1-1-2010

Robust Observers And Controllers For Marine Surface Vessels Undergoing Maneuvering And Course-Keeping Tasks

Nassim Khaled
Wayne State University

ROBUST OBSERVERS AND CONTROLLERS FOR MARINE SURFACE VESSELS UNDERGOING MANEUVERING AND COURSE-KEEPING TASKS

by

NASSIM SAADDINE KHALED

DISSERTATION

Submitted to the Graduate School

of Wayne State University,

Detroit, Michigan

in partial fulfillment of the requirements

for the degree of

DOCTOR OF PHILOSOPHY

2010

MAJOR: MECHANICAL ENGINEERING

Approved by:

_____

Advisor Date

_____

_____

_____

_____

DEDICATION

I dedicate this work to my parents, my wife and to my advisor.

ACKNOWLEDGMENTS

My parents sacrificed more than I can mention to provide me with the best education. I thank you and may God give me strength to try to pay you back. My wife, Asmaa, is my inspiration. Her understanding and support in the past four years were unlimited. If I could, I would add her as a second author for this work. As for my professor, Dr. Chalhoub, his continuous guidance and supervision for this research work were essential in the completion of this thesis. I've learned a lot from him. He helped me understand the essence of non-linear control theory. He taught me to criticize my own work, before others get to criticize it. His systematic approach tackling engineering problems is unique. The knowledge that he transmitted to me can't be read off a book.

I would like to acknowledge the financial support of the ONR (award number N00014-05-1-0040) and to the program director Dr. Kelly B. Cooper. I am truly thankful for their support throughout my PhD program

TABLE OF CONTENTS

LIST OF TABLES

LIST OF FIGURES

NOMENCLATURE

$\overset{o}{\underset{\sim}{(.)}}$ = denotes the time derivative of the components of the vector with respect to time.

$\dot{\underset{\sim}{(.)}}$ = denotes a total time derivative of a vector with respect to time.

A_T, A_L = transverse and longitudinal areas of the ship's superstructure

$A_{rud}, A_{propeller\_disk}$ = area of the rudder and the propeller disk, respectively

α = rudder angle

D_{pr} = diameter of the propeller

$H_{1/3}$ = average height of the highest one-third peaks of the wave

k, β = wave number for infinite sea depth and incident wave angle, respectively

L, L_{Bp} = overall length and length between the perpendiculars of the ship, respectively

m, I = mass and mass moment of inertia of the ship

u, v, w = translational velocity of the ship along the $\underset{\sim}{i}$, $\underset{\sim}{j}$ and $\underset{\sim}{k}$ directions, respectively

p,q,r	=	angular velocity of the ship along the $\underset{\sim}{i}_o, \underset{\sim}{j}_o$ and $\underset{\sim}{k}_o$ directions, respectively
T	=	draft of the ship
x_G, y_G, z_G	=	coordinates of the ship mass center with respect to the body-fixed frame
ρ_{water}, ρ_{air}	=	density of water and air, respectively
ψ,θ,ϕ	=	yaw, pitch and roll angular displacements of the ship, respectively

CHAPTER 1 “INTRODUCTION”

Autonomous operation and robust performance of marine surface vessels are essential for minimizing human errors in ship navigation and control as well as for efficient operation of marine vessels under different sea states and harsh environmental conditions. This goal presents a formidable task due to the inherent nonlinearities of ship dynamics, modeling imprecision, under-actuated ship configuration along with considerable and unpredictable environmental disturbances.

The motivation and goals of the current study are discussed in detail in the next Section. Subsequently, a brief review of the literature, regarding ship modeling and control, is presented. Then, an overview of the dissertation is included in Section 1.3.

1.1 Motivation and Objective

The majority of marine vessels are equipped with a single screw propeller and a rudder to provide the required thrust and steering capability to keep the ship on track. These vessels possess only two actuators to yield the desired heading angle, ψ, and the global position, (X,Y), of the ship. This results in an under-actuated configuration of the ship, whereby only two actuators are used to control three degrees of freedom, namely, X, Y, and ψ. Typically, the propeller thrust is employed in the control of the forward or surge speed of the ship. The challenge brought about by the under-actuated configuration stems from the fact that the rudder action is now required to simultaneously control the sway displacement and the heading angle of the marine vessel.

Side thrusters have been added to make ships fully-actuated at low speeds. This approach has significantly improved the maneuverability of marine vessels in harbors

and canals (Breivik, 2003). However, side thrusters are ineffective at high ship speeds; thus, causing marine vessels, equipped with side thrusters, to act as an under-actuated system in an open-sea.

To overcome this issue, modern cruise ships are supplied with podded propellers, which are thrusters that are capable of rotating 360^0 and operate at all speeds. The podded propellers enable the ship to regain its fully-actuated configuration. However, they are expensive and their malfunction will revert the ship to an under-actuated configuration.

A plausible and promising approach for enabling under-actuated marine vessels to accurately track their desired trajectories is to implement a fully integrated guidance and control system. This approach has many advantages. It does not require additional hardware to be installed on the ship. Moreover, it has the potential of improving the efficiency of ship operation under harsh environmental conditions. It also allows autonomous operation of the ship once the desired trajectory is defined; thus, significantly minimizing human errors in both navigation and control that have resulted in the past in many catastrophic accidents (BC Ferries Press Release, 2006). For instance, the Queen of the North Ferry sunk in 2006 shortly after it ran into the rocks of Gil Island when the helmsman failed to make the required course change. As a matter of fact, the majority of sinking ships are caused by human errors, which may be induced by fatigue of the crew, rough sea conditions, reduced visibility due to fog and/or unsuccessful maneuvering of the ship between obstacles.

However, the development of a fully integrated guidance and control system is still a very active research area that presents researchers with many challenges. For

example, the inherent nonlinearities of the ship dynamics, modeling imprecision, considerable and unpredictable environmental disturbances are very difficult control issues that have to be addressed in the development of a robust guidance and control system. Bear in mind that ships may experience extremely different weather conditions during a single trip, which can significantly vary the wave excitation forces, sea-current and wind loads, and may also involve ice accretion on the ship hull, and ship-ice impact.

Therefore, the main focus of this study is to develop an integrated guidance and control system that enables under-actuated marine surface vessels to operate autonomously and yield robust tracking performance in spite of significant external disturbances and modeling imprecision.

1.2 Literature Survey

The current work deals with two main topics, namely, engine friction and nonlinear robust observers. Therefore, two subsections are included to briefly discuss previous work done in these areas.

1.2.1 Literature Survey on Ship Modeling

The dynamic behavior of marine surface vessels is highly nonlinear (Nayfeh et al., 1973, 1974; Nayfeh and Mook, 1979; Barr et al., 1981; Bernitsas and Papoulias, 1986 & 1990; Sagatun and Fossen, 1991; Sagatun, 1992; Fossen, 1994; Vassalos, 1999; Vassalos et al., 2000; Suleiman, 2000; El-Hawary, 2001; Lewandowski, 2004; Bulian, 2005; Perez, 2005). Such nonlinearities include the effects of centripetal and coriolis accelerations (Fossen, 1994; El-Hawary, 2001; Lewandowski, 2004; and Perez, 2005; Khaled and Chalhoub, 2009a) and the interaction between the ship hull and its surrounding fluid, which is highly dependent on the hull geometry, the pressure

distribution in the fluid around the hull, and the wave height with respect to the hull (Korvin-Kroukovsky, 1955; Oglivie and Tuck, 1969; Norrbin, 1970; Salvesen et al., 1970; Vugts, 1970; Salvesen and Smith, 1971; Ogilvie, 1974 & 1977; Van Dyke, 1975; Wang, 1976; Newman, 1977; Sarpkaya, 1981; Korsmeyer et al., 1988; Lee and Sclavounos, 1989; Lee, 1989; Lee and Newman, 1991 & 2004; Faltinsen, 1990; Fossen, 1994; Tao and Incecik, 1998; Brian, 2003; Kristiansen and Egeland, 2003; Bertram, 2004; Perez, 2005; Kristiansen et al., 2005; Bungartz and Schafer, 2006). This solid-fluid interaction results in hydrostatic and hydrodynamic forces (Newman, 1977; Faltinsen, 1990; Fossen, 1994; Perez, 2005; Bungartz and Schafer, 2006). Among the major forces acting on the ship are the hydrostatic or buoyancy forces (Newman, 1977; Faltinsen, 1990; Fossen, 1994; Derrett and Barrass, 1999; El-Hawary, 2001; Brian, 2003; Bulian, 2005; Perez, 2005). The majority of the work reported in the literature computes these forces based on the ship's metacentric height, the position of the center of gravity and the center of buoyancy. To reduce the complexity of the computation, small roll and pitch angles are assumed. Moreover, the buoyancy forces are calculated with respect to the calm sea surface. These simplifying assumptions limit the computation of the restoring forces to the linear range of the righting-arm curve of the ship (Newman, 1977; Faltinsen, 1990; Fossen, 1994; Journée and Massie, 2001; Journée and Pinkster, 2002; Perez, 2005).

Unlike the restoring forces, the hydrodynamic forces are non-zero whenever the fluid surrounding the hull or the hull itself is in motion (Korvin-Kroukovsky, 1955; Oglivie and Tuck, 1969; Norrbin, 1970; Salvesen et al., 1970; Vugts, 1970; Salvesen and Smith, 1971; Ogilvie, 1974 & 1977; Van Dyke, 1975; Wang, 1976; Newman, 1977;

Sarpkaya, 1981; Korsmeyer et al., 1988; Lee and Sclavounos, 1989; Lee, 1989; Wu and Taylor, 1990; Lee and Newman, 1991 & 2004; Faltinsen, 1990; Fossen, 1994; Tao and Incecik, 1998; Kristiansen and Egeland, 2003; Bertram, 2004; Perez, 2005). These forces are the first and second order wave excitations forces (Newman, 1977; Sarpkaya, 1981; Lee and Sclavounos, 1989; Lee, 1989; Lee and Newman, 1991 & 2004; Faltinsen, 1990; Fossen, 1994; Kristiansen and Egeland, 2003; Bertram, 2004; Perez, 2005; Pinkster, 1980; Newman, 1993; Prins, 1995; Prins and Hermans, 1996; Hermans, 1991 & 1999), the radiation forces or the so-called “memory” effect (Newman, 1977; Perez, 2005), viscous forces (Fossen, 1994; Perez, 2005).

Moreover, ship maneuvering tasks are significantly influenced by varying and unpredictable environmental disturbances induced by winds (Isherwood, 1973; Oil Companies International Marine Forum, 1994; Fossen, 1994; Perez, 2005), sea-currents (Oil Companies International Marine Forum, 1994; Fossen, 1994; Perez, 2005), ice accretion (Golubev, 1972; Minsk, 1977; Ryerson, 1995; Derrett and Barrass, 1999) and ice impact (Cammaert and Tsinker, 1981; Cammaert et al., 1983; Cammaert and Muggeridge, 1988; Grace and Ibrahim, 2008). Thus, a realistic ship model should incorporate many, if not all, of the above mentioned effects.

Furthermore, the actuators, such as the propellers, fins and rudders, are nonlinearly coupled with the six-degree of freedom model of the ship (Abbott and Doenhoff, 1958; Kuiper, 1992; Carlton, 1994; Breslin and Andersen, 1994; Fossen, 1994; Molland and Turnock, 1993, 1994 & 1996; Molland et al., 1996; Bachmayer et al., 2000; Journée and Pinkster, 2002; Perez, 2005), which significantly increases the complexity of the problem.

Various ship models have been developed in the literature with different levels of complexity depending on the application for which they were intended for. For instance, when considering design and/or stability applications, one degree-of-freedom models have been developed to capture the roll dynamics of the ship induced by external excitations (Dunwoody, 1989; Falzarano and Troesch, 1992; Fortuna and Muscato, 1996; Bulian et al., 2003 & 2004; Yang et al., 2004; Grace and Ibrahim, 2008). Fortuna and Muscato (1996) considered a second order ordinary differential equation to describe the roll motion of the ship that is subjected to sinusoidal wave excitations. Other roll oscillation models take into consideration the stabilizing restoring moment. Yang et al. (2004) introduced a linear term representing the buoyancy moment into the second order roll equation of motion. Others used an n^{th}-order polynomial to add more precision in the computation of the restoring moment (Nayfeh and Balachandran; 1995, Arnold et al., 2004; Bulian, 2005). Furthermore, some models considered the nonlinear terms of the roll angle and its time derivatives along with a nonlinear buoyancy moment and some coupling terms between the pitch and roll motions of the ship (Falzarano and Troesch, 1992; Grace and Ibrahim, 2008). Recently, Ibrahim and Grace (2009) accounted for the effects of both pitch and heave in their formulation of the ship roll equation of motion. In addition, they used Taylor series expansion to approximate the restoring force and moments of the ship.

One degree-of-freedom models have also been developed to model and control the heading of the ship (Nomoto et al., 1956). These models consider the heading of the ship and use the rudder moment as an input. A commonly used one degree-of-freedom model for steering is the one developed by Nomoto et al. (1956). It consists of a transfer

function between the ship heading and the rudder angle-of-attack. This transfer function has been formulated to represent a first order system (Nomoto et al., 1956; Van Amerongen, 1975; Lopez et al., 1992; Fossen, 1994; Journée, 2001; Clarke, 2003 ; Moreira et al., 2007 ; Peng and Wu, 2007) or a second order system (Nomoto et al., 1957; Lopez et al., 1992; Layne and Passino, 1993; Fossen, 1994; Journée, 2001; Clarke, 2003 ; Moreira et al., 2007; Peng et al., 2007 ; Minghui et al., 2008).

To handle the control problem of ships operating in a calm sea states with slow turning maneuvers, three degree-of-freedom models should be considered (Hirano, 1980; Fossen, 1994; Fossen et al., 1998; Pettersen et al., 2001; Jiang, 2002). These models take into account the surge, sway and yaw motions of the ship under the effect of external disturbances and control forces.

Four degree-of-freedom ship models have also been developed. They account for the surge, sway, roll and yaw motions of the ship (Abkowitz, M. A., 1964; Chislett and Stom-Tejsen, 1965; Blanke and Jensen, 1997; Perez and Blanke, 2002; Perez et al., 2006; Kim et al., 2007). These models are suitable to examine and control high speed maneuvers of ships operating in calm sea states.

To accurately model the dynamics of the ship under various maneuvering speeds, one has to account for all six degrees of freedom of the ship including their coupling terms. Traditionally, these models have been formulated by assuming calm sea states and ignoring wave excitation forces and so-called “memory effect”. This class of problems are widely referred to in the literature as the “maneuvering” problem and used in studies focusing on course changing or ship stopping tasks under calm sea states (Bailey et al., 1997; Perez, 2005; Perez and Fossen, 2007; Abkowitz, 1694). The

actuators employed in these studies are limited to the propeller and the rudder (Journée and Pinkster, 2002; Bertram, 2004; Fossen, 1994; Perez, 2005; Perez and Fossen, 2007).

However, the wave excitation forces and the so-called “memory effect” strongly influence the dynamic behavior of the ship. They should be accounted for in any study that examines ship maneuvering under various environmental conditions. These forces are commonly computed based on linear harmonic motions of the ship having small amplitudes. The linear formulations have traditionally assumed constant or zero surge speed with a constant heading angle (Bingham et al.; 1994, Maury et al., 2003; Perez, 2005; Perez and Fossen, 2007). This problem is referred to in the literature as the “seakeeping” problem.

Both maneuvering and seakeeping problems have been heavily studied and reasonable models in both fields have been established (Newman, 1977; Bailey et al., 1997; Kristiansen and Egeland, 2003; Fossen, 2005; Kristiansen et al; 2005; Perez, 2005; Perez and Fossen, 2006 & 2007; Skejic and Faltinsen, 2007 & 2008). However, due to the independent development of maneuvering and seakeeping problems, different coordinate frames and assumptions have been adopted to describe the motion of the ship (Bailey et al., 1997; Perez, 2005; Perez and Fossen, 2006 & 2007). Thus, to formulate a maneuvering ship problem that accounts for the effects of sea waves, models from both maneuvering and seakeeping fields have to be considered simultaneously and combined appropriately. This is done herein by using the force superposition method to couple the seakeeping and maneuvering problems. The perturbations around moving averages of the ship velocity components in the

maneuvering problems have been used as inputs to the seakeeping problem. The latter is employed herein to determine the forces induced by wave excitations and “memory” effect. These forces are then considered among the external forces applied on the ship in the maneuvering problem, which is being solved to determine the overall response of the ship (Bailey et al., 1997; Fossen, 2005; Perez, 2005; Perez and Fossen, 2006 & 2007; Skejic and Faltinsen, 2007 & 2008).

In the current work, a nonlinear six degree-of-freedom dynamic model for a marine surface vessel is presented. The formulation incorporates recent advances that have been reported in the literature pertaining to both maneuvering and seakeeping theories (Newman, 1977; Journée and Pinkster, 2002; Fossen, 1994 & 2005; Bailey et al., 1997; Fossen and Grovlen 1998; Bertram, 2004; Perez, 2005; Perez and Fossen, 2006 & 2007). It accounts for the effects of inertial forces including those associated with coriolis and centripetal accelerations, wave excitation forces, retardation forces induced by the “memory” effect, nonlinear restoring forces, linear viscous damping terms, wind and sea-current loads. The current model differs from the existing literature on ship modeling by accounting for the physical limitations of both the ship propulsion system and the rudder. It includes a seventh degree-of-freedom to capture the dynamics of the rudder. Furthermore, it implements a 3-D mesh to determine the nonlinear restoring force based on the instantaneous free-surface of the sea rather than using the righting arm curves that are generated based on a calm sea surface.

1.2.2 Literature Survey on Ship Controllers

There are many challenging issues to be dealt with in the development of a fully integrated guidance and control system that will enable under-actuated ships to operate

autonomously while yielding a robust performance in tracking a desired trajectory. The dynamics of the ship is highly nonlinear and not fully known. Quite often ship models involve significant structured and unstructured uncertainties (Pettersen and Nijmeijer, 2001; Morel, 2009). The structured uncertainties stem from the fact that the ship parameters are not exactly known, particularly, when the marine vessel is operated under severe weather conditions that may result in ice accretion on the ship hull (Derrett and Barrass, 1999; Laranjinha et al., 2002; International Maritime Organization, 2007; Falzarano and Lakhotia, 2008). The unstructured uncertainties are associated with omitted higher order dynamics of the ship. Most controllers designed for under-actuated ships are designed based on a reduced-order model that only accounts for the surge, sway and yaw motions. However, these controllers are applied on the full-order model that involves all six degrees of freedom of the ship. In such situations, the controlled system would exhibit significant unstructured uncertainties.

Another problem that the ship controller must overcome stems from the fact that ships are required to operate in a constantly varying environmental conditions that are capable of producing significant and unpredictable external disturbances.

The environmental conditions under which the ship must operate along with the modeling imprecision can significantly deteriorate the performance of model-based controllers. Therefore, to address the above mentioned challenges, the ship controller must be robust to modeling imprecision and external disturbances (Godhavn et al., 1998; Lauvdal and Fossen, 1998; Fossen and Strand, 1999a and 1999b; Pettersen and Nijmeijer, 2001; Aranda et al., 2002; Do et al., 2003; Yang et al., 2003; Cimen and Banks, 2004; Li et al., 2009).

Moreover, these challenges are compounded by the fact that the ship is under-actuated, whereby the surge, sway and yaw motions must be controlled by using only two control variables, namely, the propeller thrust and the rudder moment. The handling of this problem necessitates the integration of the ship controller with a navigation system. This will empower the ship steering mechanism to simultaneously control the sway displacement and the heading yaw angle of the ship (Healey and Marco, 1992; Jiang and Nijmeijer, 1999; Pettersen and Lefeber, 2001; Jiang, 2002; Fossen, 2002; Fossen et al., 2003; Do et al., 2003 and 2005; Lefeber et al., 2003; Brevik, 2003; Moreira et al., 2007; Khaled and Chalhoub, 2010).

Industrial ship control applications involve the heading control problem, the roll stabilization problem, the dynamic positioning problem, and the desired trajectory control problem. In the automatic steering problem, the rudder is controlled to yield a desired heading angle of the ship (Minorsky, 1922; Vahedipour and Bobis, 1992; Kallstrom et al., 1979; Van Amerongen, 1984; Lopez and Rubio, 1992 ;Vukic and Milinovic, 1996; Fossen, 1999; Moreira et al., 2007; Francisco et al., 2008; Minghui, 2008). In the roll stabilization problem, the aim is on reducing large oscillations induced by the roll motion of the ship. These oscillations are discomforting to passengers, may significantly reduce crew efficiency, cause damage or result in loss of containers in cargo ships. Among the techniques for stabilizing the roll motion of the ship are anti-roll tanks (Abdel Gawad et al., 2001; Vasta et al., 1961; Stigter, 1966; Bell and Walker, 1966; Samoilescu and Radu, 2002), active and passive fins (Kawazoe et al., 1992; Katebi et al., 2000; Roberts et al., 1997), and rudder roll stabilization system (Roberts et al., 1997; Lloyd, 1975; Van Amerongen and Piffers, 1987).

In the dynamic positioning control problem, the ship is required to maintain a constant or zero speed while maintaining a fixed heading angle (Balchen et al., 1980; Sorensen et al., 1996; Aamo and Fossen, 1999; Lindegaard, 2003; Breivik et al., 2006). However, in the path following problem, the ship is required to follow a prescribed or desired trajectory defined by a set of way points. The current study addresses the path following control problems of under-actuated marine surface vessels.

Minorsky performed pioneering work on the development of an automatic steering system for US Navy ships (Minorsky, 1922). He observed the way helmsmen steered the ship and tried to mimic their reactions by implementing a proportional-integral-derivative (PID) controller to automatically steer the ship. Since then, PID controllers have been extensively used in the control problem of ship heading. Their popularity stems from their ease of implementation. They also led to satisfactory ship response under mild weather conditions (Vahedipour and Bobis, 1992; Kallstrom et al., 1979; Vukic and Milinovic, 1996; Fossen, 1999; Moreira et al., 2007; Francisco et al., 2008; Minghui, 2008). As expected, the performance of PID controllers significantly deteriorates when the ship undergoes large maneuvers or operates under severe environmental conditions (Kallstrom et al., 1979). This is because PID controllers are not suitable to handle strong nonlinearities and considerable external disturbances. To enhance the performance of PID controllers, some studies have varied the gains of the controller based on the ship speed (Kallstrom et al., 1979). Van Amerongen proposed a model-based adaptive steering controller based on a linear steering model (Van Amerongen, 1984). Others have implemented the optimal control theory, such as the linear quadratic regulator (LQR) and the linear quadratic tracking (LQT), to control the

ship steering problem (Lopez and Rubio 1992). These controllers tend to suffer from their susceptibility to modeling imprecision.

Nonlinear control theory has been extensively used in both track-keeping and course-changing maneuvers of marine vessels (Fossen, 2000; Pivano et al., 2007; Berge et al., 1998; Fossen, 1993; Moreira et al., 2007). However, many of these compensators, such as state feedback linearization techniques (Moreira et al., 2007; Berge et al., 1998; Fossen, 1993), output feedback controllers and back-stepping schemes (Fossen and Grovlen, 1998; Godhavn, 1996; Strand et al., 1998; Fossen and Strand, 1999; Pettersen and Nijmeijer, 2001) are model-based schemes. As a consequence, these techniques are not robust to modeling uncertainties.

Fuzzy logic controllers have been presented, by many studies, as a potential and a viable control scheme for handling modeling imprecision and varying environmental conditions. Their attractiveness stems from the fact that fuzzy logic controllers are inherently robust compensators and do not require a model of the plant. They have been implemented to control the ship steering and surge speed (Layne and Passino, 1993; Polkinghorne et al., 1995; Yansheng and Jiang, 2004; Minghui et al., 2008). However, the design of fuzzy logic controllers does not take advantage of the available knowledge about the physical plant and their proof of stability is hard to prove. Moreover, the good performance of fuzzy logic controllers hinges upon the construction of an appropriate rule-base and the fine-tuning of the gains, which can be time consuming and exhaustive procedures. Moreover, the construction of the rule-base is usually based on an expert's knowledge on the behavior of the plant. This knowledge may not be available. To deal with these drawbacks, adaptive fuzzy controllers have

emerged in the literature (Procyk and Mamdani, 1979; Sutton, R. and Towill, 1987; Sutton and Jess, 1991; Maeda and Murakami, 1992; Chih-Hsun, C. and Hung-Ching, 1994). A self-tuning fuzzy logic controller, developed by Procyk and Mamdani (1979), consists of a fuzzy logic controller with a tuning algorithm that changes the input and/or output values of the controller based on the performance of the closed-loop system. Several modified versions of the original self-tuning procedure have been presented in the literature (Sutton, R. and Towill, 1987; Sutton and Jess, 1991; Maeda and Murakami, 1992; Chih-Hsun, C. and Hung-Ching, 1994; Tönshoff and Walter, 1994; Velagic, 2003; Jie, 2007; and Yu, 2009; Yeh, 1994; Wai et al., 2002; Abreu and Ribeiro, 2002; Velagic, 2003; and Yu, 2009). Similar to the fixed-rule based fuzzy logic controllers, the majority of adaptive fuzzy controllers lack a proof for stability of their corresponding closed-loop system. Furthermore, they don't make use of the available knowledge regarding the dynamics of the system.

On the other hand, controllers based on the variable structure systems (VSS) theory are nonlinear compensators. They make use of the available knowledge about the system's dynamics. However, they do not require exact knowledge of the system. Their robustness and stability are guaranteed as long as the upper bounds on the plant nonlinearities and/or uncertainties are known (Slotine and Li, 1991; Khalil, 1996; Utkin, 1981; Rundell et al., 1996; Drakunov, 1983; Kim and Inman, 2004; Chalhoub et al., 2006; Le et al., 2004; Khaled and Chalhoub, 2010b). The design of sliding mode controllers has been proven, in many studies, to be robust to both structured and unstructured uncertainties.

Two types of robust controllers are presented in this study to control the surge speed and the heading angle of a marine surface vessel. The ship is assumed to be under-actuated. The first controller is a sliding mode controller, which is based on the variable structure theory (VSS) (Utkin, 1981). It has been proven to yield a robust tracking performance when applied on nonlinear systems whose dynamics are not fully known as long as the upper bounds of the uncertainties are known (Chalhoub and Khaled, 2009; Khaled and Chalhoub; 2009a & 2009b).

The second controller is a self-tuning fuzzy-sliding mode controller (Khaled and Chalhoub, 2010a). It combines the advantages of the variable structure systems (VSS) theory with the self-tuning fuzzy logic controller. Neither the development of an accurate dynamic model of the ship nor the construction of a rule-based expert system is required for designing this controller. The only requirement is that the upper bound of the modeling uncertainties has to be known. Moreover, the stability of the controlled system is ensured by forcing the tuning parameter to satisfy the sliding condition.

1.2.3 Literature Survey on Nonlinear State Estimators

The implementation of the controllers in the current study necessitates the availability of the state variables of the marine vessel, which represent the global X and Y position coordinates and the heading angle of the ship, ψ, along with their time derivatives. Typically, the global X and Y coordinates are available through direct measurement by a global positioning system (GPS). The heading angle can be measured by an on-board Gyro compass system (Fossen and Strand, 1999; Parkinson and Spilker, 1996; Kongsberg Maritime Corporation, 2010). $\dot{X}$, $\dot{Y}$, and $\dot{\psi}$ are not measured. They cannot be deduced from the measured signals through differentiation

because such a scheme tends to significantly magnify the noise level in $\dot{X}$, $\dot{Y}$, and $\dot{\psi}$. Therefore, a state estimator or an observer must be used to estimate the state variables that are needed for the computation of the control signals (Vik et al., 1999; Vik, 2000; Lindegaard and Fossen, 2001; Vik and Fossen, 2001; Kim and Inman, 2004; Chalhoub and Kfoury, 2005; Chalhoub et al., 2006; Chalhoub and Khaled, 2009). Since the dynamics of the ship are not fully known and the vessel may experience significant external disturbances then only robust nonlinear observers can be useful for the current work (Pettersen and Nijmeijer, 2001; Morel, 2009; Chalhoub et al., 2006; Godhavn et al., 1998; Lauvdal and Fossen, 1998; Fossen and Strand, 1999; Aranda et al., 2002; Do et al., 2003; Yang et al., 2003; Cimen and Banks, 2004; Kfoury, 2008; Li et al., 2009).

Many types of observers have been presented in the literature. In the case of linear time-invariant systems with fully known plant parameters, the Luenberger observer has been shown to yield accurate estimates of the state variables (Luenberger, 1964, 1966 & 1979; Kailath, 1980; Chen, 1970; Friedland, 1986; Ogata, 2002). Some studies attempted to extend the use of the Luenberger observer to nonlinear systems (Zeitz, 1987). Yanada and Shimahara (1997) applied the gain scheduling scheme in an attempt to enable the Luenberger observer to cope with variations in plant parameters. The drawbacks of the Luenberger observer stem from the fact that it is only applicable to linear time-invariant systems with no external disturbances. Any modeling imprecision or the presence of external disturbances would result in severe deterioration in the accuracy of the estimated state variables (Nandam and Sen, 1990).

Kalman filters have been extensively implemented to estimate the state variables of stochastic linear systems in the presence of measurement noise (Sorenson, 1985;

Lewis, 1986; Anderson and Moore, 1990; Sorensen et al., 1996; Sandler et al. 1996; Jwo and Cho, 2007). The major drawback of this observer is due to the requirement of exact knowledge of the plant dynamics.

For systems satisfying the Lipschitz conditions, quadratic Lyapunov functions can be used to design nonlinear asymptotic observers (Thau, 1973; Kou et al., 1975; Banks, 1981; Tsinias, 1989; Yaz, 1993; Boyd et al., 1994; Raghavan and Hedrick, 1994; and Rajamani, 1998). Bestle and Zeitz (1983) proposed a nonlinear observer whereby the nonlinear equations of the system are converted to the observable canonical form by using a nonlinear time-variant transformation matrix. The major drawback of such approach is the difficulty to find such a nonlinear transformation matrix.

For the class of systems where the nonlinearities are dependent on the measured outputs, the nonlinearity can be canceled by using an “output injection” term (Krener and Isidori, 1983; Besancon, 1999).

A promising class of nonlinear observers, capable of handling modeling uncertainties and external disturbances, has been developed based on the variable structure systems (VSS) theory (Walcott and Zak, 1986; Slotine et al., 1987; Misawa and Hedrick, 1989; Rundell et al., 1996; Kim and Inman, 2004; Chalhoub and Kfoury, 2005; Kfoury and Chalhoub, 2007; Kfoury, 2008). Similar to sliding mode controllers, these observers do not require exact knowledge of the dynamics of the system. The convergence of the estimated state variables to the actual ones is guaranteed as long as the upper bounds on the modeling imprecision are known.

Two types of observers have been presented in the current study. The first is a nonlinear sliding mode observer while the second is a self-tuning fuzzy-sliding mode

observer. These observers were implemented herein to accurately estimate the global position of the ship and its heading angle along with their time derivatives. Both observers were developed based on a reduced-order model of the ship, which only accounts for the surge, sway and yaw motions. The proof for their asymptotic stability was also considered.

1.2.4 Literature Survey on Guidance Systems

Prior to the implementation of guidance systems, multi-input multi-output controllers were implemented to control the motion of under-actuated marine surface vessels. The number of control actions was considered to be smaller than the number of degrees of freedom of the system. The desired heading angle and surge speed are specified as functions of time. The drawback of such an approach is due to the fact that the ship may diverge from its desired trajectory even in the case when the controller succeeds in yielding the desired values of the heading angle and surge speed. In the presence of environmental disturbances, the ship may experience a substantial drift in the sway direction while the controller maintains the desired orientation of the ship. The drift may grow with time if the desired heading angle is specified as a function of time. However, if the desired heading angle is defined based on the instantaneous cross track error then a successful implementation of the controller will prevent the drift in the sway motion to grow with time. Consequently, the ship will remain in the vicinity of its desired trajectory. Therefore, a promising solution to this problem is to fully integrate the guidance system to the controller of the ship. The guidance system will determine the desired heading angle based on the instantaneous cross track error, which is the relative position of the ship with respect to its desired trajectory. While the task of the

controller would be to ensure that the actual heading angle and surge speed converges to their desired values.

In under-actuated marine surface vessels, the propeller is dedicated to the control of the surge speed. The rudder has to simultaneously control the sway motion and provide the desired heading angle of the ship (Breivik, M., 2003; Moreira et al.; 2007). Such a task requires the ship controller to be integrated with a guidance system as indicated earlier. The latter provides desired values for the heading angle that will enable the ship to converge and remain on its desired trajectory.

The guidance system should always be able to guide the system regardless of the magnitude of the cross track error. The computation of the desired heading angle based on the instantaneous cross track error ensures a smooth and fast convergence of the ship to its desired path. Moreover, once the ship is on track, the guidance system should prevent the marine vessel from oscillating around its desired trajectory (Breivik, 2003; Moreira et al., 2007).

Furthermore, a potential problem has emerged during the implementation of guidance systems for under-actuated marine vessels (Godhavn, 1996; Berge and Fossen 1998; Fossen et al., 1998; Breivik, 2003; Moreira et al., 2007). It causes the ship to track the desired trajectory while moving backward. This problem is inherent in guidance systems. Therefore, guidance schemes should have a provision in their design to prevent such a problem from occurring.

A guidance system, based on the line-of-sight (LOS) concept, has been reported in the literature (Fossen, 2002; Fossen et al., 2003; Healey and Marco, 1992; Breivik, 2003; Moreira et al., 2007). The initial concept (Moreira et al., 2007) incorporates a

circle with a constant radius, R. Such a scheme fails to provide any guidance and becomes inapplicable whenever the cross-track error exceeds the radius. Moreira and his co-workers (2007) presented a guidance scheme that varies R linearly with the cross-track error. This technique will always yield an appropriate value for the desired heading angle that will guide the ship to the desired trajectory irrespective of the magnitude of the cross-track error (Moreira et al., 2007).

In the current work, a guidance scheme is presented based on the concepts of the variable radius line-of-sight (LOS) and the acceptance radius. It differs from existing literature by varying the radius of line-of-sight exponentially rather than linearly with the cross track error (Khaled and Chalhoub, 2010b). The rationale is to yield a faster convergence rate of the ship to its desired trajectory than those achievable by existing guidance systems. Moreover, the current technique can handle large cross-track errors and has a provision in its design to prevent the ship from tracking the desired trajectory while moving backward.

1.3 Dissertation Overview

The purpose of the current work is to develop control and guidance schemes that allow under-actuated ships to operate autonomously and exhibit robust tracking characteristic in the presence of considerable external disturbances and modeling imprecision.

A dynamic model, capable of predicting the dynamic behavior of under-actuated marine vessels under various environmental conditions, has been developed. It is used herein as a test bed to assess the performance of the proposed guidance and control systems. The model is described in detail in Chapter 2. Its formulation accounts for the

inertial forces, wave excitation forces, retardation forces or so-called “memory” effect, nonlinear restoring forces, linear viscous damping terms, wind and current loads. It takes into consideration the physical limitations of both the ship propulsion system and the rudder. Moreover, an additional degree-of-freedom has been introduced in the model to capture the dynamics of the rudder.

Chapter 3 describes the design of a sliding mode controller to control the surge speed and the heading angle of a marine surface vessel. The simulation results assess the performance of the controller in the presence of significant structured and unstructured uncertainties along with external disturbances.

In Chapter 4, a nonlinear observer, based on the sliding mode methodology, is presented. The objective is to estimate all the state variables that are needed for the computation of the control signals. The simulation results assess the accuracy of the estimated state variables in spite of modeling imprecision and external disturbances. Moreover, it covers simulation results that were generated by computing the control actions based on estimated rather than actual state variables.

In Chapter 5, a new self-tuning fuzzy-sliding mode controller is described. The proposed controller is an attempt to combine the advantages of the variable structure systems (VSS) theory with the self-tuning fuzzy logic controller. Simulation results are also included in order to assess the robustness and performance of the controller.

A novel self-tuning fuzzy-sliding mode observer is presented in Chapter 6. A detailed stability analysis of the observer design has also been included. The simulation results examine the performance of the proposed observer as well as the combined response of the self-tuning fuzzy-sliding mode controller and observer.

Chapter 7 covers the details of a modified guidance system, which aims at yielding a faster convergence rate of the ship to its desired trajectory than those achievable by existing guidance systems. The simulation results test the combined performance of the proposed guidance and control systems, which incorporate the proposed observer designs.

Finally, the work is summarized in Chapter 8. Its main results and contributions are clearly defined. Moreover, prospective research topics are suggested.

CHAPTER 2 “NONLINEAR DYNAMIC MODEL OF A MARINE SURFACE VESSEL”

The formulation for a nonlinear dynamic model of a marine surface vessel is discussed in detail in this Chapter. The model considers the six rigid body degrees of freedom of the ship. It accounts for the physical limitations of both the ship propulsion system and the rudder. Moreover, the model incorporates environmental conditions that can potentially alter the dynamic behavior of the ship.

The model emulates the dynamic behavior of a marine surface vessel operating under various sea states. It will be used herein as a test bed to assess the performances of guidance and control systems, which involve robust and self-tuned controllers and observers.

2.1 Dynamic Model of a Marine Vessel

The dynamic behavior of marine surface vessels is highly nonlinear. Moreover, it is significantly influenced by environmental disturbances induced by winds, random sea waves and currents. The present model closely follows the existing literature on ship modeling (Fossen, 1994; Perez, 2005; Newman, 1977). Its formulation includes the wave excitation forces, retardation forces, inertial forces, nonlinear restoring forces, wind and current loads along with linear viscous damping terms. Moreover, the physical limitations of both the ship propulsion system and the rudder are accounted for in the model.

The ship is treated in the current study as a rigid body having six degrees of freedom, namely, surge, sway, heave, roll, pitch and yaw. This is illustrated in Fig. 2-1. Two coordinate systems have been used. The first one is an inertial frame $\{X,Y,Z\}$ whose origin is located at an arbitrary point on the calm sea surface. The second

coordinate system, $\{x, y, z\}$, is a non-inertial, body-fixed coordinate system attached to the ship at point o, which coincides with the center of floatation of the ship. The $(x, z)-$plane is chosen to coincide with the vertical plane of symmetry of the ship hull. The $x-$ and $y-$axes are directed towards the bow and the starboard of the ship.

Following the SNAME convention (1950), both the position and orientation of the ship are defined with respect to the inertial frame. However, the ship translational and angular velocity vectors are expressed with respect to the body-fixed frame.

The position vector of the mass center of the ship can be written as

$$\underset{\sim}{r}^{*} = \underset{\sim}{r}_{o} + \underset{\sim}{r}_{G} \tag{2.1}$$

where $\underset{\sim}{r}_{G}$ is the position vector of the ship mass center defined with respect to the body-fixed coordinate system. It is given by

$$\underset{\sim}{r}_{G} = x_{G}\,\underset{\sim}{i}_{o} + y_{G}\,\underset{\sim}{j}_{o} + z_{G}\,\underset{\sim}{k}_{o} \tag{2.2}$$

It should be pointed out that x_G, y_G and z_G are constant. $\underset{\sim}{r}_{o}$ represents the position vector of point o with respect to the inertial coordinate system. It is expressed as follows

$$\underset{\sim}{r}_{o} = x\,\underset{\sim}{I} + y\,\underset{\sim}{J} + z\,\underset{\sim}{K} \tag{2.3}$$

Next, the velocity vector of the mass center of the ship is determined from

$$\dot{\underset{\sim}{r}}^{*} = \dot{\underset{\sim}{r}}_{o} + \dot{\underset{\sim}{r}}_{G} = \dot{\underset{\sim}{r}}_{o} + \underset{\sim}{\omega} \times \underset{\sim}{r}_{G} \tag{2.4}$$

$\dot{\underset{\sim}{r}}_{o}$ can be written with respect to the inertial frame as

$$\dot{\underset{\sim}{r}}_o = \dot{x}\,\underset{\sim}{I} + \dot{y}\,\underset{\sim}{J} + \dot{z}\,\underset{\sim}{K} \tag{2.5}$$

The velocity vector of point o, $\dot{\underset{\sim}{r}}_o$, and the angular velocity vector of the ship, $\underset{\sim}{\omega}$, are both defined with respect to the body-fixed coordinate system as

$$\dot{\underset{\sim}{r}}_o = u\,\underset{\sim}{i} + v\,\underset{\sim}{j} + w\,\underset{\sim}{k} \tag{2.6}$$

$$\underset{\sim}{\omega} = p\,\underset{\sim}{i} + q\,\underset{\sim}{j} + r\,\underset{\sim}{k} \tag{2.7}$$

where u, v and w terms in Eq. (2.6) are related to $\dot{x}, \dot{y}$ and $\dot{z}$ in Eq. (2.5) through a composite rotation matrix as follows

$$\begin{aligned}\begin{pmatrix}\dot{x}\\ \dot{y}\\ \dot{z}\end{pmatrix} &= R_{XYZ}^{xyz}(\psi,\theta,\phi)\begin{pmatrix}u\\ v\\ w\end{pmatrix}\\ &= \begin{pmatrix} c\psi c\theta & -s\psi c\phi + c\psi s\theta s\phi & s\psi s\phi + c\psi s\theta c\phi\\ s\psi c\theta & c\psi c\phi + s\psi s\theta s\phi & -c\psi s\phi + s\psi s\theta c\phi\\ -s\theta & c\theta s\phi & c\theta c\phi\end{pmatrix}\begin{pmatrix}u\\ v\\ w\end{pmatrix}\end{aligned} \tag{2.8}$$

Furthermore, the roll, p, pitch, q, and yaw, r can be directly related to the Euler angles ψ, θ and ϕ as follows

$$\begin{aligned}\begin{pmatrix}p\\ q\\ r\end{pmatrix} &= \begin{pmatrix}\dot{\phi}\\ 0\\ 0\end{pmatrix} + \begin{pmatrix}1 & 0 & 0\\ 0 & c\phi & s\phi\\ 0 & -s\phi & c\phi\end{pmatrix}\begin{pmatrix}0\\ \dot{\theta}\\ 0\end{pmatrix} + \begin{pmatrix}c\theta & 0 & -s\theta\\ 0 & 1 & 0\\ s\theta & 0 & c\theta\end{pmatrix}\begin{pmatrix}1 & 0 & 0\\ 0 & c\phi & s\phi\\ 0 & -s\phi & c\phi\end{pmatrix}\begin{pmatrix}0\\ 0\\ \dot{\psi}\end{pmatrix}\\ &= \begin{pmatrix}1 & 0 & -s\theta\\ 0 & c\phi & s\phi c\theta\\ 0 & -s\phi & c\phi c\theta\end{pmatrix}\begin{pmatrix}\dot{\phi}\\ \dot{\theta}\\ \dot{\psi}\end{pmatrix} = J_2^{-1}(\psi,\theta,\phi)\begin{pmatrix}\dot{\phi}\\ \dot{\theta}\\ \dot{\psi}\end{pmatrix}\end{aligned} \tag{2.9}$$

Alternatively, one can write

$$\begin{pmatrix}\dot{\phi}\\ \dot{\theta}\\ \dot{\psi}\end{pmatrix} = J_2(\psi,\theta,\phi)\begin{pmatrix}p\\ q\\ r\end{pmatrix} = \begin{pmatrix}1 & s\phi t\theta & c\phi t\theta\\ 0 & c\phi & -s\phi\\ 0 & s\phi/c\theta & c\phi/c\theta\end{pmatrix}\begin{pmatrix}p\\ q\\ r\end{pmatrix} \tag{2.10}$$

Next, the acceleration vector of the ship mass center is obtained by differentiating $\dot{r}^*$ with respect to time as follows

$$\ddot{r}^* = \overset{o}{\dot{r}}_o + \omega \times \dot{r}_o + \overset{o}{\omega} \times r_G + \omega \times \left(\omega \times r_G\right) \tag{2.11}$$

The scalar equations, describing the translational motion of the ship, are derived from the linear momentum balance. They are given as

$$m\left[\dot{u} - vr + wq - x_G(q^2 + r^2) + y_G(pq - \dot{r}) + z_G(pr + \dot{q})\right] = F_X \tag{2.12a}$$

$$m\left[\dot{v} - wp + ur - y_G(r^2 + p^2) + z_G(qr - \dot{p}) + x_G(pq + \dot{r})\right] = F_Y \tag{2.12b}$$

$$m\left[\dot{w} - uq + pv - z_G(p^2 + q^2) + x_G(rp - \dot{q}) + y_G(rq + \dot{p})\right] = F_Z \tag{2.12c}$$

where F_X, F_Y and F_Z are the components of the resultant force, F, of all externally applied forces on the ship along the i, j and k directions, respectively. Moreover, the angular momentum balance of the ship around point o can be written as

$$m\, r_G \times \left(\overset{o}{\dot{r}}_o + \omega \times \dot{r}_o\right) + I_o\, \overset{o}{\omega} + \omega \times \left(I_o\, \omega\right) = M_o \tag{2.13}$$

Its corresponding three scalar equations, governing the rotational motion of the marine vessel, are:

$$\begin{aligned} I_x\dot{p} - I_{xy}\dot{q} - I_{xz}\dot{r} - I_{xz}pq - I_{yz}q^2 + I_z rq + I_{xy}pr - I_y qr + I_{yz}r^2 \\ + my_G(\dot{w} + pv - uq) - mz_G(\dot{v} + ur - pw) = M_X^o \end{aligned} \tag{2.14a}$$

$$-I_{xy}\dot{p}+I_y\dot{q}-I_{yz}\dot{r}+I_{xz}p^2+I_{yz}pq-I_zrp+I_xpr-I_{xy}qr-I_{xz}r^2 + mz_G(\dot{u}+qw-vr)-mx_G(\dot{w}+pv-uq)=M_Y^o \tag{2.14b}$$

$$-I_{xz}\dot{p}-I_{yz}\dot{q}+I_z\dot{r}-I_{xy}p^2+I_ypq-I_{yz}pr-I_xpq+I_{xy}q^2+I_{xz}rq + mx_G(\dot{v}+ur-pw)-my_G(\dot{u}+qw-vr)=M_Z^o \tag{2.14c}$$

where M_X^o, M_Y^o and M_Z^o are the components of the resultant moment, $\underset{\sim}{M}_o$, of all externally applied moments on the ship along the $\underset{\sim}{i}$, $\underset{\sim}{j}$ and $\underset{\sim}{k}$ directions, respectively. Both $\underset{\sim}{F}$ and $\underset{\sim}{M}_o$ reflect the effects of wave excitations, retardation forces, wind and current loads, linear viscous damping terms, nonlinear restoring forces along with the control actions generated by the propeller, and the rudder.

Long-crested sea waves are considered in the current study. The wave height, h, at an arbitrary point (X,Y), defined with respect to the inertial frame, is commonly described by (Newman, 1977; Perez, 2005)

$$h(X,Y,t)=\sum_{i=1}^{650}A_i\cos\left(\omega_i t+\varepsilon_i-k\left(X\cos\beta+Y\sin\beta\right)\right) \tag{2.15}$$

where A_i and ε_i are the amplitude and the phase angle of the i^{th} frequency component of the wave height, respectively. ε_i is considered to be a random variable with a uniform distribution between 0 and 2π. A_i is determined from $\sqrt{2S(\omega_i)\Delta\omega}$ where $S(\omega)$ is the wave spectrum. The latter is assumed to be the Modified Pierson-Moskowitz wave spectrum. It is defined as (Perez, 2005)

$$S(\omega)=\frac{A_S}{\omega^5}e^{\left(-B_S/\omega^4\right)} \tag{2.16a}$$

$$A_S=0.312H_{1/3}^2\omega_o^4 \tag{2.16b}$$

$$B_S = 1.25\omega_o^4 \tag{2.16c}$$

where ω_o is the modal frequency at which the wave spectrum reaches its maximum value. The wave spectrum corresponding to $H_{1/3} = 5\ m$ and $\omega_0 = 0.69$ rad/s is shown in Fig. 2-2. Moreover, to avoid risking $h(X,Y,t)$ from being repeated, ω_i is selected randomly in the interval $\left[(i-1)\Delta\omega, i\Delta\omega\right]$ (Perez, 2005). It should be noted that $\Delta\omega$ is considered to be constant and equal to 0.01 rad/s.

The formulation of the seakeeping problem, which customarily considers the ship motion to be harmonic with small amplitudes, has been used herein to determine the wave excitation forcing functions along with the frequency dependent added mass and wave damping terms (Faltinsen, 1990; Newman, 1977; Perez, 2005). In addition, the fluid is assumed to be inviscid, incompressible and irrotational. The wave excitation forces and moments are computed as follows

$$F_j^{w-e}(t) = \sum_{i=1}^{650} \left| X_j(\chi,\omega_i) \right| \sqrt{2S(\omega_i)\Delta\omega}\cos\left(\omega_i t + \varepsilon_i - k\left(X\cos\beta + Y\sin\beta\right) + \varphi_j(\chi,\omega_i)\right) \quad \textit{for} \quad j=1,\cdots,6 \tag{2.17}$$

where $\chi = \beta - \psi$ is the wave encounter angle. Moreover, $\left|X_j(\chi,\omega_i)\right|$ and $\varphi_j(\chi,\omega_i)$ are the magnitude and phase angle of the force transfer function defined by the ratio of the wave excitation force influencing the j^{th} degree-of-freedom of the ship over the wave amplitude. The six force transfer functions are determined numerically by using a 3-D potential theory software WAMIT (Lee and Newman, 2004). It should be mentioned that the latter does not account for the effect of the ship forward speed.

The frequency dependent added mass, $a_{ml}(\omega)$, and wave damping, $b_{ml}(\omega)$ terms are also computed by using WAMIT (Lee and Newman, 2004) for a frequency range between 0 and 6.5 rad/sec. The impulse response $k_{ml}(t)$ in the m^{th} direction due to a unit velocity impulse in the l^{th} direction can be related to the wave damping term, $b_{ml}(\omega)$, as follows (Ogilivie, 1964; Kristiansen et al., 2005)

$$k_{ml}(t) = \frac{2}{\pi}\int_0^\infty \left[b_{ml}(\omega) - b_{ml}(\infty)\right]\cos(\omega t)\, d\omega \tag{2.18}$$

The convolution integral associated with $k_{ml}(t)$, based on an arbitrary velocity term $\dot{\zeta}_l$ in the l^{th} direction, can be written as

$$\int_0^\infty k_{ml}(t-\tau)\dot{\zeta}_l(\tau)\, d\tau \quad for \quad m,l = 1,\cdots,6 \tag{2.19}$$

This will result in a 6×6 retardation matrix $K(t)$. Following the procedure outlined by Kristiansen et al. (2005), the singular value decomposition method was used to generate a non-minimal state space realization for a single-input single-output (SISO) system whose input and output variables are $\dot{\zeta}_l(t)$ and $y_{kl}(t)$, respectively. A model reduction procedure was then implemented to reduce the order of the state space realization to eight without significantly compromising its accuracy. This is illustrated in Fig. 2-3 for the case of $k_{15}(t)$. The state space representation corresponding to the (k,l) entry of the retardation matrix $K(t)$ can be described as

$$\begin{aligned} \dot{\underset{\sim}{\xi}}^{(kl)} &= A^{(kl)}\underset{\sim}{\xi}^{(kl)} + B^{(kl)}\dot{\zeta}_l \\ y_{kl} &= C^{(kl)}\underset{\sim}{\xi}^{(kl)} + D^{(kl)}\dot{\zeta}_l \end{aligned} \tag{2.20}$$

In the current study, the seakeeping problem will be influenced by the actual motion of the ship through the input term, which is considered herein to be the perturbation in the l^{th} velocity component of the ship. Therefore, $\dot{\zeta}_l$ is defined to be the variations around the moving average value of the instantaneous l^{th} velocity component of the ship. The moving average is determined by implementing a "forgetting" factor, which puts significantly heavier weights on recent than on older data of the ship velocity. Furthermore, the retardation force, $F_k^{retardation}$, representing the so-called "memory effect" in the k^{th} equation of motion of the ship can be evaluated from $\sum_{l=1}^{6} y_{kl}$.

Next, the buoyancy force and moment are computed based on the instantaneous submerged volume of the ship with respect to the sea free-surface. These forcing functions, which are balanced by the ship's own weight, are determined by integrating over the entire submerged volume of the ship. This is done herein by defining a 3-D mesh that partitions the ship hull into 32000 cubes (see Fig. 2-4). The dimensions of each cube are selected to be 5, 2 and 0.04 m in the $\underset{\sim}{i}_o, \underset{\sim}{j}_o$ and $\underset{\sim}{k}_o$ directions, respectively. The computation of the instantaneous submerged volume of the ship involves the evaluation of a "degree of submergence", α, for each block. α_i corresponding to the i^{th} block is defined by

$$\alpha_i = sat\left(\frac{Z_c^i - h\left(X_c^i, Y_c^i, t\right)}{block\ thickness} + \frac{1}{2}\right) \tag{2.21}$$

where $\left(X_c^i, Y_c^i, Z_c^i\right)$ are the coordinates of the centroid of the i^{th} block (see Fig. 2-4), $block\ thickness = 0.04\ \ m$ (height of the block) and h is the elevation of the sea free-

surface at (X_c^i, Y_c^i). Both the centroid and h are defined with respect to the inertial frame. The lower and upper saturation limits are set to 0 and 1, respectively. Note that $\alpha_i = 0$ reflects the case in which the i^{th} block is located above the sea free-surface. However, $\alpha_i = 1$ and $0 < \alpha_i < 1$ correspond to total and partial submergence of the i^{th} block, respectively. The instantaneous submerged volume of the ship can now be computed from $V_{sub} = \sum_{i=1}^{32000} \alpha_i V_{i_{block}}$. The coordinates of the center of buoyancy (CB) are calculated as follows

$$x_{CB} = \frac{\sum_{i=1}^{32000} \left(x_{i_{block}}\right)\left(\alpha_i V_{i_{block}}\right)}{V_{sub}} \tag{2.22a}$$

$$y_{CB} = \frac{\sum_{i=1}^{32000} \left(y_{i_{block}}\right)\left(\alpha_i V_{i_{block}}\right)}{V_{sub}} \tag{2.22b}$$

$$z_{CB} = \frac{\sum_{i=1}^{32000} \left(\alpha_i z_{i_{block}}\right)\left(\alpha_i V_{i_{block}}\right)}{V_{sub}} \tag{2.22c}$$

The righting arm curve of the current ship is shown Fig. 2-5, which reveals a range of stability of around 84.3^o. It should be noted that the hydrostatic moment is determined with respect to the origin of $\{x, y, z\}$ coordinate system. Moreover, linear viscous damping forces and moments are introduced as $\left[\left(mb_u\right)u, \left(mb_v\right)v, \left(mb_w\right)w, \left(I_x b_p\right)p, \left(I_y b_q\right)q, \left(I_z b_r\right)r\right]^T$ where b_u, b_v, b_w, b_p, b_q and b_r are chosen herein to be 1, 1, 3, 8, 8 and 8, respectively (Ueng et al., 2008).

Next, the formulation reflecting the resistive forces and moments, induced by wind and sea-currents, is discussed. The wind can impact the dynamic behavior of vessels in different ways. Its direct effect is due to the wind forces and moments exerted on the portion of the ship that is exposed to air. However, its indirect effect stems from the fact that the wind generates waves, which apply forces and moments on the wetted portion of the ship. It should be emphasized that the present study accounts only for the direct effect of wind on the ship.

The formulations used herein to determine wind resistive forces and moments exerted on ships are adopted from the widely accepted work of Isherwood (1973) in both ship design (Journée and Massie, 2001; El-Hawary, 2001) and ship motion control (Faltinsen, 1990; Fossen, 1994; Tragardh et al., 2005). In his book, Faltinsen (1990) referred to Isherwood's paper for determining the wind loads on passenger ships, ferries, cargo ships, tankers, ore carriers, stern trawlers and tugs. Journée and Massie (2001) described Isherwood's formulations as a "reliable method for estimating the wind resistance".

Numerous studies addressing the wind resistive forces and moments on merchant ships have been reviewed by Isherwood (1973) who deemed them to be incomplete due to their lack of covering the entire range of merchant ships. Therefore, in his work, Isherwood (1973) performed a comprehensive analysis of data collected from wind resistance experiments that were conducted at different test establishments on models covering a wide range of merchant ships. Based on his analysis, he provided formulations for computing the wind resistive force and yawing moment that are suitable for any merchant ship subjected to wind from any direction.

In a similar manner, Remery and Oortmerssen collected wind data for eleven different tanker hulls (1973). They expanded the coefficients, used in calculating wind forces and moments, by a Fourier series as a function of the incident angle. Such fifth order series were found to be reasonably accurate in representing the data for preliminary design purposes (Remery and Oortmerssen, 1973).

Moreover, due to significant variations in the prediction of wind loads on very large crude carriers (VLCC, i.e., tankers having deadweights between 150,000 to 500,000 Tons), the Oil Companies International Marine Forum charged the Mooring and Mooring Equipment Committee of the Piers and Docks Forum with the task of defining a general set of wind coefficients (OCIMF, 1977 & 1994). The latter will be useful for specifying mooring equipment and for determining a minimum acceptable criterion for designing marine terminals for VLCC's.

Since the scope of the current study is limited to ships that are significantly smaller in size than those of the VLCC's then the formulation of Isherwood will be implemented herein for the computation of wind loads (Isherwood, 1973).

The wind resistive forces and yawing moment are computed as follows (Isherwood, 1973; Journée and Massie, 2001; Fossen, 1994; Perez, 2005; OCIMF, 1977 & 1994)

$$f_{x_w} = \frac{1}{2} C_{x_w} \rho_{air} A_T V_{r_w}^2 (10) \tag{2.23a}$$

$$f_{y_w} = \frac{1}{2} C_{y_w} \rho_{air} A_L V_{r_w}^2 (10) \tag{2.23b}$$

$$m_{z_w} = 0.5 C_{z_w} \rho_{air} A_L V_{r_w}^2 (10) L \tag{2.23c}$$

where $V_{r_w}(10)$ is the wind velocity relative to the ship evaluated at 10 m above the calm sea surface. Note that m_{z_w} is applied around an axis perpendicular to the calm sea surface and passing through the midpoint between the aft and forward perpendiculars of the ship (see Fig 2-6). The formulation for determining C_{x_w}, C_{y_w} and C_{z_w} coefficients are provided by Isherwood (1973).

The formulation used for computing the current induced forces and yawing moment are similar to those employed in the calculation of the wind loads with the exception that they are only being applied on the submerged portion of the ship. They are given by (OCIMF, 1977 & 1994)

$$f_{x_c} = \frac{1}{2} C_{x_c} \rho_{water} V_{r_c}^2 L_{pp} T \tag{2.24a}$$

$$f_{y_c} = \frac{1}{2} C_{y_c} \rho_{water} V_{r_c}^2 L_{pp} T \tag{2.24b}$$

$$m_{z_c} = \frac{1}{2} C_{z_c} \rho_{water} V_{r_c}^2 L_{pp} T \tag{2.24c}$$

where V_{r_c} is the velocity of the current relative to the ship. The numerical values for C_{x_c}, C_{y_c} and C_{z_c} are obtained from the OCIMF report (1994).

The propeller thrust, F_{th}, is one of the control variables responsible for keeping the ship on track. In determining F_{th}, a mean value for the entrance speed of the fluid at the propeller disk, V_{pr}, is considered. It is determined as follows (Journée and Massie, 2001; Blanke, 1982; Journée, 2001)

$$V_{pr} = (1 - w) U \tag{2.25}$$

where the wake fraction number, w_f, is usually determined from open-water tests. Its typical values are between 0.1 and 0.4 (Fossen, 1994). It is assumed herein to be 0.1.

The present work considers a fixed pitch, sub-cavitating, Wageningen B-screw open-propeller. Due to its simple form and good performance, the B-screw is the most widely used type of fixed-pitch open-propellers (Journée and Massie, 2001; Journée, 2001; Roddy et al., 2006). Numerous tests were conducted on the Wageningen B-screw propellers; thus, resulting in a large body of experimental data covering around 210 B-screw propellers (Journée and Massie, 2001; Roddy et al., 2006). Kuiper (1992) has provided a comprehensive summary of this data. In the present work, the B4-70 propeller series has been employed.

For ship maneuvering tasks, four-quadrant data on dimensionless thrust, C_T, and torque, C_Q, coefficients should be used (Kuiper, 1992; Journée and Massie, 2001; Journée, 2001; Roddy at al, 2006). Kuiper (1992) provided such data for a B4-70 open-propeller as a function of the hydrodynamic pitch angle, δ, which is illustrated in Fig. 2-7 and calculated at $r = 0.7\left(D_{pr}/2\right)$ as follows (Journée and Massie, 2001; Journée, 2001)

$$\beta_{0.7\left(D_{pr}/2\right)} = \arctan\left(\frac{V_{pr}}{1.4\pi n_{pr} D_{pr}}\right) \tag{2.26}$$

The propeller thrust, F_{th}, and the corresponding torque, T_{pr}, that should be applied on the propeller shaft are determined from (Journée and Massie, 2001)

$$T_{pr} = (\pi/8) C_Q \rho_{water} V_r^2 D_{pr}^3 \tag{2.27a}$$

$$F_{th} = (\pi/8) C_T \rho_{water} V_r^2 D_{pr}^2 \tag{2.27b}$$

where V_r is the speed of the flow in the blade section evaluated at $0.7(D_{pr}/2)$. It is given by

$$V_r = \sqrt{V_{pr}^2 + \left(0.7\pi n_{pr} D_{pr}\right)^2} \tag{2.28}$$

where n_{pr} is the angular velocity of the propeller shaft.

To make the ship model and its corresponding controller more realistic and suitable for real life applications, the physical limitations of the powertrain system of the ship have been accounted for in the current formulation by applying the deliverable propeller thrust, F_{th_deliv}, on the ship instead of the desired thrust, F_{th_cont}, assigned by the controller. F_{th_deliv} is determined based on a computationally efficient numerical scheme, which is illustrated schematically in the flowchart of Fig. 2-8. By using Eq. (2-26), one can define the following normalized propeller force and torque:

$$T_{pr\_norm} = \frac{T_{pr}}{(\pi/8)\rho_{water} V_{pr}^2 D_{pr}^3} = C_Q(\beta)\left(1 + \frac{1}{\tan^2(\beta)}\right) \tag{2.29a}$$

$$F_{th\_norm} = \frac{F_{th}}{(\pi/8)\rho_{water} V_{pr}^2 D_{pr}^2} = C_T(\beta)\left(1 + \frac{1}{\tan^2(\beta)}\right) \tag{2.29b}$$

Two look-up tables are generated for each of F_{th_norm} and T_{pr_norm}. The first table is constructed for $0 \le \beta \le 180^o$ while the second table covers the range corresponding to $180^o \le \beta \le 360^o$. This is done to make the mapping between β and the right hand side of Eqs. (2.29a) and (2.29b) to be single valued.

At this stage, the procedure outlined in the flowchart of Fig. 2-8 is followed. F_{th_norm} is computed based on F_{th_cont}, as assigned by the controller, and V_{pr} from

the previous time step. A candidate value for β will now be determined from the table look-up between β and F_{th_norm}. Based on β_{cand}, T_{pr_cand} will be determined. If the latter is within the physical limitations of the ship propulsion system than both F_{th_cont} and T_{pr_cand} become F_{th_deliv} and T_{pr_deliv}, respectively. Otherwise, T_{pr_cand} is set to T_{bound} where the latter takes on a maximum or a minimum value of the engine torque depending on the conditions specified in the flowchart. Now, T_{pr_norm} is computed based on T_{bound} and the table look-up between β and T_{pr_norm} is used to determine the numerical value of β. The latter will then be used to determine F_{th_deliv}.

Next, the forces and moments associated with the rudder are considered. The rudder serves as an actuator to steer the ship. It is positioned near the stern of the ship and in the propeller stream in order to improve its effectiveness (Journée and Pinkster, 2002). The interaction between the rudder and the fluid flow in its viscinity results in lift and drag forces exerted on the rudder surface as illustrated in Fig. 2-9 (Perez, 2005). The lift and drag forces are perpendicular and tangential to the fluid flow velocity, respectively. The point of application of these forces is commonly referred to in the literature as the center of pressure (C_P)(Fig. 2-9). It is located at the mid-span $\left(\frac{s_P}{2}\right)$ of the rudder (Fig. 2-10) and at an "e_{rud}" distance away from the leading edge. It should be emphasized that e_{rud} depends on the angle of attack of the rudder. For small angles, the center of pressure is around $e_{rud} \approx 0.25\bar{c}$, where $\bar{c}$ is the mean cord of the

rudder (Perez, 2005; Journée and Pinkster, 2002). For an arbitrary shape of the rudder, $\overline{c}$ can be written as

$$\overline{c} = \frac{A_{rud}}{\overline{s}_P} \tag{2.30}$$

However, for large angles of attack and before the rudder stalls, C_P shifts backward and e_{rud} increases to around $0.4\,\overline{c}$ (Journée and Pinkster, 2002). This is due to the flow separation occurring on the suction side of the rudder.

The magnitudes of both the lift, F_{lift}, and drag, F_{drag}, forces are determined as follows (Perez, 2005; Journée and Pinkster, 2002)

$$F_{lift} = \frac{1}{2} C_L \rho_{water} V_{rud}^2 A_{rud} \tag{2.31a}$$

$$F_{drag} = \frac{1}{2} C_D \rho_{water} V_{rud}^2 A_{rud} \tag{2.31b}$$

The numerical values for C_L and C_D, based on an aspect ratio (AR) of 6 and a rudder section between 0.06 and 0.18, are provided by Abbott and Von Doenhoff (1958) and Journée and Pinkster (2002). Furthermore, V_{rud} is computed herein by considering two components of the flow velocity as follows

$$V_{rud} = \sqrt{V_{surge\_rud}^2 + V_{sway\_rud}^2} \tag{2.32}$$

where V_{surge_rud} represents the velocity of the fluid approaching the rudder after being influenced by the propeller (Perez 2005; Lewis 1988). The effect of the propeller on the flow heading towards the rudder has been accounted for by considering an idealized, steady, one-dimensional flow through the propeller. The latter is modeled by a thin actuator disk across which, the flow velocity is considered to be continuous while the

pressure is assumed to undergo a sudden change. Based on this simplified model, one can express V_{surge_rud} as (Fox and McDonald, 1992; Perez, 2005; Lewis, 1988; Khaled and Chalhoub, 2009)

$$V_{surge\_rud} = \sqrt{\left(\frac{2F_{th\_deliv}}{\rho_{water} A_{propeller\_disk}} + V_{pr}^2 \right)} \tag{2.33}$$

Next, V_{sway_rud} is considered to be the fluid velocity component induced by the sway motion of the ship (Fig. 2-9). It is equated to $-v$. As a consequence, the overall direction and magnitude of the flow approaching the rudder are given by

$$\alpha_e = \text{atan2}\left((-v) / V_{surge\_rud} \right) \tag{2.34a}$$

$$V_{rud} = \sqrt{V_{surge\_rud}^2 + v^2} \tag{2.34b}$$

The difference between the rudder angle, α, and the overall fluid flow direction, α_e, is given by $(\alpha - \alpha_e)$ (Fig. 2-9). It is used in determining both C_L and C_D for Eqs. (2_31a) and (2_31b) from the data provided by Abbott and von Doenhoff (1958) and Journée and Pinkster (2002).

Both the lift and drag forces result in the following rudder vector force expressed with respect to the body-fixed frame as

$$\underset{\sim}{F}_{rud} = \left(-F_{drag} \cos\alpha_e - F_{lift} \sin\alpha_e \right) \underset{\sim}{i}_o + \left(-F_{drag} \sin\alpha_e + F_{lift} \cos\alpha_e \right) \underset{\sim}{j}_o \tag{2.35}$$

By applying the angular momentum balance around the axis of rotation of the rudder, one can obtain the following rudder equation of motion:

$$I_{rud} \ddot{\alpha} = T_{rud} + \left[\underset{\sim}{r}_{o_r C_P} \times \underset{\sim}{F}_{rud} \right] \cdot \underset{\sim}{k} \tag{2.36}$$

where T_{rud} is the control torque specified by the ship controller. The above equation is implemented to determine the unconstrained angular rotation of the rudder, which corresponds to $-22.5^o \le \alpha \le 22.5^o$. When α exceeds its bounding values, the rudder motion becomes constrained. T_{rud} is now calculated from an algebraic equation obtained by setting $\ddot{\alpha}$ in the above equation to zero.

Additional constraints have also been imposed herein on the slew rate of the rudder by limiting the range of $\dot{\alpha}$ to $\left[-19.5\text{deg/sec}, 19.5\text{deg/sec}\right]$.

2.2 Model Validation

Digital simulations have been carried out to examine the capability of the nonlinear dynamic model in predicting the ship behavior during circle-turning maneuvers. The results were generated based on a barge of 100 m in length, 20 m in beam and 4.8 m in draft sailing in a following sea. The wind speed was considered to be 30 m/sec and the current speed was defined to be 1 m/sec. Moreover, the Modified Pierson-Moskowitz wave spectrum, discussed in the previous Section, was used in the simulation.

In assessing the performance of the ship model, a two-segment maneuver was used. The first segment consists of a straight line while the second segment is a turning-circle maneuver with the wave encounter angle varying based on the instantaneous heading of the ship. The propeller thrust, F_{th}, was kept constant at its maximum value of 5×10^7 N, while the rudder angle of attack, α, was assigned 0^o and 25^o values in the first and second segments of the maneuver, respectively. The simulation results are illustrated in Fig. 2-11. The tactical diameter, D_T (see Fig. 2-11), is found to be 340.6 m. This leads to a non-dimensional tactical diameter of 2.43

($D_T^{'} = \left[D_T \left| \alpha_{rud} \right| / 35 L_{pp} \right]$), which agrees with experimental data provided by Lewis (1988) and Barr et al. (1981) for ships of comparable geometric dimensions and weight. Furthermore, ships undergoing turning-circle maneuvers are expected to exhibit lateral drifts (Lewis, 1988). This fact is confirmed in Fig. (2-11), which reveals a lateral drift, L_D, of 4.5 m.

The simulation results serve to partially validate the performance of the ship model discussed in the present Chapter.

2.3 Summary

A nonlinear six degree-of-freedom dynamic model for a marine surface vessel has been presented in the current Chapter. The formulation closely follows the existing literature on ship modeling. It accounts for the effects of inertial forces, wave excitation forces, retardation forces, nonlinear restoring forces, linear viscous damping terms, wind and current loads. Furthermore, a seventh degree-of-freedom has been added in the model to capture the dynamics of the rudder. In addition, the physical limitations of the propulsion system and the rudder dynamics are accounted for in the model formulation of the ship.

The model has been partially validated by examining its performance in predicting the ship dynamic response during circle-turning maneuvers. The ship model will serve as a test bed to assess the performances of the guidance system, controllers and observers that will be covered in the next Chapters.

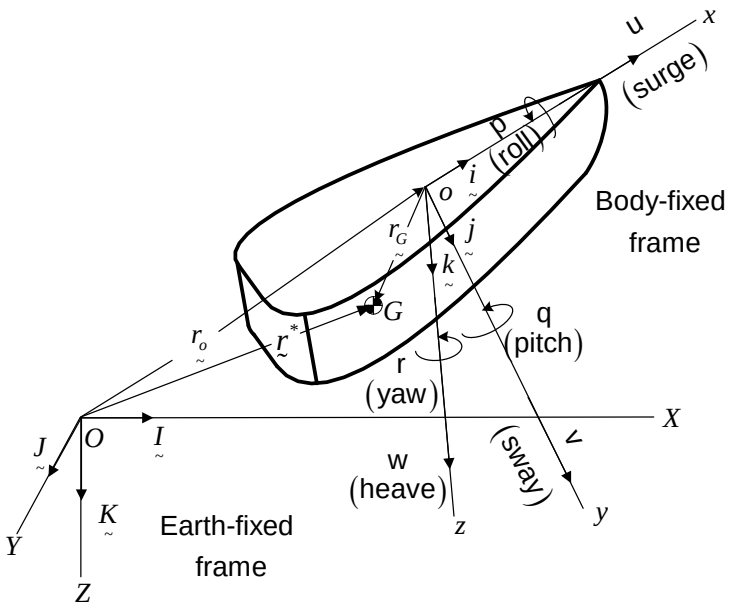

Fig. 2-1. Schematic of the ship hull.

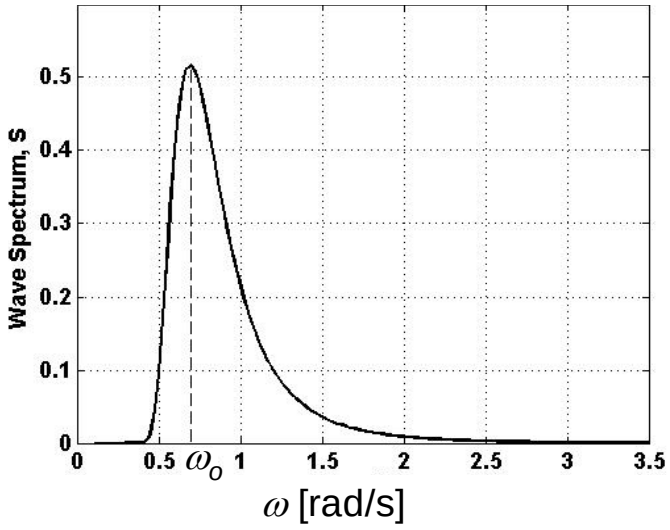

Fig. 2-2. Modified Pierson-Moskowitz wave spectrum.

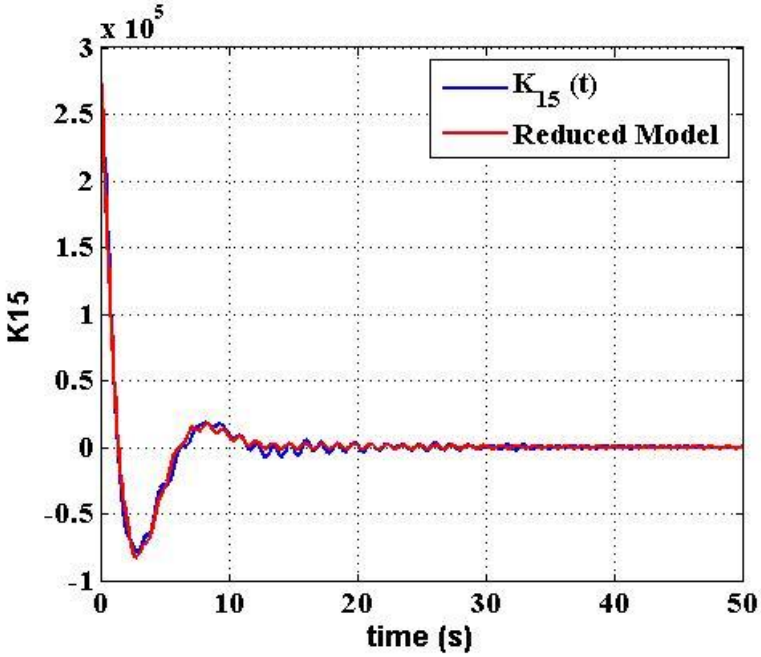

Fig. 2-3. Curves illustrating the accuracy of the state space formulation.

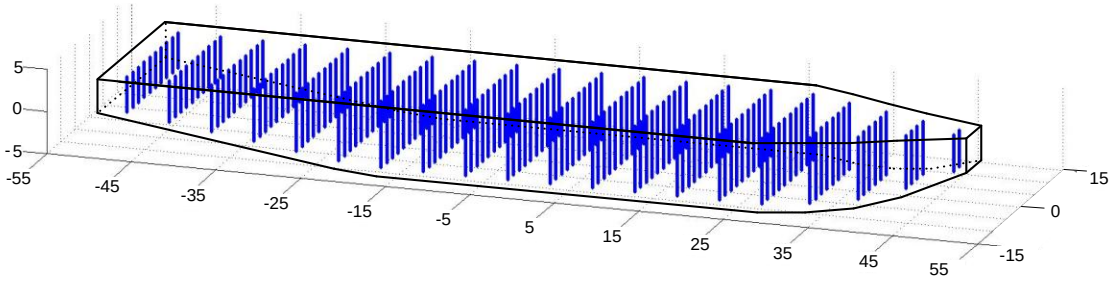

Fig. 2-4. Centroids of the blocks in the 3-D mesh of the ship.

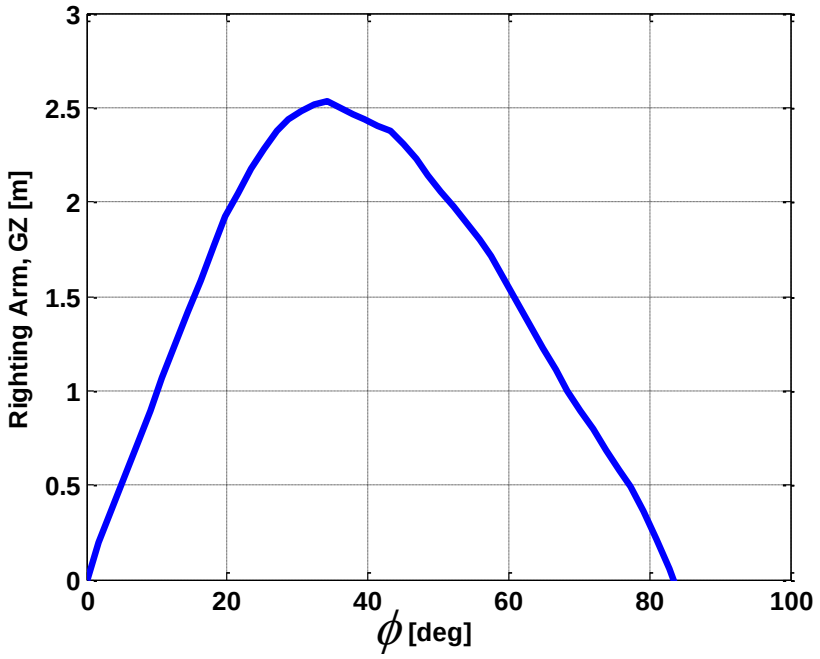

Fig. 2-5. Righting arm curve of the ship.

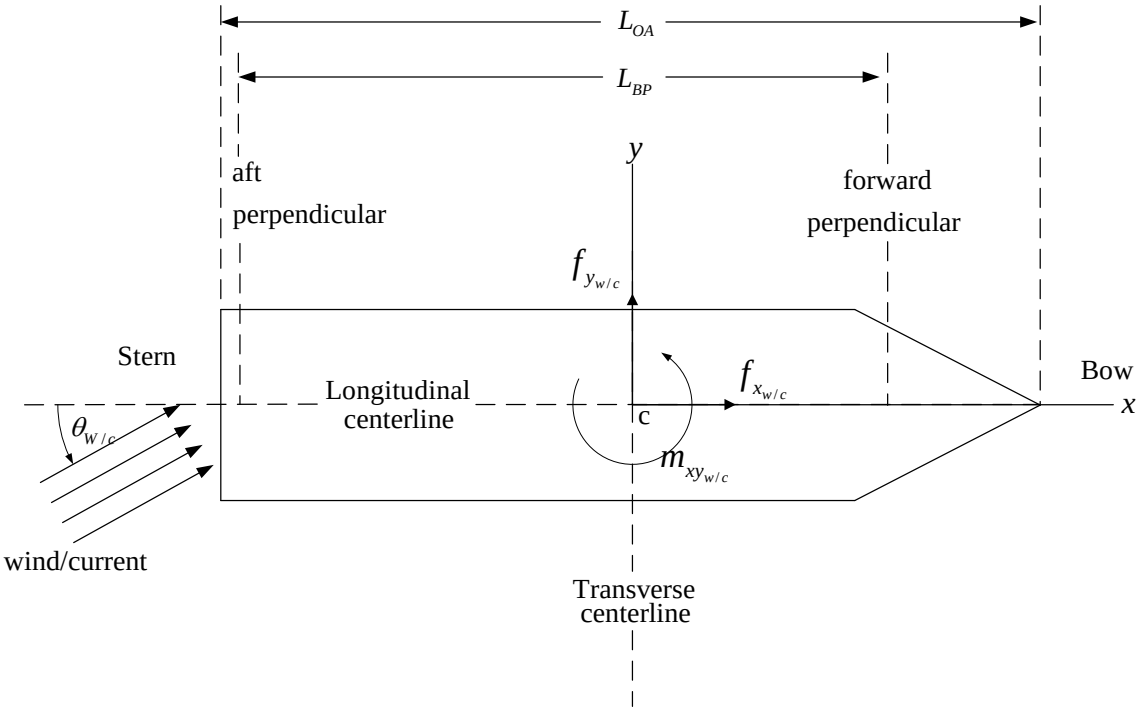

Fig. 2-6 Schematic of a ship illustrating the wind and current angle of attack along with the positive directions of the wind and current induced loads.

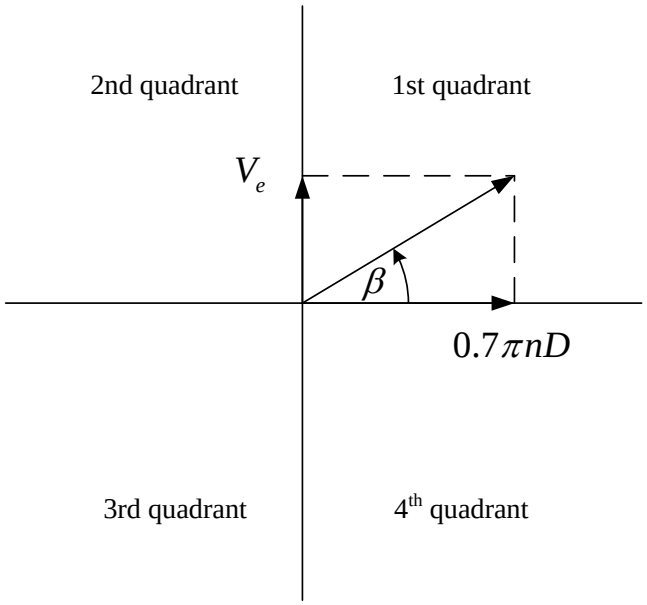

(Adopted from Journée and Massie, 2001)

Fig. 2-7 Four quadrants of the hydrodynamic pitch angle, β .

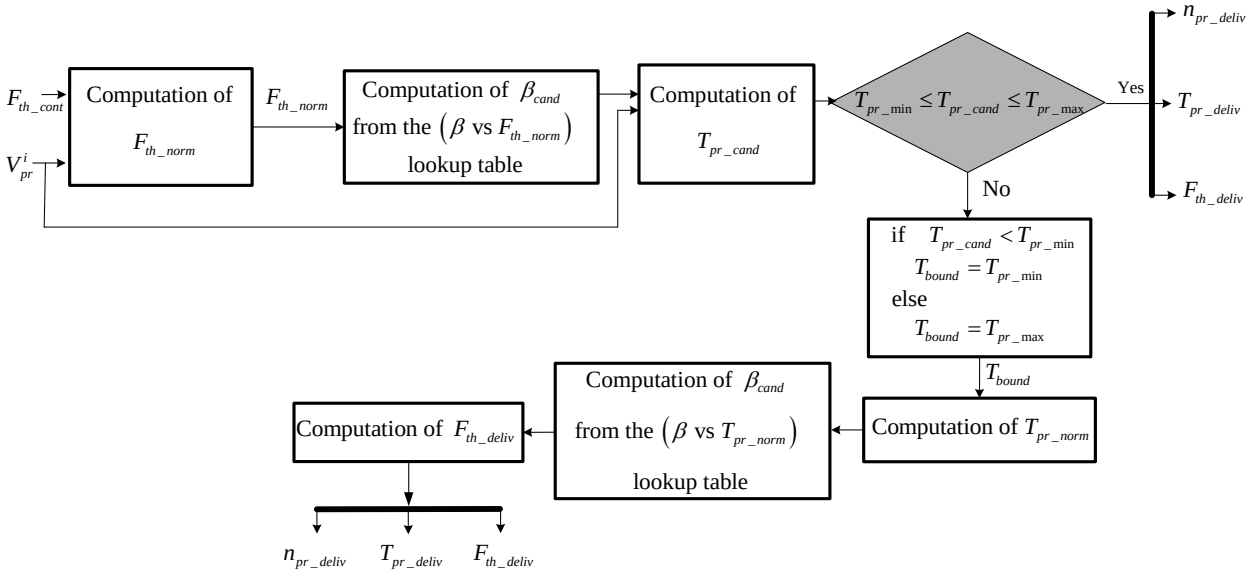

Fig. 2-8 Flowchart reflecting the physical limitations of the ship propulsion system.

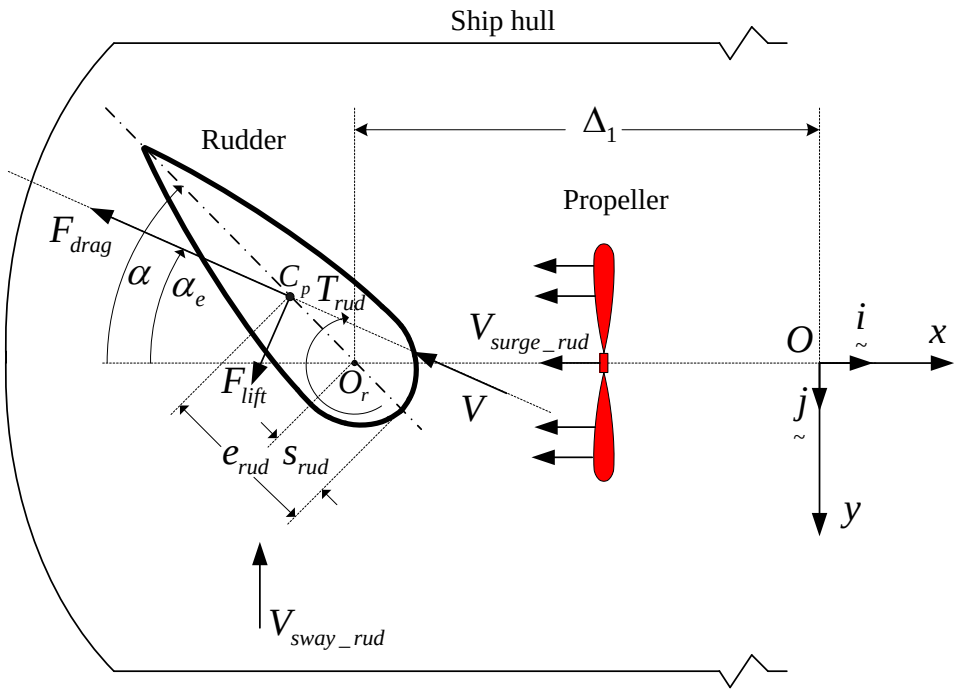

Fig. 2-9 Schematic of the rudder and propeller configuration along with the lift and drag forces induced by the fluid flow.

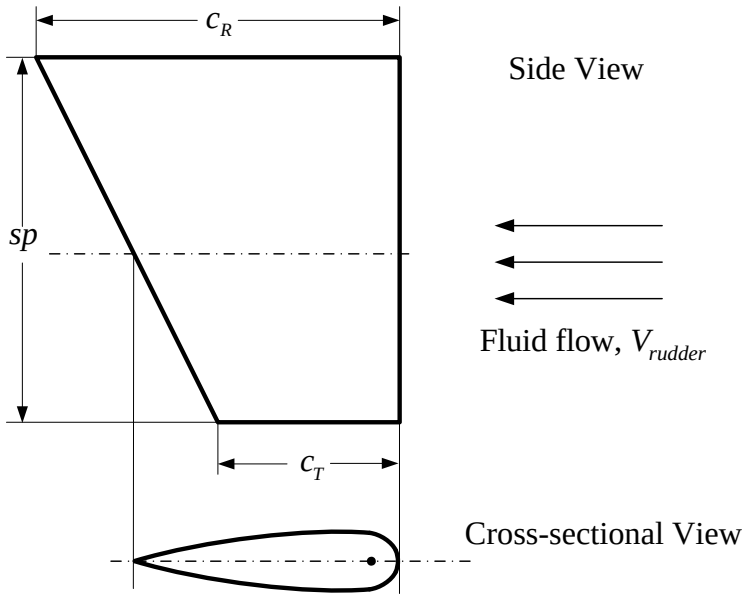

Fig. 2-10 Geometry of the rudder

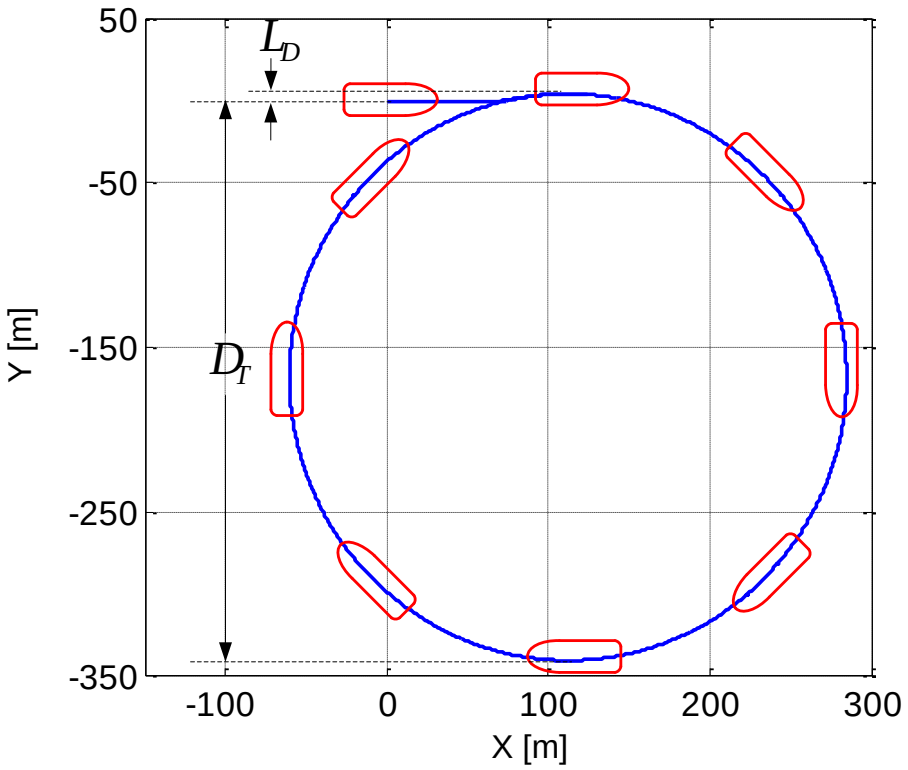

Fig. 2-11 Turning-circle maneuver of the ship.

CHAPTER 3 “DESIGN OF A SLIDING MODE CONTROLLER FOR A MARINE VESSEL”

Ships are required to operate under extreme environmental conditions that are capable of producing considerable external disturbances. This problem is compounded by the modeling imprecision of marine vessels. Therefore, good tracking characteristic of ships can only be achieved if their controllers are robust to both structured and unstructured uncertainties along with external disturbances.

The focus of the present Chapter is to design a sliding mode controller for the purpose of controlling the surge speed and the heading angle of a marine surface vessel. Such controllers are based on the variable structure theory (VSS) (Utkin, 1981). They have been proven to yield robust performances when applied on nonlinear systems whose dynamics are not fully known as long as the upper bounds on the uncertainties are bounded and known.

The controller design is presented in the next Section. Subsequently, the simulation results are shown. They demonstrate the robust performance of the controller in yielding the desired surge speed and heading angle of the ship.

3.1 Design of the Sliding Mode Controller of the ship

A sliding mode controller is designed in this Section to control both the surge speed and the heading angle of a marine vessel. All state variables of the ship are assumed to be available through measurement and the actuators are considered to be the propeller and the rudder. The controller is designed based on a reduced-order model of the ship, which consists of two nonlinear second order ordinary differential equations of motion reflecting the surge and yaw motions of the ship. These equations were derived

in Chapter 2 and given in Eqs. (2.12) & (2.14). All terms, pertaining to the sway, heave, pitch and roll motions of the vessel, have been ignored in the reduced-order model of the ship that was used in the design of the controller. The resulting surge equation of motion can be written in the following compact form:

$$\dot{u} = f_1 + b_1 F_{th} \tag{3.1.1}$$

where $b_1 = m_{ship}^{-1}$. It is considered to satisfy the following inequality:

$$0 < b_{1_{\min}} \le b_1 \le b_{1_{\max}} \tag{3.1.2}$$

The simplified yaw equation had to be modified in order to account for the rudder dynamics. The rationale is to generate a direct relation between $\dot{r}$ and T_{rud}. This is done by first writing the yaw equation with respect to the body-fixed coordinate system as follows

$$\dot{r} = \bar{f}_2 - \frac{\Delta_1}{I_z} F_{rud_y} + \frac{T_{rud}}{I_z} \tag{3.1.3}$$

where $F_{rud_y} = -F_{drag}\sin(\alpha_e) + F_{lift}\cos(\alpha_e)$. The rudder dynamics are governed by the following equation:

$$I_{rud}\ddot{\alpha} = (s_{rud} - e_{rud})\left[\cos(\alpha)F_{rud_y} - \sin(\alpha)F_{rud_x}\right] - T_{rud} \tag{3.1.4}$$

where $F_{rud_x} = -F_{drag}\cos(\alpha_e) - F_{lift}\sin(\alpha_e)$. Moreover, s_{rud}, e_{rud} and Δ_1 are geometric parameters defined in Fig. 3-1. Using Eq. (3.1.4) into Eq. (3.1.3) yields a direct relation between the yaw angular acceleration to the rudder control torque:

$$\dot{r} = \bar{f}_2 - \frac{\Delta_1}{I_z}\left[\frac{J_{rud}\ddot{\alpha}}{(s_{rud} - e_{rud})\cos(\alpha)} + \tan(\alpha)F_{rud_x}\right] + T_{rud}\left[\frac{1}{I_z} - \frac{\Delta_1}{I_z(s_{rud} - e_{rud})\cos(\alpha)}\right] \tag{3.1.5}$$

For simplicity in the derivation of the controller, the above equation is written as

$$\dot{r} = f_2 + b_2 T_{rud} \tag{3.1.6}$$

where f_2 and b_2 are defined as

$$f_2 = \bar{f}_2 - \frac{\Delta_1}{I_z}\left[\frac{I_{rud}\ddot{\alpha}}{(s_{rud} - e_{rud})\cos(\alpha)} + \tan(\alpha) F_{rud_x}\right] \tag{3.1.7a}$$

$$b_2 = \left[\frac{1}{I_z} - \frac{\Delta_1}{I_z (s_{rud} - e_{rud})\cos(\alpha)}\right] \tag{3.1.7b}$$

where b_2 is considered to satisfy the following inequality:

$$0 < b_{2_{\min}} \le b_2 \le b_{2_{\max}} \tag{3.1.8}$$

In designing the controller, the dynamics of the plant are not considered to be fully known. Thus, the following nominal equations of motion are used:

$$\dot{u} = \hat{f}_1 + \hat{b}_1 F_{th} \tag{3.1.9a}$$

$$\dot{r} = \hat{f}_2 + \hat{b}_3 T_{rud} \tag{3.1.9b}$$

Since both roll and pitch angular displacements are ignored in the reduced-order model of the ship then $\int_0^t r\, d\tau$ and r become equal to ψ and $\dot{\psi}$, which are the ship yaw angle and its time derivative with respect to the inertial frame. On the other hand, the $\int_0^t u\, d\tau$ term has no physical meaning and its value is not available for the computation of the control signal. This issue has been addressed in the current work by considering three state equations to represent the surge and yaw motions of the ship as well as for choosing different sliding surfaces in the control of the surge and heading motions of the

ship. As a consequence, the state equations of the reduced-order model, given by Eqs. (3.1.1) and (3.1.6), can now be expressed in the following vector form:

$$\dot{\underset{\sim}{x}}_r = \underset{\sim}{f}_r(\underset{\sim}{x}_r) + b_r(\underset{\sim}{x}_r)\underset{\sim}{u}_c \tag{3.1.10}$$

where the state vector, $\underset{\sim}{x}_r$, and the control vector, $\underset{\sim}{u}_c$, are defined as $\left[\int_0^t r\,d\tau, u, r\right]^T$ and $[\,F_{th}, T_{rud}\,]^T$, respectively. However, the nominal vector state equation, which will be used in the design of the controller, are based on Eqs. (3.1.9a) and (3.1.9b). They are written as

$$\dot{\underset{\sim}{x}}_r = \hat{\underset{\sim}{f}}_r(\underset{\sim}{x}_r) + \hat{b}_r(\underset{\sim}{x}_r)\underset{\sim}{u}_c \tag{3.1.11}$$

The upper bounds on the modeling imprecision of the entries of $\hat{\underset{\sim}{f}}_r(\underset{\sim}{x}_r)$ are assumed to be known and given by

$$F_i = \left| f_{r_i}(\underset{\sim}{x}_r) - \hat{f}_{r_i}(\underset{\sim}{x}_r) \right| \qquad i = 2 \ \textit{and} \ 3 \tag{3.1.12}$$

The sliding surface, implemented in the surge speed control, is selected to be:

$$\begin{aligned} s_s(e_s, \dot{e}_s) &= \left(\frac{d}{dt} + \lambda_s\right)^2 \int_0^t e_s\,d\tau \\ &= \dot{e}_s + 2\lambda_s e_s + \lambda_s^2 \int_0^t e_s\,d\tau \qquad \textit{with} \quad e_s \triangleq \int_0^t (u - u_d)\,d\tau \end{aligned} \tag{3.1.13}$$

where u and u_d are the actual and desired surge speeds, respectively. A comment is in order regarding s_s and e_s. The above definition of s_s involves a double integration of the surge speed error, which is basically a single integration of the surge position error of the ship. The problem had to be formulated in this form, as it will be explained in the

next Chapter, because the $\int u d\tau$ term cannot be estimated by an observer given the available type of ship position and orientation measurements. Since such a term is not available for the computation of the control signal then s_s is defined as in Eq. (3.1.13) to prevent the use of $\int u d\tau$ term in the control algorithm.

The sliding surface for the heading angle is chosen to be:

$$s_h(e_h, \dot{e}_h) = \dot{e}_h + \lambda_h e_h \quad with \quad e_h \triangleq \int_0^t r\, d\tau - \left(\int_0^t r\, d\tau \right)_d \simeq \psi - \psi_d \tag{3.1.14}$$

where ψ and ψ_d are the actual and desired yaw angles, respectively. To handle the upper and lower bounds imposed on the b_i terms, in Eqs. (3.1.2) and (3.1.8), the following terms are defined (Slotine and Li, 1991):

$$\hat{b}_i = \sqrt{b_{i_{\min}} b_{i_{\max}}} \qquad and \qquad \beta_i = \sqrt{\frac{b_{i_{\max}}}{b_{i_{\min}}}} \qquad i = 2 \; and \; 3 \tag{3.1.15}$$

Based on the sliding mode methodology, the entries of $\underset{\sim}{u}_c$ can be written as

$$\begin{aligned} u_{c_i} &= u_{i_{eq}} - \frac{k_i}{\hat{b}_{i+1}} \operatorname{sgn}(s_k) \\ &= u_{i_{eq}} - \frac{k_i}{\hat{b}_{i+1}} sat\left(\frac{s_k}{\Phi_k} \right) \qquad i = 1 \; and \; 2 \end{aligned} \tag{3.1.16}$$

where the index k can be either "s" or "h". Note that both $\operatorname{sgn}(s_s)$ and $\operatorname{sgn}(s_h)$ are substituted by $sat(s_s/\Phi_s)$ and $sat(s_h/\Phi_h)$ terms, which are basically saturation functions. The rationale is to alleviate the chattering problem associated with the switching terms, $\operatorname{sgn}(s_s)$ and $\operatorname{sgn}(s_h)$. Φ_s and Φ_h are the thicknesses of boundary layers surrounding the s_s and s_s sliding surfaces, respectively.

The equivalent control signals are obtained by setting $\dot{s}_i = 0$ for $i = 1 \, and \, 2$ as follows

$$u_{1_{eq}} = \frac{1}{\hat{b}_2}\left\{\dot{u}_d - 2\lambda_1 \dot{e}_s - \lambda_1^2 e_s - \hat{f}_2\right\} \tag{3.1.17a}$$

$$u_{2_{eq}} = \frac{1}{\hat{b}_3}\left\{\ddot{\psi}_d - \lambda_2 \dot{e}_h - \hat{f}_3\right\} \tag{3.1.17b}$$

The k_1 gain is determined by satisfying the following sliding condition:

$$\frac{1}{2}\frac{d}{dt}\left(s_s^2\left(e_s, \dot{e}_s\right)\right) \le -\bar{\eta}_s \left|s_s\left(e_s, \dot{e}_s\right)\right| \tag{3.1.18}$$

This will lead to

$$k_1 \ge \beta_1\left(\bar{\eta}_s + F_2\right) + \left|\beta_1 - 1\right|\left|\lambda_1 \dot{e}_s - \dot{u}_d + \hat{f}_2\right| \tag{3.1.19}$$

Similarly, k_2 is selected to satisfy the following sliding condition:

$$\frac{1}{2}\frac{d}{dt}\left(s_h^2\left(e_h, \dot{e}_h\right)\right) \le -\bar{\eta}_h \left|s_h\left(e_h, \dot{e}_h\right)\right| \tag{3.1.20}$$

This will lead to

$$k_2 \ge \beta_2\left(\bar{\eta}_h + F_3\right) + \left|\beta_2 - 1\right|\left|\lambda_2 \dot{e}_h - \ddot{\psi}_d + \hat{f}_3\right| \tag{3.1.21}$$

To prevent the controller from over reacting when the system is in the vicinity of the sliding surfaces, both k_1 and k_2 have been varied without violating the sliding conditions in Eqs. (3.1.18) and (3.1.20). This is done by linearly varying the control parameters $\bar{\eta}_s$ and $\bar{\eta}_h$ with $\bar{d}_s$ and $\bar{d}_h$, respectively, which represent distances from the current location of the system to the sliding surfaces. They are computed from

$$\bar{\eta}_s = Sat\left(\bar{d}_s\right) = Sat\left(\frac{\left|s_s\right|}{\sqrt{1+\lambda_1^2}}\right) \tag{3.1.22a}$$

$$\bar{\eta}_h = Sat\left(\bar{d}_h\right) = Sat\left(\frac{|s_h|}{\sqrt{1+\lambda_2^2}}\right) \tag{3.1.22b}$$

where the "Sat" is a saturation function. The variations of $\bar{\eta}_s$ and $\bar{\eta}_h$ based on $\bar{d}_s$ and $\bar{d}_h$ is illustrated graphically in Figs. 3-2 and 3-3.

3.2 Assessment of the Sliding Mode Controller

The sliding mode controller has been designed based on a reduced-order model of the ship, which only accounts for the surge and yaw motions. To test its performance under considerable unstructured uncertainties, the controller is applied on the full order model of the ship that was presented in Chapter 2, which considers the surge, sway, heave, roll, pitch, and yaw motions of the ship. Furthermore, structured uncertainties were introduced by intentionally using nominal equations in the reduced-order model that are significantly different from the exact ones. The nominal values are given in Table 3-1. Note that the nominal values for $\hat{f}_{r_2}(x)$ and $\hat{f}_{r_3}(x)$ have been set to zero in order to demonstrate that these terms can actually be ignored in the design of the controller as long as the upper bounds F_2 and F_3 are known. The ship geometric dimensions, control parameters, and environmental conditions, used in performing the simulations, are also listed in Table 3-1. The simulation results were generated by assuming zero initial conditions for the state variables of the ship except for the initial surge speed which was set to $u(0) = 5.5\ m/\sec$.

The desired surge speed and heading angle are assigned as follows

$$u_d = \begin{cases} 6 \quad m/\sec & 0 \le t \le 50 \sec \\ \dfrac{-(t-50)}{110} + 6 \quad m/\sec & 50 \le t \le 160 \sec \\ 5 \quad m/\sec & t \ge 160 \sec \end{cases} \tag{3.2a}$$

$$\psi_d = \begin{cases} 0 \quad rad & 0 \le t \le 180 \sec \\ \dfrac{0.8(t-180)}{120} \quad rad & 180 \le t \le 300 \sec \\ 0.8 \quad rad & t \ge 300 \sec \end{cases} \tag{3.2b}$$

Figure 3-4 shows the wave height at the mass center of the ship. Figures 3-5 to 3-8 demonstrate the robustness of the sliding mode controller in yielding good tracking characteristic for both the surge speed and the heading angle in spite of the presence of significant modeling imprecision and external disturbances. Baring the initial errors due to the initial position and orientation of the ship, Figs. 3-7 and 3-8 reveal tracking errors in the order of 10^{-4} and 10^{-3} for the surge speed and the heading angle, respectively. The heave displacement along with the roll and pitch angular displacements of the ship are given in Figs. 3-9 to 3-11. Note that during the first 180 seconds of the simulation, the waves had 90^o incident angle with respect to the ship; thus, resulting in larger excitations in the roll angle than in the pitch angle. However, this trend has gradually been reversed after 180 sec with the beginning of the turning maneuver of the ship, which is reflected by the increase in the actual heading angle of the ship. This is shown in Figs. 3-10 and 3-11.

3.3 Summary

A sliding mode controller has been presented in this Chapter to control both the surge speed and the heading angle of a marine surface vessel. The simulation results demonstrate the robustness of the controller in yielding good tracking characteristic of

the controlled system in spite of the presence of significant environmental disturbances and modeling imprecision.

In the next Chapter, a nonlinear robust observer, based on the sliding mode methodology, will be designed and coupled with the controller of the current Chapter.

Ship Data	
Length of the ship L_{PP}	100 m
Mass of the ship m_{ship}	7264000 Kg
Beam B	25 m
Draught T	8 m
Rudder Area A_{rud}	6 m^2
Maximum rudder angle $\alpha_{\max}$	22.5^0
Maximum rudder slew rate $\dot{\alpha}_{\max}$	19.5^0/sec
Environmental Conditions	
$H_{1/3}$ of the wave	8 m
Period of the wave spectrum T_0	9.01 sec
Incident angles of the wave, wind and current	90^0
Wind speed	20 m/s
Current speed	2 m/s
Surge Controller Parameters	
$\hat{f}_{r_2}$	0 m/sec^2
F_2	8 m/sec^2
$b_{2_{\min}} = b_{2_{\max}}$	m_{ship}^{-1} Kg^{-1}
λ_s	10
Φ_s	0.05
Heading Angle Controller Parameters	
$\hat{f}_{r_3}$	0 rad/sec^2
F_3	0.3 rad/sec^2
$b_{3_{\min}}$	$0.8\left[\frac{1}{I_z} - \frac{\Delta_1}{I_z\left(s_{rud} - e_{rud}\right)}\right]$
$b_{3_{\max}}$	$1.2\left[\frac{1}{I_z} - \frac{\Delta_1}{I_z\left(s_{rud} - e_{rud}\right)\cos\left(\alpha_{\max}\right)}\right]$
λ_h	0.2
Φ_h	0.001

Table 3-1Ship data, environmental conditions and controller parameters

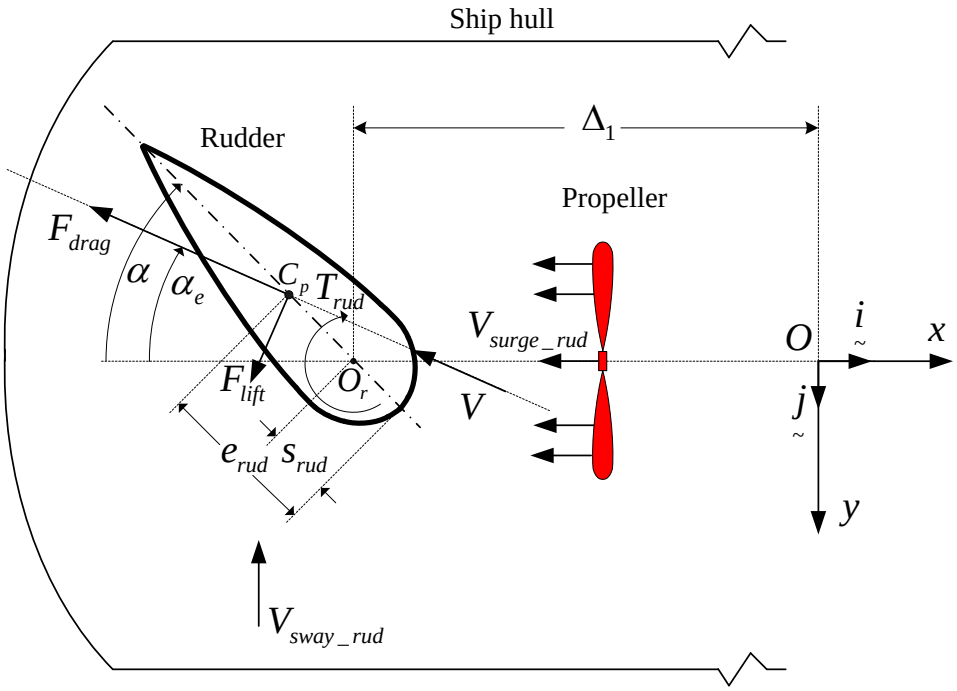

Fig. 3-1 Schematic of the rudder

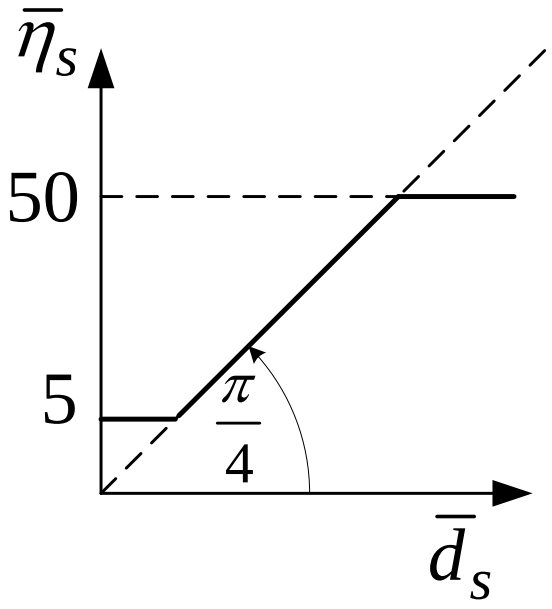

Fig. 3-2 Variation profile proposed for $\bar{\eta}_s$

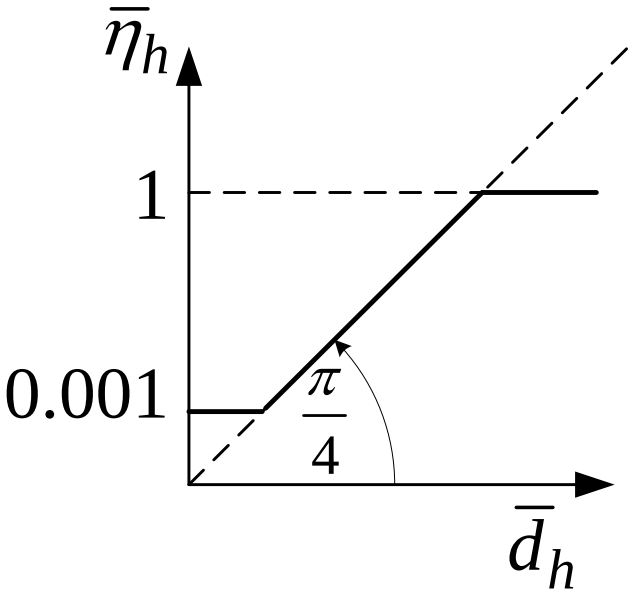

Fig. 3-3 Variation profile proposed for $\bar{\eta}_h$

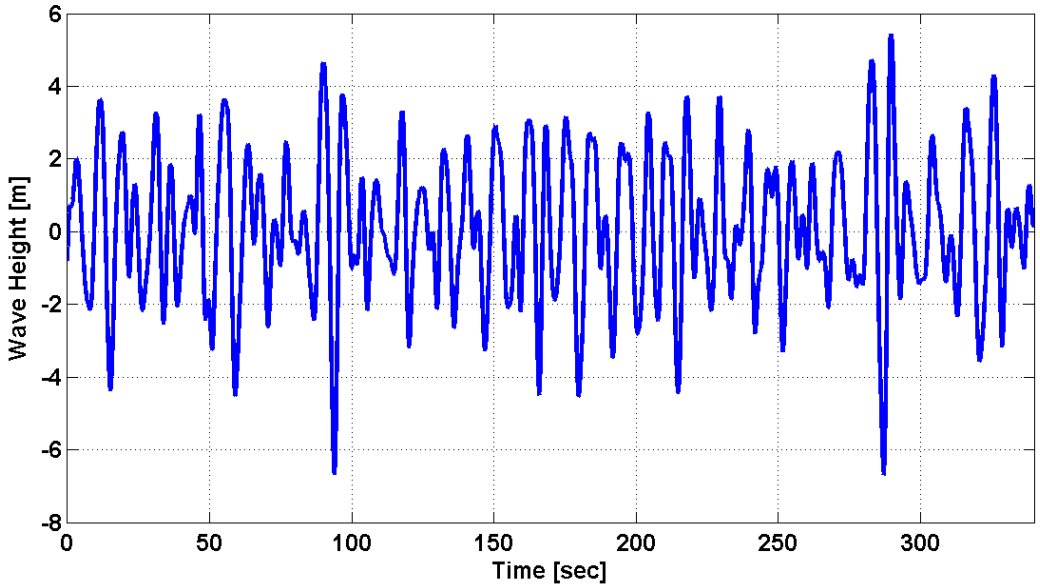

Fig. 3-4 Wave Height at the mass center of the ship

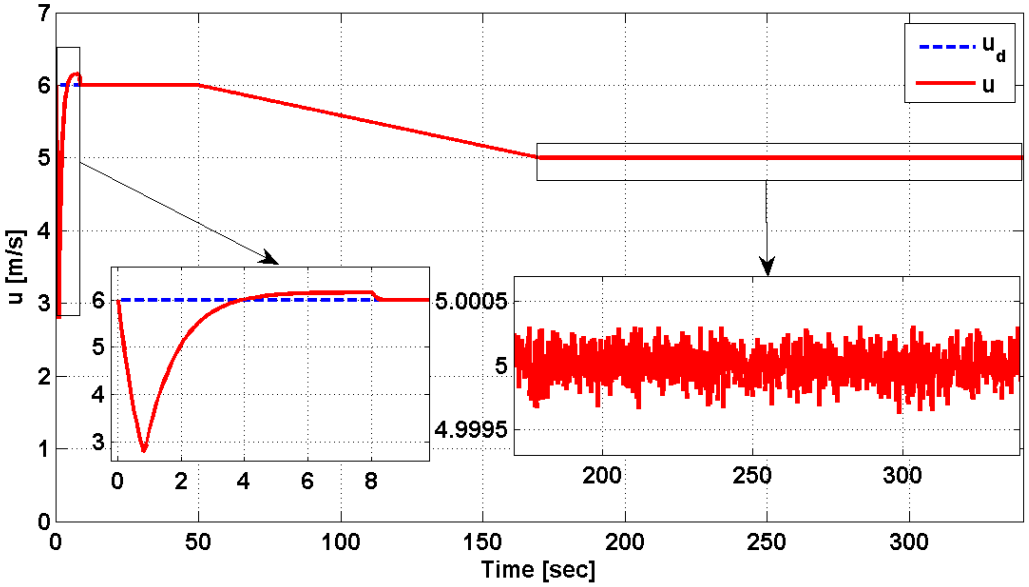

Fig. 3-5 Actual and desired surge speed of the ship

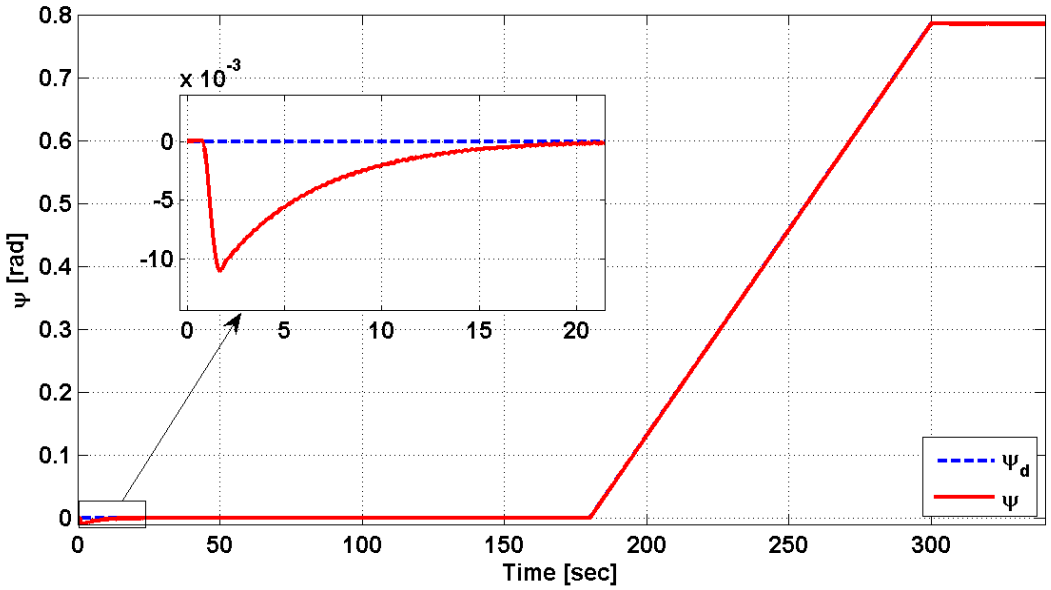

Fig. 3-6 Actual and desired heading angle of the ship

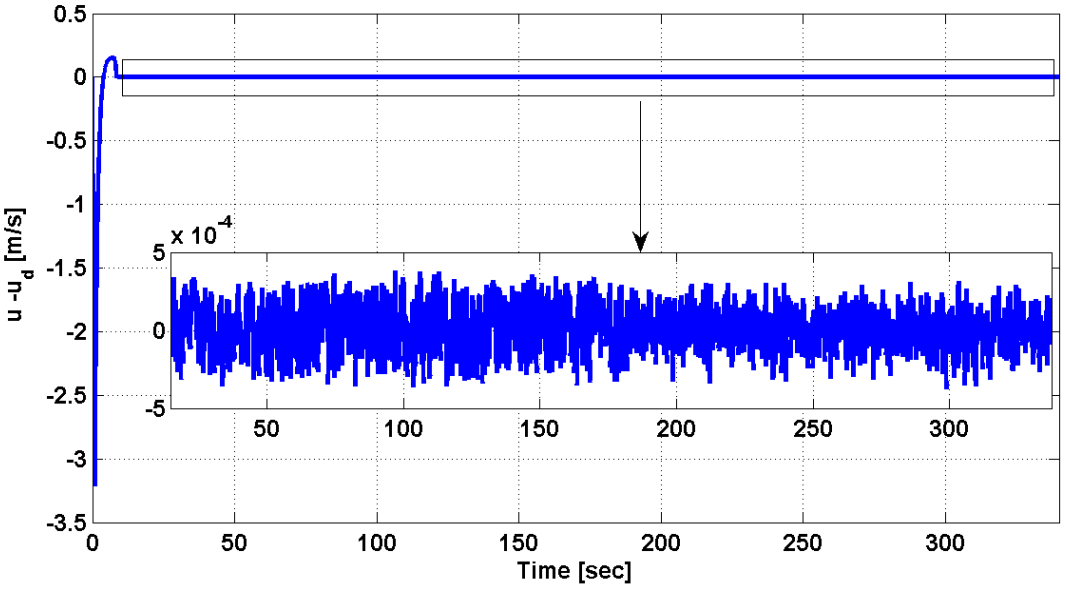

Fig. 3-7 Error between the actual and desired surge speed of the ship

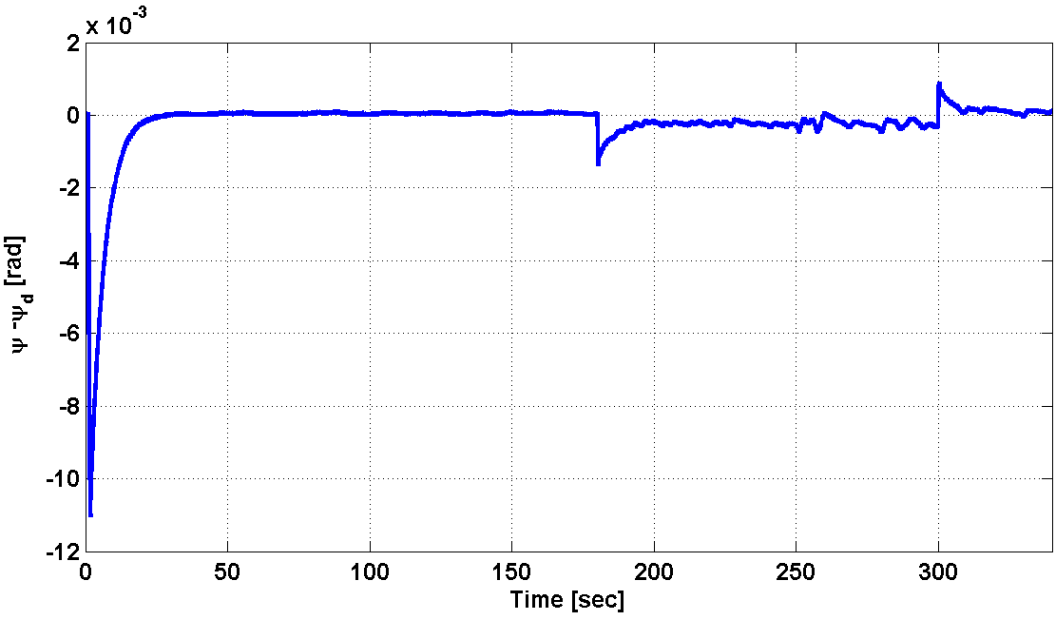

Fig. 3-8 Error between the actual and desired heading angle of the ship

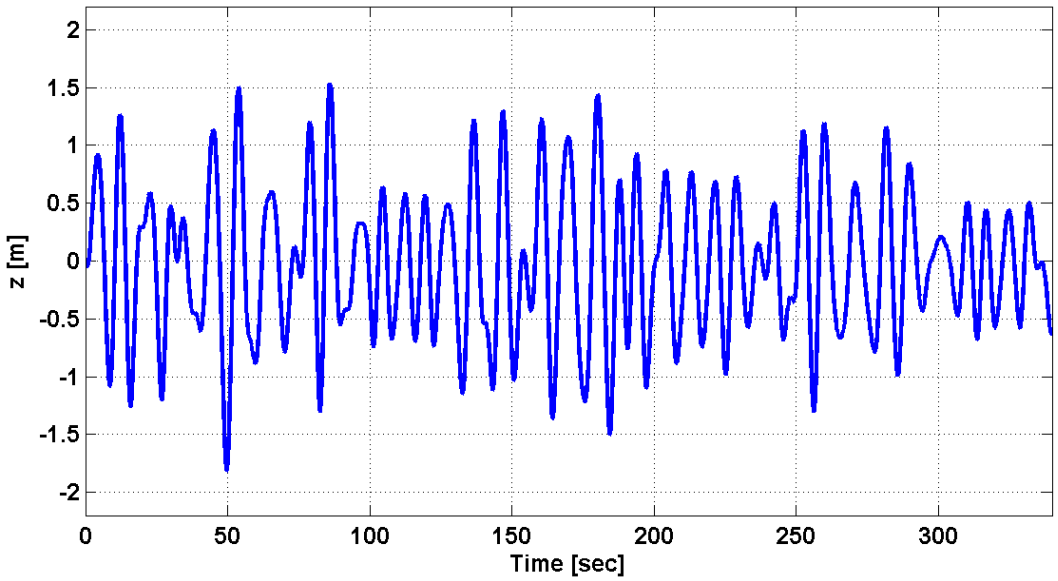

Fig. 3-9 Heave motion at the mass center of the ship

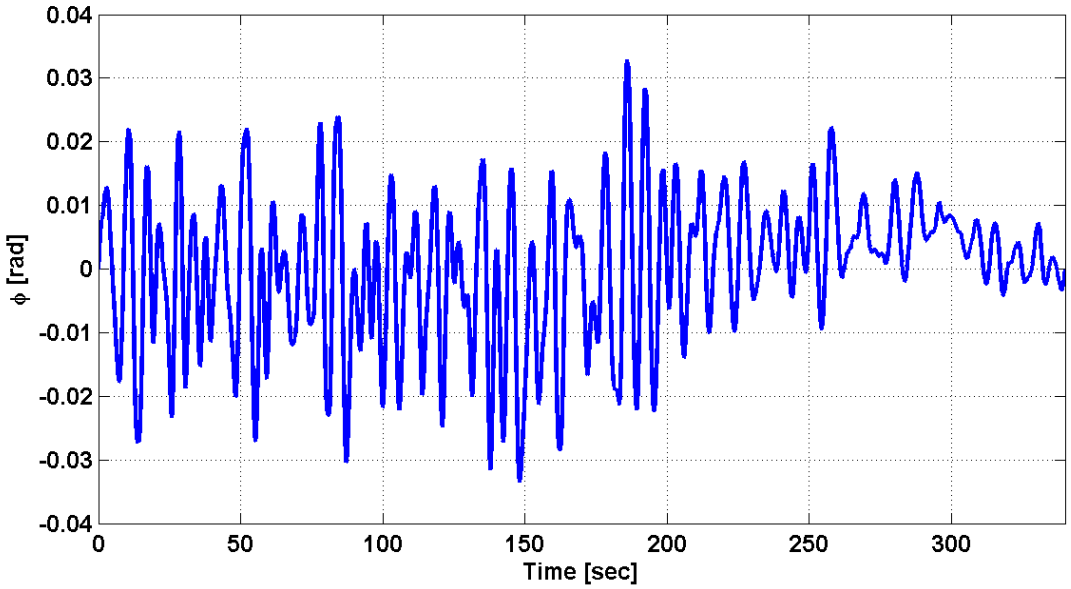

Fig. 3-10 Roll angular displacement of the ship

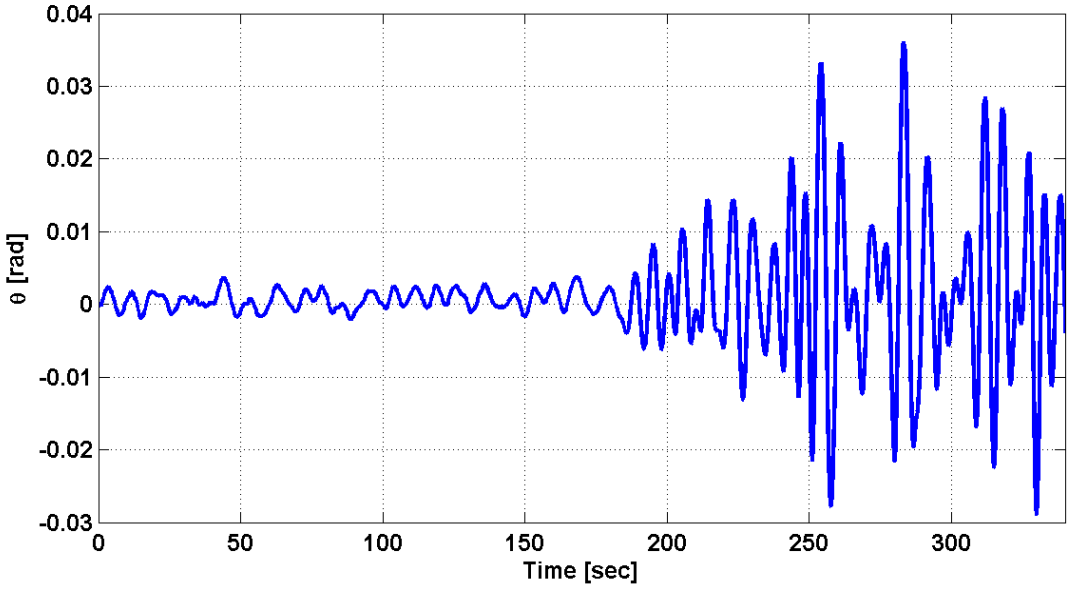

Fig. 3-11 Pitch angular displacement of the ship

CHAPTER 4 "DESIGN OF A NONLINEAR ROBUST SLIDING MODE OBSERVER"

In this Chapter, a nonlinear observer, based on the sliding mode methodology, is presented. The objective is to estimate the state variables that are needed for the computation of the control signals of the sliding mode controller that was covered in the previous Chapter. The estimation of the state variables is required to be accurate in spite of significant modeling imprecision and external disturbances.

The observer is applied in this Chapter to estimate the state variables of a marine vessel. By using the full-order model of the ship as a test bed, the observer performance will be assessed under considerable unstructured uncertainties in addition to external disturbances and structured uncertainties. Later on in the Chapter, both sliding mode controller and observer will be coupled and the closed-loop performance of the ship will be examined through digital simulations.

4.1 Sliding Mode Observer for a Marine Vessel

A sliding mode observer is designed to accurately estimate the state variables pertaining to the surge and yaw motions of the ship. The available measurements are considered to be the heading angle along with the X and Y coordinates of the ship with respect to the inertial reference frame. This is because both X and Y coordinates can be obtained from a global positioning system (GPS) while the yaw angle, ψ, can be measured by an on-board gyro compass system (Fossen and Strand, 1999). It should be stressed that the measured variables are defined with respect to the inertial frame $\{X,Y,Z\}$. They are different from $\int_0^t r\,d\tau, u$ and r, which are defined with respect to the body-fixed reference frame $\{x,y,z\}$ and required for the computation of the control

signals of the sliding mode controller covered in the previous Chapter (see Fig. 2-1). This issue, briefly discussed in the previous Chapter, tends to complicate the estimation process. To tackle this problem, the observer is now designed to estimate $X, Y,$ and ψ along with their time derivatives. The required state variables, with respect to the body-fixed coordinate system, are then deduced from the estimated ones by using the following transformation matrix, given in Eq. (2.8), as follows

$$\begin{pmatrix} u \\ v \\ w \end{pmatrix} = \begin{pmatrix} c\psi c\theta & -s\psi c\phi + c\psi s\theta s\phi & s\psi s\phi + c\psi s\theta c\phi \\ s\psi c\theta & c\psi c\phi + s\psi s\theta s\phi & -c\psi s\phi + s\psi s\theta c\phi \\ -s\theta & c\theta s\phi & c\theta c\phi \end{pmatrix}^{-1} \begin{pmatrix} \dot{X} \\ \dot{Y} \\ \dot{Z} \end{pmatrix} \tag{4.1.1}$$

Note that both sliding mode controller and observer are designed based on a reduced-order model, which only accounts for the surge and yaw motions of the ship. Therefore, both roll and pitch angles are set in the above equation to zero. This will lead to:

$$\left(\int r d\tau\right)_e = \psi_e \tag{4.1.2a}$$

$$r_e = \dot{\psi}_e \tag{4.1.2b}$$

$$\begin{aligned} \begin{pmatrix} u_e \\ v_e \\ w_e \end{pmatrix} &= \begin{pmatrix} c\psi c\theta & -s\psi c\phi + c\psi s\theta s\phi & s\psi s\phi + c\psi s\theta c\phi \\ s\psi c\theta & c\psi c\phi + s\psi s\theta s\phi & -c\psi s\phi + s\psi s\theta c\phi \\ -s\theta & c\theta s\phi & c\theta c\phi \end{pmatrix}^{-1}_{\substack{\theta=0 \\ \phi=0 \\ \psi=\psi_e}} \begin{pmatrix} \dot{X}_e \\ \dot{Y}_e \\ \dot{Z}_e \end{pmatrix} \\ &= \begin{pmatrix} c\psi_e & s\psi_e & 0 \\ -s\psi_e & c\psi_e & 0 \\ 0 & 0 & 1 \end{pmatrix} \begin{pmatrix} \dot{X}_e \\ \dot{Y}_e \\ \dot{Z}_e \end{pmatrix} \quad \Rightarrow \quad u_e = c\psi_e \dot{X}_e + s\psi_e \dot{Y}_e \end{aligned} \tag{4.1.2c}$$

It should be mentioned that the errors in the deduced values of $\int_0^t r\, d\tau, u$ and r are adversely affected by the roll and pitch angles of the ship. In addition, the use of u_e to

calculate the variable $\left(\int_0^t u\,d\tau\right)_e$ is bound to fail because a persistent steady-state error in u_e will cause $\int_0^t u_e\,d\tau$ to diverge from the actual value. Thus, the control algorithm, of the previous Chapter, was formulated such that it does not require the knowledge of the variable $\int_0^t u\,d\tau$. This is the rationale for using the expressions, given in Eq. (3.1.13), to define the sliding surface, s_s, and the error, e_s.

Therefore, the observer is formulated based on the following state equations representing the dynamics of the system with respect to the inertial frame:

$$\begin{Bmatrix} \dot{x}_1 = \dot{X} \\ \dot{x}_2 = \dot{Y} \\ \dot{x}_3 = \dot{\psi} \\ \dot{x}_4 = \ddot{X} \\ \dot{x}_5 = \ddot{Y} \\ \dot{x}_6 = \ddot{\psi} \end{Bmatrix} = \begin{Bmatrix} x_4 \\ x_5 \\ x_6 \\ f_4^o(\underset{\sim}{x}, u_c) \\ f_5^o(\underset{\sim}{x}, u_c) \\ f_6^o(\underset{\sim}{x}, u_c) \end{Bmatrix} \tag{4.1.3}$$

In the design of the observer, the $f_4^o(\underset{\sim}{x}, u_c)$, $f_5^o(\underset{\sim}{x}, u_c)$ and $f_6^o(\underset{\sim}{x}, u_c)$ are considered to be unknown functions. Thus, they are approximated by $\hat{f}_4^o(\underset{\sim}{\hat{x}}, u_c)$, $\hat{f}_5^o(\underset{\sim}{\hat{x}}, u_c)$ and $\hat{f}_6^o(\underset{\sim}{\hat{x}}, u_c)$, which are assigned the following simplified expressions:

$$\hat{f}_4^o(\underset{\sim}{\hat{x}}, u_c) = \frac{1}{m_{ship}}\left(F_{th} - 10^7\right)\cos\hat{x}_3 \tag{4.1.4a}$$

$$\hat{f}_5^o(\underset{\sim}{\hat{x}}, u_c) = \frac{1}{m_{ship}}\left(F_{th} - 10^7\right)\sin\hat{x}_3 \tag{4.1.4b}$$

$$\hat{f}_6^o(\hat{\underset{\sim}{x}},u_c)=\frac{-F_{rud_y}\Delta_1}{I_z} \tag{4.1.4c}$$

Note that the expressions, assigned to $\hat{f}_4^o(\hat{\underset{\sim}{x}},u_c)$, $\hat{f}_5^o(\hat{\underset{\sim}{x}},u_c)$ and $\hat{f}_6^o(\hat{\underset{\sim}{x}},u_c)$, are intentionally oversimplified in order to introduce significant structured and unstructured uncertainties in the design of the observer.

Now consider the following structure for the sliding mode observer:

$$\dot{\hat{x}}_i=\hat{x}_{i+3}-K_i^o\,\mathrm{sgn}(s_{o_i}) \qquad i=1,\cdots,3 \tag{4.1.5a}$$

$$\dot{\hat{x}}_j=\hat{f}_j^o(\hat{\underset{\sim}{x}},u_c)-K_j^o\,\mathrm{sgn}\left(s_{o_{j-3}}\right) \quad j=4,\cdots,6 \tag{4.1.5b}$$

The sliding surfaces are defined as

$$s_{o_i}\triangleq\hat{x}_i-x_i\triangleq\tilde{x}_i \qquad i=1,\cdots,3 \tag{4.1.6}$$

Define the estimation error vector, $\tilde{\underset{\sim}{x}}$, to be:

$$\tilde{\underset{\sim}{x}}\triangleq\hat{\underset{\sim}{x}}-\underset{\sim}{x} \tag{4.1.7}$$

This will yield the following error equations:

$$\dot{\tilde{x}}_i=\tilde{x}_{i+3}-K_i^o\,\mathrm{sgn}(s_{o_i}) \qquad i=1,\cdots,3 \tag{4.1.8a}$$

$$\dot{\tilde{x}}_j=\Delta f_j^o-K_j^o\,\mathrm{sgn}\left(s_{o_{j-3}}\right) \quad j=4,\cdots,6 \tag{4.1.8b}$$

where Δf_j^o, given by $\hat{f}_j^o(\hat{\underset{\sim}{x}},u_c)-f_j^o(\underset{\sim}{x},u_c)$, are not known. However, their upper bounds, $F_j^o\geq\left|f_j^o(\hat{\underset{\sim}{x}},u_c)-f_j^o(\underset{\sim}{x},u_c)\right|$ for $j=4,\cdots,6$, are considered to be known. The gains K_i^o's are computed by satisfying the following sliding conditions:

$$\frac{1}{2}\frac{d}{dt}\left(s_{o_i}^2\right)\leq-\eta_{o_i}\left|s_{o_i}\right| \tag{4.1.9}$$

This results in the following expressions:

$$K_i^o \geq \eta_{o_i} + \left|\tilde{x}_{i+3}\right|_{upper\ bound} \qquad i = 1,\cdots,3 \tag{4.1.10}$$

On the sliding surfaces, one has

$$\dot{s}_{o_i} = \dot{\tilde{x}}_i = 0 \quad \Rightarrow \quad \tilde{x}_{i+3} = K_i^o \,\mathrm{sgn}(s_{o_i}) \qquad i = 1,\cdots,3 \tag{4.1.11}$$

Introduce the following Lyapunov functions:

$$V_j = \frac{1}{2}\tilde{x}_j^2 \qquad j = 4,\cdots 6, \tag{4.1.12}$$

The estimation error, $\tilde{x}_j$ for $j = 4,\cdots,6$, can be constantly decreased by selecting the K_j^o gains such that $\dot{V}_j < 0$ for $j = 4,\cdots,6$. This will yield to the following expressions for the gains:

$$K_j^o \geq \frac{F_j^o K_{j-3}^o}{\left|\tilde{x}_j\right|_{desired\_accuracy}} \quad for \quad j = 4,\cdots,6 \tag{4.1.13}$$

where Δf_j for $i = 3,\cdots,6$ are substituted by their upper bounds, F_j^o, respectively.

4.2 Assessment of the Sliding Mode Observer

The sliding mode observer is used herein to estimate the heading angle, ψ, the X and Y coordinates of the ship along with their time derivatives. The full-order nonlinear model of the ship along with the sliding mode controller of the previous Chapter has been used to obtain the controlled response of the ship. The observer was only implemented to estimate the state variables. Thus, the actual state variables are used in the computation of the control signals as shown in Fig. 4-1.

The simulation conditions are considered to be the same as those used in generating the results of the sliding mode controller. Therefore, the ship parameters and

environmental conditions, listed in Table 3-1, are used in the assessment of the observer. The nominal model of the ship, given in Eqs. (4.1.3 and 4.1.4), has been incorporated in the formulation of the observer. The observer parameters are listed in Table 4-1. The initial conditions of the ship were selected to be:

$$\begin{aligned} X(0) &= 4 \text{ m} & \dot{X}(0) &= 5.5 \text{ m/s} \\ Y(0) &= 4 \text{ m} & \dot{Y}(0) &= 0 \text{ m/s} \\ \psi(0) &= 0 \text{ rad} & \dot{\psi}(0) &= 0 \text{ rad/s} \end{aligned} \tag{4.2.1}$$

However, the initial conditions of the observer were defined as follows

$$\begin{aligned} \hat{X}(0) &= 5 \text{ m} & \dot{\hat{X}}(0) &= 0 \text{ m/s} \\ \hat{Y}(0) &= 5 \text{ m} & \dot{\hat{Y}}(0) &= 0 \text{ m/s} \\ \hat{\psi}(0) &= 0.05 \text{ rad} & \dot{\hat{\psi}}(0) &= 0 \text{ rad/s} \end{aligned} \tag{4.2.2}$$

In addition, all the body-fixed state variables of the ship were initially set to zero except for the surge speed which was set initially to $u(0) = 5.5\ m/\sec$.

Figures 4-2 to 4-7 demonstrate the capability of the sliding mode observer to yield accurate estimates of the state variables X, Y, ψ, $\dot{X}$, $\dot{Y}$, and $\dot{\psi}$ in the presence of significant external disturbances, structured and unstructured uncertainties.

Moreover, Figs. 4-8 and 4-9 show the desired, actual, and estimated ship surge speeds. Figure 4-8 demonstrates that the sliding mode controller is capable of forcing the actual surge speed, u, to accurately track the desired surge speed, u_d. However, the error between u and the estimated surge speed reflects the adverse effect of ignoring the roll and pitch angles in the computation of u_e in Eq. (4.1.2c). This is illustrated in Fig. 4-9. Same reasoning can be used to explain the discrepancies

between r and r_e in Fig. 4-10 where r_e is considered to be $\dot{\psi}_e$ while r is generated by the full-order model of the ship, which accounts for the roll and pitch angles.

4.3 Integrated Sliding Mode Controller and Observer for a Ship

To couple the sliding mode controller and observer, the control signals are now being computed based on estimated rather than actual state variables (see Fig. 4-11). The robustness of the observer in yielding accurate estimates of the state variables is exhibited in Figs. 4-12 to 4-17. However, by comparing Figs. 4-2 to 4-7 with their counterparts in Figs. 4-12 to 4-17, one can realize that the estimation convergence rate becomes slower.

Unlike the results of the previous Section, Fig. 4-18 exhibits an error between the actual and desired surge speeds of the ship. This error is caused by the computation of u_e, which ignores the roll and pitch angles in the transformation matrix of Eq. 4.1.2c. This is shown in Fig. 4-19. However, the results in Figs. (4-18 and 4-20) prove the robustness and good tracking characteristic of the integrated system of sliding mode controller and observer.

4.4 Summary

A sliding mode observer has been designed in the current Chapter to accurately estimate the state of a marine vessel. The simulation results illustrate the robustness and the rapid convergence rate of the observer. In addition, the sliding mode controller of the previous Chapter was coupled with the sliding mode observer of the present Chapter. The integrated system has lead to a robust performance of the closed-loop system in spite of significant modeling imprecision and external disturbances.

In the next Chapter, a self-tuning fuzzy sliding mode controller is developed to enable the ship to adapt to its varying environmental conditions.

Ship Data	
Length of the ship L_{PP}	100 m
Mass of the ship m_{ship}	7264000 Kg
Beam B	25 m
Draught T	8 m
Rudder Area A_{rud}	6 m^2
Maximum rudder angle $\alpha_{\max}$	22.5^0
Maximum rudder slew rate $\dot{\alpha}_{\max}$	19.5^0/sec
Environmental Conditions	
$H_{1/3}$ of the wave	8 m
Period of the wave spectrum T_0	9.01 sec
Incident angles of the wave, wind and current	90^0
Wind speed	20 m/s
Current speed	2 m/s
Sliding Mode Observer Parameters	
Φ_1	0.01
Φ_2	0.01
Φ_3	0.001
η_{o_1}	0.001
η_{o_2}	0.001
η_{o_3}	0.001
$\lvert\tilde{x}_4\rvert_{upper\ bound}$	9 m/sec^2
$\lvert\tilde{x}_5\rvert_{upper\ bound}$	1 m/sec^2
$\lvert\tilde{x}_6\rvert_{upper\ bound}$	0.1 rad/ sec^2

Table 4-1 Ship data, environmental conditions and observer parameters.

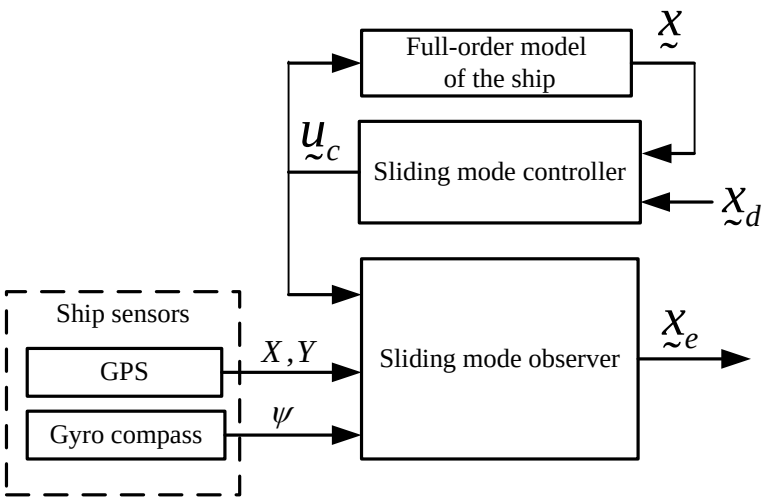

Fig. 4-1 Closed-loop system used in evaluating the sliding mode observer.

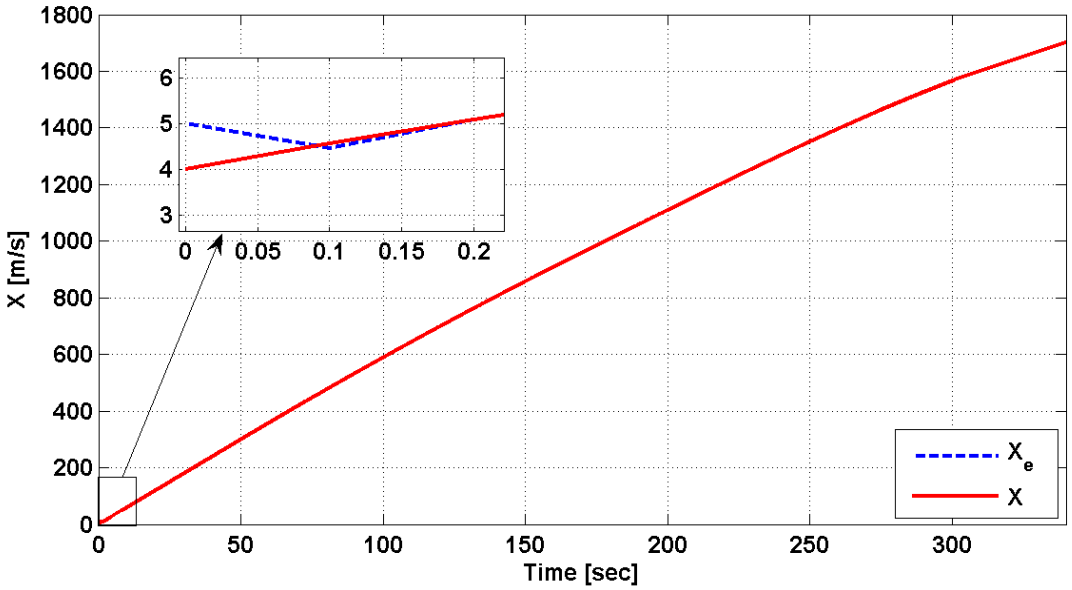

Fig. 4-2 Actual and estimated X coordinate of the ship with respect to the inertial frame.

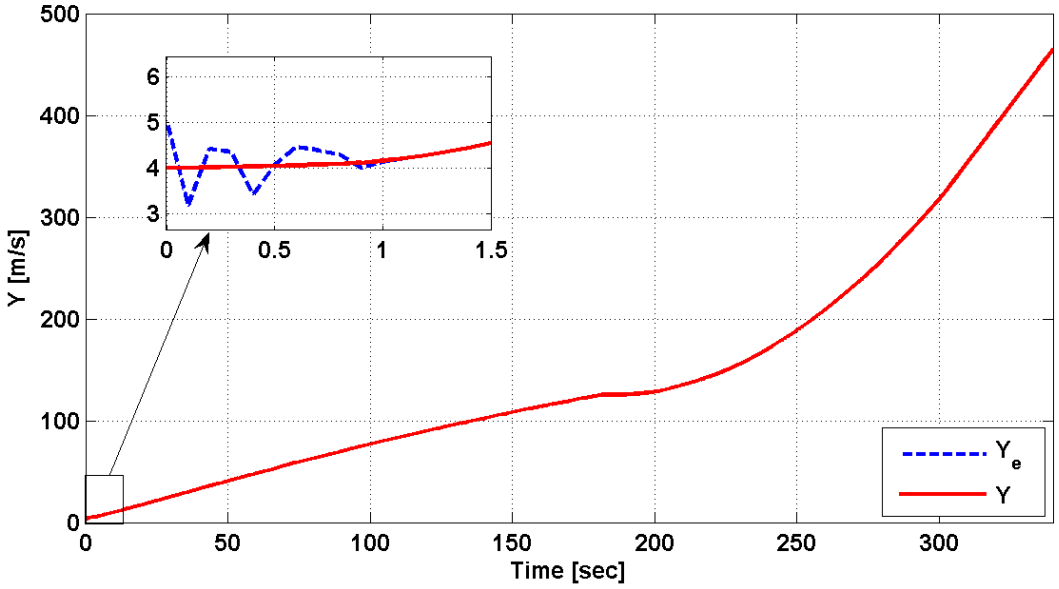

Fig. 4-3 Actual and estimated Y coordinate of the ship with respect to the inertial frame.

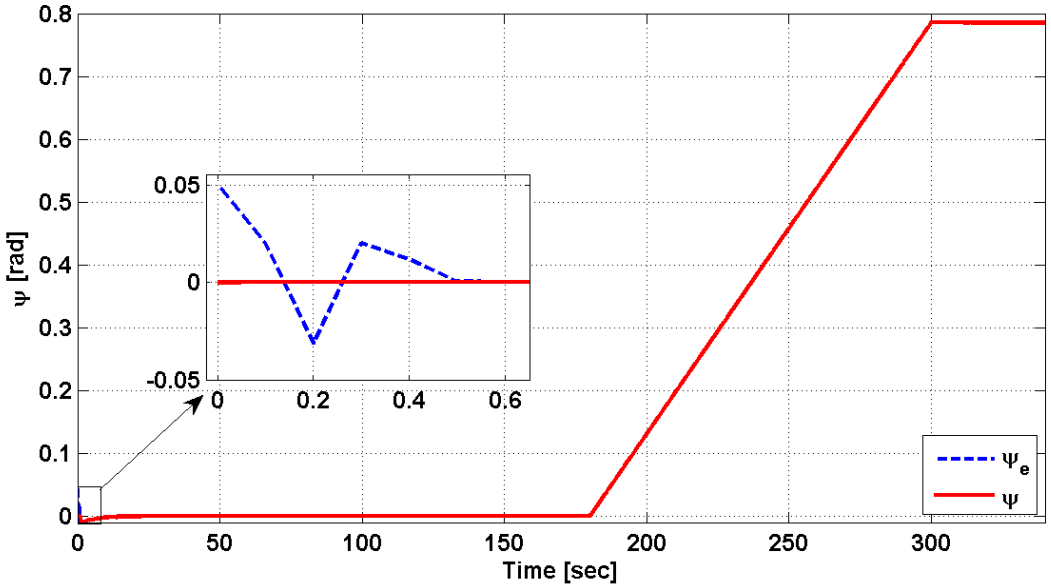

Fig. 4-4 Actual and estimated ψ coordinate of the ship with respect to the inertial frame.

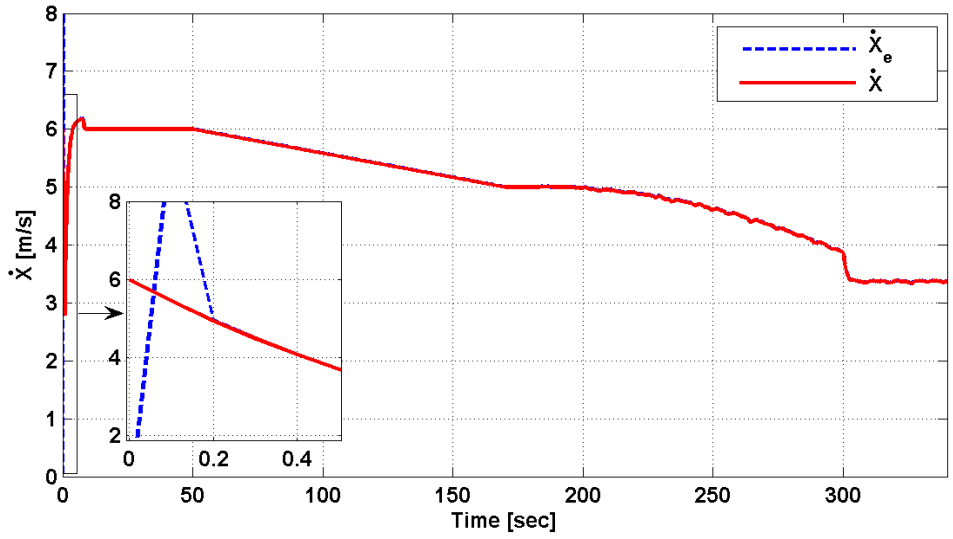

Fig. 4-5 Actual and estimated speed of the ship along the $X-$axis.

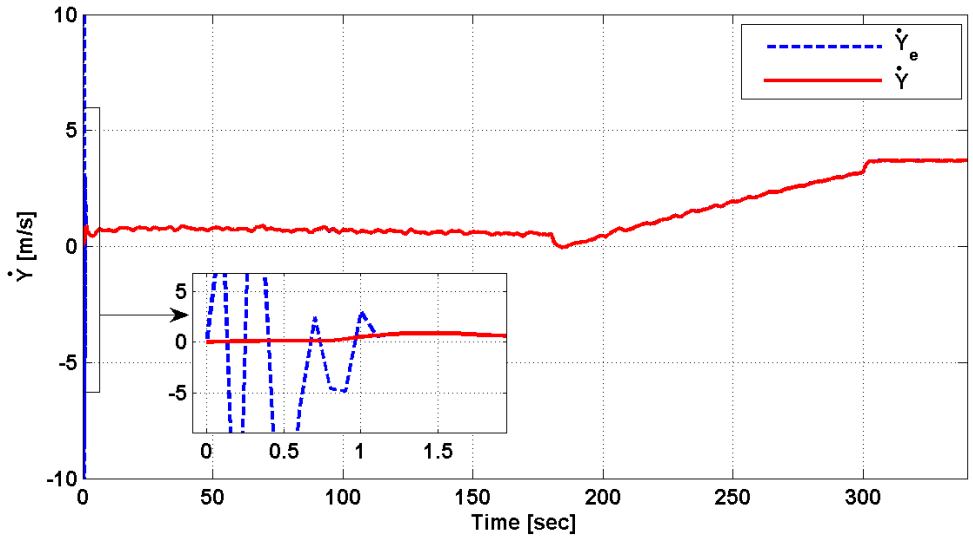

Fig. 4-6 Actual and estimated speed of the ship along the Y – axis.

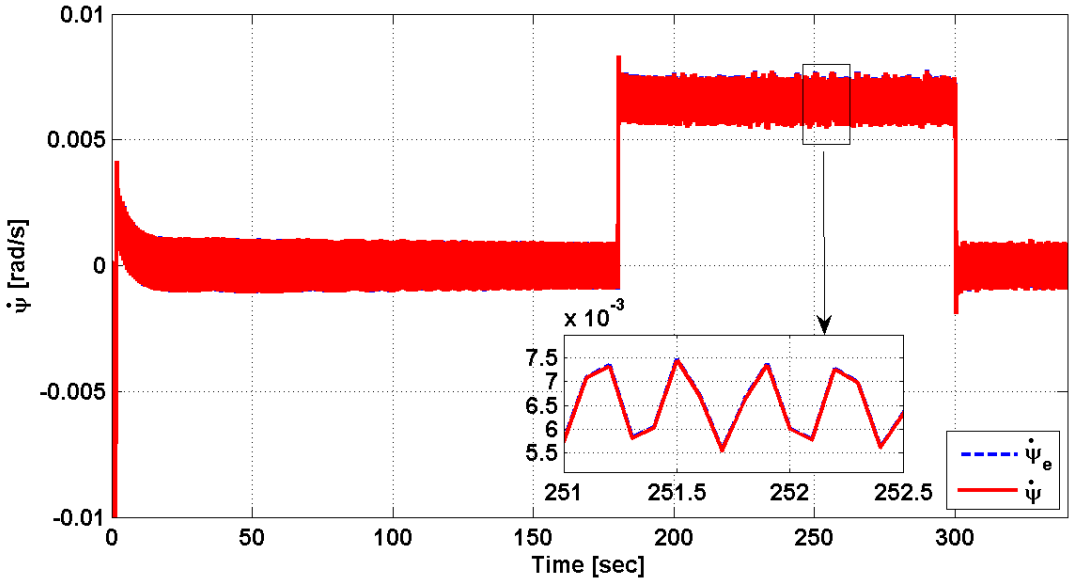

Fig. 4-7 Actual and estimated time rate of change of the heading angle around the Z – axis.

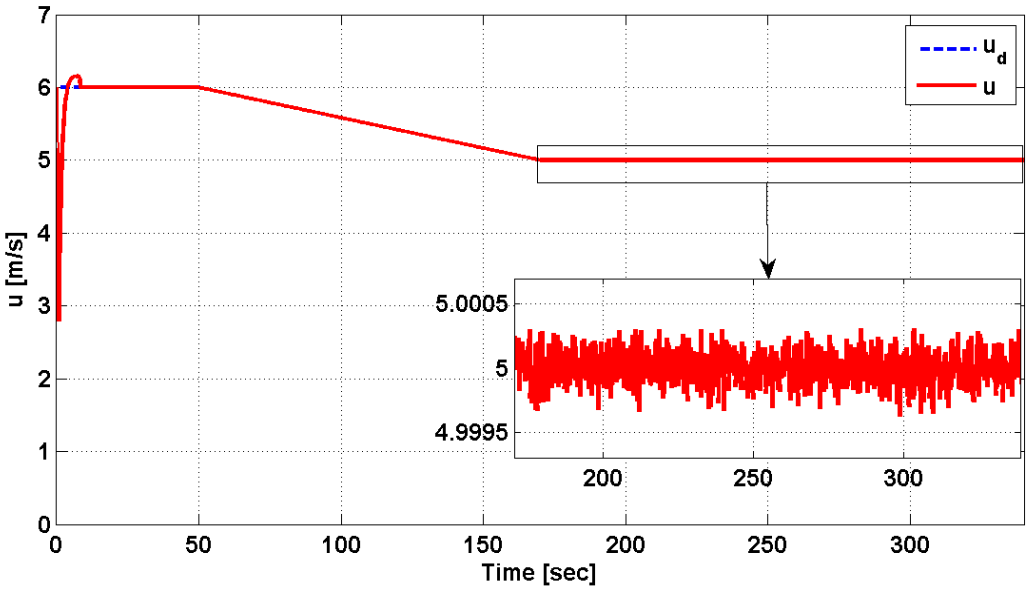

Fig. 4-8 Actual and desired speed of the ship defined with respect to the body-fixed coordinate system.

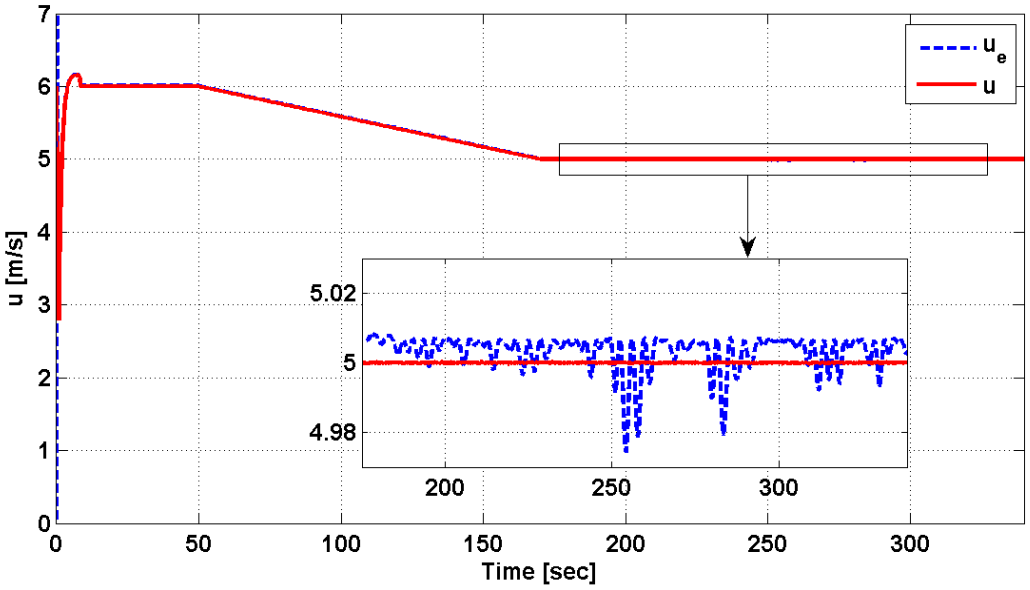

Fig. 4-9 Actual and estimated speed of the ship defined with respect to the body-fixed coordinate system.

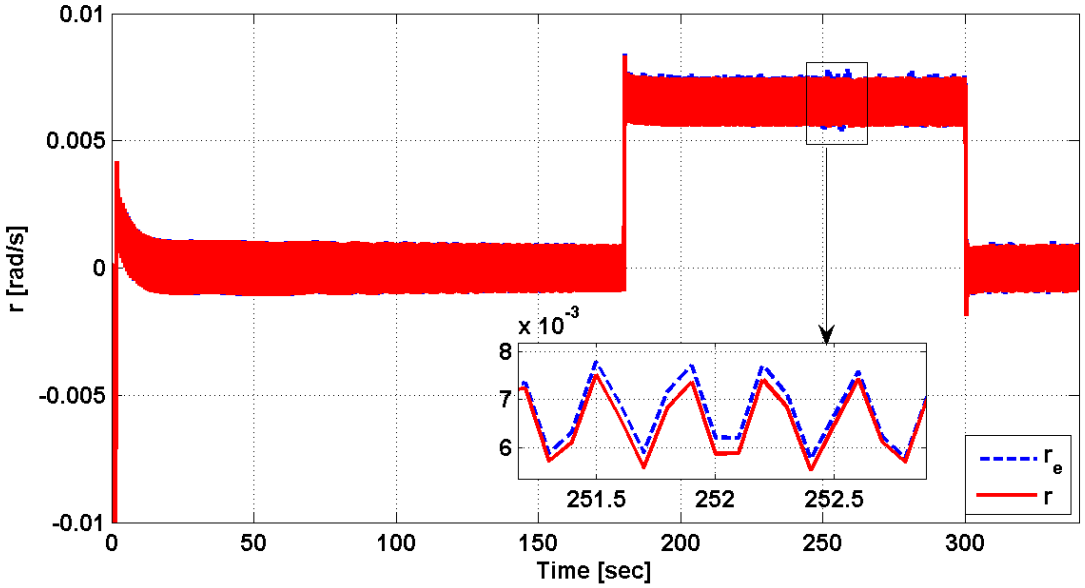

Fig. 4-10 Actual and estimated time rate of change of the ship heading with respect to the body-fixed coordinate system.

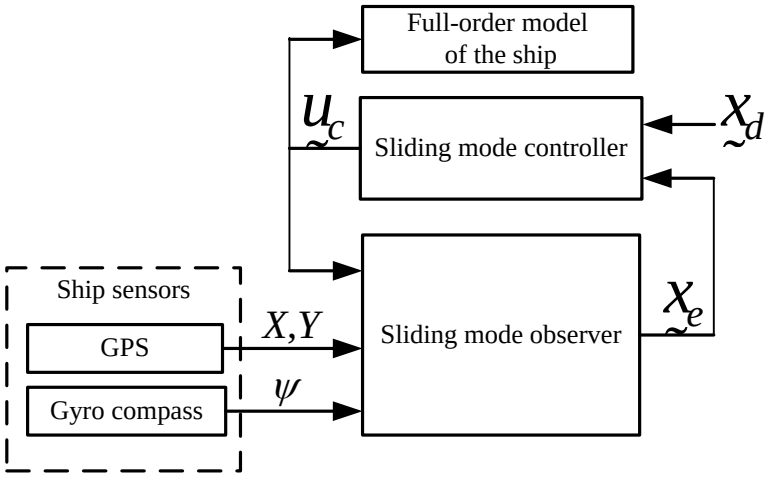

Fig. 4-11 Closed-loop system configuration used in assessing the performance of the integrated controller and observer system.

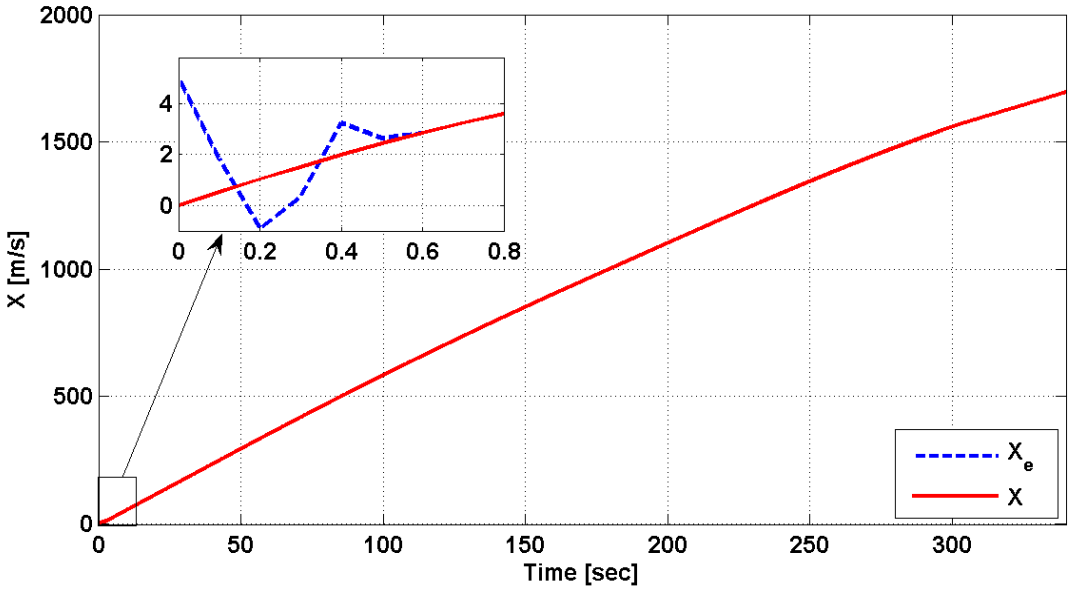

Fig. 4-12 Actual and estimated X coordinate of the ship with respect to the inertial frame.

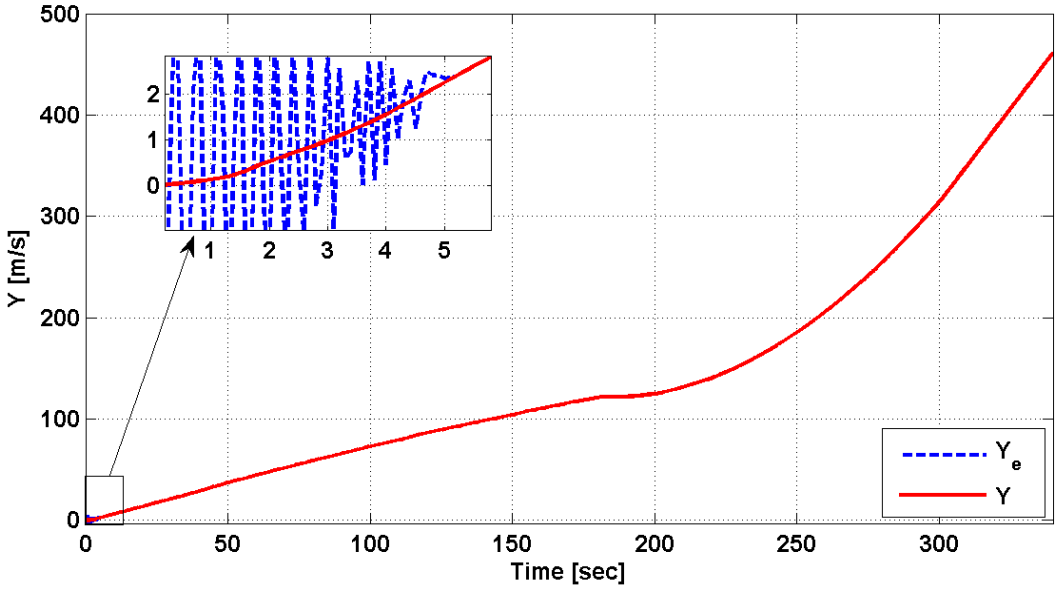

Fig. 4-13 Actual and estimated Y coordinate of the ship with respect to the inertial frame.

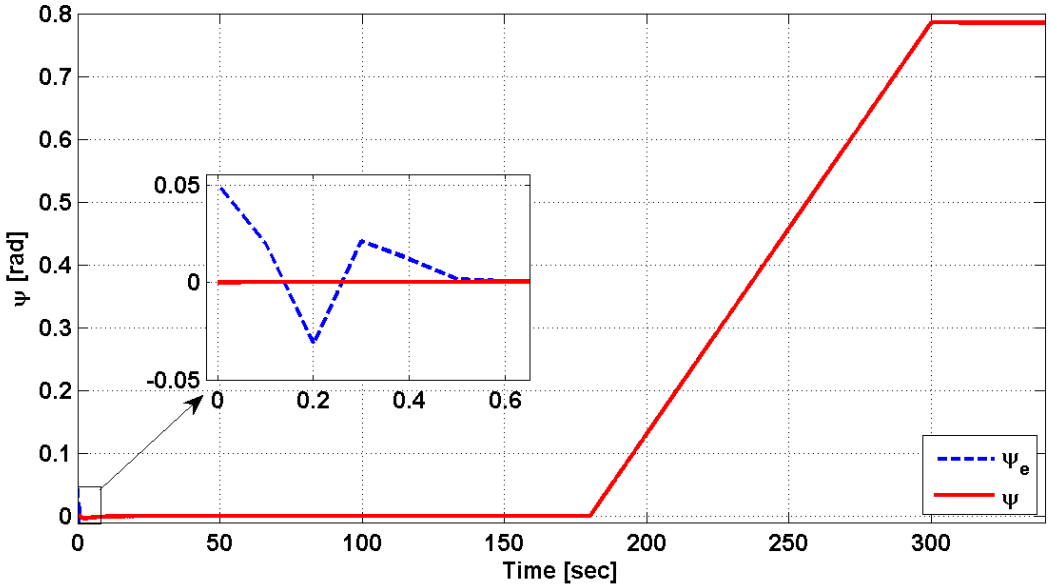

Fig. 4-14 Actual and estimated ψ coordinate of the ship with respect to the inertial frame.

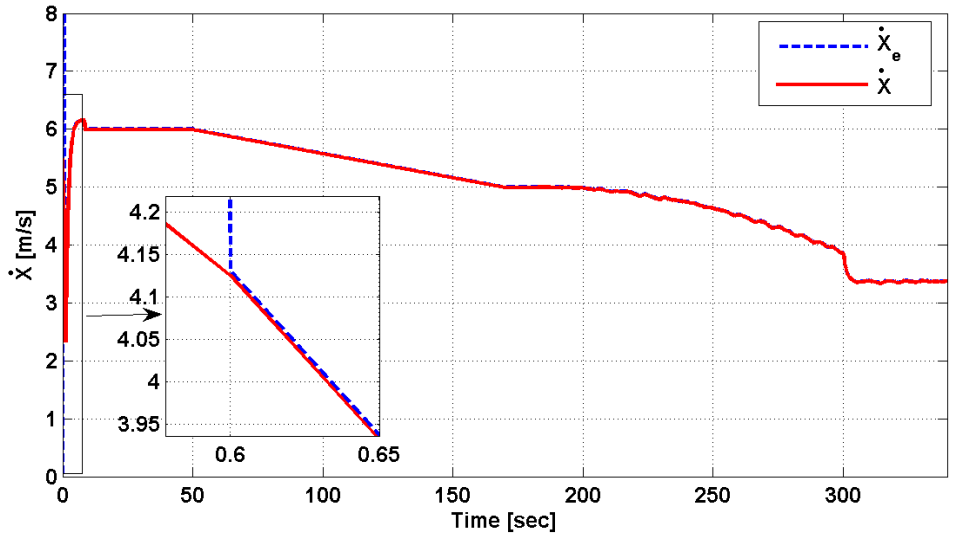

Fig. 4-15 Actual and estimated speed of the ship along the $X-$axis.

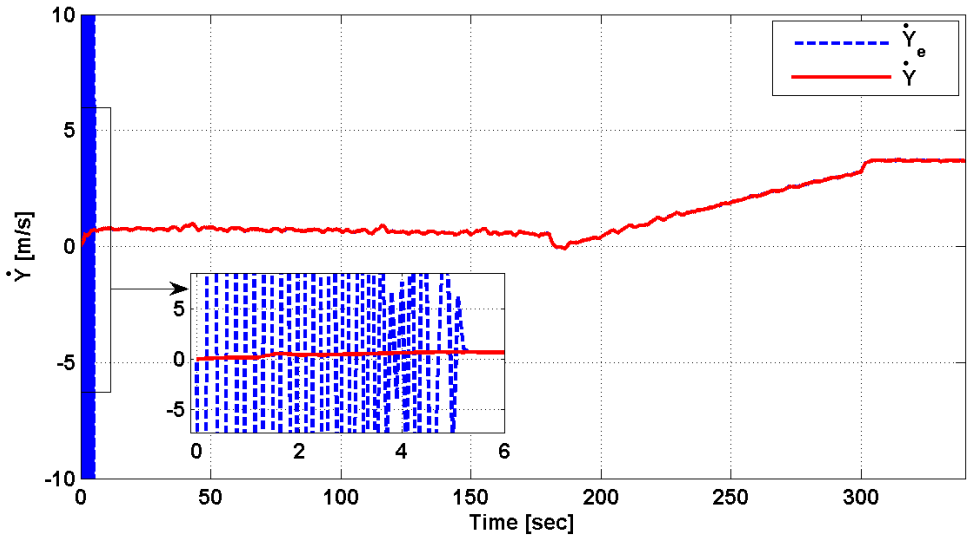

Fig. 4-16 Actual and estimated speed of the ship along the Y – axis.

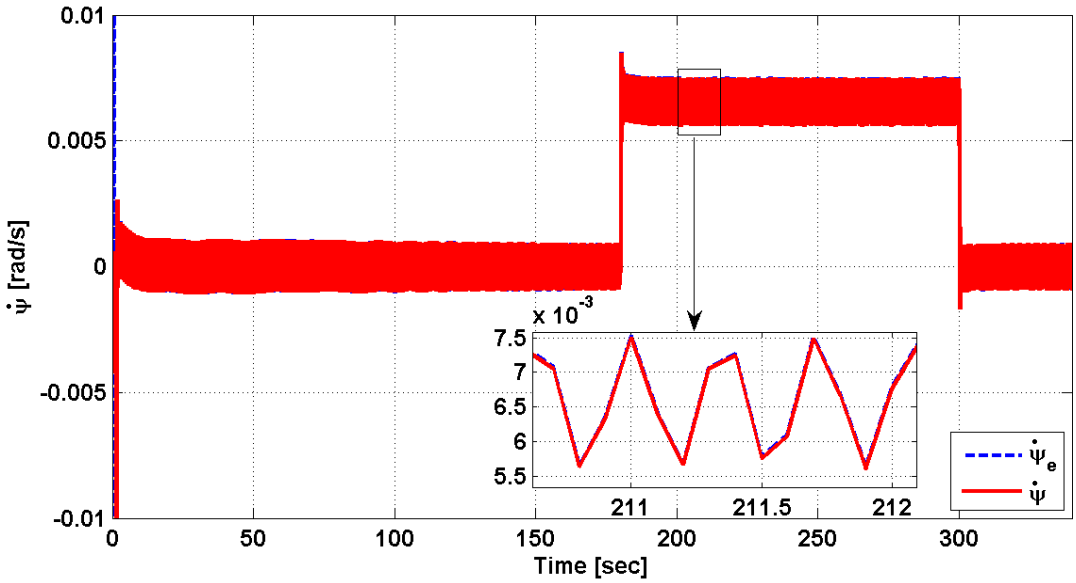

Fig. 4-17 Actual and estimated time rate of change of the heading angle around the Z – axis.

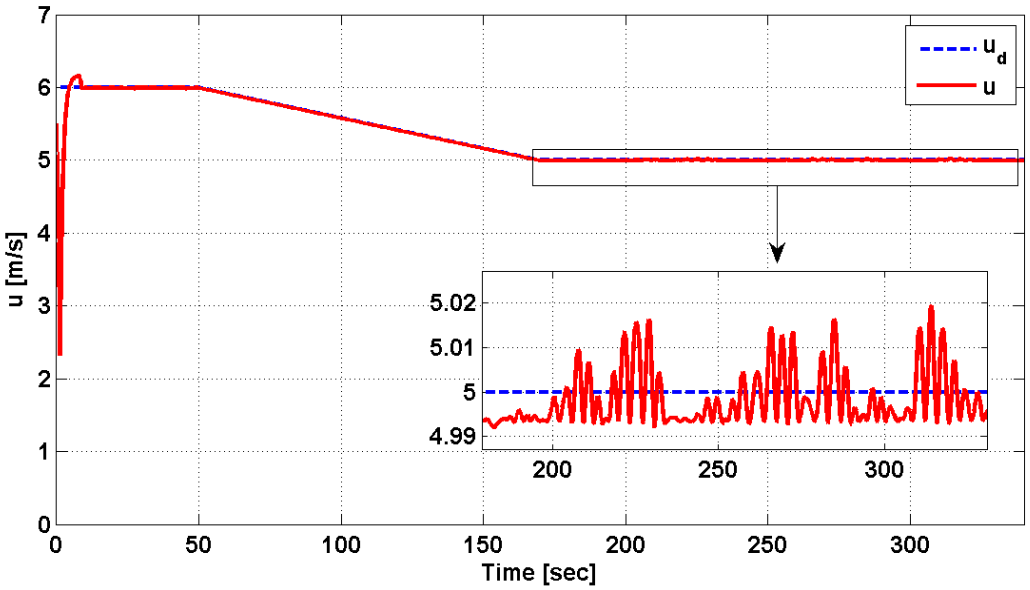

Fig. 4-18 Actual and desired surge speed of the ship.

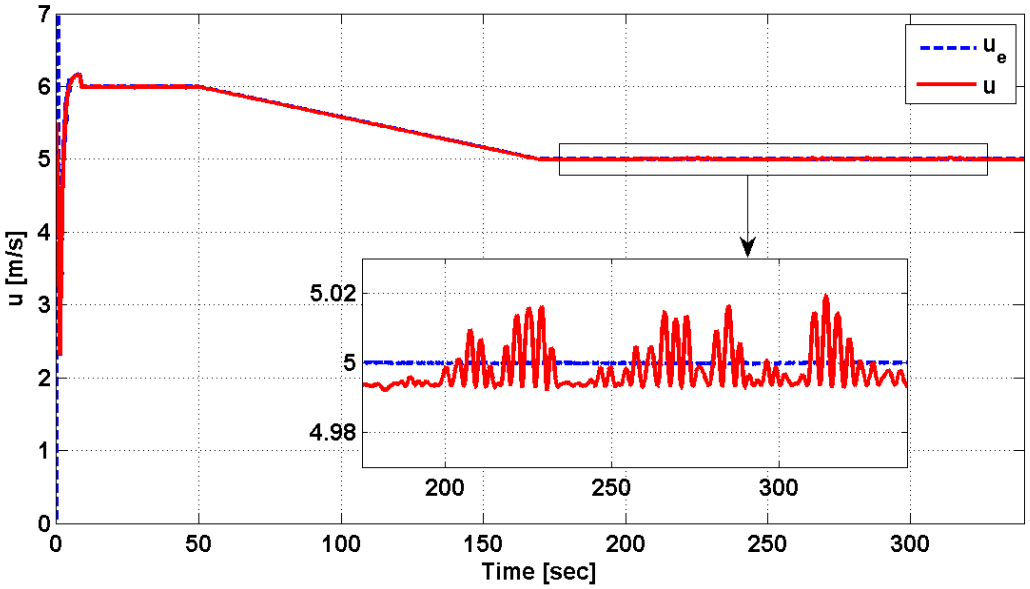

Fig. 4-19 Actual and estimated surge speed of the ship.

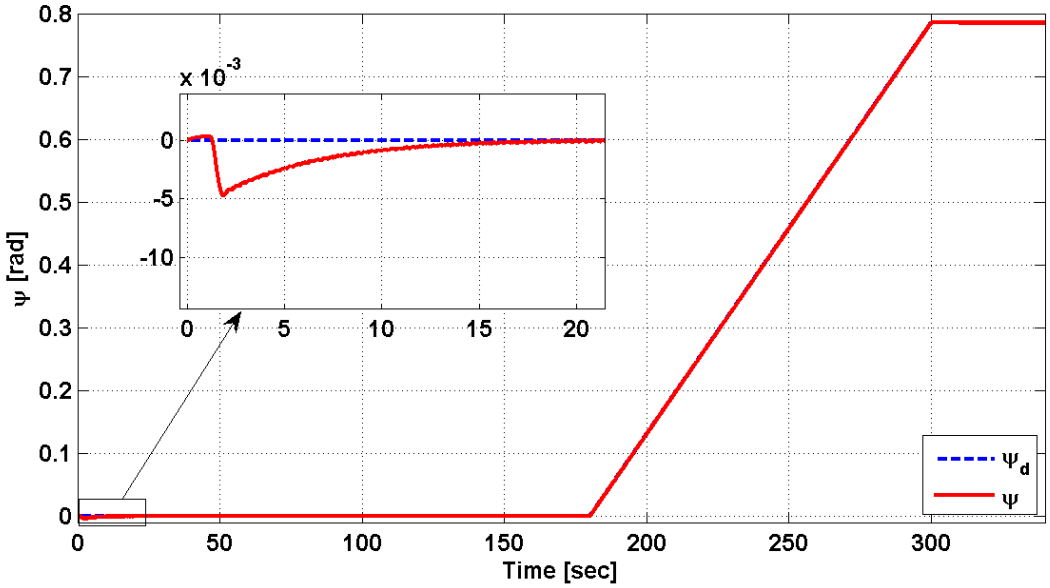

Fig. 4-20 Actual and desired heading angle of the ship.

CHAPTER 5 “DESIGN OF A SELF-TUNING FUZZY SLIDING MODE CONTROLLER”

Marine surface vessels are required to operate in constantly changing and unpredictable environmental conditions that are capable of producing unexpected and considerable disturbances. A self-tuning fuzzy sliding mode controller is presented in this chapter as a potential approach for controlling the ship motion in the presence of modeling uncertainties and significant external disturbances.

The general procedure for designing the self-tuning fuzzy sliding mode controller will be covered in details in the next section. Subsequently, the controller will be applied to control the motion of an under-actuated marine surface vessel. The simulation results, illustrating the performance of the controller, will be included in section 5-3. They will be followed by concluding remarks regarding the performance of the proposed controller.

5.1 Procedure for designing a self-tuning fuzzy sliding mode controller

The self-tuning fuzzy sliding mode controller is an attempt to combine the advantages of the variable structure systems (VSS) theory with the self-tuning fuzzy logic controller. Its salient feature emanates from the fact that neither an accurate dynamic model of the plant nor the construction of a rule-based expert fuzzy inference system is required for the design of the controller. However, its stability analysis requires the knowledge of the upper bound of the modeling uncertainties and external disturbances. The controller will be robust to both structured and unstructured uncertainties of the plant and will be able to adapt to its varying environmental conditions.

The current controller design considers the dynamics of the plant to be governed by the following nonlinear second order differential equation:

$$\ddot{x} = f(x, \dot{x}) + b(x) u_c \tag{5.1.1}$$

where $f(x, \dot{x})$ is not fully known and $b(x)$ satisfies the inequality $0 < b_{\min} \le b(x) \le b_{\max}$. Therefore, in designing the controller, both $f(x)$ and $b(x)$ are represented by their nominal expressions $\hat{f}(x)$ and $\hat{b}(x)$, respectively. In addition, the upper bound, F, of $\left| f(x) - \hat{f}(x) \right|$ is considered to be known.

Based on the Sugeno-type fuzzy inference system (FIS), the control variable, u_c, can be expressed as (Sugeno and Kang, 1988; Takagi and Sugeno, 1985)

$$u_c = \frac{\sum_{i=1}^{m} w_i r_{i_t}}{\sum_{i=1}^{m} w_i} = \frac{\sum_{i=1}^{m} w_i (r_i - \gamma |s| s \frac{w_i}{\sum_{i=1}^{m} w_i})}{\sum_{i=1}^{m} w_i} \tag{5.1.2}$$

where the expression between parentheses represents the tuned singleton output membership function, r_{i_t}, of the i^{th} rule. The tuning procedure is motivated by the steepest descent method (Kirk, 1970; Yeh, 1994), which is an efficient scheme to minimize a given cost function. The latter has been selected herein to be $\frac{1}{2} s^2(e, \dot{e})$. The selection of the sliding surface expression, $s(e, \dot{e})$, is motivated by the problem at hand.

By expanding Eq. (5.1.2), one gets

$$u_C = \frac{\sum_{i=1}^{m} w_i r_i}{\sum_{i=1}^{m} w_i} - \gamma |s| s \frac{\sum_{i=1}^{m} w_i^2}{\left(\sum_{i=1}^{m} w_i \right)^2} \tag{5.1.3}$$

The first term in the above equation is a typical output of a Sugeno-type FIS. It is a weighted average of the outputs of all the rules where the general form of the i^{th} rule can be expressed as

If "input" is "A" then "output" is $r_i \quad i = 1, \cdots, m$ (5.1.4)

All singleton output membership functions, r_i's, can be initially set to zero. Therefore, at time t, r_i refers to the tuned value of the output membership function of the i^{th} rule during the period $[0, t)$.

The second term in Eq. (5.1.3) is a switching term, which is inspired by the variable structure systems (VSS) theory (Utkin, 1977). Its objective is to modify the control action so that the controlled system is either continuously driven toward the sliding surface or forced to remain on $s(e, \dot{e})$. As a consequence, the robustness of the controlled system to external disturbances and modeling uncertainties will be significantly enhanced. It should also be emphasized that the switching term is heavily relied on during the initial phase of tuning the controller.

Stability conditions should now be derived in order to ensure that the real-time tuning process of the rules does not cause the closed-loop system to become unstable. This is done by forcing the learning rate parameter, γ, to satisfy the following sliding condition (Khalil, 1996; Slotine and Li, 1991):

$$\frac{1}{2}\frac{d}{dt}\left(s^2(e,\dot{e})\right) \le -\eta\left|s(e,\dot{e})\right| \tag{5.1.5}$$

This control scheme is pictorially described in Fig. 5-1. It will be applied in the next section to control the surge and heading of under-actuated marine surface vessels.

5.2 Design of a self-tuning fuzzy sliding mode controller for an under-actuated ship

The self-tuning fuzzy sliding mode controller is applied in this work to control the surge and heading of an under-actuated marine surface vessel. All state variables of the ship are considered to be available through measurement. The actuators are limited to the propeller and the rudder.

The controller is designed based on a reduced-order model, which accounts for the surge and yaw motions of the ship. The yaw equation, given by Eq.(3.1.5), directly relates the yaw angular acceleration to the rudder control torque. As a consequence, the state equation governing the surge and yaw motions of the ship can be expressed in the following compact form:

$$\dot{\underset{\sim}{x}}_r = \underset{\sim}{f}_r\left(\underset{\sim}{x}_r\right) + b_r\left(\underset{\sim}{x}_r\right)\underset{\sim}{u}_c \tag{5.2.1}$$

where $\underset{\sim}{x}_r^T$ and $\underset{\sim}{u}_c^T$ are defined as $\left[\int_0^t r\,d\tau, u, r\right]$ and $\left[F_{th\_del}, T_{rud}\right]$, respectively. In addition, all terms pertaining to the sway, heave, pitch and roll motions of the vessel are ignored in the above equations. Recall that both u and r are defined with respect to the body-fixed coordinate system of the ship. In the case of the reduced-order model where the roll and pitch angular displacements of the ship are ignored, $\int_0^t r\,d\tau$ and r

become equal to ψ and $\dot{\psi}$, which are the ship yaw angle and its time derivative with respect to the inertial frame. However, the $\int_0^t u\,d\tau$ term has no physical meaning and its value is not available for the computation of the control signal. This is the rationale behind using three state equations to represent the surge and yaw motions of the ship as well as for choosing different sliding surfaces in the control of the surge and heading motions of the ship.

Both $\underset{\sim}{f}_r(\underset{\sim}{x}_r)$ and $b_r(\underset{\sim}{x}_r)$ are not considered to be fully known. They are approximated by their nominal expressions $\hat{\underset{\sim}{f}}_r(\underset{\sim}{x}_r)$ and $\hat{b}_r(\underset{\sim}{x}_r)$, respectively. The upper bounds on the modeling imprecision of the entries of $\hat{\underset{\sim}{f}}_r(\underset{\sim}{x}_r)$ are assumed to be known and defined as follows

$$F_i = \left| f_{r_i}(\underset{\sim}{x}_r) - \hat{f}_{r_i}(\underset{\sim}{x}_r) \right| \qquad i = 2 \text{ and } 3 \tag{5.2.2}$$

The $b_{r_i}(\underset{\sim}{x}_r)$ terms for $i = 2 \text{ and } 3$ are assumed to satisfy inequality conditions defined by $0 < b_{r_{i_{\min}}} \le b_{r_i}(\underset{\sim}{x}_r) \le b_{r_{i_{\max}}}$. Thus, the controller is designed based on the following nominal model

$$\dot{\underset{\sim}{x}}_r = \hat{\underset{\sim}{f}}_r(\underset{\sim}{x}_r) + \hat{b}_r(\underset{\sim}{x}_r)\underset{\sim}{u}_c \tag{5.2.3}$$

In the current work, eleven rules have been incorporated ($m = 11$) into the Sugeno-type fuzzy inference systems designed for the surge and heading of the marine vessel. The input variables are defined to be the following sliding surfaces:

$$s_s\left(e_s,\dot{e}_s\right)=\left(\frac{d}{dt}+\lambda_s\right)^2\int_0^t e_s\,d\tau$$
$$=\quad \dot{e}_s+2\lambda_s e_s+\lambda_s^2\int_0^t e_s\,d\tau \qquad with \quad e_s=\int_0^t\left(u-u_d\right)d\tau \tag{5.2.4a}$$

$$s_h\left(e_h,\dot{e}_h\right)=\dot{e}_h+\lambda_h e_h \quad with \quad e_h=\int_0^t r\,d\tau-\left(\int_0^t r\,d\tau\right)_d=\psi-\psi_d \tag{5.2.4b}$$

where ψ and ψ_d are the actual and desired yaw angles, respectively. The membership functions corresponding to the input variables, $s_s\left(e_s,\dot{e}_s\right)$ and $s_h\left(e_h,\dot{e}_h\right)$, are shown in Fig. 5-2 where Φ_s and Φ_h are selected to be 0.1 and 0.02, respectively. N1 to N5 are membership functions covering the range of negative values for the input variables, which reflect situations where the system is located beneath the sliding surface. Similarly, P1 to P5 cover all cases when the system is located above the sliding surface. However, Z reflects cases when the system is either on or in close proximity to the sliding surface. In the current work, all singleton output membership functions, r_i's, are initially assigned zero values.

Figure 5-3 provides a pictorial description of the ship controller. The control variables for the surge and heading motion of the ship can be written as

$$F_{th}=\frac{\sum_{i=1}^m w_{s_i}r_{s_i}}{\sum_{i=1}^m w_{s_i}}-\gamma_s\left|s_s\right|s_s\frac{\sum_{i=1}^m w_{s_i}^2}{\left(\sum_{i=1}^m w_{s_i}\right)^2} \tag{5.2.5a}$$

$$T_{rud} = \frac{\sum_{i=1}^{m} w_{h_i} r_{h_i}}{\sum_{i=1}^{m} w_{h_i}} - \gamma_h |s_h| s_h \frac{\sum_{i=1}^{m} w_{h_i}^2}{\left(\sum_{i=1}^{m} w_{h_i} \right)^2} \tag{5.2.5b}$$

It should be stressed that the switching terms in the above equations are heavily relied on to control the ship during the initial phase of the tuning process where the singleton output membership functions are set to zero. The asymptotic stability of the control system is ensured by selecting the tuning rates, γ_s and γ_h, such that they satisfy sliding conditions similar to that given in Eq. (5.1.5). As a consequence, the tuning rates must satisfy the following inequalities:

$$\gamma_s \geq \left(\frac{\eta_s + \left[F_2 + \hat{f}_{r_2} - \dot{u}_d + 2\lambda_s \dot{e}_s + \lambda_s e_s + b_{r_2} \frac{\sum w_{s_i} r_{s_i}}{\sum w_{s_i}} \right] \mathrm{sgn}(s_s)}{b_{r_2} \left[\frac{s_s^2 \sum w_{s_i}^2}{\left(\sum w_{s_i} \right)^2} \right]} \right)_{\sup} \tag{5.2.6a}$$

$$\gamma_h \geq \left(\frac{\eta_h + \left[F_3 + \hat{f}_{r_3} - \ddot{\psi}_d + \lambda_2 \dot{e}_2 + b_{r_3} \frac{\sum w_{h_i} r_{h_i}}{\sum w_{h_i}} \right] \mathrm{sgn}(s_h)}{b_{r_3} \left[\frac{s_h^2 \sum w_{h_i}^2}{\left(\sum w_{h_i} \right)^2} \right]} \right)_{\sup} \tag{5.2.6b}$$

The performance of the controller will be assessed in digital simulations in the next section under considerable external disturbances and modeling imprecision.

5.3 Assessment of the self-tuning fuzzy sliding mode controller

The full order model of the marine vessel, which accounts for the surge, sway, heave, roll, pitch and yaw motions of the ship along with the rudder dynamics, is used

herein as a test bed to assess the performance of the proposed controller. As a consequence, the unstructured uncertainties will be significantly increased due to the fact that the controller is designed based on a reduced-order model of the ship. The vessel geometric dimensions, control parameters, and environmental conditions, used in carrying out the digital simulations, are listed in Table 5-1. The nominal values for $\hat{f}_{r_2}(x)$ and $\hat{f}_{r_3}(x)$ have been set to zero in order to demonstrate that these terms can actually be ignored in the design of the controller as long as the upper bounds F_2 and F_3 are known. The data in Table 5-1 reveals considerable modeling uncertainties and external disturbances. The simulations assume zero initial conditions for the state variables of the ship except for the surge speed which is set initially to $u(0) = 5.5\ m/\sec$.

The desired surge speed and heading angle are assigned as follows

$$u_d = \begin{cases} 6 \quad m/\sec & 0 \le t \le 50\ \sec \\ \dfrac{-(t-50)}{110} + 6 \quad m/\sec & 50 \le t \le 160\ \sec \\ 5 \quad m/\sec & t \ge 160\ \sec \end{cases} \tag{5.3.1a}$$

$$\psi_d = \begin{cases} 0 \quad rad & 0 \le t \le 180\ \sec \\ \dfrac{0.8(t-180)}{120} \quad rad & 180 \le t \le 300\ \sec \\ 0.8 \quad rad & t \ge 300\ \sec \end{cases} \tag{5.3.1b}$$

Figure 5-4 illustrates the wave height at the mass center of the ship. Figures 5-5 to 5-8 demonstrate the capability of the controller in tracking the desired surge speed and heading angle of the ship in the presence of significant modeling imprecision and external disturbances. Figures 5-7 and 5-8 illustrate that the tracking errors are in the order of 10^{-3}. The heave displacement along with the roll and pitch angular

displacements of the ship are shown in Figs. 5-9 to 5-11. Note that during the first 180 seconds of the simulation, the waves had 90^o incident angle with respect to the ship, which resulted in larger excitations in the roll angle than in the pitch angle. However, this trend is reversed after 180 sec into the simulation when the actual heading angle of the ship started to increase (see Figs. 5-10 and 5-11).

5.4 Summary

This chapter covers the general design procedure for a self-tuning fuzzy-sliding mode controller. It illustrates the implementation of such a controller on an under-actuated marine surface vessel. The simulation results illustrate the robust performance of the proposed controller in the presence of significant modeling imprecision and external disturbances.

The next chapter will focus on the implementation aspect of the controller by coupling it to a self-tuning fuzzy sliding mode observer.

Ship Data	
Length of the ship L_{PP}	100 m
Mass of the ship m_{ship}	7264000 Kg
Beam B	25 m
Draught T	8 m
Rudder Area A_{rud}	6 m^2
Maximum rudder angle $\alpha_{\max}$	22.5^0
Maximum rudder slew rate $\dot{\alpha}_{\max}$	19.5^0/sec
Environmental Conditions	
$H_{1/3}$ of the wave	8 m
Period of the wave spectrum T_0	9.01 sec
Incident angles of the wave, wind and current	90^0
Wind speed	20 m/s
Current speed	2 m/s
Surge Controller Parameters	
η_s	0.001
$\hat{f}_{r_2}$	0 m/sec^2
F_2	8 m/sec^2
$b_{r_{2_{\min}}} = b_{r_{2_{\max}}}$	m_{ship}^{-1} Kg^{-1}
λ_s	10
Heading Angle Controller Parameters	
η_h	1
$\hat{f}_{r_3}$	0 rad/sec^2
F_3	0.3 rad/sec^2
$b_{r_3 \min}$	$0.8\left[\frac{1}{I_z} - \frac{\Delta_1}{I_z\left(s_{rud} - e_{rud}\right)}\right]$
$b_{r_3 \max}$	$1.2\left[\frac{1}{I_z} - \frac{\Delta_1}{I_z\left(s_{rud} - e_{rud}\right)\cos\left(\alpha_{\max}\right)}\right]$
λ_h	0.2

Table 5-1Ship data, environmental conditions and controller parameters

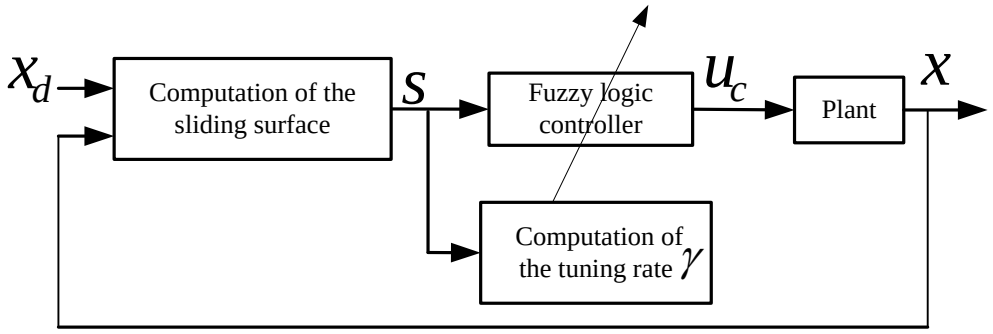

Fig. 5-1 Block diagram for a general self-tuning fuzzy sliding mode controller

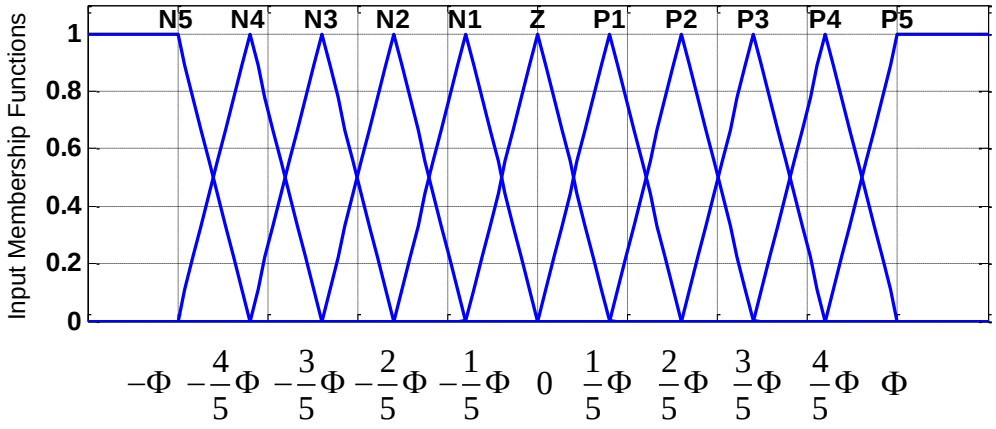

Fig. 5-2 Membership functions for the input variables s_s and s_h

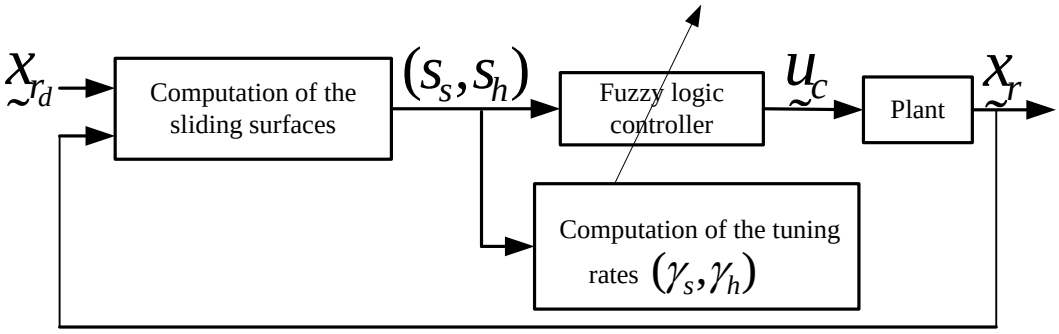

Fig. 5-3 Block diagram for the self-tuning fuzzy sliding mode controller designed for an under-actuated ship

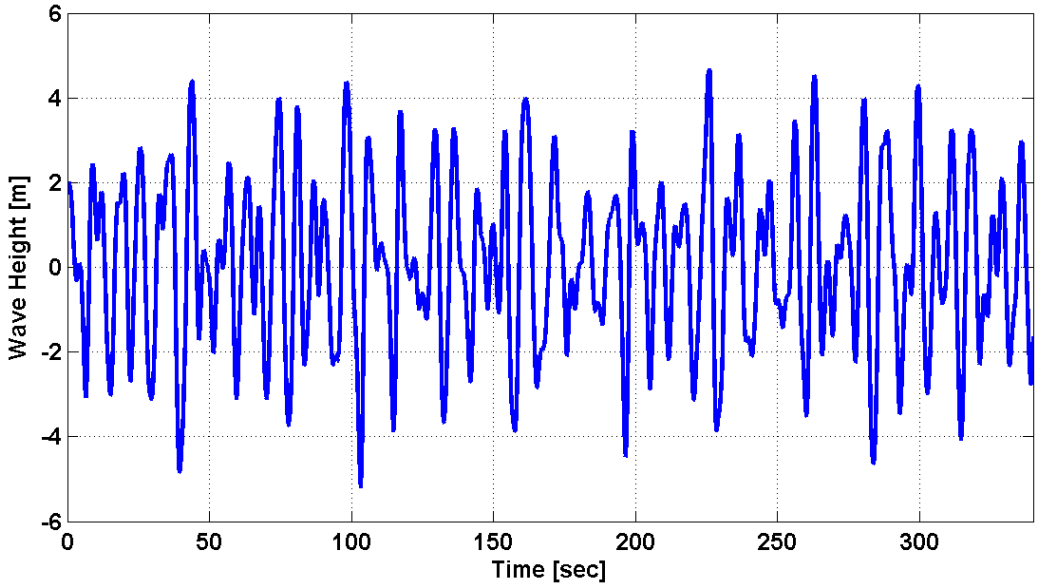

Fig. 5-4 Wave height at the mass center of the ship

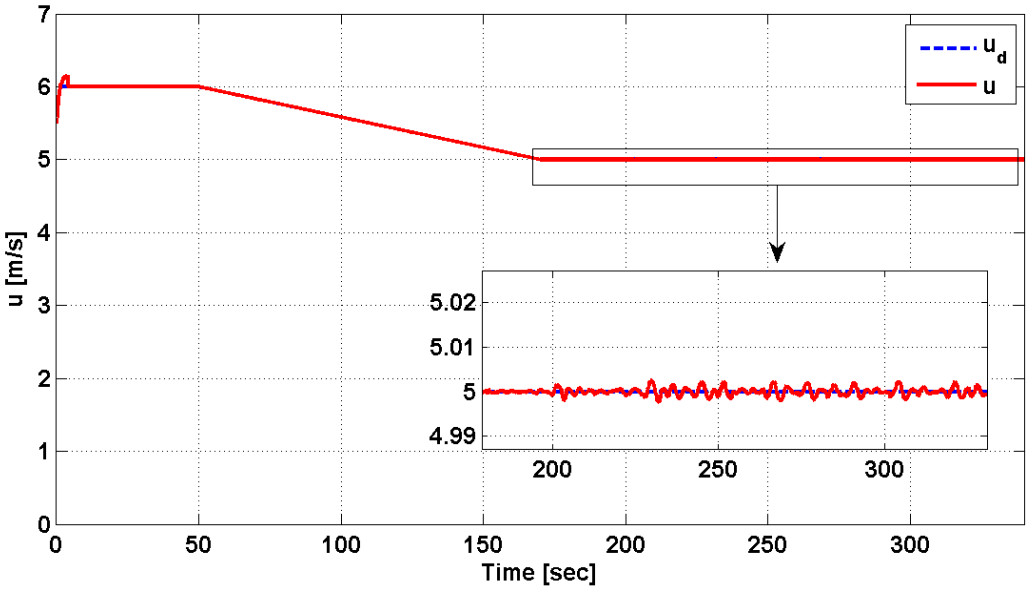

Fig. 5-5 Actual and desired surge speed of the ship

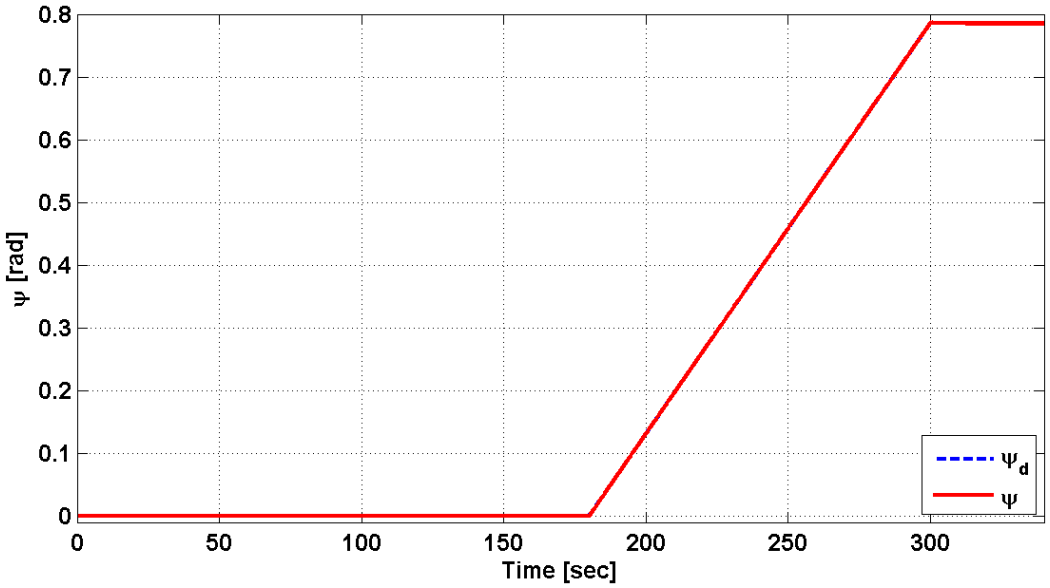

Fig. 5-6 Actual and desired heading angle of the ship

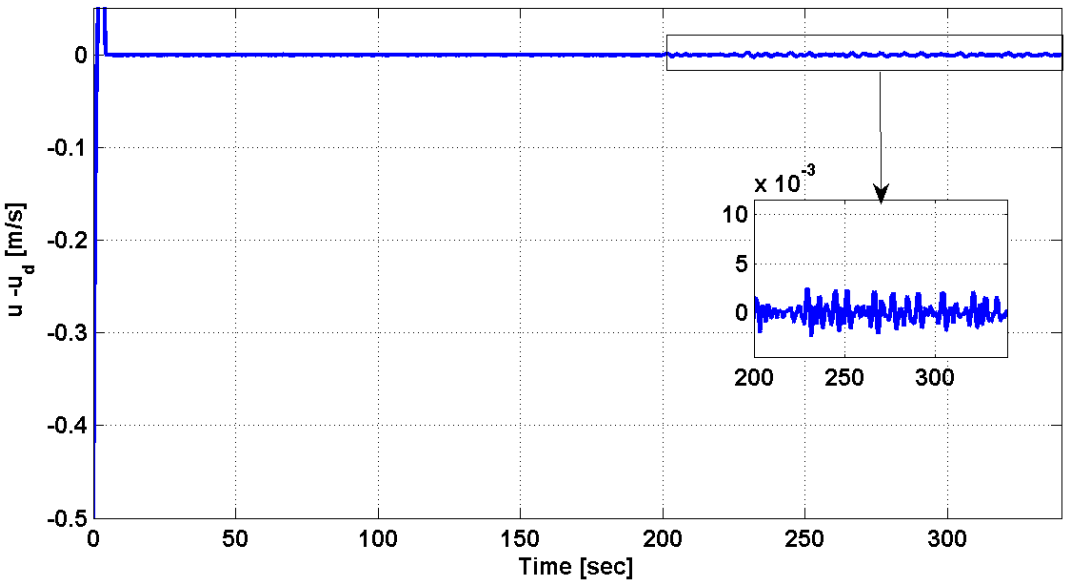

Fig. 5-7 Error between the actual and desired surge speed of the ship

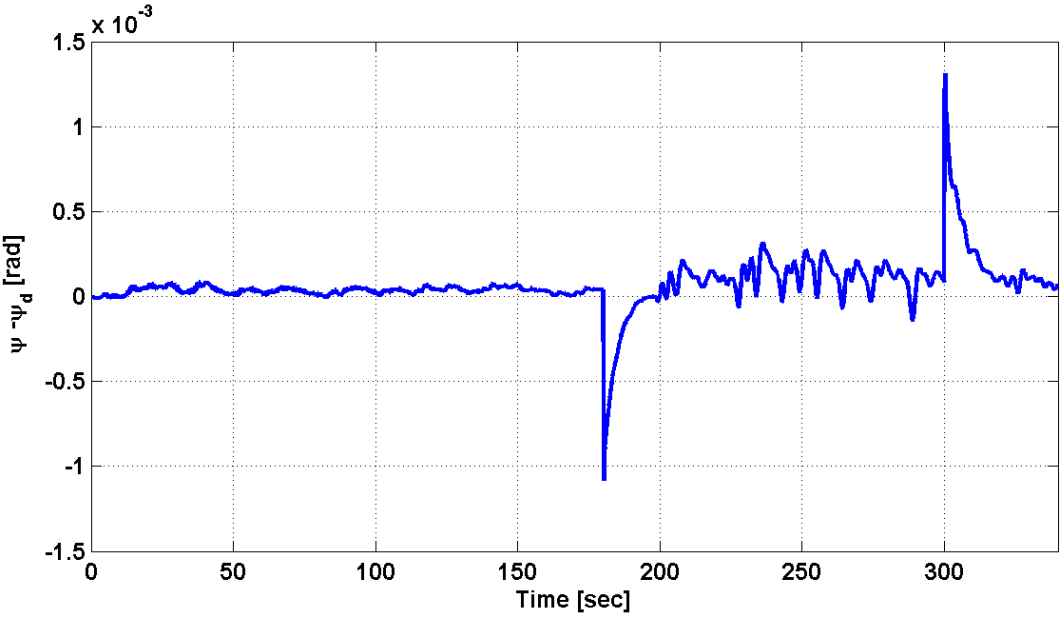

Fig. 5-8 Error between the actual and desired heading angle of the ship

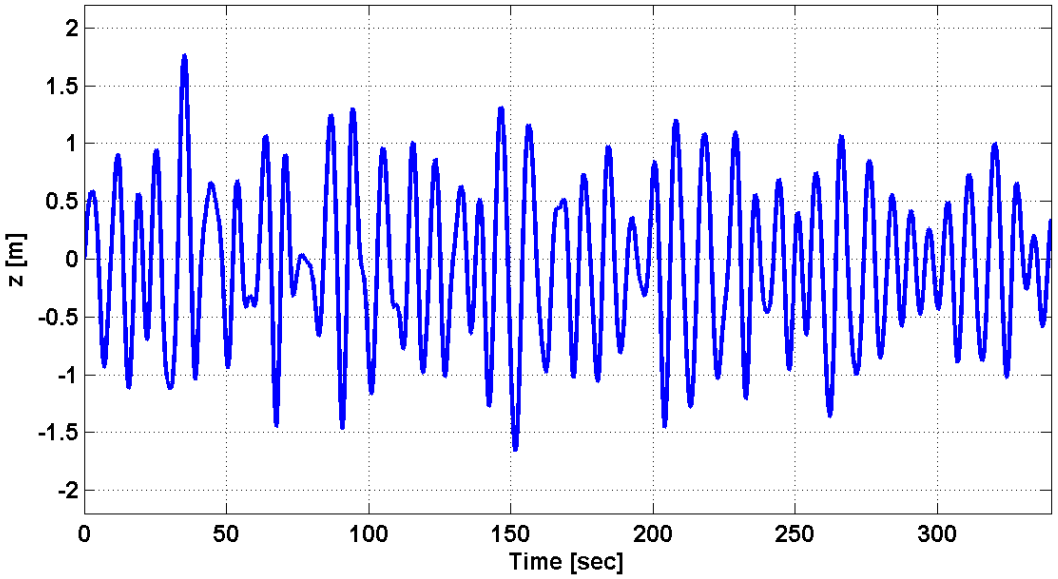

Fig. 5-9 Heave motion at the mass center of the ship

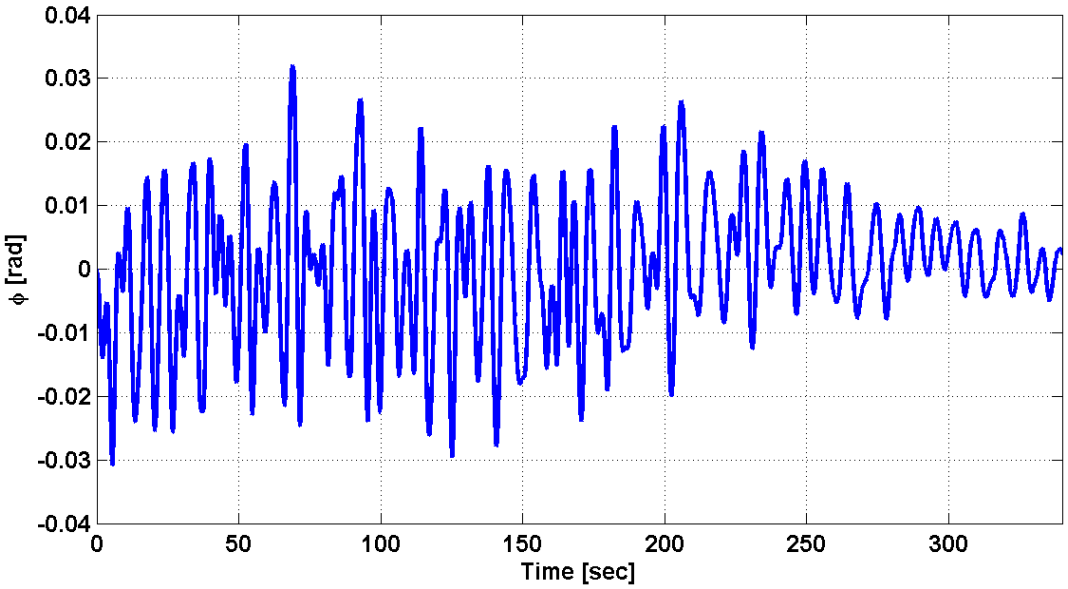

Fig. 5-10 Roll angular displacement of the ship

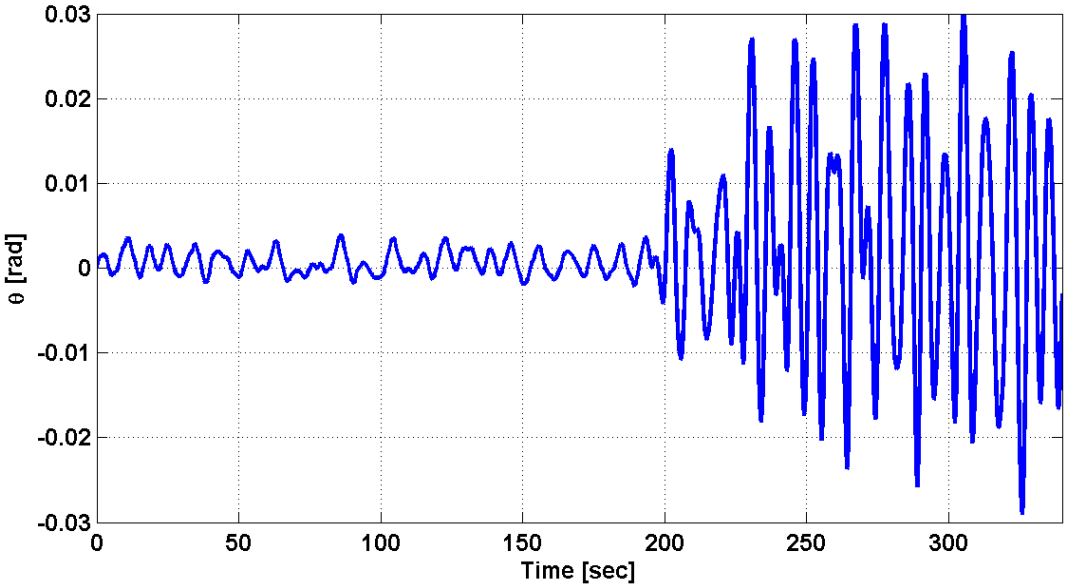

Fig. 5-11 Pitch angular displacement of the ship

CHAPTER 6 "DEVELOPMENT OF A ROBUST SELF-TUNING FUZZY SLIDING MODE OBSERVER"

In general, the implementation of the controller requires that the state variables of the system be available for the computation of the control signals. In the case where the state variables are not known through direct measurement then one has to design an observer to accurately estimate the unknown state variables in the presence of modeling uncertainties and external disturbances. The current chapter addresses this issue by providing a general procedure for designing a robust self-tuning fuzzy sliding mode observer. The observer will be applied herein to estimate the state variables of an under-actuated marine vessel. Subsequently, the observer will be coupled with the self-tuning fuzzy sliding mode controller of the previous chapter in order to generate a complete and robust control system. The simulation results will demonstrate the feasibility of the proposed control system.

6.1 General Procedure for Designing a Self-Tuning Fuzzy Sliding Mode Observer

Consider a nonlinear system whose dynamics are governed by the following second order differential equation:

$$\ddot{x} = \overline{f}\left(x, \dot{x}, u_c\right) \tag{6.1.1}$$

where u_c is the control variable and $\overline{f}\left(x, \dot{x}, u_c\right)$ is not considered to be fully known. By defining the state variables to be $x_1 \triangleq x$ and $x_2 \triangleq \dot{x}$, the equivalent state equations for (6.1.1) can be written as

$$\dot{x}_1 = x_2 = f_1\left(\underset{\sim}{x}, u_c\right) \tag{6.1.2a}$$

$$\dot{x}_2 = \overline{f}\left(x, \dot{x}, u_c\right) = f_2\left(\underset{\sim}{x}, u_c\right) \tag{6.1.2b}$$

Consider the structure of the self-tuning fuzzy sliding mode observer to be as follows

$$\dot{\hat{x}}_1 = \hat{x}_2 - K_1^o \operatorname{sgn}(s_o) \tag{6.1.3a}$$

$$\begin{aligned} \dot{\hat{x}}_2 &= \hat{f}_2\left(\underset{\sim}{\hat{x}}, u_c\right) + \frac{\sum_{i=1}^{m} w_i^{(o)} r_{i_t}^{(o)}}{\sum_{i=1}^{m} w_i^{(o)}} \\ &= \hat{f}_2\left(\underset{\sim}{\hat{x}}, u_c\right) + \left[\frac{\sum_{i=1}^{m} w_i^{(o)} r_i^{(o)}}{\sum_{i=1}^{m} w_i^{(o)}} - \gamma_o \left| s_o \right| s_o \frac{\sum_{i=1}^{m} w_i^{(o)^2}}{\left(\sum_{i=1}^{m} w_i^{(o)} \right)^2} \right] \end{aligned} \tag{6.1.3b}$$

where $\hat{f}_2\left(\underset{\sim}{\hat{x}}, u_c\right)$ is a nominal expression for the unknown function $f_2\left(\underset{\sim}{x}, u_c\right)$ evaluated based on the estimated state vector. The sliding surface for the observer, s_o, is selected to be

$$s_o \triangleq \hat{x}_1 - x_1 \triangleq \tilde{x}_1 \tag{6.1.4}$$

The first term between the square brackets of Eq. (6.1.3b) is a typical Sugeno-type FIS output. However, the second term is a switching function, which modifies the corrective action of the observer so that the estimation process is either continuously driven toward the sliding surface or forced to remain on it. By selecting the sliding surface to be the estimation error, as in Eq. (6.1.4), then the conditions of convergence to s_o or being on it become equivalent to reducing or eliminating the estimation error. As a

result, the robustness of the estimation scheme to external disturbances and modeling imprecision will be significantly enhanced. Furthermore, it should be noted that the switching term is heavily relied on to provide the corrective action of the observer during the initial phase of tuning the estimator.

Next, the estimation error vector is defined as

$$\underset{\sim}{\tilde{x}} \triangleq \underset{\sim}{\hat{x}} - \underset{\sim}{x} \tag{6.1.5}$$

Using Eqs. (6.1.2) and (6.1.3), the error equations can be written as

$$\dot{\tilde{x}}_1 = \tilde{x}_2 - K_1^o \operatorname{sgn}(s_o) \tag{6.1.6a}$$

$$\dot{\tilde{x}}_2 = \Delta f_2 + \frac{\sum_{i=1}^{m} w_i^{(o)} r_i^{(o)}}{\sum_{i=1}^{m} w_i^{(o)}} - \gamma_o |s_o| s_o \frac{\sum_{i=1}^{m} w_i^{(o)^2}}{\left(\sum_{i=1}^{m} w_i^{(o)} \right)^2} \tag{6.1.6b}$$

where Δf_2 is $\hat{f}_2(\underset{\sim}{\hat{x}}, u_c) - f_2(\underset{\sim}{x}, u_c)$. The gain K_1^o is determined by satisfying the following sliding condition (Chalhoub et al., 2006):

$$\frac{1}{2}\frac{d}{dt}\left(s_o^2\right) \le -\eta_o |s_o| \tag{6.1.7}$$

which leads to

$$K_1^o \ge \eta_o + \left|\tilde{x}_2\right|_{upper\ bound} \tag{6.1.8}$$

On the sliding surface, one would have

$$\dot{s}_o = \dot{\tilde{x}}_1 = 0 \quad \Rightarrow \quad \tilde{x}_2 = K_1^o \operatorname{sgn}(s_o) \tag{6.1.9}$$

Next, the following Lyapunov function is considered:

$$V_2 = \frac{1}{2}\tilde{x}_2^2 \tag{6.1.10}$$

The estimation error, $\tilde{x}_2$, can be constantly decreased by selecting the tuning rate parameter, γ_o, such that $\dot{V}_2 < 0$. This leads to the following inequality:

$$\frac{\Delta f_2}{\tilde{x}_2}\frac{K_1^o}{s_o^2}\frac{\left(\sum_{i=1}^{m} w_i^{(o)}\right)^2}{\sum_{i=1}^{m} w_i^{(o)^2}} + \frac{\sum_{i=1}^{m} w_i^{(o)} r_i^{(o)}}{\sum_{i=1}^{m} w_i^{(o)}}\frac{K_1^o}{s_o^2}\frac{\left(\sum_{i=1}^{m} w_i^{(o)}\right)^2}{\sum_{i=1}^{m} w_i^{(o)^2}}\frac{1}{\tilde{x}_2} < \gamma_o \tag{6.1.11}$$

Since Δf_2 is not known then it will be substituted in the above expression by its upper bound F_2^o. To avoid the overestimation of γ_o, $\tilde{x}_2$ in the second term of the above equation is substituted by $K_1^o \operatorname{sgn}(s_o)$ from Eq. (6.1.9), which is the value of $\tilde{x}_2$ when the system is on the sliding surface. This substitution is justifiable since the system will be kept either on or in the vicinity of s_o by ensuring that K_1^o satisfies the sliding condition in Eq. (6.1.7). Consequently, Eq. (6.1.11) can now be written as

$$\gamma_o > \frac{F_2^o}{\left|\tilde{x}_2\right|_{desired\_accuracy}}\frac{K_1^o}{s_o^2}\frac{\left(\sum_{i=1}^{m} w_i^{(o)}\right)^2}{\sum_{i=1}^{m} w_i^{(o)^2}} + \frac{\sum_{i=1}^{m} w_i^{(o)} r_i^{(o)}}{\sum_{i=1}^{m} w_i^{(o)}}\frac{\left(\sum_{i=1}^{m} w_i^{(o)}\right)^2}{\sum_{i=1}^{m} w_i^{(o)^2}}\frac{\operatorname{sgn}(s_o)}{s_o^2} \tag{6.1.12}$$

6.2 Design of a Self-Tuning Fuzzy Sliding Mode Observer for an Under-Actuated Ship

The general procedure, described in the previous Section, will now be implemented to design an observer for an under-actuated marine surface vessel. The rationale is to provide accurate estimates of the state variables, $\int_0^t r\,d\tau, u$ and r, which are needed for the implementation of the controllers described in Chapters 3 and 5.

In the current work, the available measurements are considered to be the heading angle along with the X and Y coordinates of the ship with respect to the inertial reference frame. The X and Y coordinates can be obtained from a global positioning system (GPS) while the yaw angle can be measured by an on-board gyro compass system (Fossen and Strand, 1999). Note that the measured variables are with respect to the inertial frame $\{X,Y,Z\}$ while the variables, needed for the computation of the control signals, should be defined with respect to the body-fixed reference frame $\{x,y,z\}$ (see Fig. 2-1). This issue has been resolved in this work by designing the observer to estimate the $X,Y,\psi,\dot{X},\dot{Y}$ and $\dot{\psi}$ variables with respect to the inertial frame. The variables, needed for the implementation of the controller, can be related to the estimated ones by rewriting Eq. (2.8) as follows

$$\begin{pmatrix} u \\ v \\ w \end{pmatrix} = \begin{pmatrix} c\psi c\theta & -s\psi c\phi + c\psi s\theta s\phi & s\psi s\phi + c\psi s\theta c\phi \\ s\psi c\theta & c\psi c\phi + s\psi s\theta s\phi & -c\psi s\phi + s\psi s\theta c\phi \\ -s\theta & c\theta s\phi & c\theta c\phi \end{pmatrix}^{-1} \begin{pmatrix} \dot{X} \\ \dot{Y} \\ \dot{Z} \end{pmatrix} \tag{6.2.1}$$

Since both roll and pitch angles are ignored in the design of the controller then their values can be set to zero. This yields the following relations:

$$\left(\int r d\tau\right)_e = \psi_e \tag{6.2.2a}$$

$$r_e = \dot{\psi}_e \tag{6.2.2b}$$

$$\begin{aligned}\begin{pmatrix} u_e \\ v_e \\ w_e \end{pmatrix} &= \begin{pmatrix} c\psi c\theta & -s\psi c\phi + c\psi s\theta s\phi & s\psi s\phi + c\psi s\theta c\phi \\ s\psi c\theta & c\psi c\phi + s\psi s\theta s\phi & -c\psi s\phi + s\psi s\theta c\phi \\ -s\theta & c\theta s\phi & c\theta c\phi \end{pmatrix}^{-1}_{\substack{\theta=0 \\ \phi=0 \\ \psi=\psi_e}} \begin{pmatrix} \dot{X}_e \\ \dot{Y}_e \\ \dot{Z}_e \end{pmatrix} \\ &= \begin{pmatrix} c\psi_e & s\psi_e & 0 \\ -s\psi_e & c\psi_e & 0 \\ 0 & 0 & 1 \end{pmatrix} \begin{pmatrix} \dot{X}_e \\ \dot{Y}_e \\ \dot{Z}_e \end{pmatrix} \quad \Rightarrow \quad u_e = c\psi_e \dot{X}_e + s\psi_e \dot{Y}_e\end{aligned} \tag{6.2.2c}$$

The observer is now designed based on the following state equations representing the dynamics of the system with respect to the inertial frame:

$$\begin{Bmatrix} \dot{x}_1 = \dot{X} \\ \dot{x}_2 = \dot{Y} \\ \dot{x}_3 = \dot{\psi} \\ \dot{x}_4 = \ddot{X} \\ \dot{x}_5 = \ddot{Y} \\ \dot{x}_6 = \ddot{\psi} \end{Bmatrix} = \begin{Bmatrix} x_4 \\ x_5 \\ x_6 \\ f_4(\underset{\sim}{x}, u_c) \\ f_5(\underset{\sim}{x}, u_c) \\ f_6(\underset{\sim}{x}, u_c) \end{Bmatrix} \tag{6.2.3}$$

All $f_4(\underset{\sim}{x}, u_c)$, $f_5(\underset{\sim}{x}, u_c)$ and $f_6(\underset{\sim}{x}, u_c)$ are considered to be unknown functions. They are roughly approximated by $\hat{f}_4(\underset{\sim}{\hat{x}}, u_c)$, $\hat{f}_5(\underset{\sim}{\hat{x}}, u_c)$ and $\hat{f}_6(\underset{\sim}{\hat{x}}, u_c)$, which are assigned the following simplified expressions:

$$\hat{f}_4(\underset{\sim}{\hat{x}}, u_c) = \frac{1}{m}\left(F_{th} - 10^7\right)\cos\hat{x}_3 \tag{6.2.4a}$$

$$\hat{f}_5(\underset{\sim}{\hat{x}}, u_c) = \frac{1}{m}\left(F_{th} - 10^7\right)\sin\hat{x}_3 \tag{6.2.4b}$$

$$\hat{f}_6(\underset{\sim}{\hat{x}}, u_c) = \frac{-F_{ry}\Delta_1}{I_z} \tag{6.2.4c}$$

The expressions of $\hat{f}_4(\hat{\underset{\sim}{x}},u_c)$, $\hat{f}_5(\hat{\underset{\sim}{x}},u_c)$, and $\hat{f}_6(\hat{\underset{\sim}{x}},u_c)$ are intentionally oversimplified in order to introduce considerable structured and unstructured uncertainties in the design of the observer.

Consider the following structure of the self-tuning fuzzy sliding mode observer:

$$\dot{\hat{x}}_i = \hat{x}_{i+3} - K_i^o \operatorname{sgn}(s_{o_i}) \qquad i = 1,\cdots,3 \tag{6.2.5a}$$

$$\dot{\hat{x}}_j = \hat{f}_j(\hat{\underset{\sim}{x}},u_c) + \left[\frac{\sum_{i=1}^{m} w_i^{(o_{j-3})} r_i^{(o_{j-3})}}{\sum_{i=1}^{m} w_i^{(o_{j-3})}} - \gamma_{o_{j-3}} \left| s_{o_{j-3}} \right| s_{o_{j-3}} \frac{\sum_{i=1}^{m} w_i^{(o_{j-3})^2}}{\left(\sum_{i=1}^{m} w_i^{(o_{j-3})} \right)^2} \right] \quad j = 4,\cdots,6 \tag{6.2.5b}$$

The sliding surfaces are defined as

$$s_{o_i} \triangleq \hat{x}_i - x_i \triangleq \tilde{x}_i \qquad i = 1,\cdots,3 \tag{6.2.6}$$

Define the estimation error vector as

$$\tilde{\underset{\sim}{x}} \triangleq \hat{\underset{\sim}{x}} - \underset{\sim}{x} \tag{6.2.7}$$

This will yield the following error equations:

$$\dot{\tilde{x}}_i = \tilde{x}_{i+3} - K_i^o \operatorname{sgn}(s_{o_i}) \qquad i = 1,\cdots,3 \tag{6.2.8a}$$

$$\dot{\tilde{x}}_j = \Delta f_j + \frac{\sum_{i=1}^{m} w_i^{(o_{j-3})} r_i^{(o_{j-3})}}{\sum_{i=1}^{m} w_i^{(o_{j-3})}} - \gamma_{o_{j-3}} \left| s_{o_{j-3}} \right| s_{o_{j-3}} \frac{\sum_{i=1}^{m} w_i^{(o_{j-3})^2}}{\left(\sum_{i=1}^{m} w_i^{(o_{j-3})} \right)^2} \quad j = 4,\cdots,6 \tag{6.2.8b}$$

where Δf_j is given by $\hat{f}_j(\hat{\underset{\sim}{x}},u_c) - f_j(\underset{\sim}{x},u_c)$. The gains K_i^o's are computed by satisfying the following sliding conditions:

$$\frac{1}{2}\frac{d}{dt}\left(s_{o_i}^2\right) \le -\eta_{o_i} \left| s_{o_i} \right| \tag{6.2.9}$$

This results in the following expressions:

$$K_i^o \geq \eta_{o_i} + \left|\tilde{x}_{i+3}\right|_{upper\ bound} \qquad i = 1,\cdots,3 \tag{6.2.10}$$

On the sliding surfaces, one has

$$\dot{s}_{o_i} = \dot{\tilde{x}}_i = 0 \quad \Rightarrow \quad \tilde{x}_{i+3} = K_i^o \,\mathrm{sgn}(s_{o_i}) \qquad i = 1,\cdots,3 \tag{6.2.11}$$

Introduce the following Lyapunov functions:

$$V_j = \frac{1}{2}\tilde{x}_j^2 \qquad j = 4,\cdots 6, \tag{6.2.12}$$

The estimation error, $\tilde{x}_j$ for $j = 4,\cdots,6$, can be constantly decreased by selecting the tuning rate parameter, γ_{o_i} for $i = 1,\cdots,3$, such that $\dot{V}_j < 0$ for $j = 4,\cdots,6$. Thus, one would get

$$\gamma_{o_i} > \frac{F_{i+3}^o}{\left|\tilde{x}_{i+3}\right|_{desired\_accuracy}} \frac{K_i^o}{s_{o_i}^2} \frac{\left(\sum_{i=1}^{m} w_i^{(o_i)}\right)^2}{\sum_{i=1}^{m} w_i^{(o_i)^2}} + \frac{\sum_{i=1}^{m} w_i^{(o_i)} r_i^{(o_i)}}{\sum_{i=1}^{m} w_i^{(o_i)}} \frac{\left(\sum_{i=1}^{m} w_i^{(o_i)}\right)^2}{\sum_{i=1}^{m} w_i^{(o_i)^2}} \frac{\mathrm{sgn}(s_{o_i})}{s_{o_i}^2} \quad i = 1,\cdots,3 \tag{6.2.13}$$

where Δf_{i+3} for $i = 1,\cdots,3$ are substituted by their upper bound values F_{i+3}^o, respectively.

6.3 Assessment of the Self-Tuning Fuzzy Sliding Mode Observer

The proposed self-tuning fuzzy logic observer has been implemented in the current work to estimate the heading angle, ψ, around the inertial $Z-$axis along with the X and Y coordinates of the ship with respect to the inertial reference frame. The simulation conditions, used in generating the results of Chapter 5, have also been adopted to produce the results of the current Chapter. Therefore, the full order nonlinear model of the ship along with the self-tuning fuzzy-sliding mode controller has

been used herein to generate the controlled response of the ship. The observer was only implemented to estimate the state variables. Since the simulation results are being generated for the sole purpose of assessing the performance of the observer then the actual state variables have been used in the computation of the control signals as shown in Fig. 6-1. The simulations were performed based on the ship parameters and environmental conditions listed in Table 5-1. The nominal model of the ship, given in Eqs. (6.2.3 and 6.2.4), has been incorporated in the design of the observer. The observer parameters are listed in Table 6-1.The initial conditions of the ship have been selected to be:

$$\begin{aligned} X(0) &= 4 \text{ m} & \dot{X}(0) &= 5.5 \text{ m/s} \\ Y(0) &= 4 \text{ m} & \dot{Y}(0) &= 0 \text{ m/s} \\ \psi(0) &= 0 \text{ rad} & \dot{\psi}(0) &= 0 \text{ rad/s} \end{aligned} \tag{6.3.1}$$

However, the initial conditions of the observer were defined as follows

$$\begin{aligned} \hat{X}(0) &= 5 \text{ m} & \dot{\hat{X}}(0) &= 0 \text{ m/s} \\ \hat{Y}(0) &= 5 \text{ m} & \dot{\hat{Y}}(0) &= 0 \text{ m/s} \\ \hat{\psi}(0) &= 0.05 \text{ rad} & \dot{\hat{\psi}}(0) &= 0 \text{ rad/s} \end{aligned} \tag{6.3.2}$$

In addition, all the body-fixed state variables of the ship were initially set to zero except for the surge speed which was set initially to $u(0) = 5.5\ m/\sec$.

Figures 6-2 to 6-7 demonstrate the capability of the proposed self-tuning fuzzy-sliding mode observer in accurately estimating X, Y, ψ along with their time derivatives in spite of significant modeling imprecision and external disturbances.

Figures 6-8 and 6-9 illustrate the desired, actual, and estimated ship surge speeds. The controller is proven to accurately track the desired surge speed in Fig. 6-8. However, the error between the actual and estimated surge speeds in Fig. 6-9 stems from ignoring the roll and pitch angles in the transformation matrix of Eq. 6.2.2c, which is being used to determine the surge speed, u_e, from the estimated ship variables $\dot{X}_e$, $\dot{Y}_e$, and ψ_e. Similarly, the discrepancies between r and r_e in Fig. 6-10 are due to the fact that r_e is considered to be $\dot{\psi}_e$, which was estimated based on a reduced-order model that ignores both roll and pitch angles. However, r was generated by the full-order model of the ship that accounts for the coupling between the roll, pitch and yaw angles.

6.4 Self-Tuning Fuzzy Sliding Mode Controller and Observer for an Under-Actuated Marine Vessel

The same set-up used in the previous section has been employed here with the exception that the control signals are now being computed based on estimated rather than actual values of the state variables (see Fig. 6-11). The robust performance of the observer is illustrated in Figs. 6-12 to 6-17.

Figure 6-18 reveals an error between the actual and desired surge speeds of the ship. This error is not caused by the inability of the controller in tracking the desired surge speed. Instead, it is induced by the estimation error in u_e, which is due to ignoring both the roll and pitch angles in the transformation matrix of Eq. 6.2.2c (see Fig. 6-19). Both Figs. (6-18 and 6-20) serve to demonstrate the good tracking characteristic of the proposed self-tuning fuzzy sliding mode observer and controller.

6.5 Summary

A general procedure for designing a self-tuning fuzzy sliding mode observer has been presented. The robust performance of the observer has been demonstrated by applying it to accurately estimate the state variables of an under-actuated marine surface vessel. Furthermore, the results demonstrate the viability of coupling the proposed observer with the self-tuning fuzzy sliding mode controller

In the next Chapter, the proposed controller/observer system will be integrated with a guidance system in order to construct a marine vessel that is capable of operating in an autonomous fashion.

Ship Data	
Length of the ship L_{PP}	100 m
Mass of the ship m_{ship}	7264000 Kg
Beam B	25 m
Draught T	8 m
Rudder Area A_{rud}	6 m^2
Maximum rudder angle $\alpha_{\max}$	22.5^0
Maximum rudder slew rate $\dot{\alpha}_{\max}$	19.5^0/sec
Environmental Conditions	
$H_{1/3}$ of the wave	8 m
Period of the wave spectrum T_0	9.01 sec
Incident angles of the wave, wind and current	90^0
Wind speed	20 m/s
Current speed	2 m/s
Self-tuning Fuzzy Sliding Mode Observer Parameters	
η_{o_1}	0.001
η_{o_2}	0.001
η_{o_3}	0.001
$\lvert\tilde{x}_4\rvert_{upper\ bound}$	9 m/sec^2
$\lvert\tilde{x}_5\rvert_{upper\ bound}$	1 m/sec^2
$\lvert\tilde{x}_6\rvert_{upper\ bound}$	0.1 rad/ sec^2

Table 6-1Ship data, environmental conditions and observer parameters.

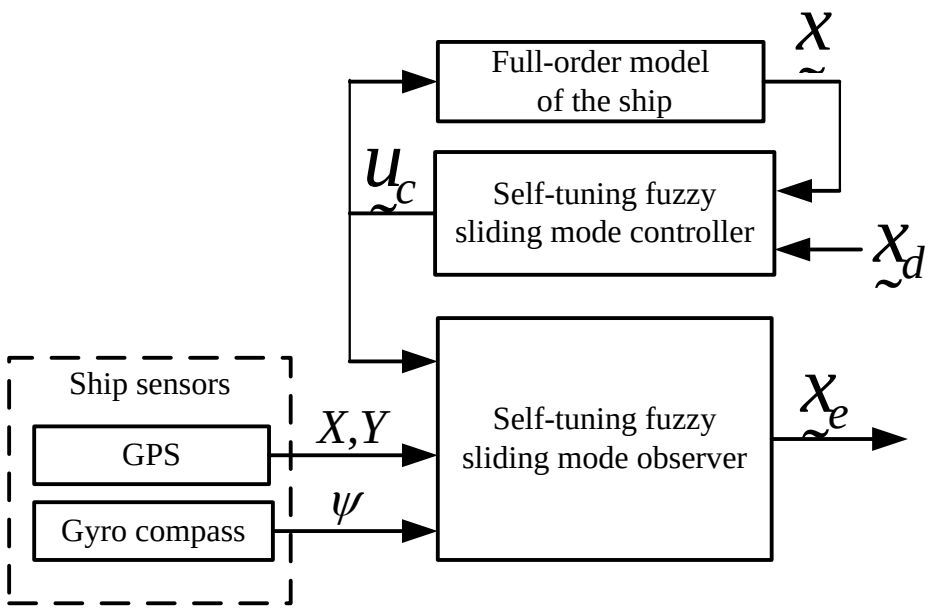

Fig. 6-1 Closed-loop system configuration used in assessing the performance of the observer.

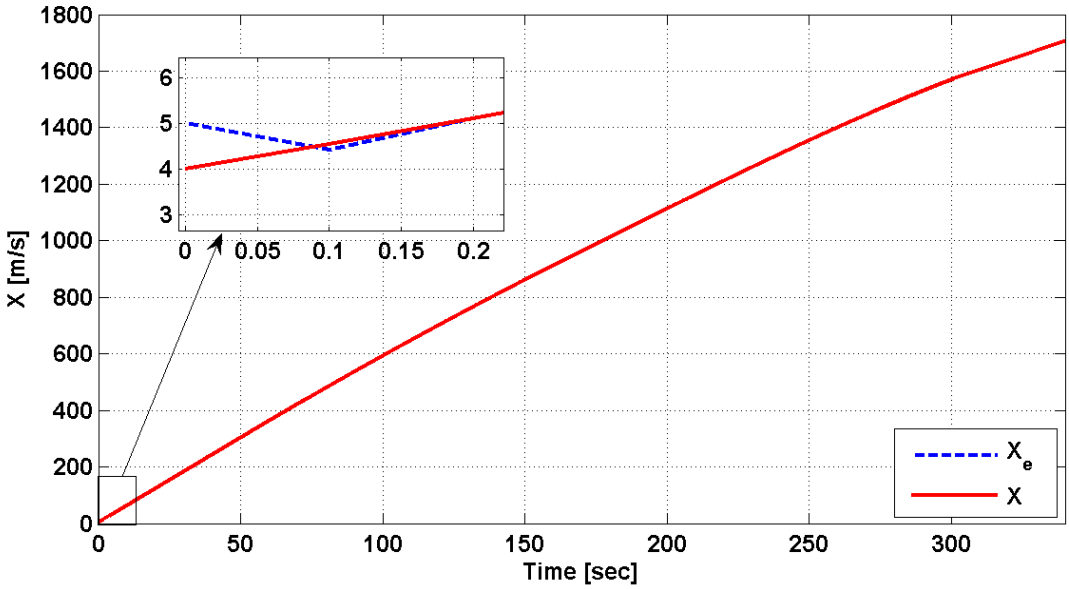

Fig. 6-2 Actual and estimated X coordinate of the ship with respect to the inertial frame.

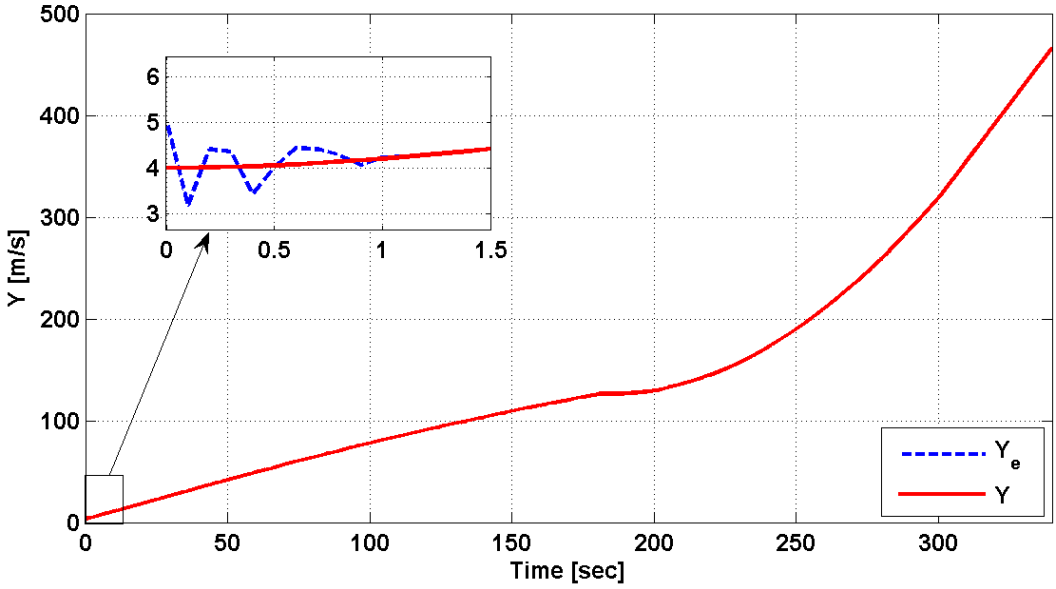

Fig. 6-3 Actual and estimated Y coordinate of the ship with respect to the inertial frame.

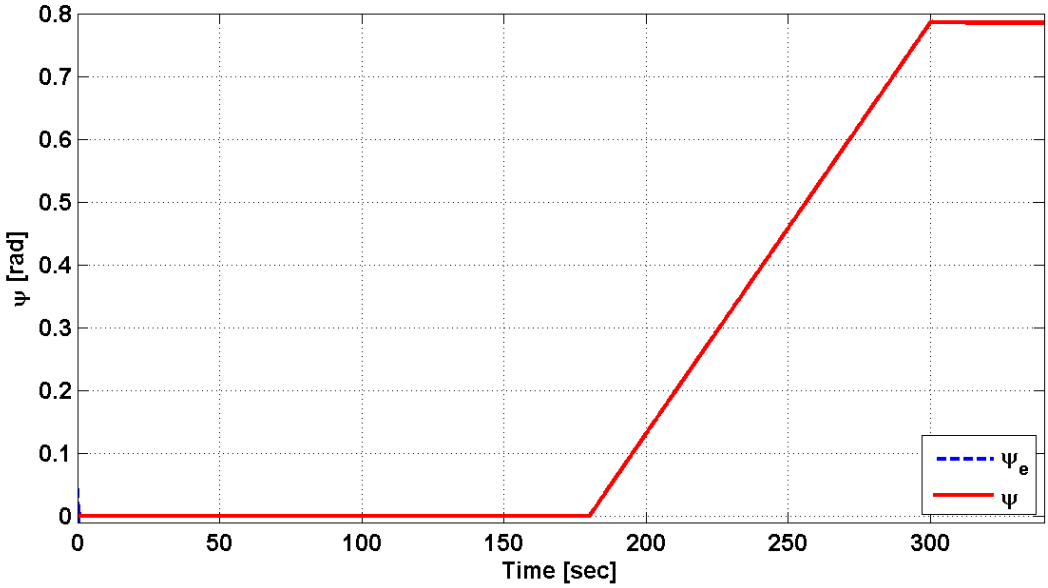

Fig. 6-4 Actual and estimated ψ coordinate of the ship with respect to the inertial frame.

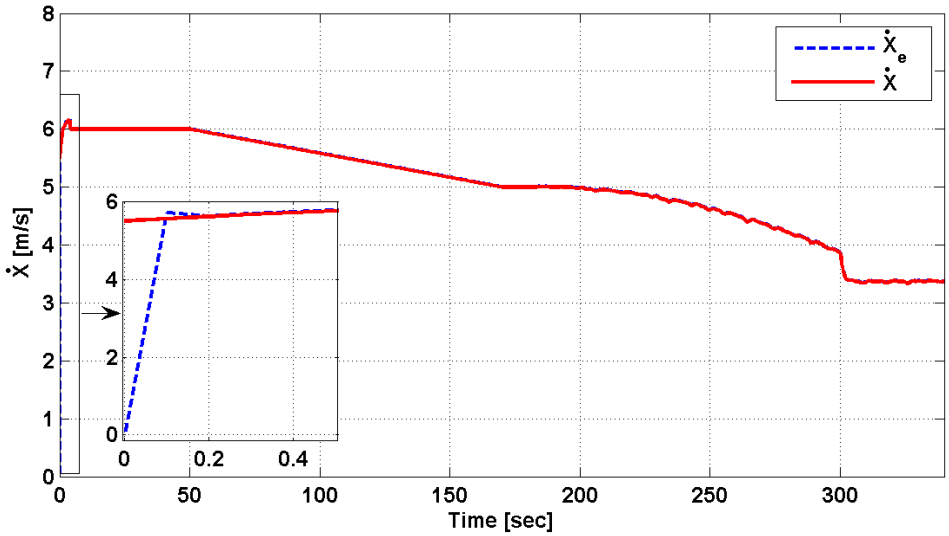

Fig. 6-5 Actual and estimated speed of the ship along the $X-$axis.

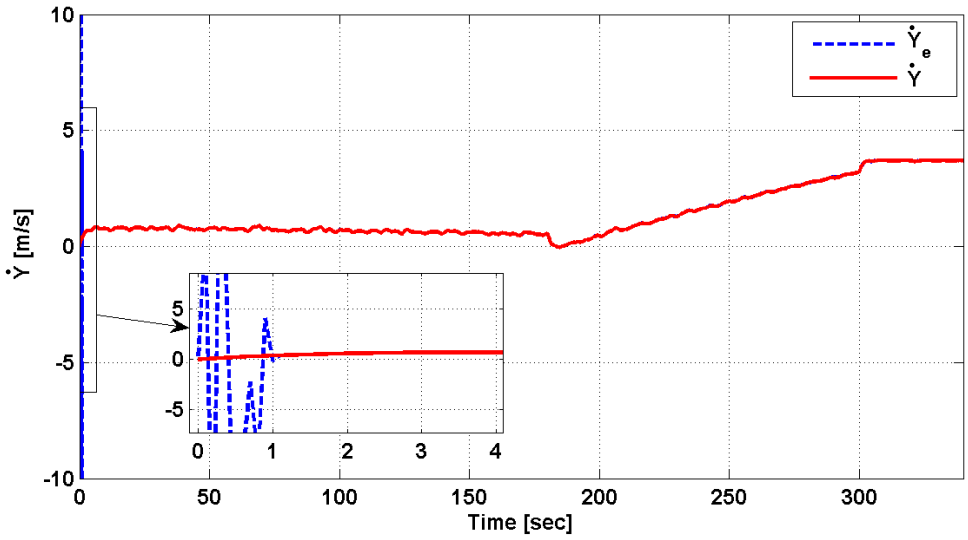

Fig. 6-6 Actual and estimated speed of the ship along the Y – axis.

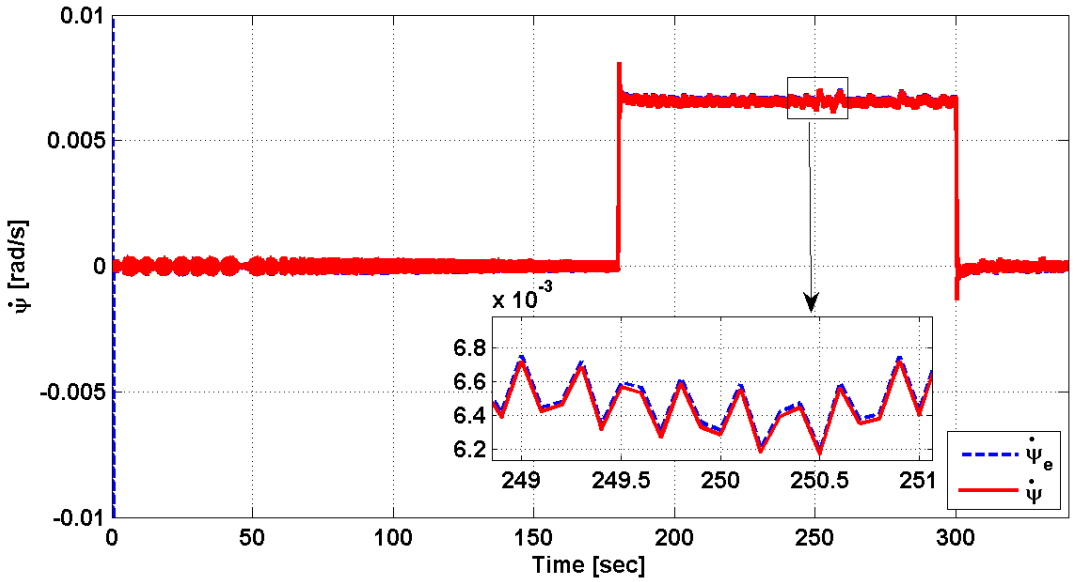

Fig. 6-7 Actual and estimated time rate of change of the heading angle around the Z – axis.

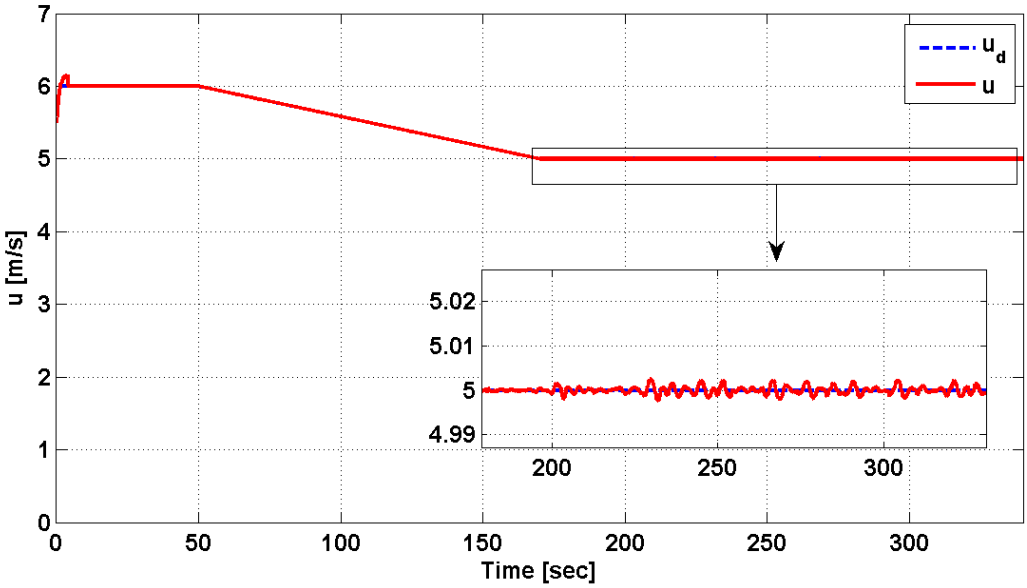

Fig. 6-8 Actual and desired speed of the ship defined with respect to the body-fixed coordinate system.

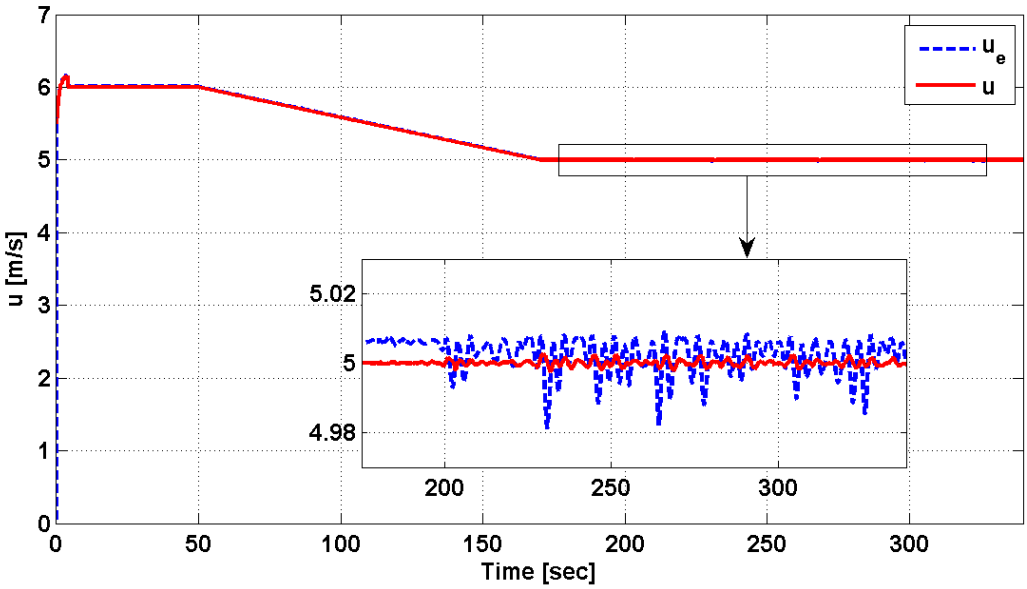

Fig. 6-9 Actual and estimated speed of the ship defined with respect to the body-fixed coordinate system.

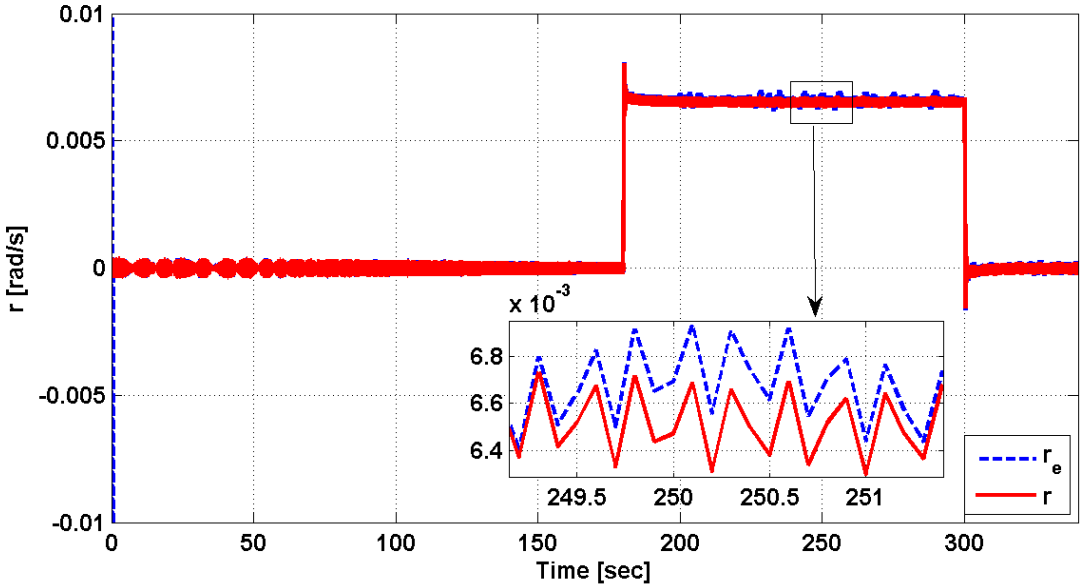

Fig. 6-10 Actual and estimated time rate of change of the ship heading with respect to the body-fixed coordinate system.

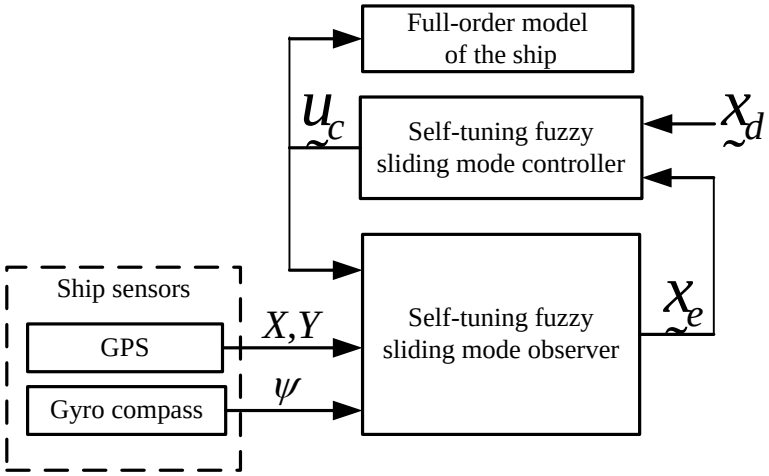

Fig. 6-11 Closed-loop system configuration used in assessing the performance of the coupled controller and observer.

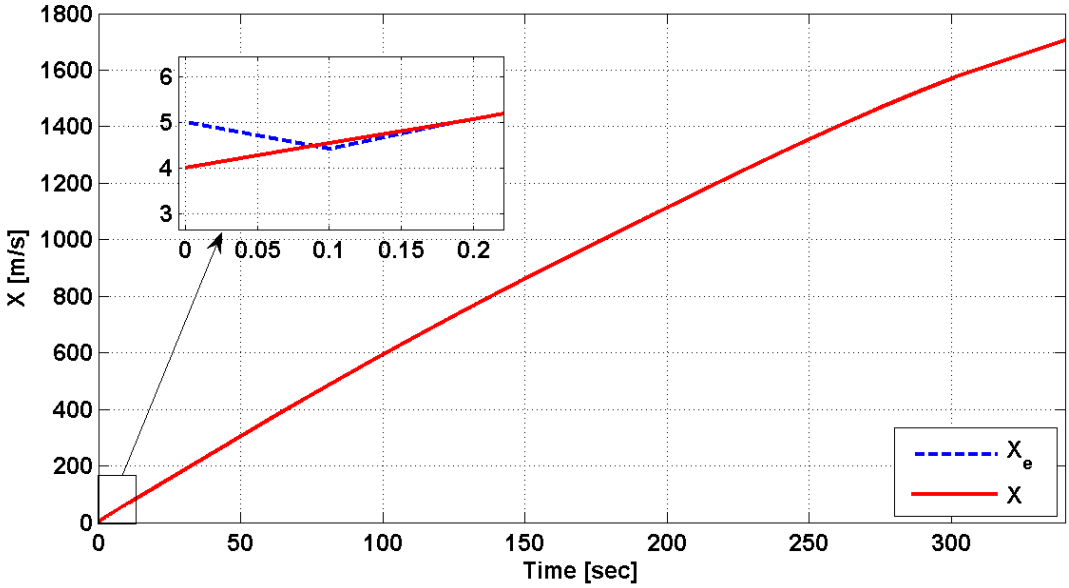

Fig. 6-12 Actual and estimated X coordinate of the ship with respect to the inertial frame.

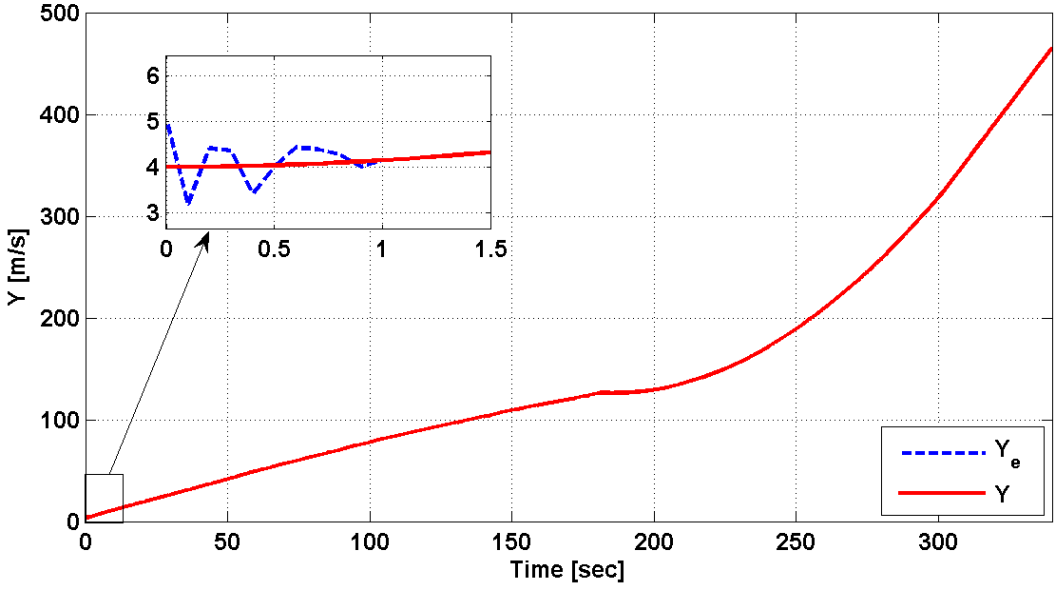

Fig. 6-13 Actual and estimated Y coordinate of the ship with respect to the inertial frame.

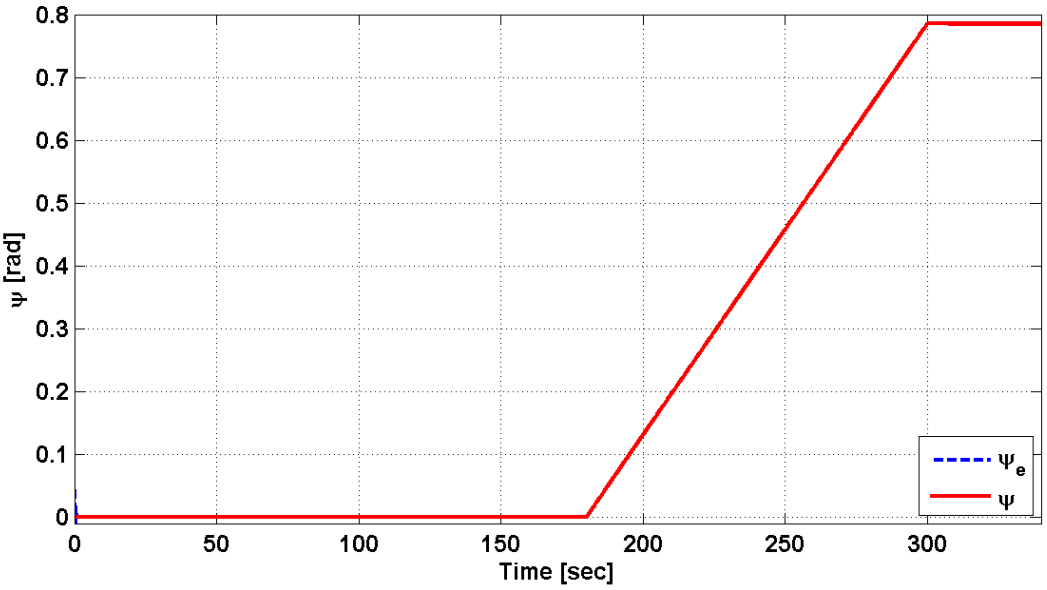

Fig. 6-14 Actual and estimated ψ coordinate of the ship with respect to the inertial frame.

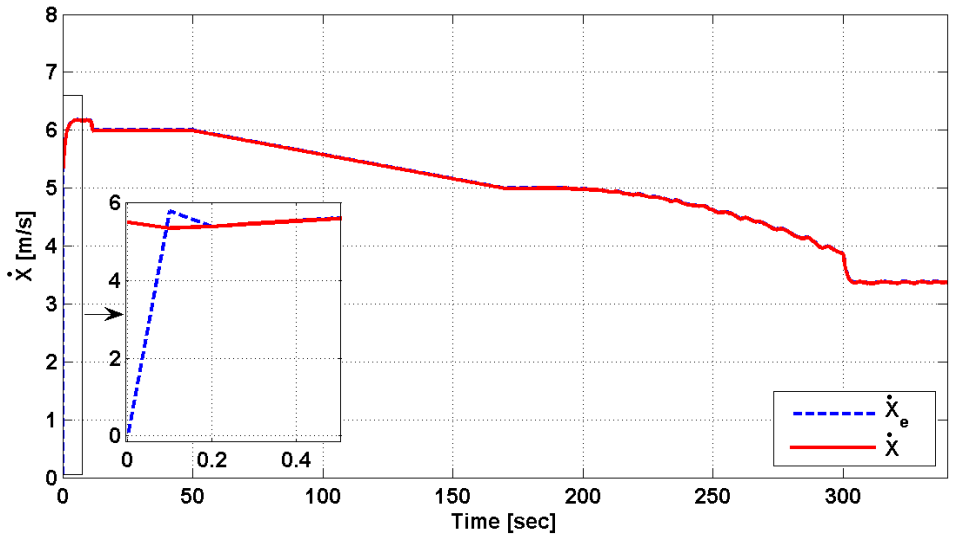

Fig. 6-15 Actual and estimated speed of the ship along the $X-$axis.

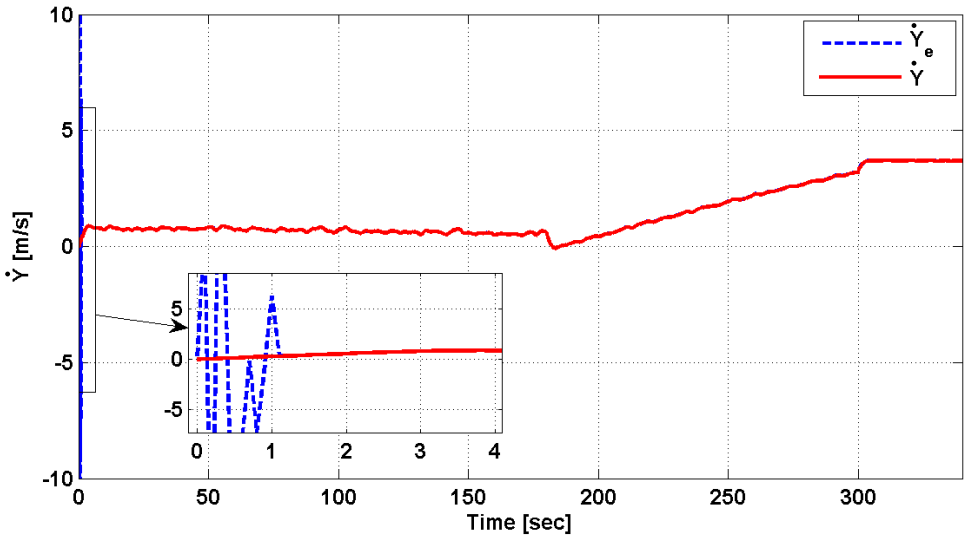

Fig. 6-16 Actual and estimated speed of the ship along the Y – axis.

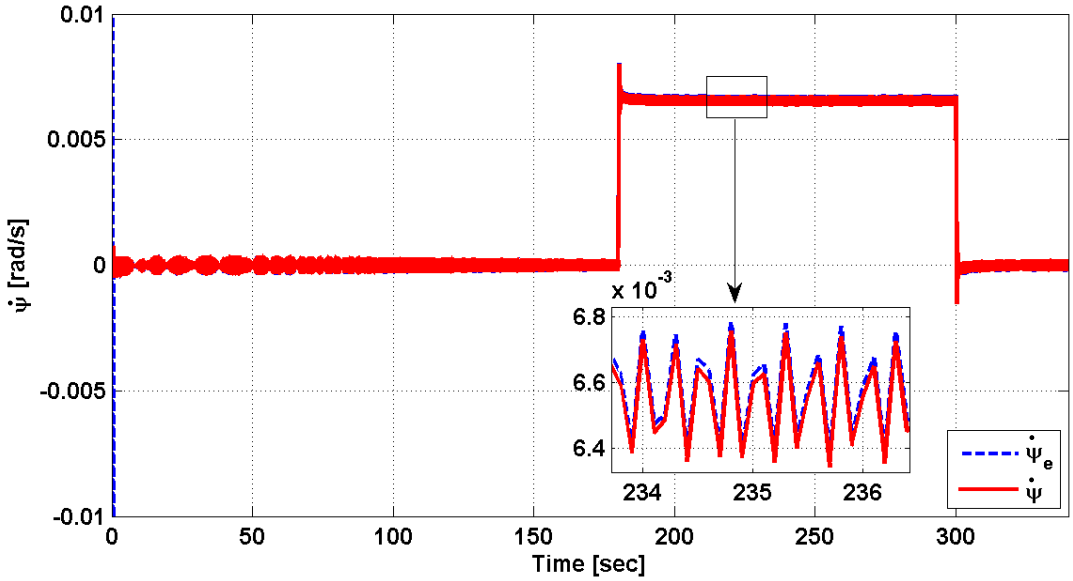

Fig. 6-17 Actual and estimated time rate of change of the heading angle around the Z – axis.

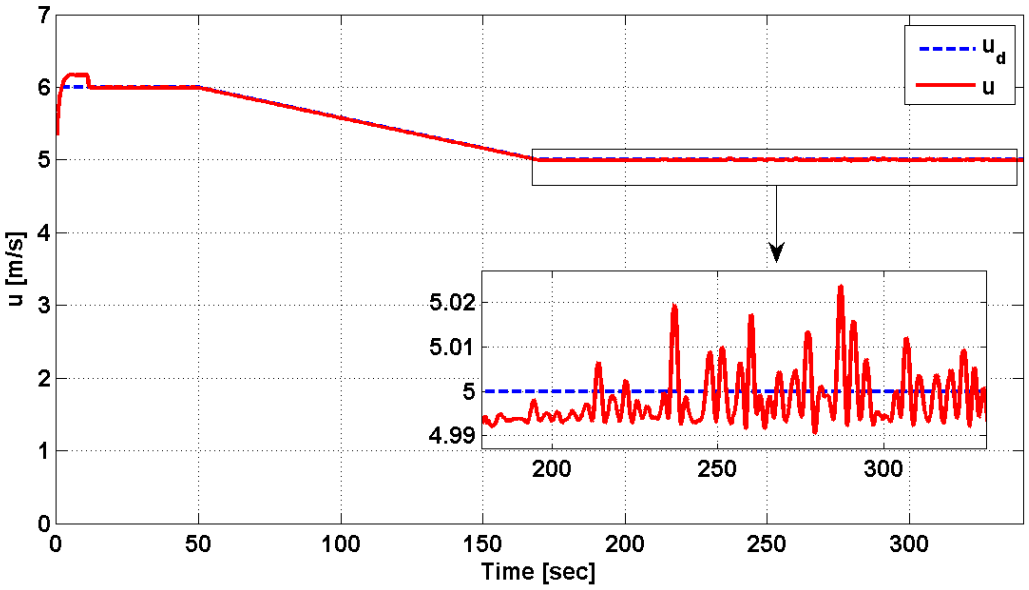

Fig. 6-18 Actual and desired surge speed of the ship.

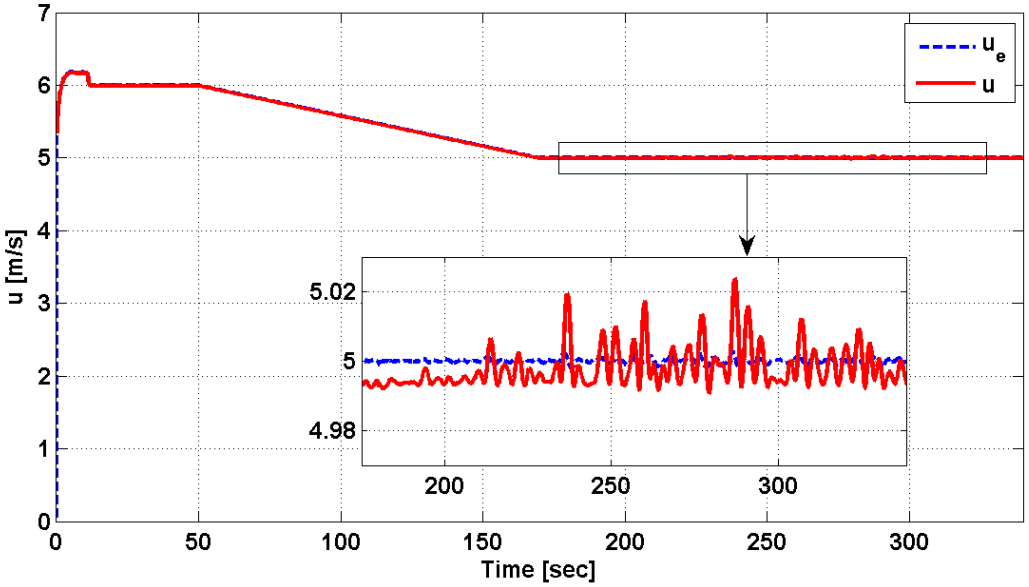

Fig. 6-19 Actual and estimated surge speed of the ship.

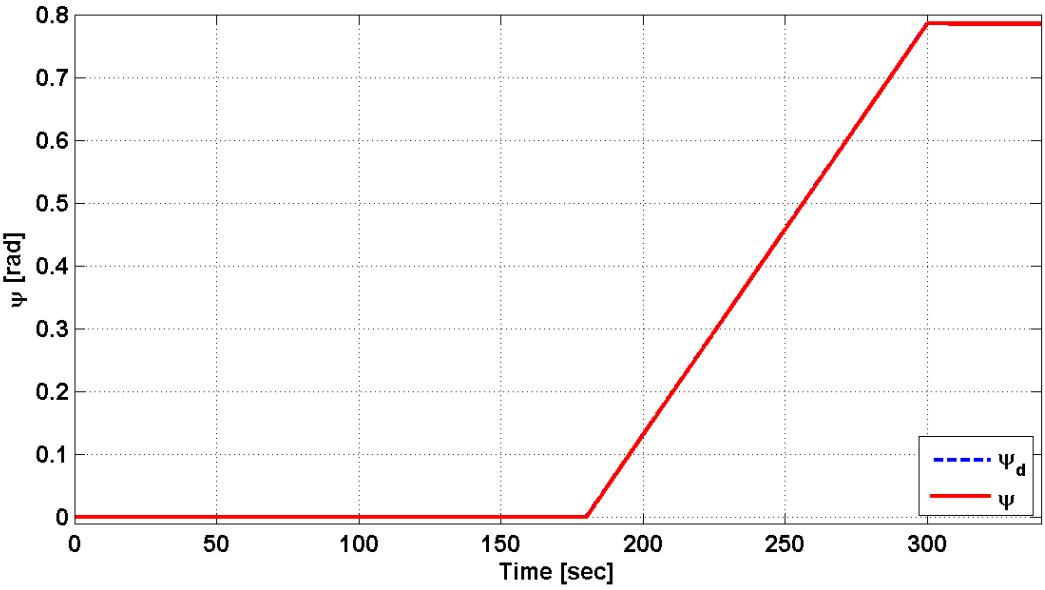

Fig. 6-20 Actual and desired heading angle of the ship.

CHAPTER 7 "GUIDANCE AND CONTROL SYSTEM FOR UNDERACTUATED MARINE SURFACE VESSELS"

Under-actuated marine surface vessels have a smaller number of actuators than the number of degrees of freedom that need to be controlled. This challenging control problem is usually dealt with by integrating the ship controller with a guidance system. Such an integrated system enables the ship to operate autonomously in pursuing a specified trajectory.

The present Chapter covers a newly proposed guidance system, which aims at yielding a faster rate of convergence over existing schemes in guiding the ship to its desired trajectory. The simulation results illustrate the robust performance of an under-actuated marine surface vessel operated autonomously by the proposed guidance and control systems. These systems consist of a guidance system with a sliding mode controller and observer or a guidance system with a self-tuning fuzzy sliding mode controller and observer.

7.1 Motivation for an Integrated guidance and Control System

The development of autonomous marine surface vessels necessitates the integration of the guidance system with the control algorithm. This is particularly true for under-actuated vessels whereby the ship has six rigid body degrees of freedom while the control actions are limited to the propeller thrust, F_{th}, and the rudder torque, T_{rud}. These two control actions are basically relied on to yield the desired position and orientation of under-actuated marine surface vessels. The propeller thrust is mainly used for forward or surge speed control. While the rudder torque yields the desired rudder angle of attack, which is relied on to steer the marine vessel to the desired

trajectory. By coupling the controller with the guidance system, the steering controller will be empowered to simultaneously address control issues pertaining to sway displacement and ship heading (Fossen, 2002; Fossen et al., 2003; Healey and Marco, 1992; Breivik, 2003; Moreira et al., 2007).

7.2 Current Guidance Systems of Marine Surface Vessels

The guidance system specifies the desired heading angle that will yield the proper orientation of the ship and reduce the cross-track error. The latter is defined to be the relative position of the ship with respect to the desired trajectory. A guidance system, based on the line-of-sight (LOS) concept, has been reported in the literature (Fossen, 2002; Fossen et al., 2003; Healey and Marco, 1992; Breivik, 2003; Moreira et al., 2007). The scheme considers that the desired trajectory is defined by a series of way-points connected by straight lines (see Fig. 7-1). Let the coordinates of the ship be given by (x, y). Assume that the ship location is in the vicinity of the straight line joining two consecutive way-points, (x_k, y_k) and (x_{k+1}, y_{k+1}), on the desired trajectory. Consider a circle centered at (x, y) with a radius, R. The latter is usually chosen to be $\bar{n}L_{pp}$, which is a multiple ship length, L_{pp}. Note that $\bar{n}$ should be greater or equal to 1; otherwise, the ship will oscillate around the desired trajectory. When the vessel is in the vicinity of the desired trajectory, the circle will intersect the line passing through (x_k, y_k) and (x_{k+1}, y_{k+1}) at two points, A_B and A_F. This is shown in Fig. 7-1 where A_F corresponds to the intersection point that is closest to the (x_{k+1}, y_{k+1}) way-point. The arrow starting at the current ship location, (x, y), and ending at point A_F is denoted by the line-of-sight (LOS). The angle between the LOS and the reference $X-$axis is given

by $a\tan 2\left(\left(y_{A_F}-y\right),\left(x_{A_F}-x\right)\right)$, which is considered to be the desired heading angle, ψ_d. This is because a ship moving along the direction of LOS will eventually head towards the desired trajectory.

The initial concept of LOS (Moreira et al., 2007) incorporates a circle with a constant radius, R. Such a scheme fails to provide any guidance and becomes inapplicable whenever the cross-track error exceeds the radius. Moreira and his co-workers (2007) presented a guidance scheme that varies R linearly with the cross-track error (see Figs. 7-2 and 7-3). By choosing R to be $d+L_{pp}$, the guidance system will always yield an appropriate value for ψ_d that will guide the ship to the desired trajectory irrespective of the magnitude of the cross-track error (Moreira et al., 2007).

7.3 Modified Guidance Systems of Marine Surface Vessels

The guidance system, used in this work, represents a modified version of the scheme presented in the previous Section (Moreira et al., 2007). It is capable of handling any cross-track error while yielding faster convergence rate of the ship to its desired trajectory than the one obtained by varying R linearly with d. This goal has been accomplished herein by varying the radius exponentially with the cross-track error. This is illustrated in Fig. 7-3, which reveals that the proposed exponential variation scheme yields significantly smaller values for R than the linear variation method for all cross-track errors. Note that the desired heading angle, ψ_d, becomes steeper as the radius is decreased. The proposed scheme, illustrated in Fig. 7-3, tend not to over-react for small cross-track errors by gradually and slowly varying R. On the other hand, it sets the radius to be equal to d for large cross-track errors; thus, causing the straight

line joining the way-points to become tangential to the circle. This translates into driving the ship at its steepest heading angle possible toward the desired trajectory. In a sense, the proposed scheme varies the radius exponentially for small values of d and linearly for large values of the cross-track error (see Fig. 7-3). The rationale is to improve the convergence rate to the desired trajectory by guiding the ship with a steep heading angle while keeping the guidance scheme applicable for any cross-track error.

The proposed exponential variation scheme for R is derived by considering two coordinate system $\{d, R\}$ and $\{d', R'\}$ where the latter frame is generated by rotating the former frame by 45^o (see Fig. 7-4). The exponential curve is defined with respect to the $\{d', R'\}$ coordinate system as follows

$$R' = R'_{\min} e^{-bd'} \tag{7.3.1}$$

Now, the portion of the exponential curve in the region where both R and d assume positive values can be expressed with respect to the $\{d, R\}$ frame as follows

$$R = d + \sqrt{2} R'_{\min} e^{-b\bar{d}'} \tag{7.3.2}$$

with

$$\bar{d}' = b^{-1}\left[Lambertw(bR'_{\min} e^{-\left(0.5\sqrt{2}bd\right)}) + 0.5\sqrt{2}bd \right] \tag{7.3.3}$$

$$R'_{\min} = \frac{R_{\min}}{\sqrt{2}} e^{-\frac{bR_{\min}}{\sqrt{2}}} \tag{7.3.4}$$

where Lambert-W function is the inverse function of $f(x) = xe^x$. $R_{\min}$ is the minimum radius allowable and b is a parameter controlling the decay rate of the exponential

term. They are selected herein to be $1.7L_{pp}$ and 0.05, respectively. Note that Eq. (7.3.2) yields $R \simeq d$ for large values of d, which results in a circle tangential to the desired trajectory . As a consequence, ψ_d now represents a normal direction to the desired trajectory. Thus, the ship will be guided along the shortest path between its current position and the desired trajectory. For low values of d, R becomes dominated by the exponential term and increases at a lower rate than the linear expression defined by $R = d + R_{\min}$ (see Fig. 7-3). Lower values of R reflect steeper angles for ψ_d, which lead to a faster convergence rate of the ship to its desired trajectory (see Fig. 7-2). Moreover, Fig. 7-3 demonstrates that the proposed approach yields smaller values for R than the linear scheme for all values of d. Thus, the proposed method is expected to provide closer guidance to the desired trajectory than the linear approach.

Furthermore, the current guidance system has been designed to shift from the pair of way-points to the succeeding $\{(x_{k+1}, y_{k+1}), (x_{k+2}, y_{k+2})\}$ pair whenever the ship enters a circle of acceptance centered at the (x_{k+1}, y_{k+1}) way-point with a radius chosen for the present work to be $2.2L_{pp}$ (see Fig. 7-2).

7.4 Digital Simulation Results

The current guidance system has been combined with the controllers and observers, discussed in earlier Chapters, to yield an integrated system that enables surface marine vessels to autonomously track desired trajectories. First, the performance of the integrated guidance system with sliding mode controller and observer is examined. Second, the performance of the guidance system with the self-tuning fuzzy-sliding mode controller and observer is assessed. All simulation results were generated based on the

same desired trajectory whose general profile was adopted from the work of Moreira et al. (2007). However, the coordinates of its way points were modified to suit the length of the ship employed in the current study. Table 7-1 lists the coordinates of the desired way points, which are plotted in Fig. 7-5. Furthermore, the vessel geometric dimensions, control and observer parameters along with the environmental conditions are listed in Table 4-1 and Table 6-1. The integrated guidance and control system has been tested on the full-order model of the ship. The initial conditions for the state variables, defined with respect to the body-fixed coordinate system, were all set to zero with the exception of the initial surge speed, which was selected to be $u(0) = 5.5\,m/s$. The initial conditions for the state variables, defined with respect to the inertial coordinate system, were considered to be the same as those defined in Eqs. (6.3.1) and (6.3.2).

7.4.1 Assessment of the Guidance System with the Sliding Mode Controller and Observer

The results in this Section were generated based on the guidance system, with an exponentially varying radius, along with the sliding mode controller and observer that were covered in Chapters 3 and 4, respectively. Figure 7-5 demonstrates the capability of the proposed guidance and control system in tracking the desired trajectory of the ship. The cross track errors near the way points are induced by the fact that the ship is a non-minimum phase system, which has a tendency to move in an opposite direction to the intended one at the onsets of maneuvers around the way points. This is clearly shown in Fig. 7-6. Figure 7-7 reveals the variations in the radius, R, that are initiated by the guidance system in order to cope with large cross-track errors.

The actual and desired heading angles of the ship are shown in Fig. 7-8. The discrepancies between the two curves are solely caused by the saturation of the rudder angle-of-attack during severe maneuvers of the ship around way points E, F, and G (see Fig. 7-5). This explanation is confirmed in Fig. 7-9, which exhibits perfect match between the estimated and actual heading angles of the ship.

The actual and desired surge speeds of the vessel are shown in Fig. 7-10. It should be stressed that the steady-state error between the u_d and u curves is caused by the estimated value of the surge speed, u_e, which led the surge speed controller to believe that it has reached its desired value, u_d (see Fig. 7-11). This is clearly illustrated in Fig. 7-12, which shows an almost zero steady-state error between u_d and u_e.

Figures 7-13 to 7-18 demonstrate the robust performance of the observer in accurately estimating X, Y and ψ along with their time derivatives in the presence of considerable modeling imprecision and external disturbances. The comparison between Figs. 7-18 and 7-19 reveals that the error between $\dot{\psi}$ and $\dot{\psi}_e$ is smaller than the error between r and r_e. This is due to the fact that r_e is determined by setting it equal to $\dot{\psi}_e$; thus, ignoring the effects of roll and pitch angles in its computation. The current approximation for r_e is justifiable for small roll and pitch angles as shown in Figs. 7-18 and 7-19.

For ease of discussion, the guidance system with a linearly varied radius is referred to throughout the remainder of this document by the “linear guidance” system. While the guidance system, with an exponentially varied radius, is called “exponential guidance” system. The performances of the linear and exponential guidance schemes

are assessed by implementing them with the same sliding mode controller and observer on the marine vessel. The results, shown in Figs. 7-20 to 7-22, demonstrate that the exponential scheme yields a faster convergence rate to the desired trajectory than the linear one. However, the same figures have also revealed that the exponential guidance system suffer from a larger cross track error than the one obtained by the linear guidance technique during a brief and specific period of the ship maneuver around a way point (see Figs. 7-23 and 7-24). This is because the exponential guidance approach causes the ship to operate at a steeper heading angle than the one specified by the linear guidance scheme. As a consequence, the rudder angle-of-attack remains locked at its saturated value for a longer period of time in the case of the exponential than the linear scheme. This causes the period, during which the ship is uncontrollable during a maneuver, to become relatively longer in the case of the exponential guidance system than in the linear one.

7.4.2 Assessment of the Guidance System with the Self-Tuning Fuzzy-Sliding Mode Controller and Observer

In this Section, the performance of the integrated system, consisting of the "exponential" guidance system with the self-tuning fuzzy-sliding mode controller and observer of Chapters 5 and 6, is assessed on the full-order model of the surface marine vessel. Figures 7-25 to 7-32 demonstrate the robust performance of the guidance and control system in tracking the desired trajectory of the ship in spite of significant modeling imprecision and external disturbances. Most of the discussion carried out in the previous Subsection are applicable to the current case and will not be repeated here.

Figures 7-33 to 7-39 concentrate on illustrating the good performance of the self-tuning fuzzy-sliding mode observer in accurately estimating the state variables with respect to the inertial reference frame. With regard to the effects of linear versus exponential variations of the radius in the guidance scheme, the results of Figs. 7-40 to 7-44 show the same pattern of response of the ship as the one observed in the case of the integrated system with the sliding mode controller and observer.

Next, the performance of the “exponential” guidance system with a sliding mode controller and observer is compared to that of an “exponential” guidance scheme with a self-tuning fuzzy-sliding mode controller and observer. Figure 7-45 reveals that the difference in the ship responses, generated by implementing the two guidance and control systems, are hardly noticeable. Therefore, the two approaches, proposed in the current work, have comparable robustness and tracking characteristics.

7.5 Summary

This Chapter gives an overview of guidance systems developed for marine surface vessels. Moreover, a guidance scheme, based on the concepts of the variable radius line-of-sight (LOS) and the acceptance radius, is presented whereby the radius of the line-of-sight is varied exponentially with the cross track error. The current technique can handle large cross-track errors while aiding the controller to quickly converge the ship to its desired trajectory. The performance of the guidance scheme is tested herein under two guidance and control systems. The first uses a sliding mode controller and observer while the second employs a self-tuning fuzzy-sliding mode controller and observer. The results demonstrate that both guidance and control systems have similar robustness and tracking characteristics.

The entire work is summarized in the next Chapter. The main conclusions are highlighted and the contributions of the current study are clearly stated. In addition, potential future research topics that can build on the outcome of the present study are suggested.

Way Point Label	X-coordinate	Y-coordinate
A	0	0
B	615.4	153.8
C	923	1538.5
D	-923	2923.1
E	0	4307.7
F	-923	4615.4
G	615.4	6000
H	0	2769.2
A	0	0

Table 7-1Desired way points coordinates

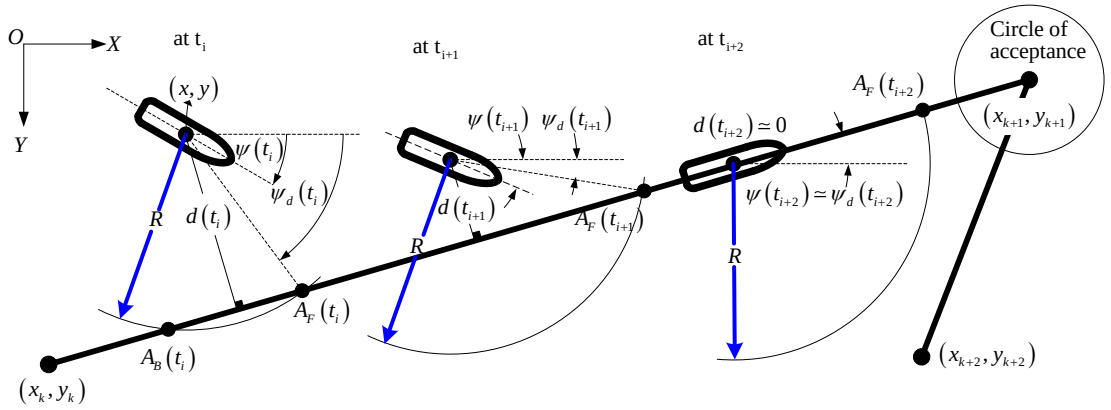

Fig. 7-1 LOS Guidance scheme based on a constant radius.

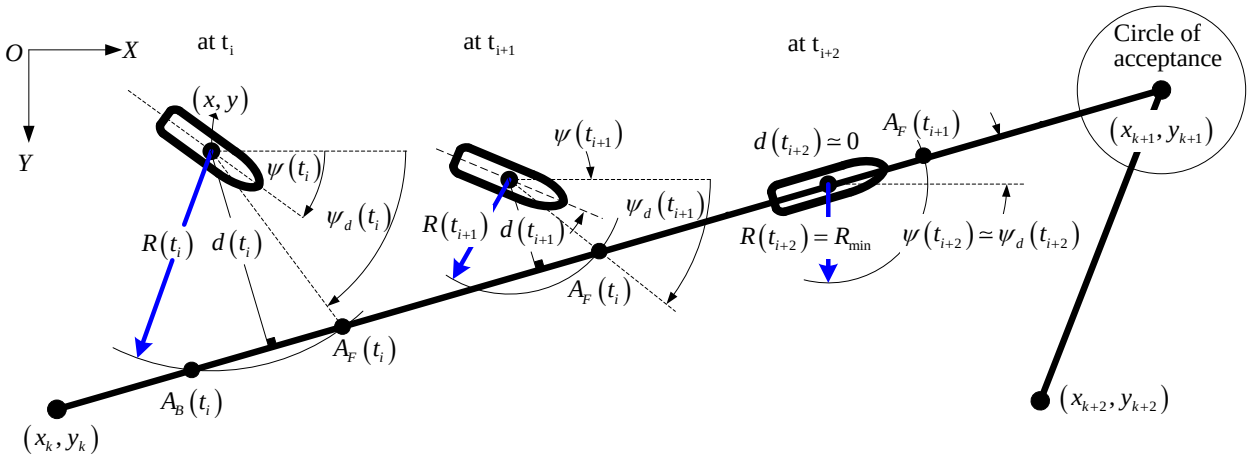

Fig. 7-2 LOS Guidance scheme based on a variable radius.

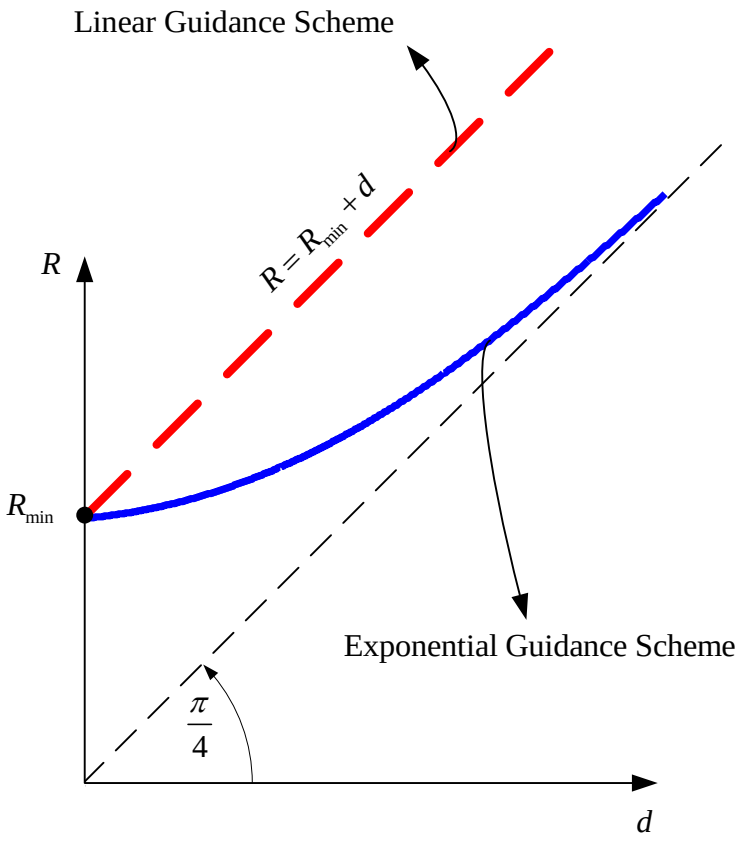

Fig. 7-3 Linear and proposed schemes for varying R.

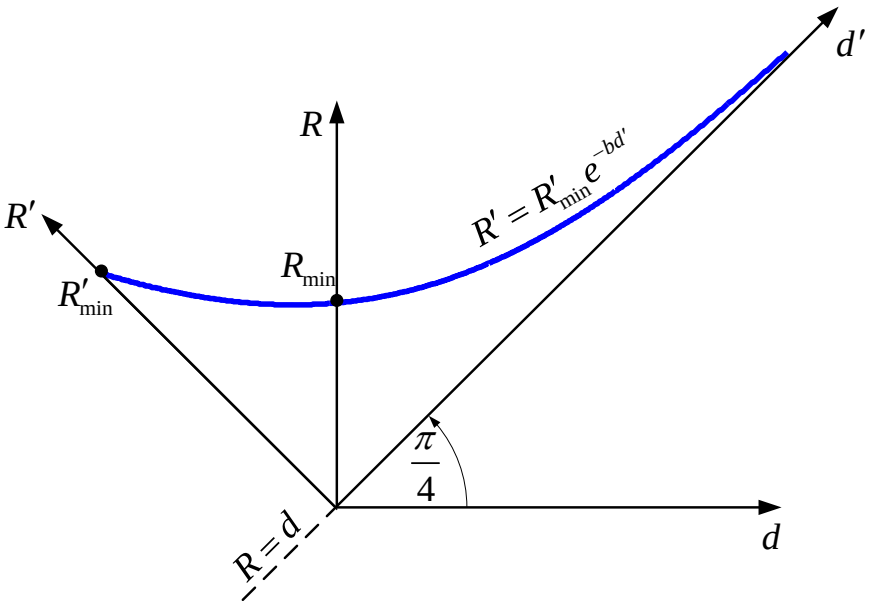

Fig. 7-4 Exponential variations of R.

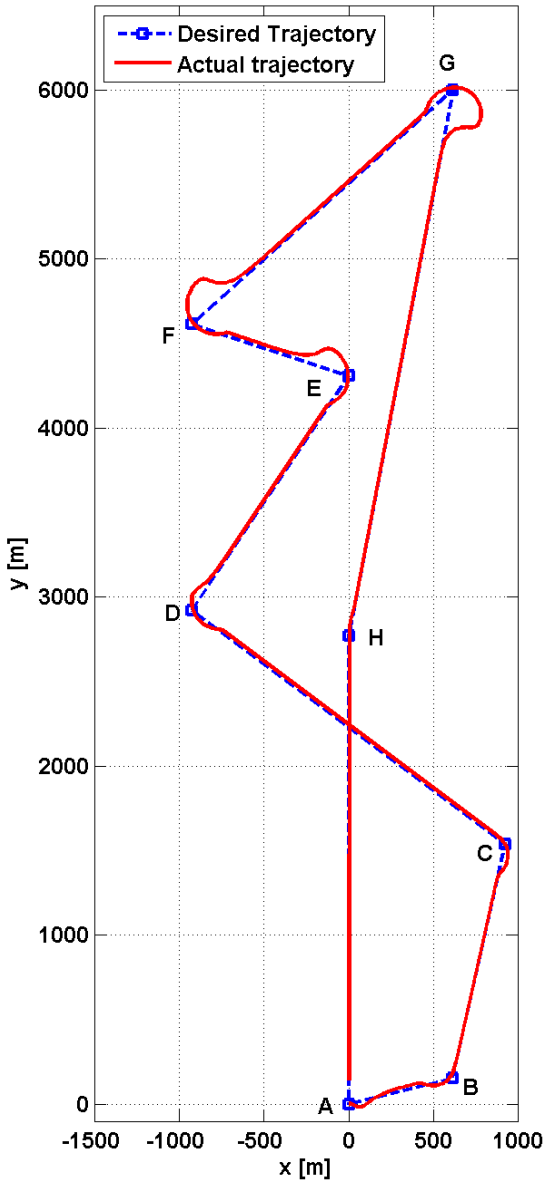

Fig. 7-5 Performance of the "exponential" guidance scheme with the sliding mode controller and observer.

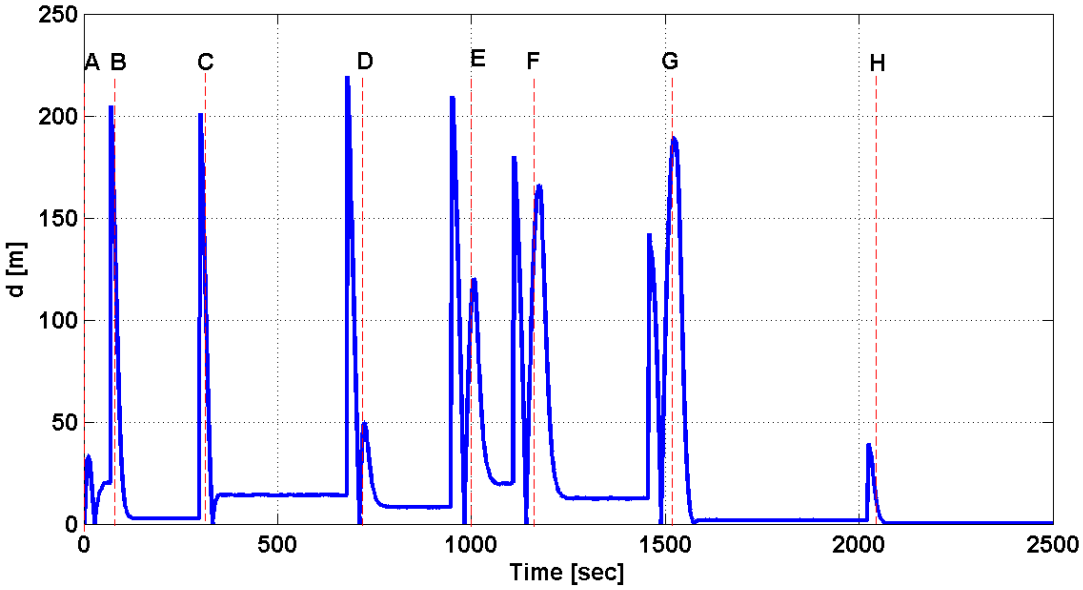

Fig. 7-6 Cross track error generated by implementing the integrated guidance, controller and observer system.

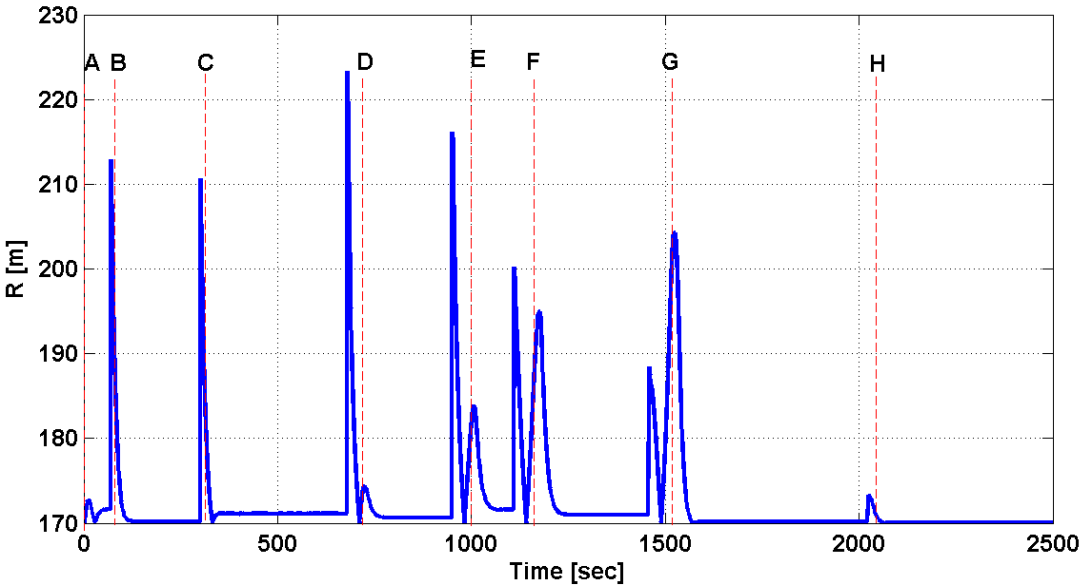

Fig. 7-7 Radius variations induced by the “exponential” guidance scheme.

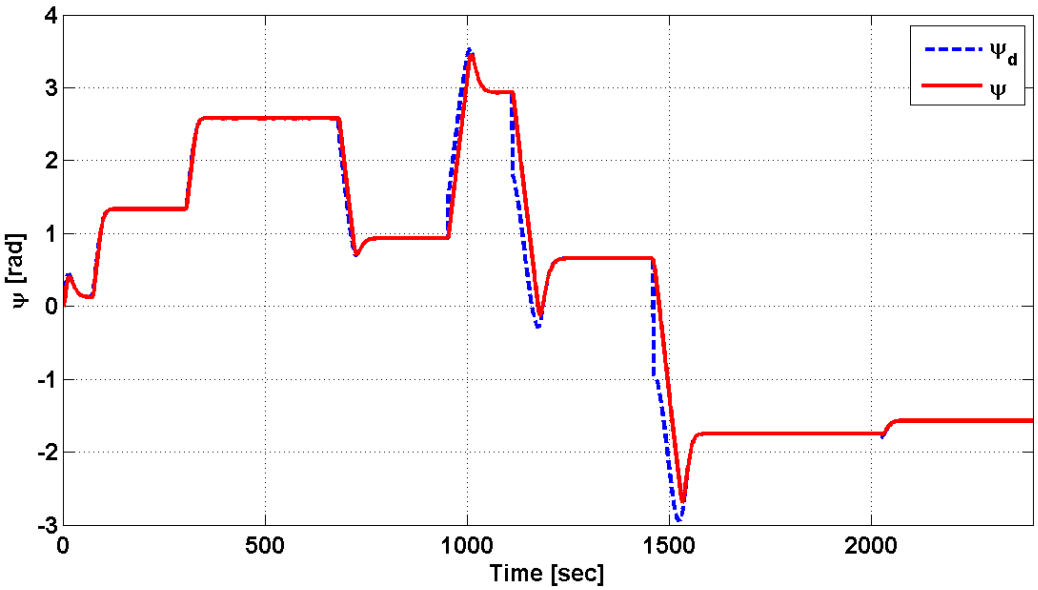

Fig. 7-8 Desired and actual heading angles of the ship.

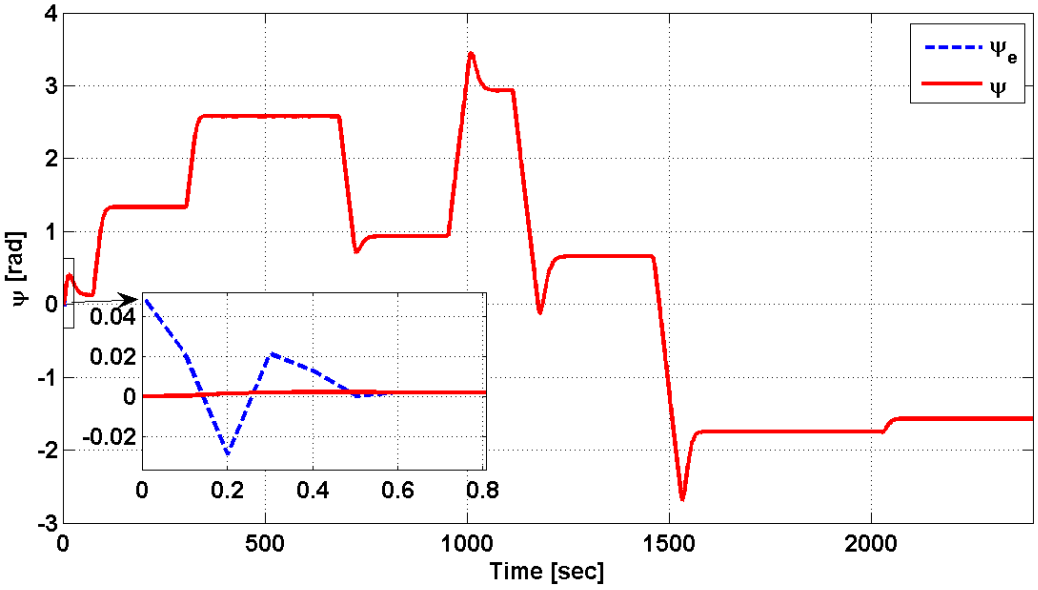

Fig. 7-9 Estimated and actual heading angles of the ship.

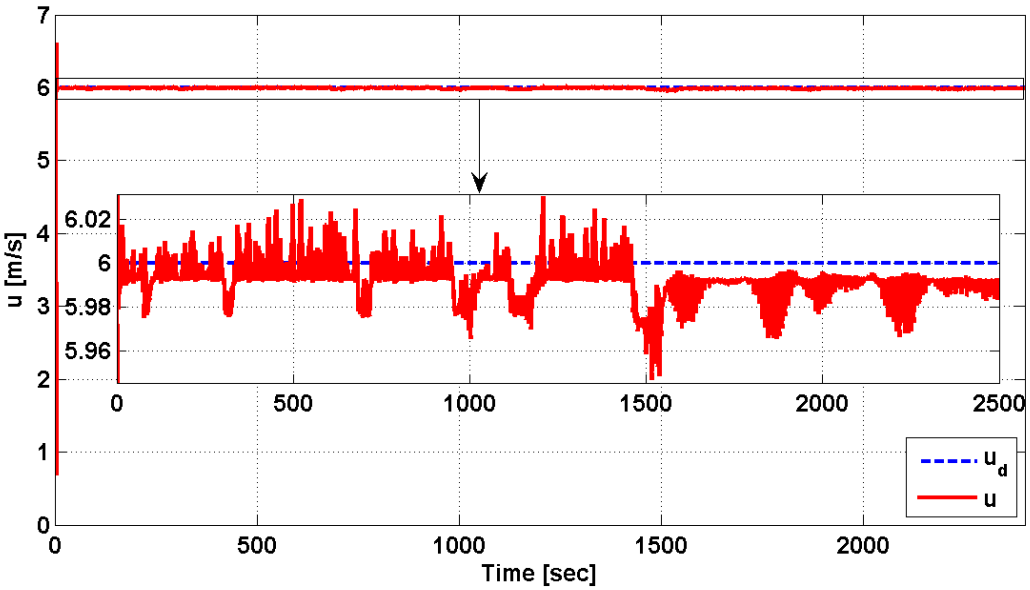

Fig. 7-10 Desired and actual surge speeds of the ship.

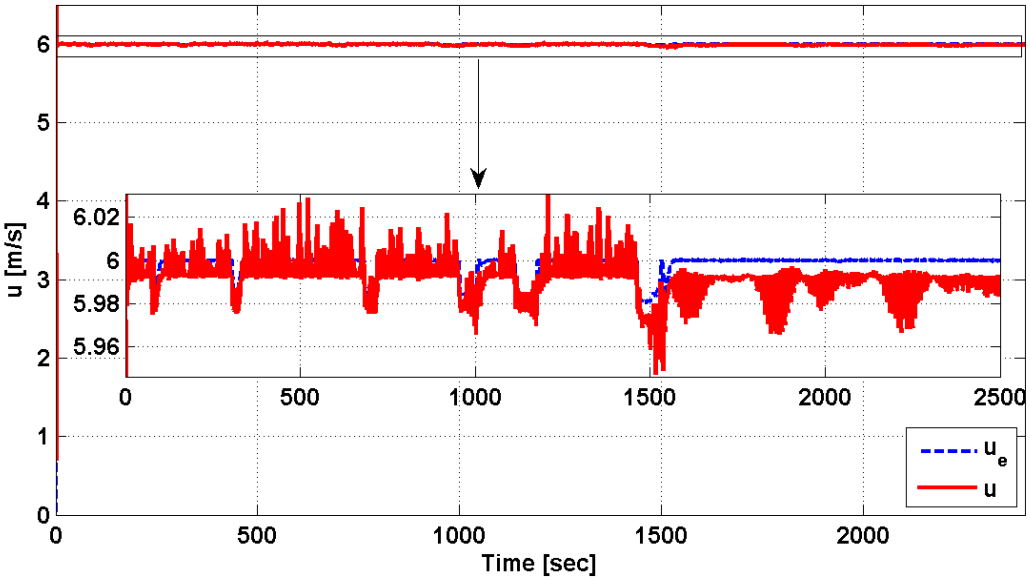

Fig. 7-11 Estimated and actual surge speeds of the ship.

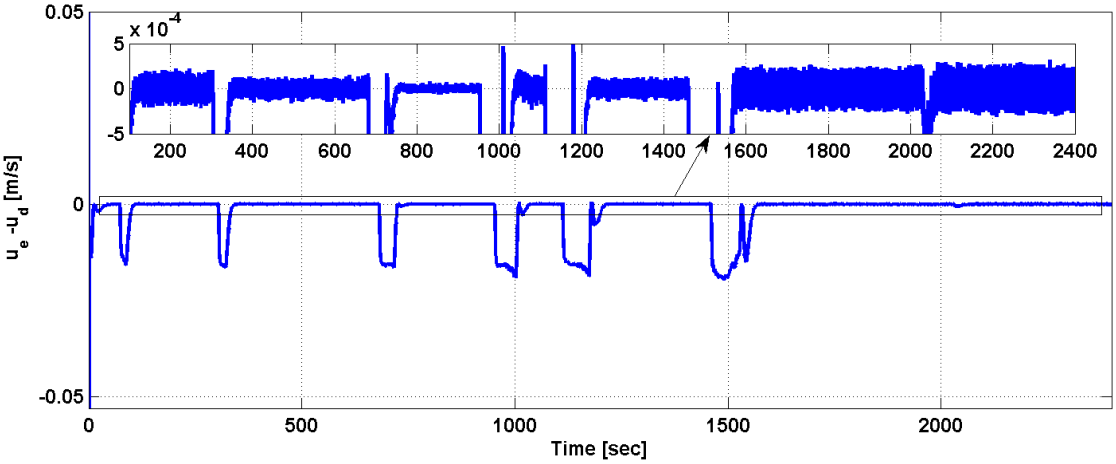

Fig. 7-12 Error between desired and estimated surge speeds of the ship.

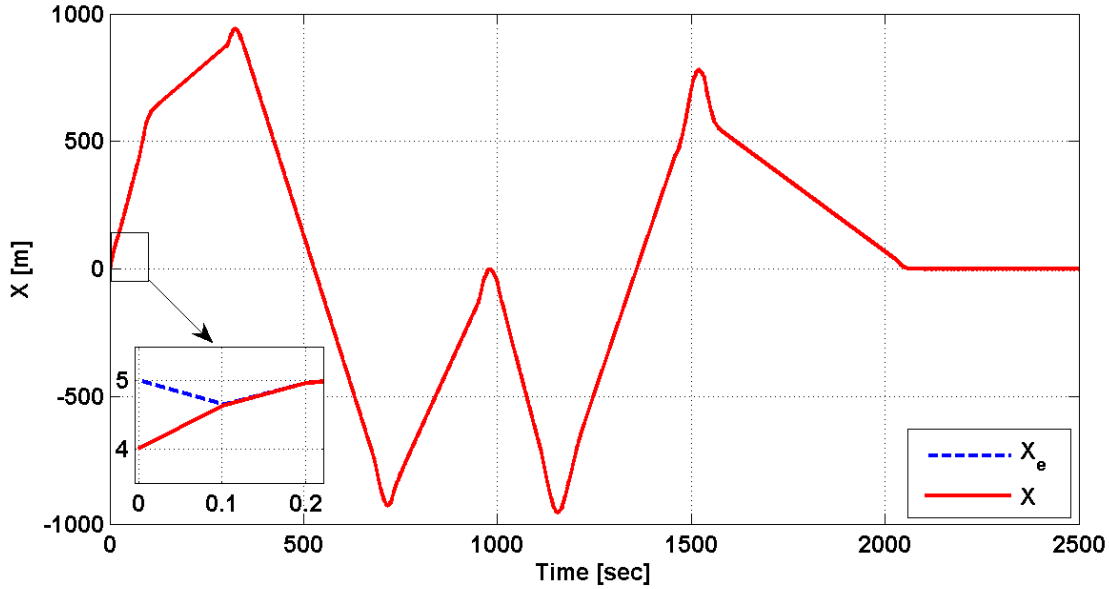

Fig. 7-13 Actual and estimated X coordinate of the ship with respect to the inertial frame.

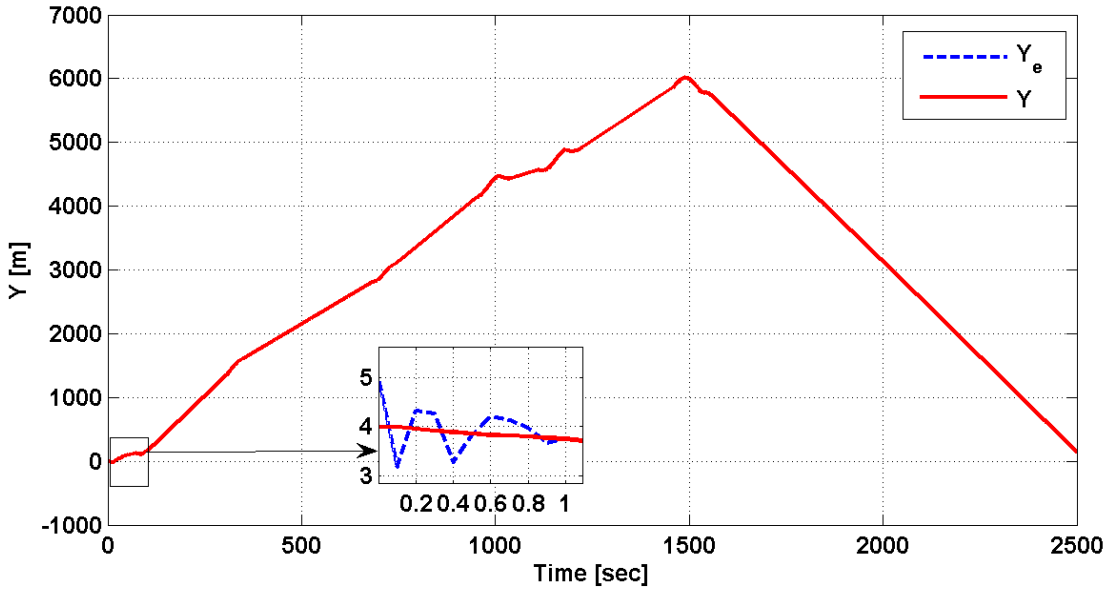

Fig. 7-14 Actual and estimated Y coordinate of the ship with respect to the inertial frame.

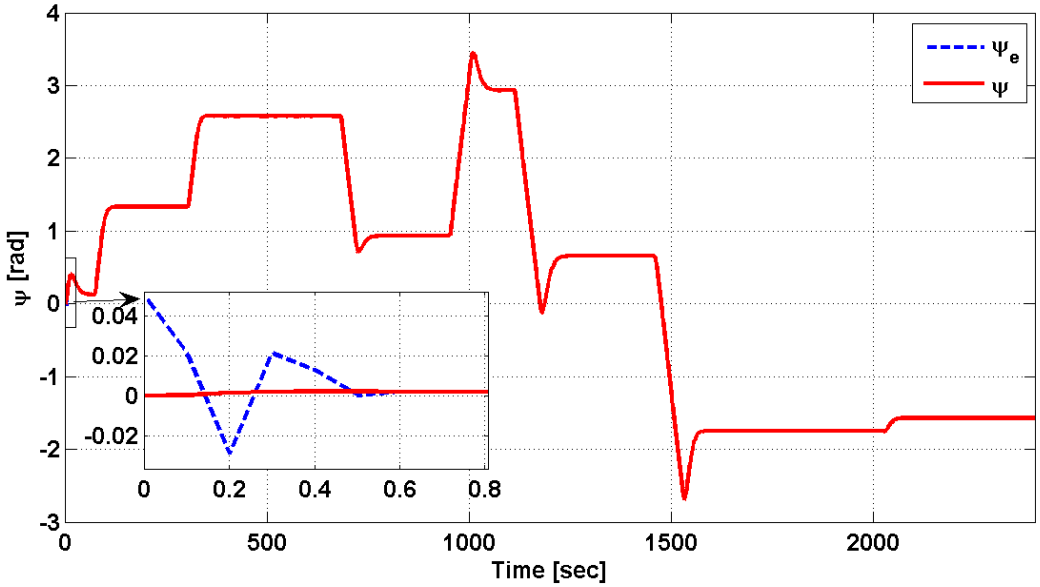

Fig. 7-15 Actual and estimated ψ coordinate of the ship with respect to the inertial frame.

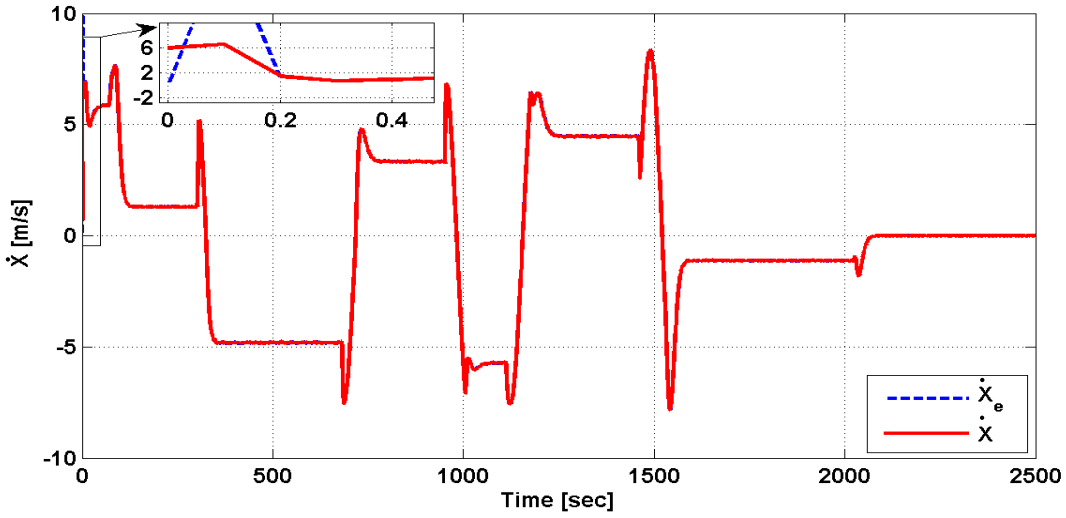

Fig. 7-16 Actual and estimated speed of the ship along the $X-$axis.

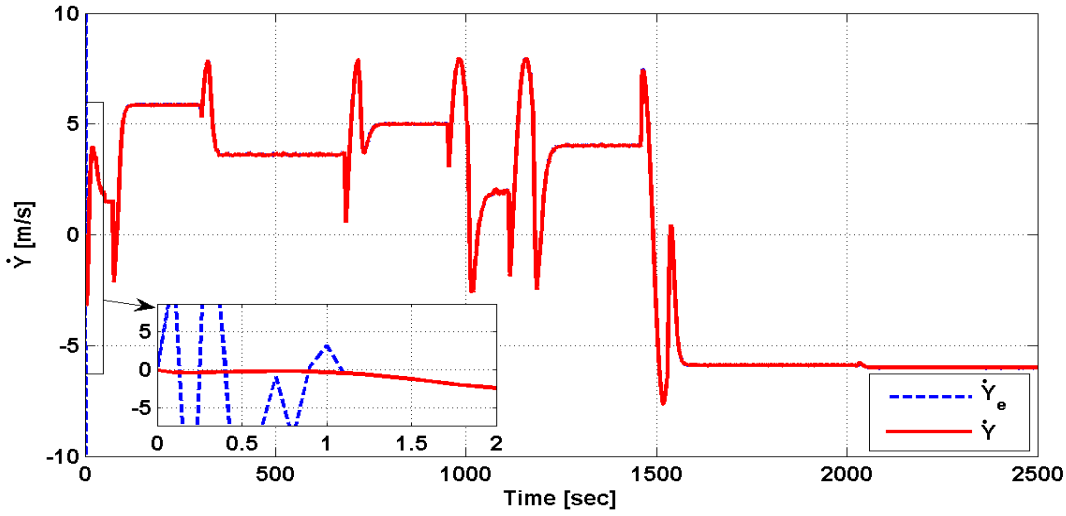

Fig. 7-17 Actual and estimated speed of the ship along the $Y-$axis.

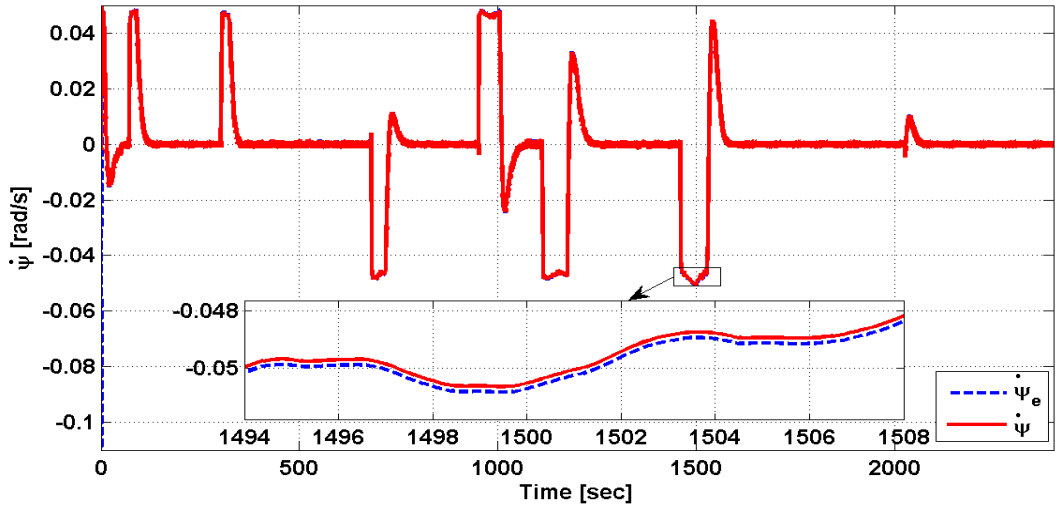

Fig. 7-18 Actual and estimated time rate of change of the heading angle around the Z – axis.

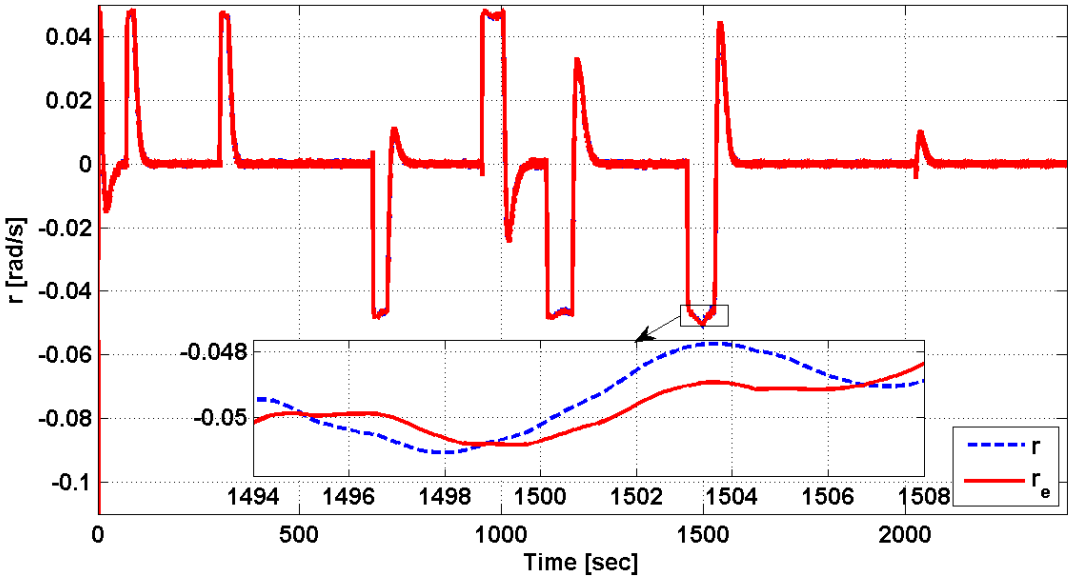

Fig. 7-19 Actual and approximated values of r.

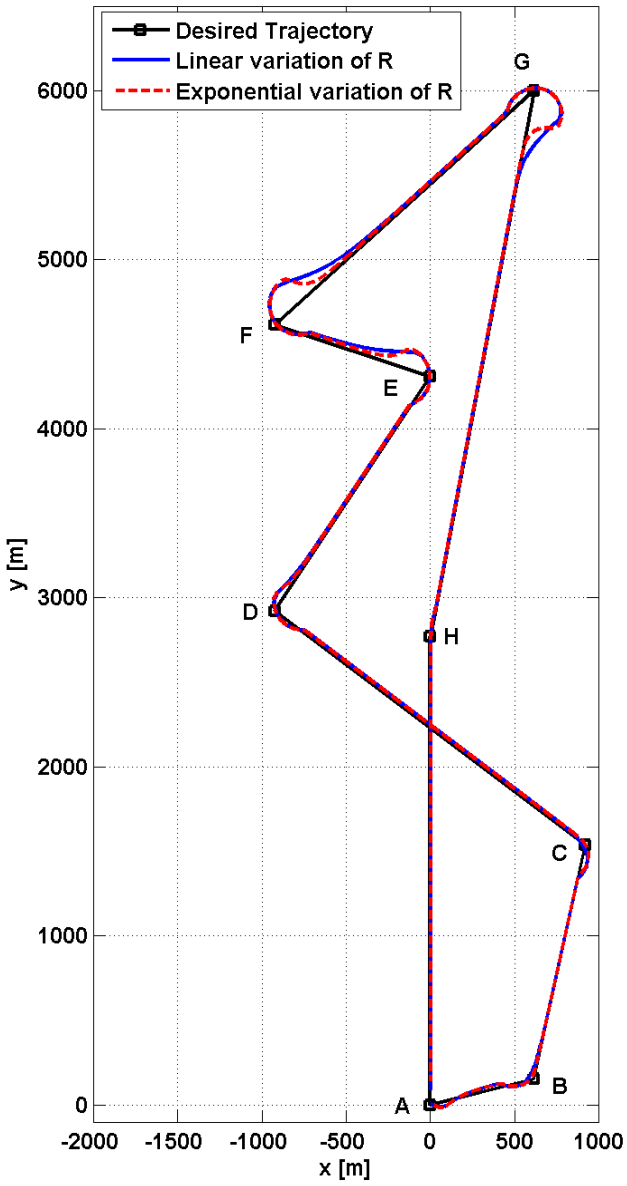

Fig. 7-20 Performances of the "linear" and "exponential" guidance systems with sliding mode controller and observer.

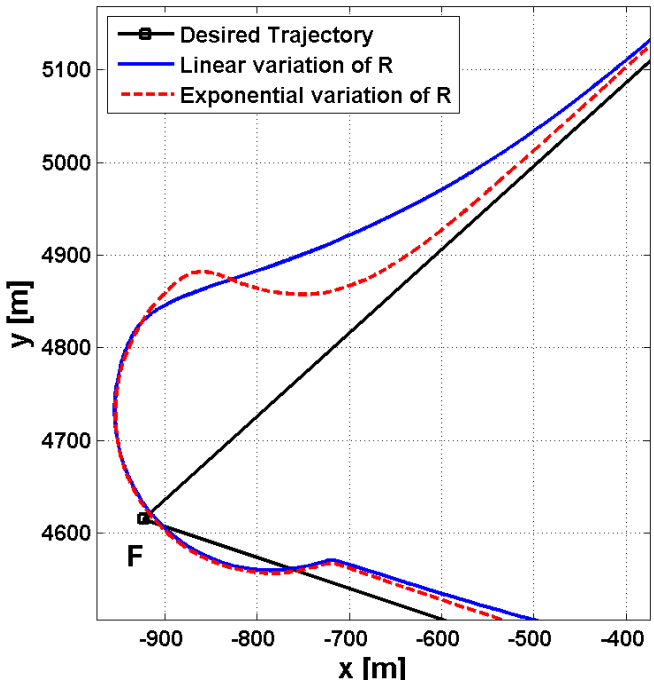

Fig. 7-21 Effects of the "linear" and "exponential" guidance schemes in the vicinity of the F way point.

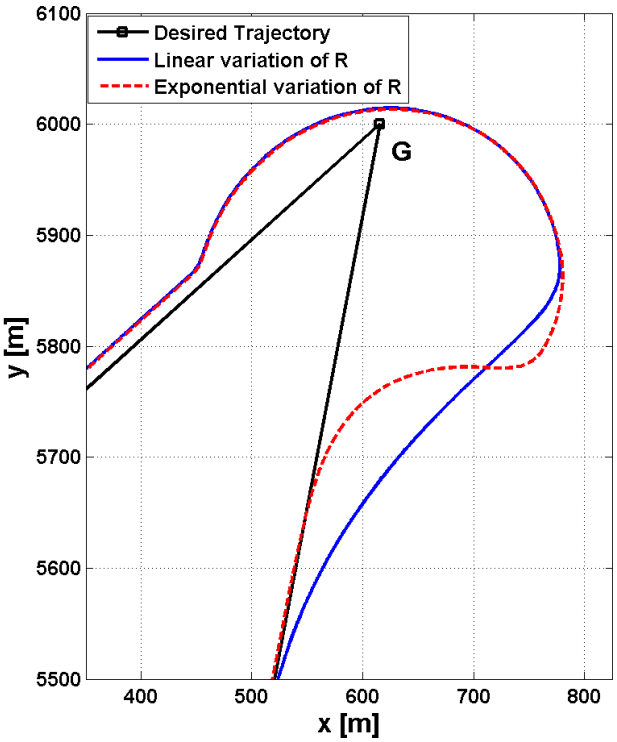

Fig. 7-22 Effects of the "linear" and "exponential" guidance schemes in the vicinity of the G way point.

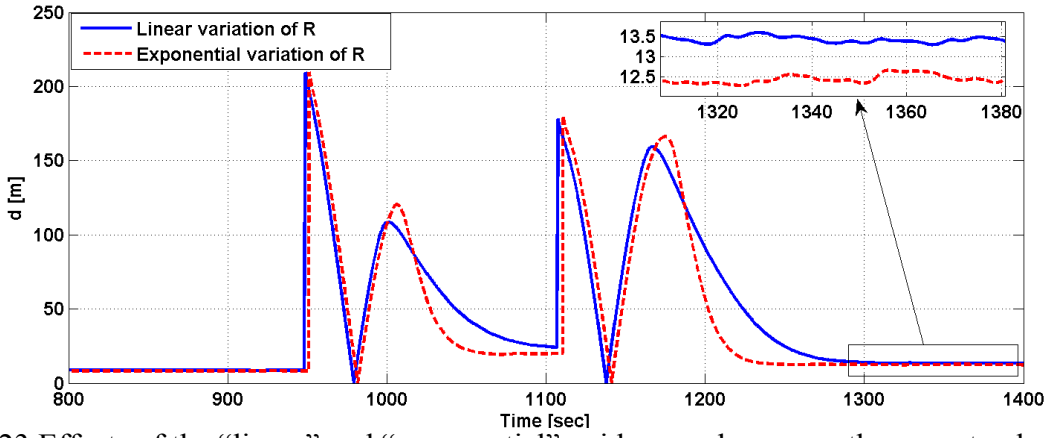

Fig. 7-23 Effects of the "linear" and "exponential" guidance schemes on the cross track error.

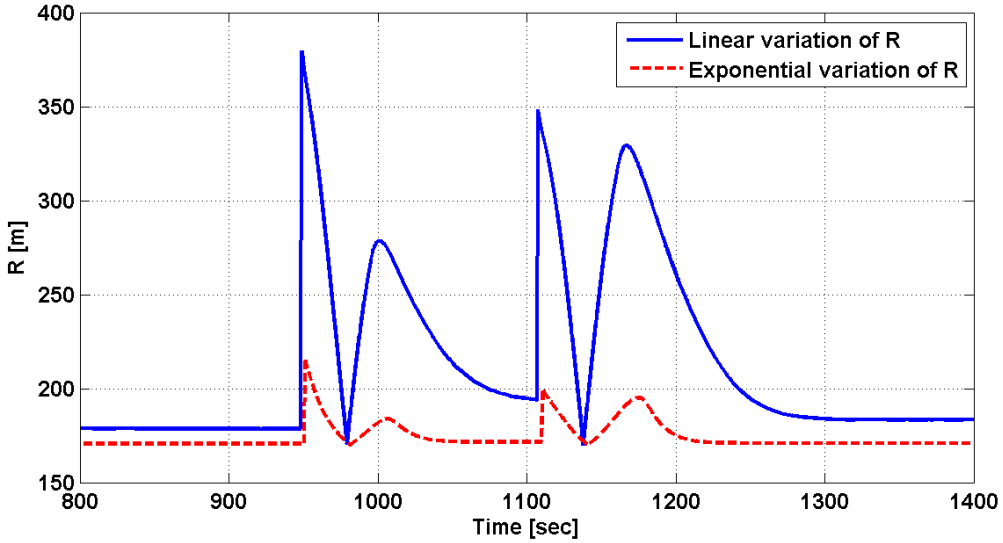

Fig. 7-24 Radius variations induced by the "linear" and "exponential" guidance schemes.

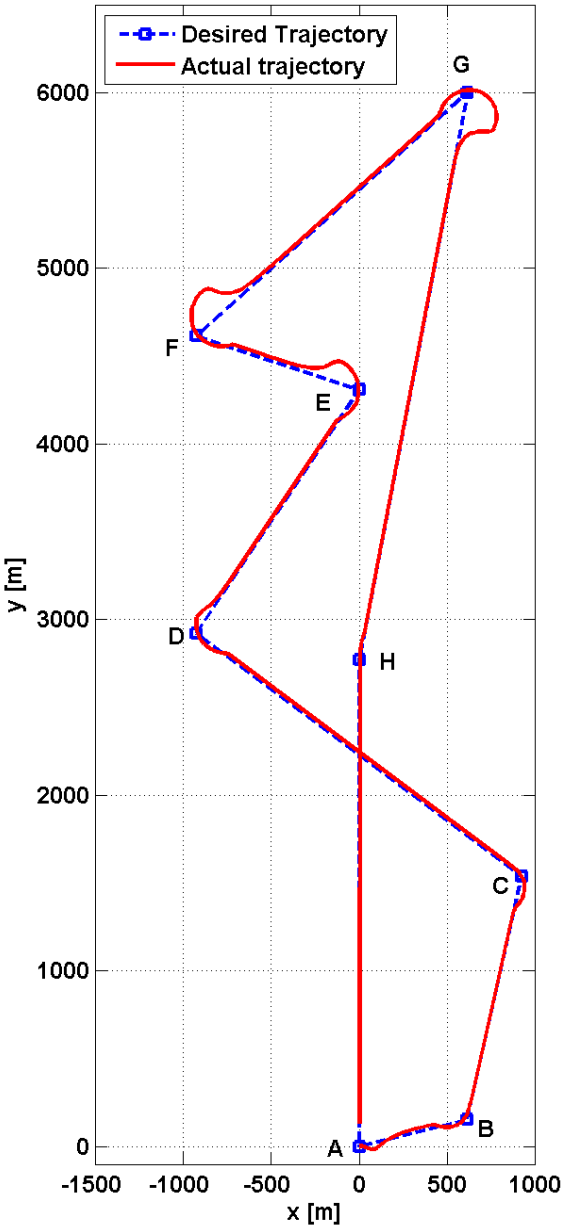

Fig. 7-25 Performance of the "exponential" guidance scheme with the self-tuning fuzzy-sliding mode controller and observer.

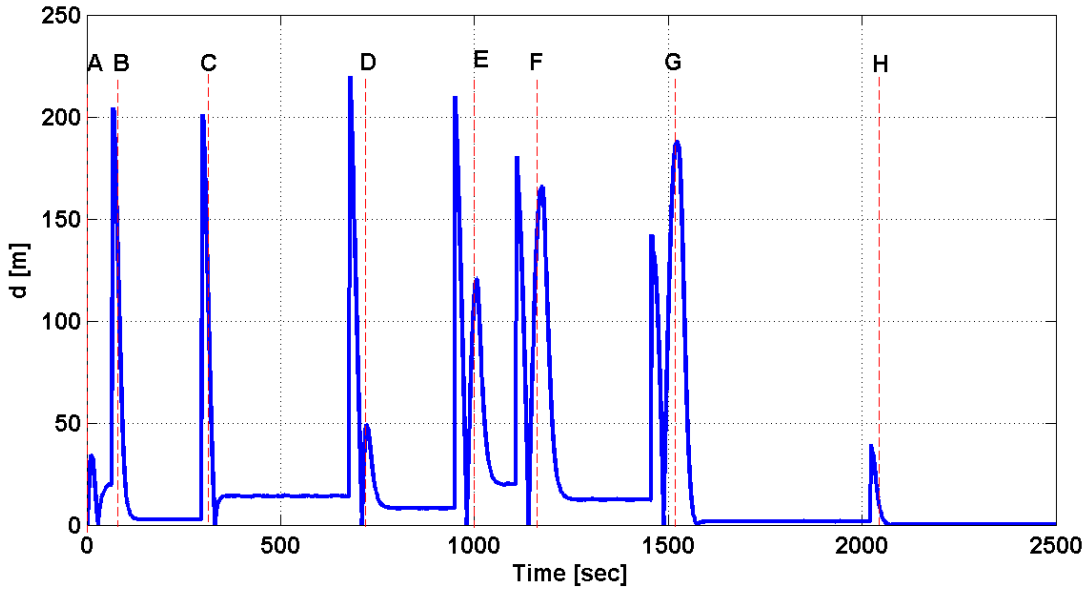

Fig. 7-26 Cross track error generated by implementing the integrated guidance, controller and observer system.

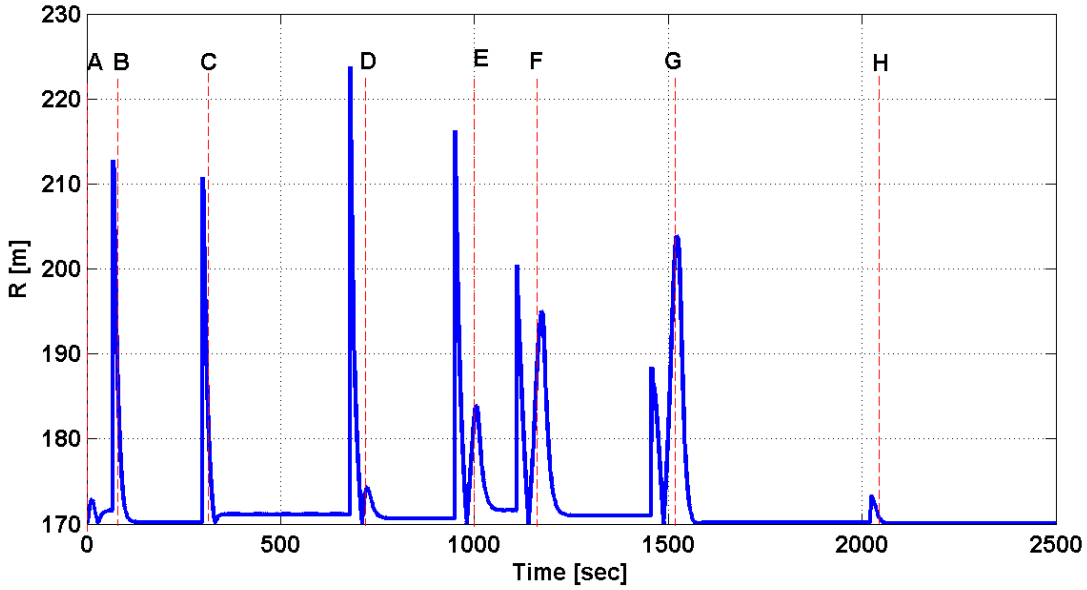

Fig. 7-27 Radius variations induced by the “exponential” guidance scheme.

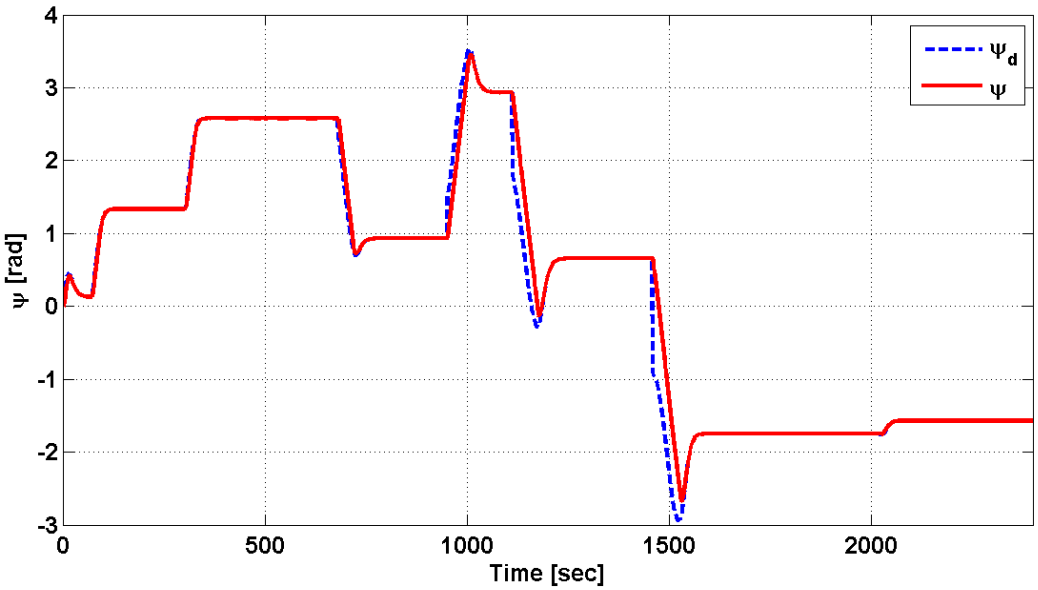

Fig. 7-28 Desired and actual heading angles of the ship.

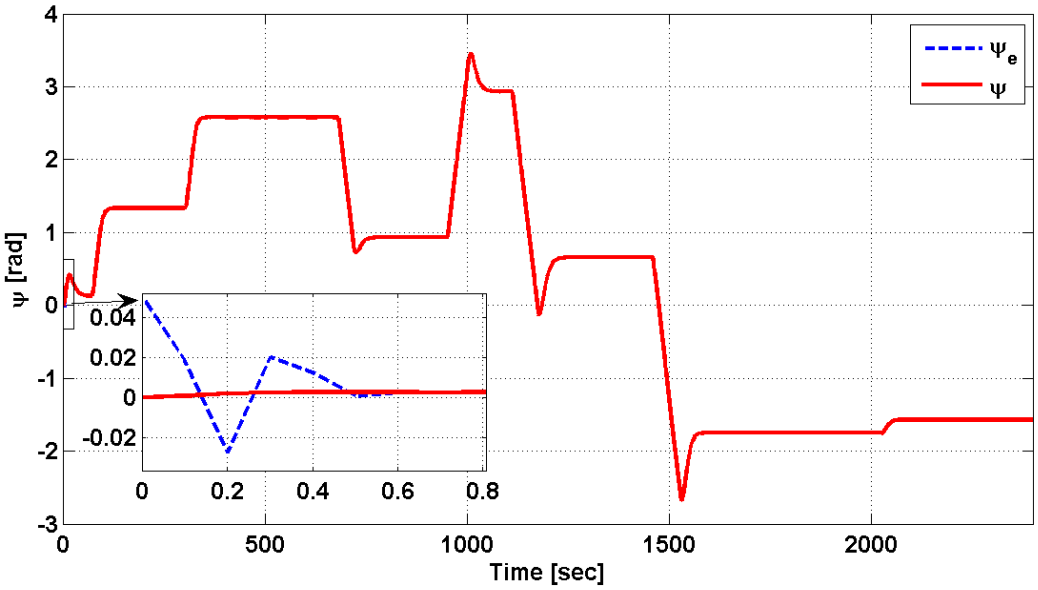

Fig. 7-29 Estimated and actual heading angles of the ship.

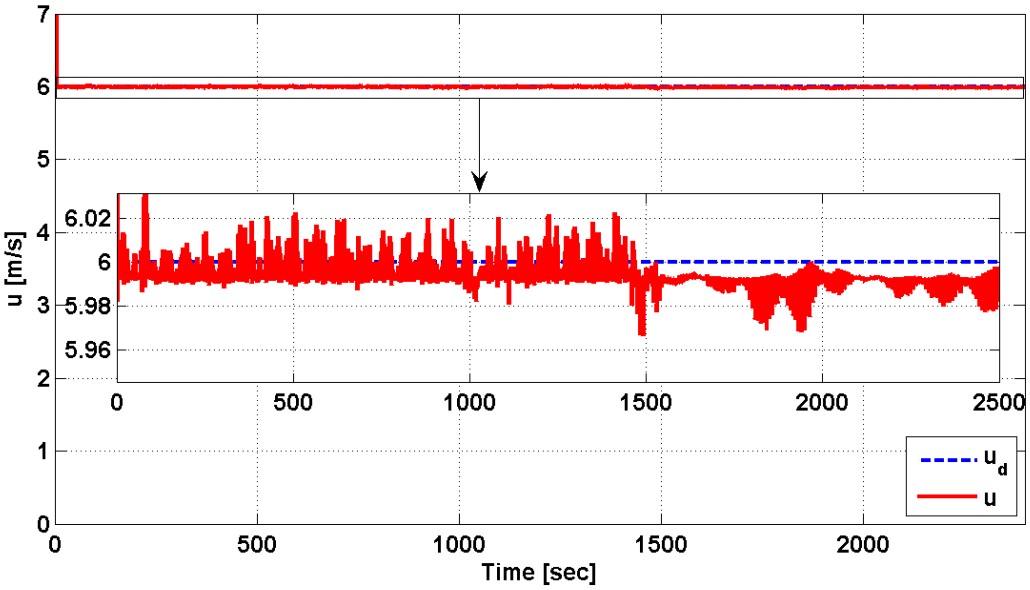

Fig. 7-30 Desired and actual surge speeds of the ship.

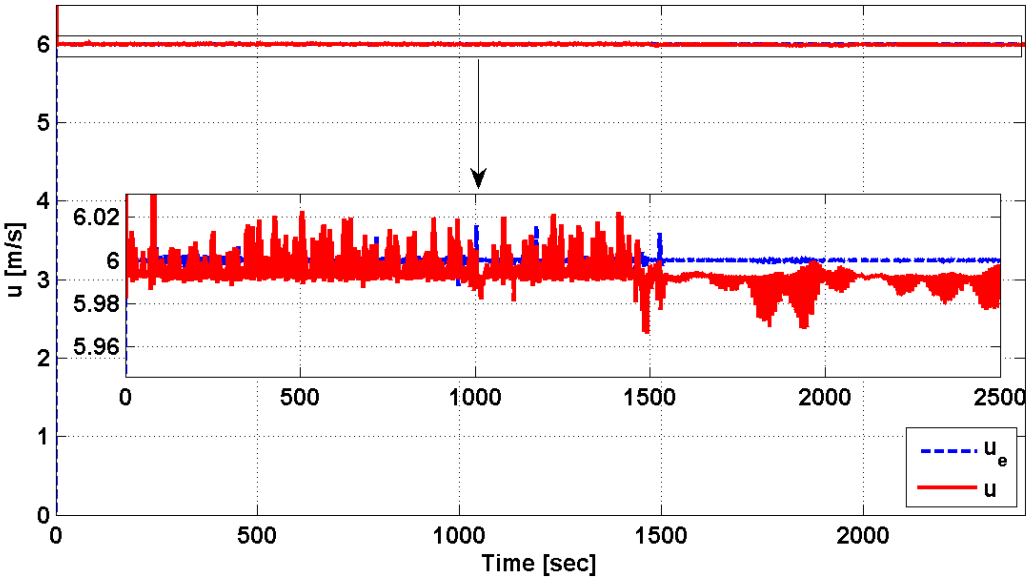

Fig. 7-31 Estimated and actual surge speeds of the ship.

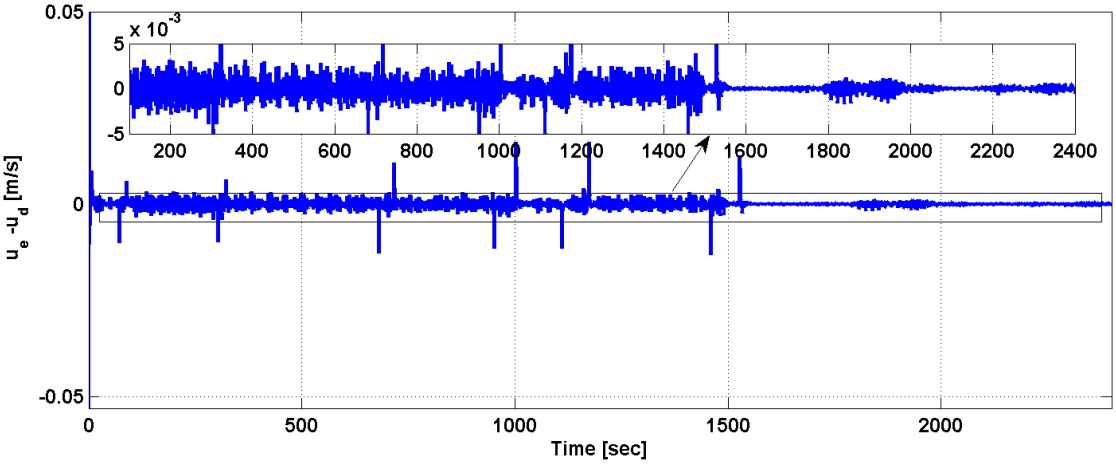

Fig. 7-32 Error between desired and estimated surge speeds of the ship.

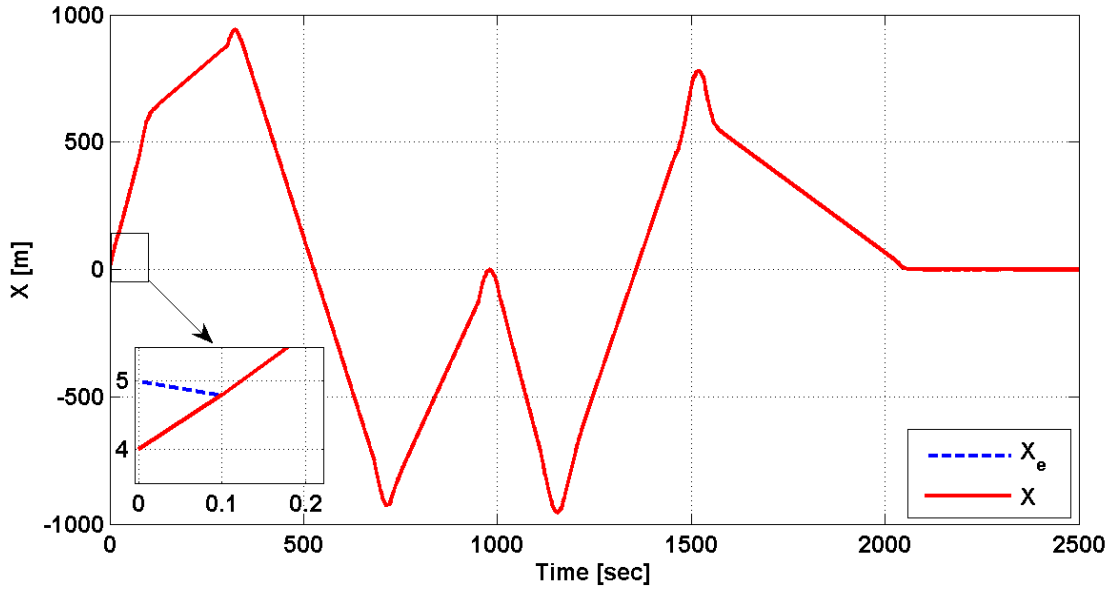

Fig. 7-33 Actual and estimated X coordinate of the ship with respect to the inertial frame.

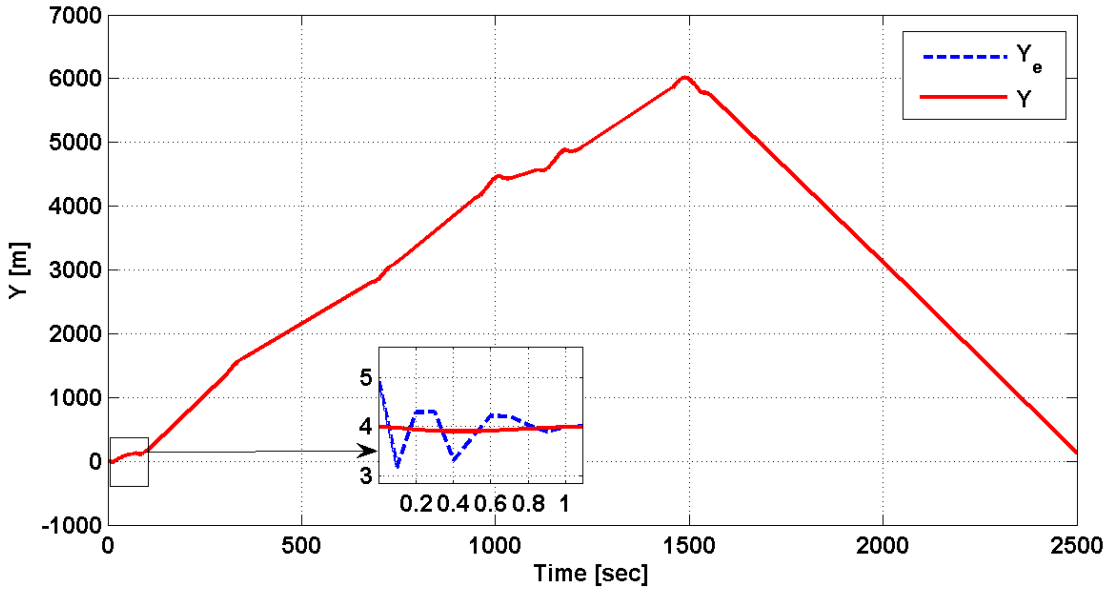

Fig. 7-34 Actual and estimated Y coordinate of the ship with respect to the inertial frame.

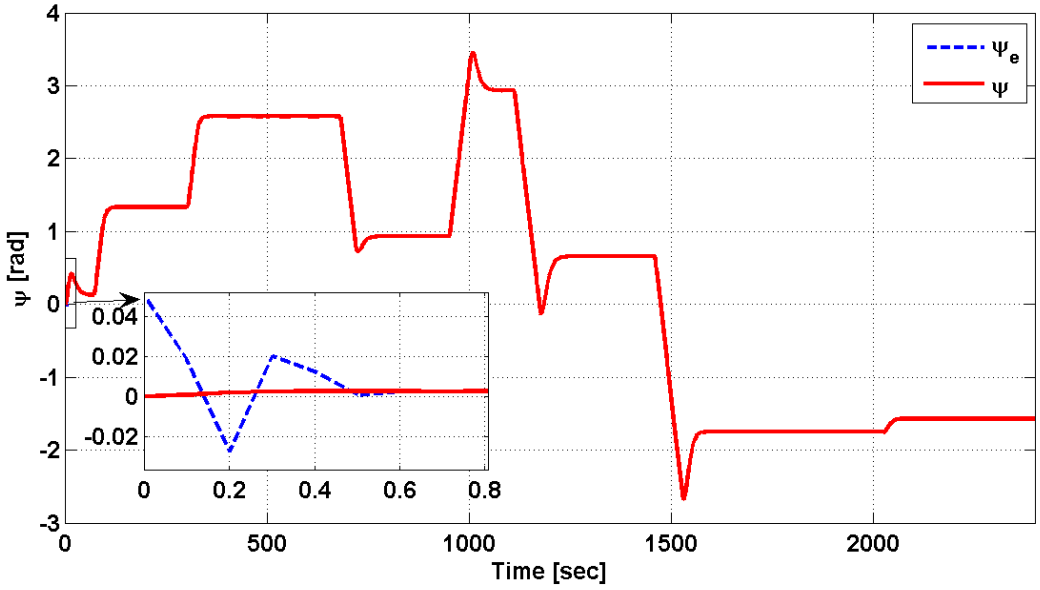

Fig. 7-35 Actual and estimated ψ coordinate of the ship with respect to the inertial frame.

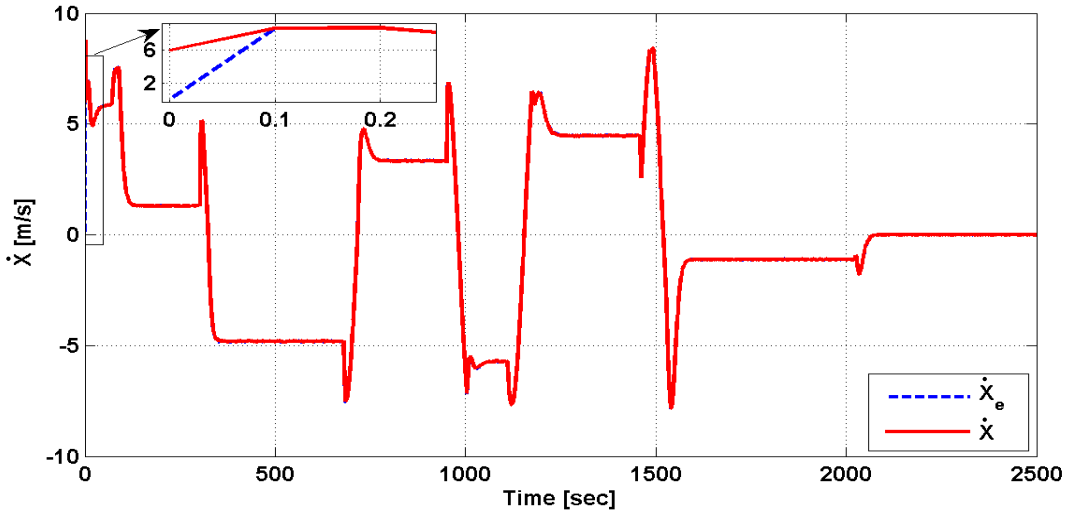

Fig. 7-36 Actual and estimated speed of the ship along the $X-$axis.

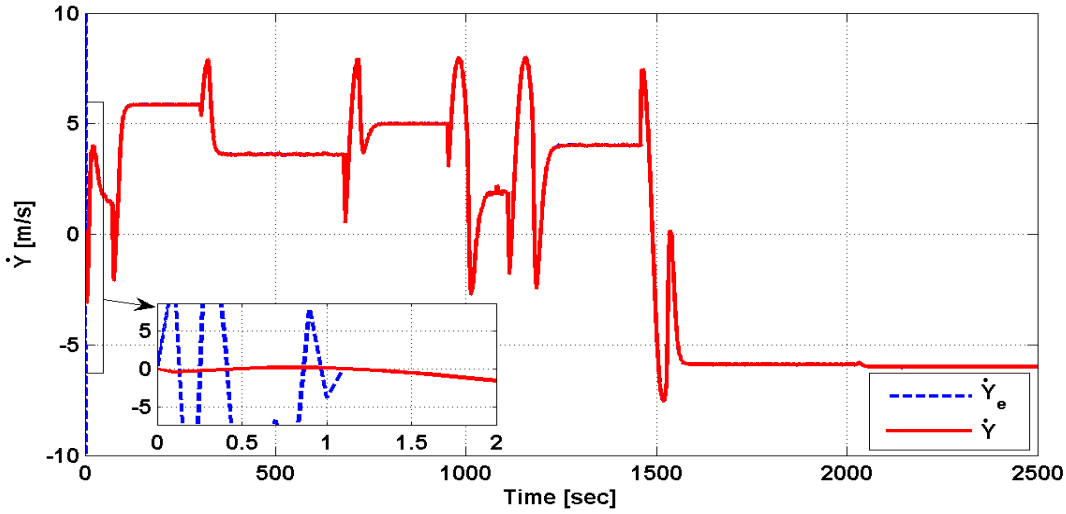

Fig. 7-37 Actual and estimated speed of the ship along the $Y-$axis.

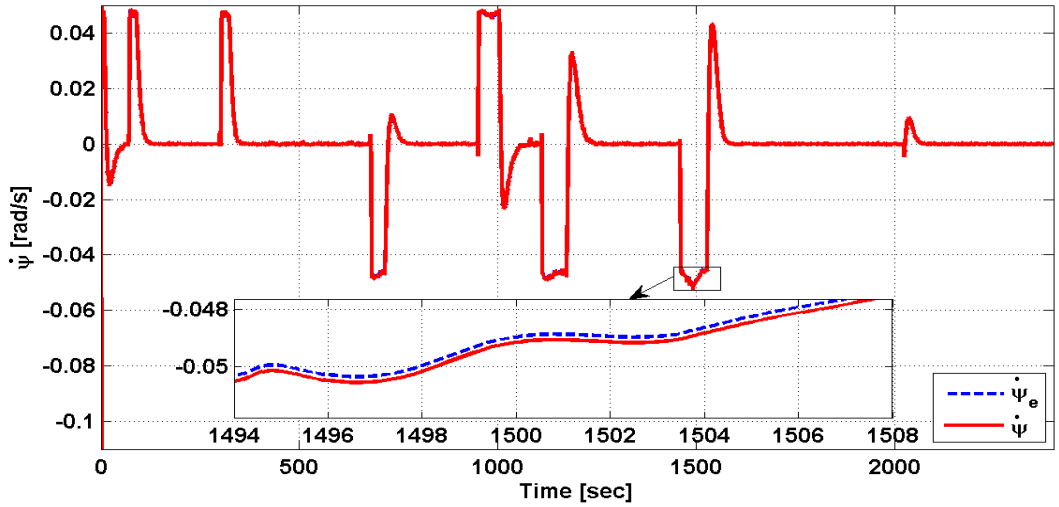

Fig. 7-38 Actual and estimated time rate of change of the heading angle around the Z – axis.

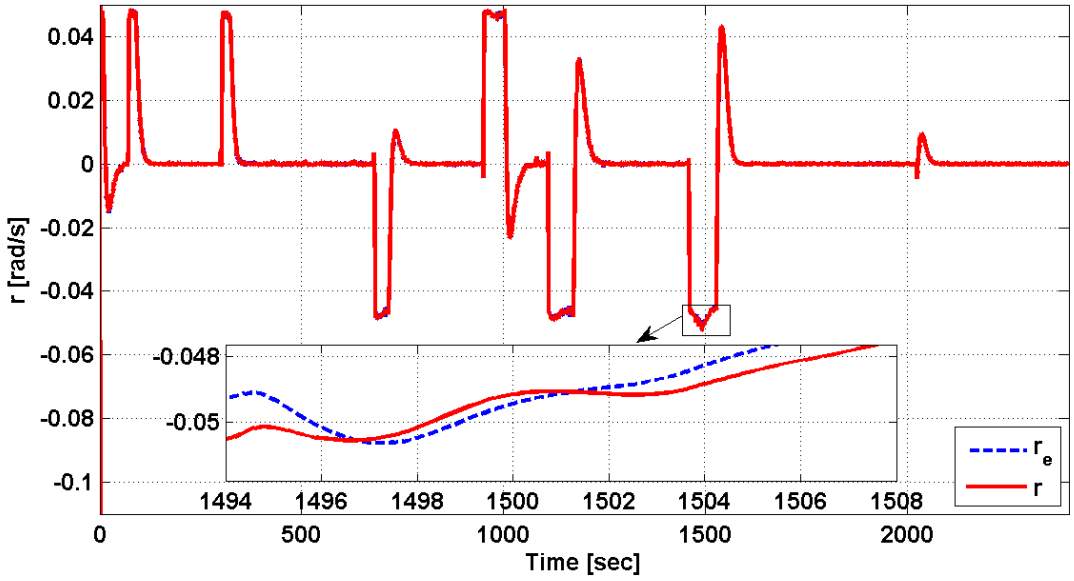

Fig. 7-39 Actual and approximated values of r.

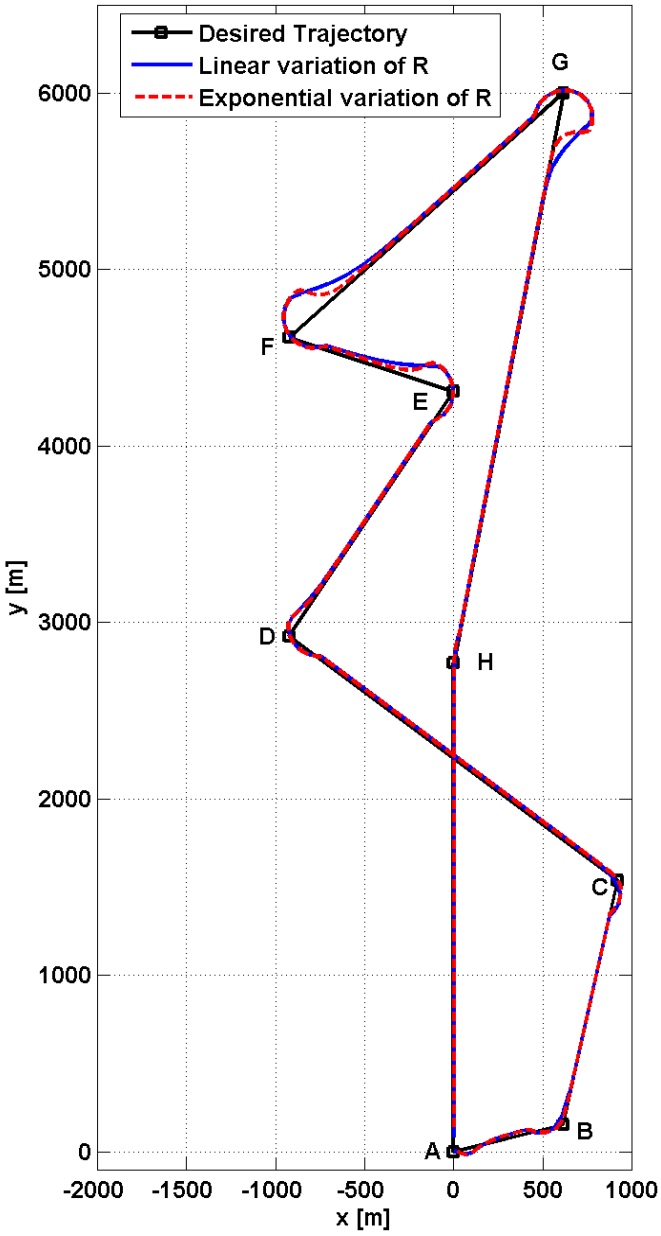

Fig. 7-40 Performances of the "linear" and "exponential" guidance systems with self-tuning fuzzy-sliding mode controller and observer.

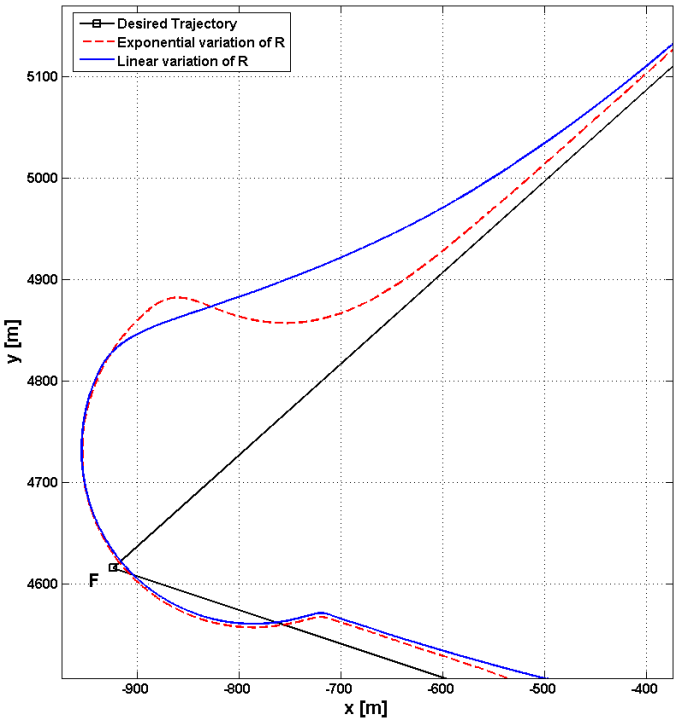

Fig. 7-41 Effects of the "linear" and "exponential" guidance schemes in the vicinity of the F way point.

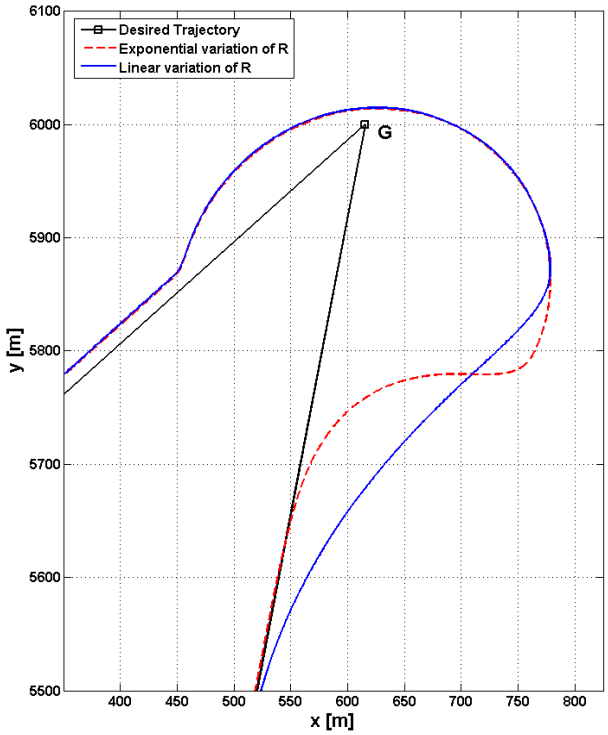

Fig. 7-42 Effects of the "linear" and "exponential" guidance schemes in the vicinity of the G way point.

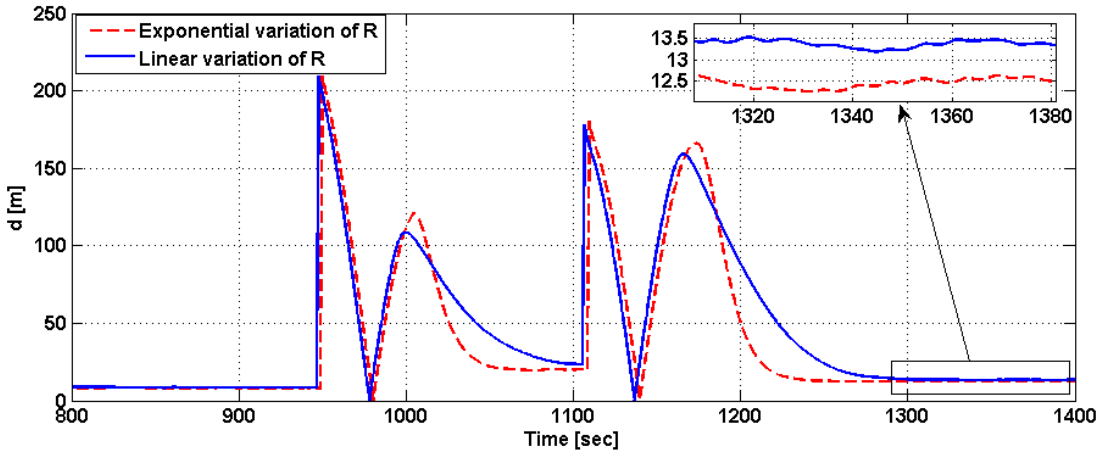

Fig. 7-43 Effects of the "linear" and "exponential" guidance schemes on the cross track error.

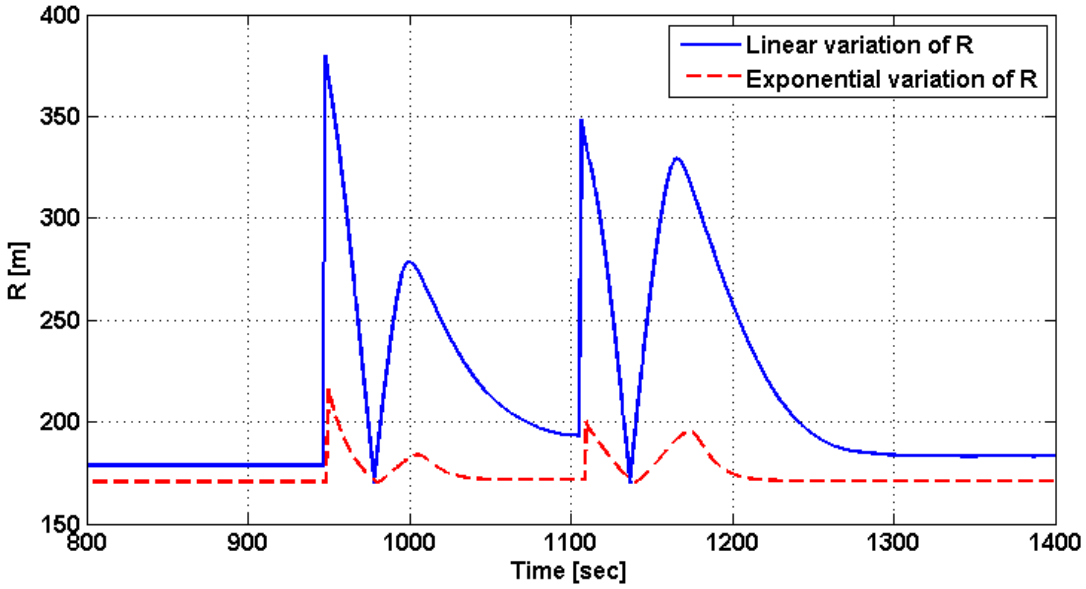

Fig. 7-44 Radius variations induced by the "linear" and "exponential" guidance schemes.

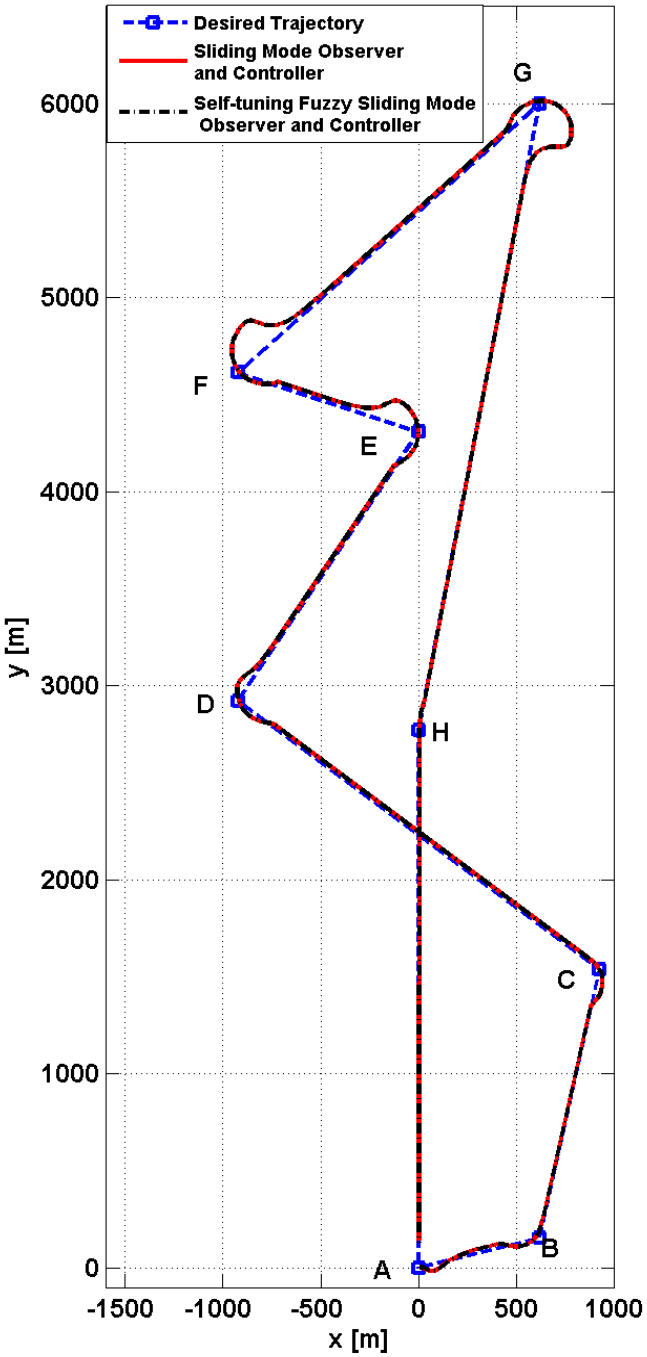

Fig. 7-45 Performances of the "exponential" guidance systems with both the sliding mode and self-tuning fuzzy-sliding mode controllers and observers.

CHAPTER 8 “SUMMARY AND CONCLUSIONS”

The present research work is summarized in this Chapter. Its main conclusions are highlighted. The contributions and the shortcomings of the work are also clearly stated. Finally, prospective research topics on the guidance, control and state estimations of marine surface vessels are recommended.

8.1 Summary and Conclusions

Maneuvering and seakeeping tasks of ships are very challenging control problems. This is because the dynamics of marine vessels are highly nonlinear and involve significant structured and unstructured uncertainties. This problem is also compounded by the fact that ships are required to operate under constantly varying environmental conditions, which are capable of producing significant external disturbances due to winds, random sea waves and currents.

The focus of this study is to develop an integrated guidance and control system that enables under-actuated marine surface vessels to operate autonomously and yield robust tracking performance in spite of significant external disturbances and modeling imprecision.

As a first step toward achieving this goal, a nonlinear ship model has been developed to serve as a test bed to assess the performances of the proposed guidance and control systems. The model closely follows the recent developments in ship modeling (Fossen, 2002; Kristiansen et al., 2005; Ogilvie, 1964; Ueng et al., 2008; Isherwood, 1973; Breivik, 2003; Moreira et al., 2007; Fossen, 2005; Perez, 2005; Newman, 1977). Its formulation considers the ship as a rigid body having six degrees of freedom. A seventh degree-of-freedom has been introduced to account for the

rudder dynamics. The model considers the effects of coriolis and centripetal accelerations, wave excitations, retardation forces, nonlinear restoring forces, wind and current loads, linear damping terms, and the control force and moment.

The excitation forces are computed by considering long-crested waves with a Modified Pierson-Moskowitz spectrum (Perez, 2005). The retardation forces are determined from a state space formulation that was generated based on the work reported in Refs. (Kristiansen et al., 2005; Perez, 2005; Ogilvie, 1964). The nonlinear restoring force and moment are calculated based on the submerged volume of the ship with respect to the instantaneous sea free-surface (Khaled and Chalhoub, 2009). Linear damping terms and load effects due to wind and sea-currents are formulated as in (Ueng et al., 2008; Isherwood, 1973; OCIMF, 1977; OCIMF, 1994). The physical limitations of the ship are accounted for in the model by including a scheme that would examine the propeller thrust, assigned by the controller, and only apply the propeller thrust that can actually be delivered by the ship propulsion system. Moreover, the rudder limitations are considered by restricting the ranges of values for the angle-of-attack and the slew rate of the rudder.

Next, the controllers are designed. The modeling imprecision and the considerable environmental disturbances prevent the implementation of model-based controllers. Therefore, two types of robust controllers were designed in the present work to control the surge speed and the heading angle of a marine surface vessel. The first one is a sliding mode controller. Such a controller is based on the variable structure theory (VSS) (Utkin, 1981). It has been proven to yield a robust tracking

performance when applied on nonlinear systems whose dynamics are not fully known as long as the upper bounds of the uncertainties are known.

The second controller is a self-tuning fuzzy-sliding mode controller. It combines the advantages of the variable structure systems (VSS) theory with the self-tuning fuzzy logic controller. Neither the development of an accurate dynamic model of the ship nor the construction of a rule-based expert system is required for designing the controller. The only requirement is that the upper bound of the modeling uncertainties has to be known. Moreover, the stability of the controlled system is ensured by forcing the tuning parameter to satisfy the sliding condition.

The digital simulation results have demonstrated that both controllers possess similar robustness in accurately tracking the desired surge speed and ship heading in spite of significant modeling imprecision and external environmental disturbances.

Next, the implementation aspect of the proposed controllers will be addressed. The controllers require that the state variables of the system be available for the computation of the control signals. In the current work, the available measurements are considered to be the heading angle along with the X and Y coordinates of the ship with respect to the inertial reference frame. The X and Y coordinates can be obtained from a global positioning system (GPS) while the yaw angle can be measured by an on-board gyro compass system (Fossen and Strand, 1999). Note that the measured variables are with respect to the inertial frame $\{X,Y,Z\}$ while the variables, needed for the computation of the control signals, should be defined with respect to the body-fixed reference frame $\{x,y,z\}$. This issue has been resolved in this work by designing the observers to estimate $X,Y,\psi,\dot{X},\dot{Y}$ and $\dot{\psi}$ variables with respect to the inertial frame.

Then the state variables, needed for the implementation of the proposed controllers, are deduced from the estimated state variables by using a rotation transformation matrix.

Two observers are designed in this work. The first is a nonlinear sliding mode observer while the second is a self-tuning fuzzy-sliding mode observer. The simulation results demonstrated the capabilities of both observers in providing accurate estimates of the state variables in the presence of significant structured and unstructured uncertainties of the system. Subsequently, the observers were coupled with the proposed controllers. This was done by computing the control signals based on estimated rather than actual values of the state variables. The rationale is to generate a complete and reliable controller-observer system. In this work, the sliding mode controller has been coupled with the sliding mode observer. Similarly, the self-tuning fuzzy-sliding mode controller and observer are combined. However, any combination of the proposed controllers and observers would have led to comparable closed-loop response. The simulation results have proven the viability of combining the proposed controllers and observers. The deterioration in the closed-loop response of the ship, due to the computation of the control signals based on estimated rather than actual values of the state variables, are hardly noticeable. This is attributed to the rapid convergence rate of the proposed estimation algorithms.

Moreover, the ship is considered herein to be under-actuated. Therefore, the number of actuators is smaller than the number of degrees of freedom that need to be controlled. For instance, the ship has six rigid body degrees of freedom while the control actions are limited to the propeller thrust and the rudder torque. These two control actions are basically relied on to yield the desired position and orientation of the

ship. The propeller thrust is mainly used for forward or surge speed control. While the rudder torque has to yield the desired rudder angle-of-attack, which is relied on to steer the marine vessel toward the desired trajectory. To enable the under-actuated vessel to operate autonomously, the desired values of the rudder angle-of-attack have to be assigned by a guidance system. This necessitates the guidance system to be coupled with the controller and observer. Such an integrated guidance and control system empowers the steering control problem to simultaneously address sway displacement and ship heading control problems (Fossen, 2002; Fossen et al., 2003; Healey and Marco, 1992; Breivik, 2003; Moreira et al., 2007).

A guidance scheme, based on the concepts of the variable radius line-of-sight (LOS) and the acceptance radius, is presented whereby the LOS radius is varied exponentially with the cross track error. The proposed technique can handle large cross-track errors while aiding the controller to quickly converge the ship to its desired trajectory. The performance of the guidance scheme is tested herein under two guidance and control configurations. The first uses a sliding mode controller and observer while the second employs a self-tuning fuzzy-sliding mode controller and observer. The results demonstrate that both guidance and control systems have similar robustness and tracking characteristics.

8.2 Main Contributions and Drawbacks of the Current Study

The main contributions of the current work can be outlined as follows

- Development of a nonlinear, six degree-of-freedom dynamic model for an under-actuated marine surface vessel, in MATLAB\Simulink, that incorporates recent advances in ship modeling, accounts for the physical limitations of the rudder and

the ship propulsion system, considers the rudder dynamics, and uses a refined mesh for the computation of the nonlinear restoring forces and moments with respect to the instantaneous sea free surface. The current model fails to consider the effect of the surge speed on the magnitude and phase angle of the force *response amplitude operators* (RAO's) that are used in the computation of the wave excitation forces.

- Design of a nonlinear robust controller and observer, based on the sliding mode methodology, to control the surge speed and the heading angle of the ship. The proposed observer-controller scheme has been proven, through digital simulations, to yield robust tracking performance in the presence of significant modeling imprecision and external disturbances.
- Development of a self-tuning fuzzy-sliding mode controller and observer to control the surge speed and the heading angle of the ship. The stability of the controller and the observer is guaranteed by ensuring that the tuning parameters satisfy the sliding conditions. The simulation results demonstrate the capability of the self-tuning fuzzy-sliding mode controller and observer to yield robust performance in spite of considerable structured and unstructured uncertainties.
- Modification of the existing guidance scheme, based on the concepts of the variable radius line-of-sight (LOS) and the acceptance radius, in order to vary the LOS radius exponentially rather than linearly with the cross track error. The simulation results demonstrated that the proposed guidance scheme enables the ship to converge to its desired trajectory faster than the existing technique.

- Integration of the guidance scheme with the controller and observer to enable under-actuated marine vessels to operate autonomously and accurately track the desired trajectory of the ship.

8.3 Future Work

The following prospective research topics are suggested:

- Account for the ice accretion and ship-ice interaction in the dynamic model of the marine vessel.
- Account for the ship surge speed in determining the magnitude and phase angle of the force *response amplitude operators* (RAO's), which are basically transfer functions defining the ratio of the wave excitation force influencing the j^{th} degree-of-freedom of the ship over the wave amplitude.
- Assess the effects of noise in the measured signals on the performance of the proposed observers.
- Validate the performance of the proposed controllers and observers through experimental studies.
- Validate the performance of the integrated guidance and control systems experimentally.

REFERENCES

[1] Aamo, O. M. and Fossen, T. I., 1999, “Controlling Line Tension in Thruster Assisted Mooring Systems,” IEEE International Conference on Control Applications (CCA’99). Honolulu, Hawaii, 1104—1109.

[2] Abkowitz, M. A., 1964, “Lectures on Ship Hydrodynamics−Steering and Manoeuverability,” Technical Report Number Hy-5, Hydro og Aerodynamisk Laboratorium, Lyngby, Denmark.

[3] Abbott, I.A. and Von Doenhoff, A.E., 1958, “Theory of Wing Sections, Including a Summary of Airfoil Data”, Dover Publications Inc., New York, USA.

[4] Abreu, G. L. and Ribeiro, J. F. 2002, “A Self-Organizing Fuzzy Logic Controller for the Active Control of Flexible Structures Using Piezoelectric Actuators,” Applied Soft Computing, 1(4), 271-283.

[5] Anderson, B. D. O. and Moore, J. B., 1990, Optimal control: Linear Quadratic Methods, Prentice-Hall.

[6] Aranda, J., De La Cruz, J. M, Díaz, J. M., Dormido Canto, S., 2002, “QFT versus Classical Gain Scheduling: Study for a Fast Ferry,” 15th IFAC World Congress.

[7] Arnold, L., Chueshov, I. and Ochs, G., 2004, “Stability and Capsizing of Ships in Random Sea – A Survey,” Nonlinear Dynamics, 36, 135-179.

[8] Bachmayer, R., Whitcomb, L. L. and Grosenbaugh, M. A., 2000, “An Accurate Four-quadrant Nonlinear Dynamical Model for Marine Thrusters: Theory and Experimental Validation,” IEEE Journal of Oceanic Engineering, 25(1), 146- 59.

[9] Bailey, P. A., Price, W. G. and Temarel, P., 1997, " A Unified Mathematical Model Describing the Manoeuvring of a Ship Travelling in a Seaway," Transactions of the Royal Institute of Naval Architects,140, 131-149.

[10] Balchen, J. G., Jenssen, N. A. Mathisen, E. and Sælid, S., 1980, "A Dynamic Positioning System Based on Kalman Filtering and Optimal Control," Modeling Identification and Control, 1(3), 135—163.

[11] Banks, S. P., 1981, "A Note on Non-linear Observers, "International Journal of Control, 34, 185‑190.

[12] Barr, R.A., Miller, E.R. and Ankudinov, V., Lee, F.C., 1981, "Technical Basis for Maneuvering Performance Standards," U.S. Coast Guard Report CG-8-81, NTIS ADA 11474.

[13] BC Ferries Press Release, BC Ferries. 22 March 2006: http://www.bcferries.com/files/AboutBCF/06-014queenofthenorth2.pdf

[14] Bernitsas, M. and Papoulias, F. A., 1986, "Stability of Single Point Mooring Systems," Applied Ocean Research, 8(1), 49-58.

[15] Bernitsas, M. and Papoulias, F. A., 1990, "Nonlinear Stability and Maneuvering Simulation of Single Point Mooring Systems," Offshore Station Keeping Symposium, Houston, TX.

[16] Bertram, V., Practical Ship Hydrodynamics, Butterworth Heinemann, 2004.

[17] Berge, S. P., Ohtsu, K. and Fossen, T. I., 1998, "Nonlinear Control of Ships Minimizing the Position Tracking Errors," Proceedings of the IFAC Conference on Control Applications in Marine Systems (CAMS'98), Fukuoka, Japan, 141-147.

[18] Besancon, G., 1999, “On Output Transformations for State Linearization Up to Output Injection, IEEE Transactions on Automatic Control, 44, 1975‑1981.

[19] Bestle, D. and Zeitz, M., 1983, “Canonical Form Observer Design for Nonlinear Time-variable Systems,” International Journal of Control, 38(2), 419-431.

[20] Bingham, H. B., Korsmeyer, F. T. and Newman, J. N., 1994, "Prediction of the Seakeeping Characteristics of Ships," 20th Symposium on Naval Hydrodynamics, Santa Barbara, California.

[21] Blanke, M., 1982, Ship Propulsion Losses Related to Automatic Steering and Prime Mover Control, PhD Thesis, Technical University of Denmark, Denmark.

[22] Blanke, M. and Jensen, A. G., 1997, “Dynamic Properties of Container Vessel with Low Metacentric Height,” Technical Report Number R-1997-4173, Department of Control Engineering, Aalborg University, Denmark.

[23] Boyd, S., El Ghaoui, L., Feron E. and Balakrishnan, V., 1994, “Linear Matrix Inequalities in System and Control Theory,” SIAM Studies in Applied Mathematics, 15, Philadelphia, PA.

[24] Breslin, J. P. Andersen, P., 1994, Hydrodynamics of Ship Propellers, Cambrigde, University Press.

[25] Breivik, M., 2003, “Nonlinear Maneuvering Control of Underactuated Ships,” Masters Thesis, Norwegian University of Science and Technology, Norway.

[26] Breivik, M., Strand, J. P. and Fossen, T. I., 2006, “Guided Dynamic Positioning for Marine Surface Vessels,” IFAC Conference on Manoeuvring and Control of Marine Craft (MCMC'06), Lisbon, Portugal, September 20-22.

[27]

[28] Brian, A., 2003, “Ship Hydrostatics and Stability,” Butterworth-Heinemann, Imprint of Elsevier.

[29] Bulian, G., Francescutto, A., Lugni, C., 2003, “A Theoretical and Experimental Study of the Threshold and Amplitude of Parametric Rolling in Regular and Irregular Waves,” Proceedings of the International Conference on Ship and Shipping Research (NAV 2003), 2, 7.6.1–7.6.12, Palermo, Italy.

[30] Bulian, G., Francescutto, A., Lugni, C., 2004, “On the Nonlinear Modeling of Parametric Rolling in Regular and Irregular Waves,” International Shipbuilding Progress, 51(2/3), 173–203.

[31] Bulian, G., 2005, “Nonlinear Parametric Rolling in Regular Waves – A General Procedure for the Analytical Approximation of the GZ Curve and its Use in Time Domain Simulations,” Ocean Engineering, 32, 309-330.

[32] Bungartz H. J., Schafer M., 2006, Fluid-Structure Interaction. Modelling, Simulation, Optimization, Springer.

[33] Cammaert, A. B., and Tsinker, G. P., 1981, “Impact of Large Ice Floes and Icebergs on Marine Structures,” Proceedings of the International Conference on Port and Ocean Engineering under Arctic Conditions-POAC’81, 2, 653-662.

[34] Cammaert, A. B., Wong, T. T., and Curtis, D. D., 1983, “Impact of Icebergs on Offshore Gravity and Floating Platforms,” Proceedings of the International Conference on Port and Ocean Engineering under Arctic Conditions-POAC, 4, 519-536.

[35] Cammaert, A. B., and Muggeridge, D. B., 1988, “Ice Interaction with Offshore Structures,” Van Nostrand Reinhold, New York.

[36] Carlton, J. S., 1994, Marine Propellers and Propulsion. Butterworth-Heinemann, Imprint of Elsevier.

[37] Chalhoub, N.G., Kfoury, G. A., 2005, “Development of a Robust Nonlinear Observer for a Single-link Flexible Manipulator”, Journal of Nonlinear Dynamics, 39(3), 217-233.

[38] Chalhoub, N.G., Kfoury, G. A. and Bazzi, B. A., 2006, “Design of Robust Controllers and a Nonlinear Observer for the Control of a Single-link Flexible Robotic Manipulator,” Journal of Sound and Vibration, 291(1-2), 437-461.

[39] Chalhoub, N.G. and Khaled, N., 2009, “Robust Controller and Observer for Marine Surface Vessels,” Proceedings of the 2009 Conference on Grand Challenges in Modeling and Simulations (GCMS’09), Istanbul, Turkey, July 13-16, 2009.

[40] Chen, C. T., 1970, Introduction to Linear Systems Theory, Holt, Rinehart and Winston.

[41] Chih-Hsun, C. and Hung-Ching, L., 1994, “A Heuristic Self-tuning Fuzzy Controller,” Fuzzy Sets and Systems, 61(3), 249-264.

[42] Chislett, M. S. and Stom-Tejsen, J., 1965, “Planar Motion Mechanism Tests and Full Scale Steering and Maneuvering Predictions of a Mariner Class Vessel,” Technical Report Number Hy-6, Hydro og Aerodynamisk Laboratorium, Lyngby, Denmark.

[43] Cimen, T. and Banks, S. P., 2004, “Nonlinear Optimal Tracking Control with Application to Super-tankers for Autopilot Design,” Automatica, 40(11), 1845-1863.

[44] Clarke, D, 2001, “Calculation of the Added Mass of Circular Cylinders in Shallow Water,” Ocean Engineering, 28(9), 1265-1294.

[45] Clarke, D, 2003, “The Foundations of Steering and Manuevering,” Proceedings of 6th Conference on Manuevering and Control of Marine Crafts (MCMC 2003), Girona, Spain, 2-16.

[46] Derrett, D. R. and Barrass, C. B., 1999, Ship Stability for Masters and Mates, 5th edition, Butterworth-Heinemann, Imprint of Elsevier.

[47] Do, K. D., Pan, J., Jiang, Z. P., 2003, “Robust Adaptive Control of Underactuated Ships on a Linear Course with Comfort,” Ocean Engineering, 30(17), 2201-2225.

[48] Do, K. D., Jiang, Z. P. and Pan, J., 2005, “Global Partial-State Feedbackand Output-Feedback Tracking Controllers for Underactuated Ships,” Systems and Control Letters, 54(10), 1015-1036.

[49] Dunwoody, A. B., 1989, “Roll of a Ship in Astern Sea- Response to GM Fluctuation, Journal of Ship Research, 33(4)284–290.

[50] El-Hawary, F., 2001, “The Ocean Engineering Handbook,” The Electrical Engineering Handbook Series, CRC Press, Boca Raton, FL.

[51] Faltinsen, O. M. 1990, Sea Loads on Ships and Offshore Structures, Cambridge University Press.

[52] Falzarano, J. M., Shaw, S. W., and Troesch, A. W., 1992, "Application of Global Methods for Analyzing Dynamical System to Ship Rolling Motion and Capsizing," International Journal of Bifurcation and Chaos, 2(1), 101–115.

[53] Falzarano, J. M. and Lakhotia, C., 2008, “Effect of Icing on Ship Maneuvering Characteristics,” The 27th International Conference on Offshore Mechanics and Arctic Engineering (OMAE2008), June 15–20, Estoril, Portugal. OMAE2008-57920, 997-1001.

[54] Fathi, D., 2004, “ShipX Vessel Responses (VERES),” Marintek AS Trondheim, Norway, http://www.marintek.sintef.no.

[55] Fortuna, L. and Muscato, G., 1996, “A Roll Stabilization System for a Monohull Ship: Modeling, Identification, and Adaptive Control,” IEEE Transactions on 481763Control Systems Technology, 4(1), 18 – 28.

[56] Fossen, T. I., 1993, “High Performance Ship Autopilot with Wave Filter,” Proceedings of the 10th Ship Control System Symposium (SCSS'93), Ottawa, Canada.

[57] Fossen, T.I., 1994, Guidance and Control of Ocean Marine Vehicles, John Wiley and Sons Limited., New York.

[58] Fossen, T. I., 1999, “Recent Developments in Ship Control Systems Design,” World Superyacht Review, Sterling Publications Limited.

[59] Fossen, T. I., 2000, “A Survey on Nonlinear Ship Control: From Theory to Practice,” Plenary Talk, Proceedings of the 5th IFAC Conference on Manoeuvring and Control of Marine Craft, Aalborg, Denmark.

[60] Fossen T. I., 2002, Marine Control Systems: Guidance, Navigation and Control of Ships, Rigs and Underwater Vehicles, Marine Cybernetics, ISBN 82-92356-00-2.

[61] Fossen, T. I., 2005, “A Nonlinear Unified State-Space Model for Ship Maneuvering and Control in a Seaway," Int. Journal of Bifurcation and Chaos, 15, 2717-2746.

[62] Fossen, T. I., Breivik, M. and Skjetne, R., 2003, “Line-Of-Sight Path Following of Underactuated Marine Craft,” Proceedings of the Sixth IFAC Conference on Maneuvering and Control of Marine Crafts (MCMC'2003), Girona, Spain, 244-249.

[63] Fossen, T.I. and Grovlen, A., 1998, “Nonlinear Output Feedback Control of Dynamically Positioned Ships Using Vectorial Observer Backstepping,” IEEE Transactions on Control Systems Technology, 6(1), 121-128.

[64] Fossen, T. I., Godhavn, J. M., Berge, S. P. and Lindegaard, K. P., 1998, “Nonlinear Control of Underactuated Ships with Forward Speed Compensation,” Proceedings of the IFAC NOLCOS 98, Enschede, The Netherlands, 121-127.

[65] Fossen, T.I., 1994, Guidance and Control of Ocean Marine Vehicles, John Wiley and Sons Ltd., New York.

[66] Fossen, T.I., 1993, “High Performance Ship Autopilot with Wave Filter,” Proceedings of the 10th Ship Control System Symposium (SCSS'93), Ottawa, Canada.

[67] Fossen, T.I. and Strand, J. P., 1999a, “A Tutorial on Nonlinear Backstepping: Applications to Ship Control,” Modelling, Identification and Control, 20(2), 83-135.

[68] Fossen, T.I. and Strand, J.P., 1999b, “Passive Nonlinear Observer Design for Ships using Lyapunov Methods: Full-scale Experiments with a Supply Vessel,” Automatica, 35(1), 3-16.

[69] Fox, R.W. and McDonald, A. T., 1992, Introduction to Fluid Mechanics, John Wiley & Sons, New York.

[70] Francisco, J., V., Elías, R., Eloy, L., Emiliano, M. and Haro Casado, M., 2008, “Simulations of an Autonomous In-scale Fast-ferry Model,” International Journal of Systems Applications, Engineering & Development, 2(3), 2008.

[71] Friedland, B., 1986, Control System Design: An Introduction to State-Space Methods, McGraw-Hill.

[72] Grace, I. F., and Ibrahim, R. A., 2008, “Modelling and Analysis of Ship Roll Oscillations Interacting with Stationary Icebergs,” Journal of Mechanical Engineering Science, 222(10), 1873-1884.

[73] Godhavn, J. M., 1996, “Nonlinear Tracking of Underactuated Surface Vessels,” in Proc. 35th Conf. Decision Control Kobe, Japan.

[74] Godhavn, J. M., Fossen, T. I., Berge, S. P., 1998, “Nonlinear and Adaptive Backstepping Designs for Tracking Control of Ships,” International Journal on Adaptive Control and Signal Processing (Special Issue on Marine Systems), 12, 649‑670.

[75] Golubev, V., 1972, “On the Structure of Ice Formed During Icing on Ships,” Issledovniye. Fizichskoy. Prirody Obledeneniya Sudo, Leningrad, Russia, 105–115.

[76] Healey, A. J. and Marco, D. B., 1992, “Slow Speed Flight Control of Autonomous Underwater vehicles: Experimental Results with the NPS AUV II,” Proceedings of the 2nd International Offshore and Polar Engineering Conference (ISOPE), SanFrancisco, California, 523-532.

[77] Hermans, A. J., 1991, “Second Order Wave forces and Wave Drift Damping,” Ship Technology Research, 38(1991), 163-172.

[78] Hermans, A. J., 1999, “Low-frequency Second-order Wave-drift Forces and Damping,” Journal of Engineering Mathematics, 35(1-2) 181-198.

[79] Hirano, M., 1980, “On the Calculation Method of Ship Maneuvering Motion at Initial Design Phase,” Journal of the Society of Naval Architects of Japan, 147, 144–153.

[80] Holzhuter, T., 1997, “LQG Approach for the High-Precision Track Control of Ships,” IEE Proceedings on Control Theory and Applications, 144(2), 121–127.

[81] Holzhuter, T. and Schultze, R., 1996, “On the Experience with a High-Precision Track Controller for Commercial Ships,” Control Engineering Practice (CEP), 4(3), 343–350.

[82] Huijsmans, R. H. M., 1996, Mathematical Modelling of the Mean Wave Drift Force in Current, a Numerical and Experimental Study, PhD Thesis, Delft University of Technology (TU Delft), Netherlands.

[83] Ibrahim, R. A. and Grace, I. F., 2010, "Modeling of Ship Roll Dynamics and Its Coupling with Heave and Pitch," Mathematical Problems in Engineering (1024-123X).

[84] International Maritime Organization (IMO), 2007, Revised IMO Intact Stability Code, www.imo.org.

[85] Isherwood, R. M., 1973, “Wind Resistance of Merchant Ships,” The Royal Institution of Naval Architects, 15, 327-338.

[86] Jiang, Z. P. and Nijmeijer, H., 1999, “A Recursive Technique for Tracking Control of Nonholonomic Systems in Chained Form,” IEEE Transactions on Automatic Control, 4(2), 265-279.

[87] Jiang, Z. P., 2002, “Global Tracking Control of Underactuated Ships by Lyapunov’s Direct method,” Automatica, 38, 301–309.

[88] Jie, J.; Li, Y. and Zheng, L., 2007, “Self-Adjusting Fuzzy Logic Control for Vehicle Lateral Control,” Fourth International Conference on Fuzzy Systems and Knowledge Discovery, 2,614 – 618.

[89] Journée, J. M. J. and Massie, W. W., 2001, Offshore Hydrodynamics, Delft University of Technology, http://www.shipmotions.nl/DUT/LectureNotes/OffshoreHydromechanics.pdf

[90] Journée, J. M. J., 2001, “A Simple Method for Determining the Maneuvering Indices k and t from Zigzag Trial Data,” DUT-SHL Technical Report 0267, Delft, Netherlands.

[91] Journée, J. M. J. and Pinkster, J., 2002, Introduction in Ship Hydromechanics, Delft University of Technology, http://www.shipmotions.nl/DUT/LectureNotes/ShipHydromechanics_Intro.pdf

[92] Jwo, D. J., Cho, T. S., 2007, “A Practical Note on Evaluating Kalman Filter Performance Optimality and Degradation,” Applied Mathematics and Computation, 193(2), 482-505,ISSN 0096-3003.

[93] Kailath, T., 1980, Linear Systems, Prentice-Hall.

[94] Kallstrom, C. G., Astrom, K. J., Thorell, N. E., Eriksson, J. and Sten, L., 1979, “Adaptive Autopilots for Tankers,” Automatica, 15(3), 241-254.

[95] Kfoury, G. A. and Chalhoub, N. G., 2007, “Development of a Robust Observer for Constrained Nonlinear Systems,” ASME International Mechanical Engineering Congress and Exposition (IMECE), Seattle, Washington, November 11-15.

[96] Kfoury, G. A., 2008, Computation of the Instantaneous Frictional Losses in Internal Combustion Engines Using Estimated Variables, PhD Thesis, Wayne State University, USA.

[97] Khaled, N. and Chalhoub, N.G., 2010a, “Self Tuning Fuzzy Sliding Controller for the Ship Heading Problem,” accepted for publication in the Proceedings of the ASME Dynamic Systems and Control Conference (DSCC 2010), Cambridge, Massachusetts, USA, September 13-15.

[98] Khaled, N. and Chalhoub, N.G., 2010b, “Guidance and Control Scheme for Under-actuated Marine Surface Vessels,” accepted for publication in the Proceedings of the 2010 American Control Conference (ACC 2010), Baltimore, Maryland, USA, June 30 – July 2.

[99] Khaled, N. and Chalhoub, N.G., 2009a, “A Dynamic Model and a Robust Controller for a Fully Actuated Marine Surface Vessel,” Journal of Vibration and Control, in press.

[100] Khaled, N. and Chalhoub, N.G., 2009b, “A Dynamic Model and a Robust Controller for a Fully Actuated Marine Surface Vessel,” Proceedings of the Vibro-Impact Dynamics of Ocean Systems, LNACM 44, 135-148.

[101] Khaled, N. and Chalhoub, N. G., 2009c, “Computationally Efficient Procedure for Handling the Powertrain Constraints In Marine Vessel Simulations”, Cairo 11th International Conference on Energy and Environment, Hurgada, Egypt, March 15-18.

[102] Khalil, H.K., 1996, Nonlinear Systems, Second Edition, Prentice-Hall.

[103] Kim, M. H., Inman, D. J., 2004, “Development of a robust non-linear observer for dynamic positioning of ships,” Proceedings of the institution of Mechanical Engineers, Part I: Journal of Systems and Control Engineering, 218(1), 1-12.

[104] Kongsberg Maritime Corporation: http://www.km.kongsberg.com/

[105] Korsmeyer, F. T., Lee, C. H., Newman, J. N., and Sclavounos, P. D., 1988, “The Analysis of Wave Interactions with Tension Leg Platforms," Offshore Mechanics and Arctic Engineering Conference (OMAE), Houston.

[106] Korvin-Kroukovsky, B. V, 1955, “Investigation of Ship Motions in Regular Waves,” Society of Naval Architects and Marine Engineers Transactions, 63, 386-435.

[107] Kou, S. R., Elliott, D. L. and Tarn, T. J., 1975, “Exponential Observers for Nonlinear Dynamic Systems,” Information and Control, 29, 204‑216.

[108]Krener, A. J. and Isidori, A., 1983, “Linearization by Output Injection and Nonlinear Observers, Systems and Control Letters, 3, 47‑52.

[109]Kristiansen, E. and Egeland, O., 2003, “Frequency Dependent Added Mass in Models for Controller Design for Wave Motion Ship Damping,” 6th IFAC Conference on Manoeuvring and Control of Marine Craft (MCMC’03), Girona, Spain.

[110]Kristiansen, E., Hjulstad, Å. and Egeland, O., 2005, “State Space Representation of Raditation Forces in Time Domain Vessel Models,” Oceanic Engineering, 32, 2195–2216.

[111]Kuiper, G., 1992, “The Wageningen Propeller Series,” MARIN Publication No. 92-001.

[112]Laranjinha, M., Falzarano, J. M. and Guedes Soares, C., 2002, “Analysis of the Dynamical Behavior of an Offshore Supply Vessel with Water on Deck,” Proceedings of Offshore Mechanics and Arctic Engineering (OMAE), June 2002, Oslo, Norway.

[113]Lauvdal, T. and Fossen, T. I., 1998, “Rudder Roll Stabilization of Ships Subject to Input Rate Saturations Using a Gain Scheduled Control Law,” Proceedings of the IFAC Conference on Control Applications in Marine Systems (CAMS'98), Fukuoka, Japan, October 27-30, 121-127.

[114]Layne, J. and Passino, K., 1993 , “Fuzzy Model Reference Learning Control for Cargo Ship Steering,” IEEE Control Systems, 13(6), 23–34.

[115]Le, M. D., Tran, Q. T., Nguyen, T.N. and Gap, V.D., 2004, “Control of Large Ship Motions in Harbor Maneuvers by Applying Sliding Mode Control,” 8th IEEE International Worshop, Avanced Motion Control, 695-700.

[116]Lee, C. H. and Newman, J. N., "First and Second-order Wave Effects on a Submerged Spheroid," Journal of Ship Research, 1991.

[117]Lee, C. H., "Kochin-type Second-order Wave Exciting Forces," 5th International Workshop on Water Waves and Floating Bodies, Manchester , UK , March 1990.

[118]Lee, C. H., and Sclavounos, P. D., "Removing the Irregular Frequencies from Integral Equations in Wave-body Interactions," Journal of Fluid Mechanics, 207, pp393-418, 1989.

[119]Lee, C. H. and Newman, J.N., 2004, “Computation of Wave Effects Using the Panel Method”, WIT Press, Southhampton.

[120]Lefeber, A. A. J., Pettersen, K. Y. and Nijmeijer, H.,2003, “Tracking Control of an Underactuated Ship, IEEE Transactions on Control Systems Technology, 11(1), 52-61.

[121]Lewandowski, E. M., 2004, “The Dynamics of Marine Craft Maneuvering and Seakeeping,” Advanced Series on Ocean Engineering, 2, World Scientific, Singapore.

[122]Lewis, F. L., 1986, Optimal Estimation with an Introduction to Stochastic Control Theory, Wiley-Interscience.

[123]Lewis, E.V., 1988, Principles of Naval Architecture, 2nd ed., Society of Naval Architects and Marine Engineers (SNAME).

[124]Li, Z., Sun, J., Oh, S., 2009, “Design, Analysis and Experimental Validation of a Robust Nonlinear Path Following Controller for Marine Surface Vessels,” Automatica, 45(7),1649-1658.

[125]Lindegaard, K. P., 2003, Acceleration Feedback in Dynamic Positioning, PhD Thesis, Norwegian University of Science and Technology, Norway.

[126]Lindegaard, K. P. and Fossen T. I., 2001, “On Global Model Based Observer Designs for Surface Vessels,” The 5th IFAC Conference on Control Applications in Marine Systems (CAMS'2001), Glasgow, UK.

[127]Lopez, M., J., Rubio, F., R., 1992, “LQG/LTR Control of Ship Steering Autopilots,” IEEE Proceedings on Intelligent Control, 447- 450.

[128]Luenberger, D. G., 1964, “Observing the State of a Linear System,“ IEEE Transactions, Military Electronics, 23, 119–125.

[129]Luenberger, D. G., 1966, “Observers for Multivariable Systems,” IEEE Transactions, Automatic Control, 11, 190–197.

[130]Luenberger, D. G., 1979, Introduction to Dynamic Systems – Theory, Models and Applications, John Wiley and Sons Limited, New York.

[131]Maeda, M. and Murakami, S., 1992, “A Self-tuning Fuzzy Controller,” Fuzzy Sets and Systems, 51(1), 29-40.

[132]Maury, C., Delhommeau, G., Ba, M., Boin, J. P., and Guilbaud, M., 2003, “Comparisons between Numerical Computations and Experiments for Seakeeping on Ship Models with Forward Speed,” Journal of Ship Research, 47, 347-364.

[133]Minghui, W., Yongquan, Y., Yun, Z. and Fei, W., 2008, “Optimization of Fuzzy Control System Based on Extension Method for Ship Course-Changing/Keeping,” IEEE World Congress on Computational Intelligence, 434 – 438.

[134]Minorsky, N., 1922, “Directional Stability of Automatically Steered Bodies,” Journal of the American Society of Naval Engineers, 342, 280-309.

[135]Minsk, D. L., 1977, “Ice Accumulation on Ocean Structures,” Cold Regions Research and Engineering Laboratory (CRREL), Hanover, NH.

[136]Misawa, E. A. and Hedrick, J. K., 1989, “Nonlinear Observers – A State-of-the-art Survey,” Journal of Dynamic Systems, Measurement, and Control, 111, 344-352.

[137]Molland, A. F. and Turnock, S. R., 1993, Wind Tunnel Investigation of the Influence of Propeller Loading on Ship Rudder Performance,” Transactions of the Royal Institution of Naval Architects (RINA), 135, 105-120.

[138]Molland, A. F. and Turnock, S. R., 1994, “Prediction of Ship Rudder-Propeller Interaction at Low Speeds and in Four Quadrants of Operation, Proceedings of the Conference on Manouevring and Control of Marine Craft (MCMC’94), 319-333.

[139]Molland, A. F. and S. R. Turnock,1996, “A Compact Computational Method for Predicting Forces on a Rudder in a Propeller Slipstream,” Transactions of the Royal Institution of Naval Architects (RINA),138, 227-244.

[140]Molland, A. F. and Turnock, S. R. and Wilson, P. A., 1996, “Performance of an Enhanced Rudder Force Prediction Model in a Ship Manoeuvring Simulator,”

Proceedings of the International Conference on Marine Simulation and Ship Manoeuvrability (MARSIM'96), Copenhagen, Denmark, 425-434.

[141] Moreira, L., Fossen, T. I. and Guedes Soares, C., 2007, "Path Following Control System for a Tanker Ship Model," Ocean Engineering (OE 2007), 34, 2074–2085.

[142] Morel, Y., 2009, Applied Nonlinear Control of Unmanned Vehicles with Uncertain Dynamics, PhD Thesis, Virginia Polytechnic Institute and State University, USA.

[143] Nandam, P. K. and Sen P. C., 1990, "A Comparative Study of a Luenberger Observer and Adaptive Observer-based Variable Structure Speed Control System Using a Self-controlled Synchronous Motor," IEEE Transactions on Industrial Electronics, 37(2), 127-132.

[144] Nayfeh, A. H., Mook, D. T., and Marchall, L. R., 1973, "Nonlinear Coupling of Pitch and Roll Modes in Ship Motions," Journal of Hydronautics 7(4), 145-152.

[145] Nayfeh, A. H., Mook, D. T., and Marshall, L. R., 1974, "Perturbation Energy Approach for the Development of the Nonlinear Equations of Ship Motion," Journal of Hydronautics 8(4), 130 - 136.

[146] Nayfeh, A. H., and Mook, D. T., 1979, "Nonlinear Oscillations," Pure and Applied Mathematics, John Wiley and Sons, New York.

[147] Nayfeh, A. H. and Balachandran, B., 1995, Applied Nonlinear Dynamics, Wiley Series in Nonlinear Science, New York.

[148] Newman, J.N., 1977, Marine Hydrodynamics, MIT Press, Cambridge, Massachusetts.

[149]Newman, J. N., 1993, “Wave-drift Damping of Floating Bodies,” Journal of Fluid Mechanics, 249 (1993), 241-259.

[150]Nomoto, K., Taguchi, K., Honda, K., 1956, “On the Steering Qualities of Ships,” Journal of Society of Naval Architects of Japan, 99, 75-82.

[151]Norrbin, N. H., 1970, “Theory and Observation on the Use of a Mathematical Model for Ship Maneuvering in Deep and Confined Waters,” Eighth Symposium on Naval Hydrodynamics, Pasadena, California.

[152]Ogata, K., 2002, Modern Control Engineering, Fourth Edition, Prentice-Hall.

[153]Ogilvie, T. F. and Tuck, E. O., 1969, “A Rational Strip Theory of Ship Motion, Part 1,” University of Michigan, Department of Naval Architecture and Marine Engineering, Report 013.

[154]Ogilvie, T. F., 1964, “Recent Progress toward the Understanding and Prediction of Ship Motion,” the ONR 5th Symposium on Naval Hydrodynamics, Bergen, Norway.

[155]Ogilvie, T. F., 1974, “Workshop on Slender-body Theory, Part 1: Free Surface Effects,” University of Michigan, Department of Naval Architecture and Marine Engineering report 162.

[156]Ogilvie, T. F., 1977, “Singular Perturbation Problems in Ship Hydrodynamics,” Advances in Applied Mechanics, 17, 92-187.

[157]Oil Companies International Marine Forum, OCIMF, 1994, Prediction of Wind and Current Loads on VLCCs, Witherby & Co., London.

[158]Oil Companies International Marine Forum, OCIMF, 1977, Prediction of wind and current loads on VLCCs, Witherby & Co., London.

[159]Parkinson, B and Spilker Jr., J. J., 1996, Global Positioning System: Theory and Applications, Volume II, American Institute of Aeronautics and Astronautics, Washington.

[160]Peng, Y., Han, J. and Wu , Z., 2007, “Nonlinear Backstepping Design of Ship Steering Controller: Using Unscented Kalman Filter to Estimate the Uncertain Parameters,” Proceedings of the IEEE International Conference on Automation and Logistics,China, 126–131.

[161]Perez, T. and Blanke, M., 2002, “Mathematical Ship Modelling for Control Applications,” Technical Report, Technical University of Denmark, Denmark, http://www.iau.dtu.dk/secretary/pdf/TP-MB-shipmod.pdf

[162]Perez, T., 2005, Ship Motion Control, Springer Verlag.

[163]Perez, T. and Fossen, T. I., 2006, “Time-Domain Models of Marine Surface Vessels for Simulation and Control Design Based on Seakeeping Computations,” Proceedings of the IFAC Conference on Manoeuvring and Control of marine Craft, Lisbon,Portugal, September 20-22.

[164]Perez, T., Ross, A. and Fossen, T. I., 2006, “A 4-DOF SIMULINK Model of a Coastal Patrol Vessel for Manoeuvring in Waves,” 7th IFAC Conference on Manoeuvring and Control of Marine Vessels MCMC, Portugal.

[165]Perez, T. and Fossen, T. I., 2007, ”Kinematic Models for Seakeeping and Maneuvering of Marine Vessels,” Modeling, Identification and Control (MIC), 28(1), 1-12.

[166]Pettersen, K. Y. and Nijmeijer, H., 1999, “Tracking Control of an Underactuated Surface Vessel,” Proceedings of the IEEE Conference on Decision and Control, Phoenix, AZ, 4561–4566.

[167]Pettersen, K.Y. and Nijmeijer, H., 2001, “Underactuated Ship Tracking Control: Theory and Experiments,” International Journal of Control, 74(14), 1435-1446.

[168]Pettersen, K. Y., Lefeber, E., 2001, “Way-point Tracking Control of Ships,” Proceedings of the 40th IEEE Conference on Decision and Control, 940–945.

[169]Pinkster, J. A., 1980, Low Frequency Second Order Wave Excitation Forces on Floating Structures, PhD Thesis, Delft University of Technology (TU Delft), Netherlands.

[170]Pivano, L., Johansen, T. A., Smogeli, O. N., Fossen, T. I., 2007, “Nonlinear Thrust Controller for Marine Propellers in Four-Quadrant Operations,” American Control Conference, New York.

[171]Polkinghorne, M. N., Roberts, G. N., Burns, R. S. and Winwood, D., 1995, “The Implementation of Fixed Rulebase Fuzzy Logic to the Control of Small Surface Ships,” Control Engineering Practice, 3(3), 321-328.

[172]Polkinghorne, M. N., Roberts, G. N. and Burns, R. S., 1997, “Intelligent Ship Control with Online Learning Ability,” Computing and Control Engineering, 8(5). 196–200.

[173]Prins, H. J., 1995, Time-domain Calculations of Drift Forces and Moments, PhD Thesis, Delft University of Technology (TU Delft), Netherlands.

[174]Prins, H. J. and Hermans, A. J., 1996, “Wave-drift Damping of a 200 kdwt Tanker,” Journal of Ship Research, 40(1996),136-143.

[175]Procyk, T.J. and Mamdani, E.H. , 1979, “A Linguistic Self-Organising Process Controller,” Automatica, 15(1), 53–65.

[176]Raghavan, S. and Hedrick, J. K., 1994, “Observer Design for a Class of Nonlinear Systems,” International Journal of Control, 59, 515‑528.

[177]Rajamani, R., 1998, Observers for Lipschitz Nonlinear Systems,” IEEE Transactions on Automatic Control 43, 397‑401.

[178]Remery, G. F. M. and Oortmerssen, G. V., 1973, The Mean Wave, Wind and Current Forces on Offshore Structures and their Role in the Design of Mooring Systems,” Offshore Technology Conference OTC 1741, Houston, USA.

[179]Roddy, R. F., Hess, D. E. and Faller, W. E., 2006, “Neural Network Predictions of the 4-Quadrant Wageningen B-Screw Series,” Fifth International Conference on Computer and IT Applications in the Maritime Industries, Leiden, Netherlands.

[180]Rundell, A.E., Drakunov, S.V. and DeCarlo, R.A., 1996, “A Sliding Mode Observer and Controller for Stabilization of Rotational Motion of a Vertical Shaft Magnetic Bearing,” IEEE Transactions on Control Systems Technology, 4(5), 598-608.

[181]Ryerson, C. C., 1995, “Superstructure Spray and Ice Accretion on a Large U.S. Coast Guard Cutter,” Atmospheric Research, 36(3-4), 321-337.

[182]Sagatun, S. I., 1992, Modeling and Control of Underwater Vehicles: A Lagrangian Approach, PhD thesis, Department of Engineering Cybernetics, The Norwegian Institute of Technology, Norway.

[183]Sagatun, S. I. and Fossen, T. I., 1991, “Lagrangian Formulation of Underwater Vehicle’s Dynamics,” Proceedings of the IEEE International Conference on Systems, Man and Cybernetics. Charlottesville, VA.

[184]Salvesen, N., Tuck, E. O. and Faltinsen, O., 1970, “Ship Motions and Sea Loads,” Society of Naval Architects and Marine Engineers Transactions, 78, 250-287.

[185]Salvesen, N. and Smith, W. E., 1971, “Comparizon of Ship-Motion Theory and Experiment for Mariner Hull and a Detroyer Hull with Bow Modification,” David Taylor Naval Ship Research and Development Center report 3337.

[186]Sandler, M., Wahl, A., Zimmermann, R., Faul, M., Kabatek, U. and Gilles, E. D., 1996, “Autonomous Guidance of Ships on Waterways,” Robotics and Autonomous Systems, 18(3), 327-335, ISSN 0921-8890.

[187]Sarpkaya, T., 1981, Mechanics of Wave Forces on Offshore Structures, Van Nostrand Reinhold Company, New York.

[188]Sira-Ramirez, H., 1999, “On the Control of the Underactuated Ship: A Trajectory Planning Approach,” IEEE Conference on Decision and Control, Phoenix, AZ.

[189]Skejic, R. and Faltinsen, O. M., 2007, “A Unified Seakeeping and Maneuvering Analysis of two Interacting Ships,” Proceedings of the 2nd International Conference on Marine Research and Transportation, 209–218, Ischia, Italy.

[190]Skejic, R. and Faltinsen, O. M., 2008, “A unified Seakeeping and Maneuvering Analysis of Ships in Regular Waves, Journal of Marine Science and Technology, 13, 371–394.

[191]Slotine, J. J. E., Hedrick, J. K. and Misawa, E. A., 1987, “On Sliding Observers for Nonlinear systems,” Journal of Dynamic Systems, Measurement, and Control, 109, 245-252.

[192]Slotine, J. J. E. and Li, W., 1991, Applied Nonlinear Control, Prentice-Hall, Englewood Cliffs, New Jersey.

[193]Sorenson, H. W., 1985, Kalman Filtering: Theory and Application, IEEE Press, New York, N.Y.

[194]Sorensen, A. J., Sagatun, S. I. and Fossen, T. I., 1996, “Design of a Dynamic Positioning System Using Model-based Control,” Control Engineering Practice, 4(3), 359-368, ISSN 0967-0661.

[195]Strand, J. P., Ezal, K., Fossen, T. I. and Kokotovic, P. V., 1998. “Nonlinear Control of Ships: A Locally Optimal Design,” Preprints of the IFAC NOLCOS'98, Enschede, The Netherlands, 732-738.

[196]Suleiman, B. M., 2000, Identification of Finite-Degree-of-Freedom Models for Ship Motions, PhD Thesis, Virginia Polytechnic Institute and State University, Blacksburg, Virginia.

[197]Sutton, R. and Towill, D.R., 1987, “A Fuzzy Model of The Helmsman Performing a Course-Keeping Task”, Applied Ergonomics, 18 (2), 137-142.

[198]Sutton, R. and Jess, I., 1991,”Real-time Application of a Self-organising Autopilot to Warship Yaw Control,” International Conference On Control, London, IEE, 332, 827 - 832.

[199]Tao, Z. and Incecik, A. , 1998, "Time Domain Simulation Of Vertical Ship Motions And Loads In Regular Head Seas," 17th International Conference on Offshore Mechanics and Arctic Engineering(OMAE'98), 2.

[200]Tonshoff, H. K. and Walter, A., 1994, "Self-tuning Fuzzy Controller for Process Control in Internal Grinding," Fuzzy Sets and Systems, 63(3), 359-373.

[201]Thau, F. E., 1973, "Observing the State of Non-linear Dynamic Systems," International Journal of Control, 17(3), 471-479.

[202]The Society of Naval Architectures and Marine Engineers, SNAME, 1950, Nomenclature for Treating the Motion of Submerged Body Through a Fluid, 74 Trinity Place, New York, N. Y. 10006.

[203]Tragardh, P., Lindell, P. and Sasaki, N., 2005, "Double Acting Tanker: Experiences from Model Tests and Sea Trials," Proceedings of the Institution of Mechanical Engineers, Journal of Engineering for the Maritime Environment, 219, 109-119.

[204]Tsinias, J., 1989, "Observer Design for Nonlinear Systems," Systems and Control Letters 13, 135‑142.

[205]Ueng, S. K., Lin, D. and Liu, C. H., 2008, "A Ship Motion Simulation System," Virtual reality, 12, 65–76.

[206]Utkin, V.I., 1981, "Principles of Identification Using Sliding Regimes," Soviet Physics – Doklady, 26(3), 271-272.

[207]Vahedipour, A. and Bobis, J. P., 1992, "Smart Autopilots," International Conference on Industrial Electronics, Control, Instrumentation, and Automation, IECON 92, San Diego, USA.

[208]Van Amerongen, J., 1975, “Model Reference Adaptive Autopilots for Ships,” Automatica, 11(1).

[209]Van Amerongen, J., 1984, “Adaptive Steering of Ships—a Model Reference Approach,” Automatica, 20 (1), 3-14.

[210]Van Dyke, M., 1975, Perturbation Methods in Fluid Mechanics, 2nd ed., Standford: Parabolic Press.

[211]Vassalos, D., 1999, “Physical Modelling and Similitude of Marine Structures,” Ocean Engineering 26, 111-123.

[212]Vassalos, D., Hamamoto, M., Papanikolaou, A. and Molneux, D., 2000, Contemporary ideas on ship stability, Amsterdam, Elsevier.

[213]Velagic, J., Vukic, Z. and Omerdic, E., 2003, “Adaptive Fuzzy Ship Autopilot for Track-keeping,” Control Engineering Practice, 11(4), 433-443.

[214]Vik, B., Shiriaev, A. and Fossen, T. I., 1999, Nonlinear Design for Integration of DGPS and INS,” New Directions in Nonlinear Observer Design (Nejmeijer, H. and Fossen, T. I.), Chapter I-8, 135-160, Springer Verlag, London.

[215]Vik, B., 2000, Nonlinear Design and Analysis of Integrated GPS and Inertial Navigation System, PhD thesis, Department of Engineering Cybernetics, Norwegian University of Science and Technology, Trondheim, Norway.

[216]Vik, B. and Fossen, T. I., 2001, “A Nonlinear Observer for Integration of GPS and Inertial Navigation Systems,” Modeling, Identification and Control,” (MIC), 21(4), 193-208.

[217]Vukic, Z., Kuljaca, L. and Milinovic, D, 1996, “Predictive Gain Scheduling Autopilot for Ships,” Electrotechnical Conference, MELECON '96., 8th Mediterranean, 2, 1133 – 136.

[218]Vugts, J. H., 1970, The Hydrodynamic Forces and Ship Motions in Waves, PhD Thesis, Delft Technological University (TU Delft), Netherlands.

[219]Wai, R.J., Lin, C. M., and Hsu, C.F., 2002, “Self-Organizing Fuzzy Control for Motor-Toggle Servomechanism Via Sliding-Mode Technique,” Fuzzy Sets and Systems, 131, 235-249.

[220]Walcott, B.L., Zak, S.H., 1986, “Observation of Dynamical Dystems in the Presence of Bounded Nonlinearities/Uncertainties”, Proceedings of the 25th Conference on Decision and Control, Athens, Greece, 2, 961-966.

[221]Wang, M., Yu, Y. and Zeng, B., 2005, “Ship Steering System Based on Fuzzy Control Using Real-Time Tuning Algorithm,” Third International Conference on Information Technology and Applications (ICITA 2005), Sydney, Australia, 577-580.

[222]Wang, S., 1976, “Dynamical Theory of Potential Flows with a Free Surface: A Classical Approach to Strip Theory of Ship Motions,” Journal of Ship Research, 20(3), 137-144.

[223]Wu, G. X. and Taylor, R. E., 1990, “The Hydrodynamic Force on an Oscillating Ship with Low Forward Speed,” Journal of Fluid Mechanics, 211, 333-353.

[224]Yanada, H., Shimahara, M., 1997, “Sliding Mode Control of an Electrohydraulic Servo Motor Using a Gain Scheduling Type Observer and Controller,”

Proceedings of the Institution of Mechanical Engineers, Part I: Journal of Systems and Control Engineering, 211(6), 407-416.

[225]Yang, Y., Zhou, C., Ren, J., 2003, “Model Reference Adaptive Robust Fuzzy Control for Ship Steering Autopilot with Uncertain Nonlinear Systems, Applied Soft Computing, 3(4), 305-316, ISSN 1568-4946.

[226]Yang, Y. and Jiang, B. 2004a, “Variable Structure Robust Fin Control for Ship Roll Stabilization with Actuator System,” In: Prococeeings of the American Control Conference. Massachusetts, USA, 5212–5217.

[227]Yang, Y. and Jiang, B. 2004b, “Robust Adaptive Fuzzy Control (RAFC) for Ship Steering with Uncertain Nonlinear Systems,” Fifth World Congress on Intelligent Control and Automation (WCICA 2004), 3, 2514- 2518.

[228]Yeh, Z. M., 1994, “A Performance Approach to Fuzzy Control Design for Nonlinear Systems,” Fuzzy Sets and Systems, 64, 339-352.

[229]Yu, F., 2009, “A Self-Tuning Fuzzy Logic Design for Perturbed Time-Delay Systems with Nonlinear Input”, Expert Systems with Applications, 36(3).

[230]Zeitz, M., 1987, “The Extended Luenberger Observer for Nonlinear Systems,” Systems Control, Letters, 9(2), 149-156.

ABSTRACT

ROBUST OBSERVERS AND CONTROLLERS FOR MARINE SURFACE VESSELS UNDERGOING MANEUVERING AND COURSE-KEEPING TASKS

by

NASSIM SAADDINE KHALED

August 2010

Advisor: Prof. Nabil G. Chalhoub

Major: Mechanical Engineering

Degree: Doctor of Philosophy

The dynamic behavior of marine surface vessels is highly nonlinear. Moreover, it is significantly influenced by environmental disturbances induced by winds, random sea waves and currents. The focus of this work is to develop an integrated guidance and control system that enables under-actuated marine surface vessels to operate autonomously and yield robust tracking performance in spite of significant external disturbances and modeling imprecision.

A nonlinear model for a marine surface vessel is developed to serve as a test bed for assessing the performance of the proposed guidance and control systems. The model incorporates recent developments in ship modeling. Its formulation considers the effects of coriolis and centripetal accelerations, wave excitations, retardation forces, nonlinear restoring forces, wind and sea-current loads, linear damping terms, and the control force and moment. Moreover, it captures the dynamics of the rudder and accounts for the physical limitations of both the rudder and the ship propulsion system.

The guidance scheme is based on the concepts of the variable radius line-of-sight (LOS) and the acceptance radius. This scheme has been modified in the current work to vary the LOS radius exponentially with the cross track error. Such a guidance system has been shown herein to yield a faster rate of convergence over existing schemes in guiding the ship toward its desired trajectory.

Two fully integrated guidance and control systems have also been introduced in this work. The first one involves a sliding mode controller and observer. The second system includes an enhanced self-tuning fuzzy-sliding mode controller and a novel design for a self-tuning fuzzy-sliding mode observer. The second guidance and control system is introduced in an attempt to combine the advantages of the variable structure systems (VSS) theory with the self-tuning fuzzy logic controller.

The simulation results demonstrate the capabilities of the proposed robust observers in yielding accurate estimates of the state variables that are needed for the computation of the control signals. Furthermore, they serve to demonstrate that the proposed guidance and control schemes allow under-actuated marine surface vessels to operate autonomously in tracking a desired trajectory. Their performance has been proven to be robust in the presence of modeling imprecision and significant environmental disturbances.

AUTOBIOGRAPHICAL STATEMENT

Nassim Khaled graduated from the Lebanese University, Lebanon, in 2003 with a Bachelor of Engineering in Mechanical Engineering. In 2005 he received his Master of Science degree in mechanical engineering at the American University of Beirut, Lebanon. The subject of his Master's thesis was Landmine detection using infra-red imaging.

In 2005 he moved to Detroit and started working at WSU towards his PhD degree as a graduate research assistant. He worked on designing robust controllers, obsersevers and a guidance system for underactuated ships. The overall system was proven to be fully autonomous.